Compressive Sensing-Based Estimation of Direction of Arrival in Antenna Arrays

Amgad A. Salama Afsa

A Thesis

in

The Department

of

Electrical and Computer Engineering

Presented in Partial Fulfillment of the Requirements

For the Degree of

Doctor of Philosophy (Electrical and Computer Engineering) at

Concordia University

Montréal, Québec, Canada

August 2017

CONCORDIA UNIVERSITY

SCHOOL OF GRADUATE STUDIES

This is to certify that the thesis prepared

By: **Amgad Adel Ibrahem SALAMA AFSA**

Entitled: **Compressive Sensing Based Estimation of Direction of Arrival in Antenna Arrays**

and submitted in partial fulfillment of the requirements for the degree of

Doctor Of Philosophy (Electrical and Computer Engineering)

complies with the regulations of the University and meets the accepted standards with respect to originality and quality.

Signed by the final examining committee:

_____ Chair
Dr. Luis Amador

_____ External Examiner
Dr. Wasfy Boushra Mikhael

_____ External to Program
Dr. Terry Fancott

_____ Examiner
Dr. Yousef R. Shayan

_____ Examiner
Dr. Wei-Ping Zhu

_____ Thesis Co-Supervisor
Dr. M.Omair Ahmad

_____ Thesis Co-Supervisor
Dr. M.N.S. Swamy

Approved by

Dr. Wei-Ping Zhu, Graduate Program Director

Monday, August 28, 2017

_____
Dr. Amir Asif, Dean
Faculty of Engineering and Computer Science

ABSTRACT

Compressive Sensing-Based Estimation of Direction of Arrival in Antenna Arrays

Amgad A. Salama Afsa, Ph.D.

Concordia University, 2017

This thesis is concerned with the development of new compressive sensing (CS) techniques both in element space and beamspace for estimating the direction of arrival of various types of sources, including moving sources as well as fluctuating sources, using one-dimensional antenna arrays. The problem of estimating the angle of arrival of a plane electromagnetic wave is referred to as the direction of arrival (DOA) estimation problem. Such algorithms for estimating DOA in antenna arrays are often used in wireless communication network to increase their capacity and throughput. DOA techniques can be used to design and adapt the directivity of the array antennas. For example, an antenna array can be designed to detect a number of incoming signals and accept signals from certain directions only, while rejecting signals that are declared as interference. This spatio-temporal estimation and filtering capability can be exploited for multiplexing co-channel users and rejecting harmful co-channel interference that may occur because of jamming or multipath effects.

In this study, three CS-based DOA estimation methods are proposed, one in the element space (ES), and the other two in the beamspace (BS). The proposed techniques do not require *a priori* knowledge of the number of sources to be estimated. Further, all these techniques are capable of handling both non-fluctuating and fluctuating source signals as well as moving signals. The virtual array concept is utilized

in order to be able to identify more number of sources than the number of the sensors used.

In element space, an extended version of the least absolute shrinkage and selection operator (LASSO) algorithm, the adaptable LASSO (A-LASSO), is presented. A-LASSO is utilized to solve the DOA problem in compressive sensing framework. It is shown through extensive simulations that the proposed algorithm outperforms the classical DOA estimation techniques as well as LASSO using a small number of snapshots. Furthermore, it is able to estimate coherent as well as spatially-close sources. This technique is then extended to the case of DOA estimation of the sources in unknown noise fields.

In beamspace, two compressive sensing techniques are proposed for DOA estimation, one in full beamspace and the other in multiple beam beamspace. Both these techniques are able to estimate correlated source signals as well as spatially-close sources using a small number of snapshots. Furthermore, it is shown that the computational complexity of the two beamspace-based techniques is much less than that of the element-space based technique. It is shown through simulations that the performance of the DOA estimation techniques in multiple beam beamspace is superior to that of the other two techniques proposed in this thesis, in addition to having the lowest computational complexity.

Finally, the feasibility for real-time implementation of the proposed CS-based DOA estimation techniques, both in the element-space and the beamspace, is examined. It is shown that the execution time of the proposed algorithms on Raspberry Pi board are compatible for real-time implementation.

To my parents,

to my sister and brother

to my wife and my son

for their love and sacrifice

ACKNOWLEDGEMENTS

My years as a Ph.D. student at Concordia University have been one of the most defining moments of my life, during which I grew intellectually and professionally. I would like to thank many who have contributed in more than one way to this journey.

First of all, I have been most fortunate to have Prof. M. Omair Ahmad and Prof. M.N.S. Swamy as my supervisors. They have inspired me to put my utmost on creativity and originality. They have provided me with invaluable support and encouragement. Without their immense knowledge, experience and supervision, this thesis would not have been possible. I am deeply indebted to them for giving me the freedom to pursue my ideas in research and providing unconditional support at every stage. I feel fortunate to work closely with two exceptional and brilliant supervisors, who have different expertise, style and interest.

Thanks to all my committee members: Prof. Wei-Ping Zhu, Prof. Yousef R. Shayan, and Prof. T. Fancott for their helpful comments during all my entire PhD program; their comments helped me really to achieve the final version of my thesis. In particular, I would like to thank Dr. Zhu for his words of encouragement and suggestions. I also learned a lot from him during my first semester from the DSP course that was taught by him. I would like to thank Dr. Shayan for his valuable comments in my comprehensive exam, thesis proposal, and seminar presentations. Also, I would like to Dr. Fancott for his inspiring words and comments.

As a past graduate student in our lab, Mohamed Naiel has been a great friend and almost a brother to me. I greatly value our conversations on various topics ranging from academic topics to life in general.

My deepest gratitude and appreciation go to my parents, my mother and my father, who have always encouraged me to move forward in my academic pursuits

and who were beside me with their hearts day after day to complete this work. I am very grateful for their prayers and support in my entire life. It is hard to find words to describe what they have contributed to my upbringing and what I am today. My deepest gratitude extends to my sister and brother for their support and goodwill.

Last but not least, I am so blessed to have an outstanding wife. Her support, encouragement, quiet patience and unwavering love were undeniably the bedrock upon which the past five years of my life have been built. Her tolerance to my occasional inability to look after my family responsibility fully is in itself a testimony of her unyielding love and devotion. I cherish and adore my son, Fares, for being the ultimate reason for finishing this thesis.

TABLE OF CONTENTS

List of Figures

List of Tables

List of Abbreviations

A-LASSO	**A**daptable **LASSO**
ACM	**A**ugmented **C**ovariance **M**atrix
AOA	**A**ngles **O**f **A**rrival
AWGN	**A**dditaive **W**hite **G**aussian **N**oise
BF	**B**eam**F**orming
BS	**B**eam-**S**pace
CBF	**C**onventional **B**eam**F**orming
CCD	**C**anonical **C**orrelation **D**ecomposition
CRB	**C**ramer-**R**ao **B**ound
CS	**C**ompressive **S**ensing
CV	**C**ross-**V**alidation
DOA	**D**irection **O**f **A**rival
DOF	**D**egrees **O**f **F**reedom
DP	**D**iscrepancy **P**rinciple
ES	**E**lement-**S**pace
FB	**F**orward-**B**ackward
FBS	**F**ull-dimension **B**eam-Space
GC	**G**eneralized **C**orrelation
GCD	**G**eneralized **C**orrelation **D**ecomposition
GCV	**G**eneralized **C**ross-**V**alidation
IoT	**I**nternet **O**f **T**hings
IP	**I**nternet **P**rotocol
KR	**K**hatri-**R**ao
LA	**L**inear **A**rray

LARS	**L**east **A**ngle **R**egression
LASSO	**L**east **A**bsolute **S**hrinkage and **S**election **O**perator
LS	**L**east **S**quare
MBS	**M**ultiple-Beam **B**eam**S**pace
ML	**M**aximum **L**ikelihood
MRA	**M**inimum **R**edundancy **A**rray
MUSIC	**MU**ltiple **S**ignal **C**lassification
MVDR	**M**inimum **V**ariance **D**istortionless **R**esponse
NLA	**N**on-Uniform **L**inear **A**rray
OLS	**O**rdinary **L**east **S**quares
POD	**P**robability **O**f **D**etection
RBS	**R**educed-Dimension **B**eam-**S**pace
RMSE	**R**oot **M**ean **S**quare **E**rror
SDPT3	**S**emi-**D**efinite Quadratic-Linear **P**rogramming
SLA	**S**parse **L**inear **A**rray
SLR	**S**ide**L**obe **R**atio
SNR	**S**ignal-to-**N**oise **R**atio
SS	**S**patially-**S**moothed
SVD	**S**ingular **V**alue **D**ecomposition
ULA	**U**niform **L**inear **A**rray
UN-MUSIC	**U**nknown **N**oise - **MUSIC**
UN	**U**known **N**oise
VA	**V**irtual **A**rray

List of Symbols

L	The number of source signals
M	The number of sensors
$\bar{M}$	The number of sensors of the virtual array
d	The inter-elements spacing
θ	The angle of arrival
k_o	The wavenumber
$\mathbf{a}$	The array steering vector
$\bar{\mathbf{a}}$	The overcomplete array steering vector
$\mathbf{x}$	The sensor array output
$\mathbf{s}$	The source signals vector
$\bar{\mathbf{s}}$	The overcomplete source signals vector
$\mathbf{A}$	The array steering matrix
$\bar{\mathbf{A}}$	The overcomplete array steering matrix
$\mathbf{n}$	The noise vector
$\bar{\mathbf{n}}$	The overcomplete noise vector
$\mathbf{y}_{bs}$	The beamspace array output
K	The number of snapshots
$\mathbf{w}$	The weight vector
$\mathbf{R}_{xx}$	The antenna array covariance matrix
$\mathbf{r}_q$	The qth column of the antenna array covariance matrix
$\mathbf{R}_{ss}$	The covariance matrix of the received signals
$\mathbf{B}$	The beamspace transformation matrix
λ	The wavelength of the propagating waves
σ_l	The lth source power

σ_n	The noise power
Ω	The set of all possible source locations
Φ	The overcomplete sensing matrix
Φ_{bs}	The beamspace overcomplete sensing matrix
τ	The regularization parameter

Chapter 1

Introduction

The ability to transmit and/or receive information without a physical connection between two locations is very attractive in many applications. Information can be delivered via electromagnetic, sonar, acoustic, or seismic waves. As the applications are becoming more complicated, they require processing of more signals and more data as well as very robust processing systems, which are beyond the capability of single sensor communication system.

A sensor array consists of a number of sensors arranged in a particular configuration. For many years, systems with multiple sensors have been used to receive or send signals through a wireless channel [1]. Sensor array systems have several advantages over single sensor systems. First, they can increase the signal-to-noise ratio (SNR) of a single sensor system M times, where M is the number of sensors, by appropriate processing of the received signals. Second, sensor arrays can steer the transmitting or receiving beams and by doing that, they can separate multiple signals [2]. This is very useful in applications such as multi-user wireless communications, which require the processing of as many signals as possible without mutual interference, or passive radar applications which need to localize signal source locations.

Array signal processing is important for many applications, such as sonar [3], radar [4], seismology [5] and radio astronomy [6]. The direction of arrival (DOA) estimation problem has been studied extensively over the past decades [7]. DOA estimation deals with the problem of determining the number and identifying the locations of multiple source signals using a sensor array. With the development of antenna arrays, DOA estimation technique has become a vital part of a smart antenna which is focused on radio direction finding, that is, estimating the direction of electromagnetic waves impinging on one or more sensors. We can classify the estimation techniques into two main categories, namely parametric and spectral-based approaches [8]. Parametric techniques make a simultaneous search for all the parameters of interest at the expense of an increased computational complexity, and these approaches often lead to more accurate outcomes. Spectral-based approaches form some spectrum-like function of the parameters of interest, and the locations of the highest peaks of the function are regarded as the DOA estimates.

Sparsity is a fundamental attribute which characterizes many signals, natural and man-made. The sparsity in signals can be observed either in the original domain, or in a transformed domain. The particular transformation under which a signal exhibits sparsity often depends on the specific application of interest. A wide variety of signals and measurements can have a natural sparse representation. Examples include images and videos, spatio-temporal spectrum of data collected by radar and sonar systems and anomalies and outliers in data used in statistical regression and inference.

1.1 A Brief Literature Review

DOA estimation has been a problem of intense research, and various algorithms have been proposed [9, 10, 11, 12]. Spectral approaches, which largely operate on

the covariance matrix and compute spectrum-like functions for the DOA estimation have been investigated. The spectral estimation method, first proposed by Bartlett [13], consists of estimating the DOA by computing the spatial spectrum and deciding the local maximum. The DOA schemes can be classified as beamforming (BF), subspace-based and maximum likelihood methods. Multiple signal classification (MUSIC) method is a well-known sub-spaced method that estimates the DOA content of a source signal using an eigenspace method proposed by Schmidt [14]. ESPRIT algorithm is another subspace-based technique [15, 16, 17] that reduces the computational and storage requirements of MUSIC, since it does not search through all the possible steering vectors to estimate DOA. However, ESPRIT suffers from the pairing problem.

Their extensions, such as root-MUSIC [18] and parallel factor analysis [19], have been proposed for the DOA estimation problem. However, these techniques require the number of sources to be known in advance and if the exact number of source signals is unknown, complete disappearance of some of the sources may happen. Furthermore, the eigenvalue decomposition-based techniques suffer from a high degradation of performance in low SNR scenarios. In such a case, the signal subspace is dominated by a high level of noise. In addition, these methods assume the source signals to be un-correlated with one another or with the noise and that a sufficient number of snapshots is available.

On the other hand, maximum likelihood methods are the most accurate DOA estimation techniques. However, they are the most time consuming ones among all the proposed DOA estimation methods. Here again, the number of source signals to be estimated is assumed to be known in advance.

It should be noted that most of the modern approaches to signal processing (including the above mentioned techniques) are model-based in the sense that they rely on certain assumptions on the data observed and these assumptions may not

hold in practice [10, 11, 12, 20, 21, 22, 23, 24, 25]. Furthermore, the number of source signals that can be detected is upper bounded by the number of actual physical sensors used in the array. We can identify only up to $(M-1)$ source signals using a sensor array containing M sensors.

The concept of a difference co-array has been investigated to extend virtually the array aperture, so that more source signals can be resolved beyond the number of the physical sensors available [26]. The co-array concept has been employed for specific array geometries in [26, 27]. In [28, 29], it was shown that by using minimum redundancy array (MRA) [30] and an augmented covariance matrix (ACM), the number of degrees of freedom can be increased.

However, the augmented ACM is not positive semidefinite for a finite number of snapshots and this violates the condition for being a covariance matrix. In [28], the proposed spatially smoothed matrix is guaranteed to be positive semidefinite for any finite number of snapshots. A transformation of the augmented matrix into a suitable positive definite Toeplitz matrix was suggested and an elaborate algorithm was provided to construct this matrix in [31, 32].

However, there are problems in this approach. First, there is no closed form expression for either the array geometry or the achievable degrees of freedom for a given sensor array containing M elements using MRAs. Second, the optimum design of MRAs is not an easy task. Furthermore, they are based on computer simulations or complicated algorithms for sensor placement [1, 33, 34, 35, 36]. Also, the algorithm for finding a suitable covariance matrix corresponding to a long array is iterative and complicated [31, 32].

Higher order cumulants was suggested to completely remove the Gaussian noise term and to yield better a DOA estimation in [37]. It was shown that using fourth order cumulants, a significant increase in the number of degrees of freedom can be achieved [38, 39, 40]. But one deficiency of this method is that it is restricted

to non-Gaussian sources.

In [41], using the concept of Khatri-Rao (KR) product and assuming quasi-stationary sources, it has been shown that one can identify upto $(2M-1)$ sources using a ULA of M elements. Unfortunately, this method imposes a constraint on the source signals in that they cannot be stationary signals. An active sensing technique was proposed in [42] to increase the degrees of freedom. Unfortunately, this method requires active sensing and passive sensing cannot be employed. Unlike the MRAs used in [28, 31, 32], the nested arrays [43] are easy to construct and an exact closed form expression for the virtual sensor locations and degrees of freedom for a given array of M sensors, can be easily determined.

In recent years, compressive sensing (CS) has evolved rapidly and has found multiple applications in various fields, such as ultrasound [44] and medical imaging [45], and radar detection [46]. Unlike the previously mentioned DOA estimation techniques, CS-based DOA estimation methods are able to identify the sources using a fewer number of snapshots. Furthermore, they can deal with both non-correlated and correlated sources without any preprocessing. Malioutov et al. [47] presented a CS-based DOA estimation technique using a single snapshot and extended it for multiple snapshots based on the singular value decomposition (SVD). However, since it is a SVD-based method, the number of sources is required to be known in advance and the performance gets highly degraded in low and very low SNR situations. In [48], a DOA estimation technique based on a sparse representation of array covariance vectors is proposed, but the computational complexity is extremely high. Xenaki et al. [49] studied the DOA estimation using CS with coherent arrivals, single-snapshot data and different array geometries. It has been shown in [49] that CS does not require the arrivals to be non-coherent.

The least absolute shrinkage and selection operator (LASSO) [50] minimizes

the residual sum of squares (subject to the sum of the absolute values of the coefficients being less than a constant) and it is popular for solving CS problems. Zou [51] proposed a new version of LASSO, whereby adaptable weights are used for penalizing different coefficients in the ℓ_1 penalty function. Panahi *et al.* [52] discussed the resolution of the LASSO-based DOA estimation; it has been shown that the LASSO-based DOA estimation is better than that of the traditional beamforming techniques.

1.2 Motivation

DOA estimation constitutes a major problem of interest in sensor array signal processing. With the development of antenna arrays, the DOA estimation technique has become a vital part of a smart antenna which is focused on radio direction finding, that is, estimating the direction of electromagnetic waves impinging on one or more sensors. We can classify the estimation techniques into two main categories, namely element-space (ES)-based and beam-space (BS)-based techniques.

In ES-based methods, the output of each element of the array is processed at the same time. BS-processing is utilized to reduce the dimensions of the the observation vector of the sensor array by projecting the received data into a subspace of lower dimension to produce BS data.

All the known classical methods as well as subspace methods and maximum likelihood techniques belong to the first category [8]. Classical methods make a simultaneous search for all the parameters of interest at the expense of an increased computational complexity, and these approaches often lead to more accurate outcomes. Yet, classical methods suffer from low resolution. Subspace-based methods depend on the orthogonality between the signal and the noise subspaces. Singular value decomposition is used to separate the signal subspace from the noise subspace,

by assigning the higher eignvalues to the signal subspace and lower eignvalues to the noise subspace. Maximum likelihood techniques are very time consuming and computationally complex among all the DOA techniques. However, they lead to more accurate results.

A fundamental aim of signal processing is to extract essential information from a set of measurements or observations. Most of the DOA estimation models have an overdetermined structure (the number of source signals to be estimated, L, is smaller than the number of sensor array elements, M). A few DOA estimation problems have considered a data model which is underdetermined ($L > M$). Recently, studying underdetermined systems by imposing sparsity on the unknown variables has become one of the important research areas.

Compressive sensing (CS) plays a significant role wherein the data models are underdetermined, and has found numerous applications such as in image and video processing, radar, channel estimation, multivariate regression, sparse Bayesian estimation, sub-Nyquist sampling of multiband signals, and monitoring and inferring from networked data. Furthermore, CS has given us the opportunity of performing DOA estimation using reduced number of observations. CS-based DOA estimation can be done using a single snapshot, which automatically result in an underdetermined problem.

Recently, the word Internet of Things (IoT) has become an important phrase in our world. IoT is not another Internet, rather it is a network of devices that are connected to the Internet and used every day to search Google, upload images and connect with friends. It's a network of products that are connected to the web, thus, they have their private Internet protocol (IP) addresses and can connect to one another to automate simple tasks.

In general, IoT promotes an elevated level of awareness about our world and a platform from which to monitor the reactions to the changing conditions. IoT

will play an important role in natural disaster management, intelligent urban management, and better health care systems. Sensor arrays are required to be small enough so that they will be compatible with IoT and machine-to-machine (M2M) applications. Simultaneously, it is expected from IoT compatible devices to be able to communicate with a large number of devices and this requires virtually extended sensor arrays. Furthermore, the DOA estimation techniques are required to be as fast as possible in order to adapt for the mobility of the connected devices.

1.3 Thesis Objectives

Based on the above motivation, it is important to design sensor array processing schemes that are capable of estimating DOA of sources that may be correlated or closely-spaced in low and very low SNR condition, and processing sources that are more in number than the number of physical sensors used. Furthermore, the DOA estimation techniques should be applicable for real-time applications. Hence, a fewer number of snapshots is required for processing and the DOA algorithms are required to have low computational complexity. It is important that the estimation methods work without an advanced knowledge of the total number of sources to be estimated or of the nature of the source signals. In other words, a blind DOA estimation technique is needed.

DOA estimation techniques assume that the noise is an additive white Gaussian noise (AWGN). In practical applications, the noise field structure is not known. Hence, it is required that the DOA estimation technique be able to perform the estimation even in the presence of unknown noise fields. Moreover, due to the crowded environment, multipath propagation is an ordinary phenomenon in any communication channel. As a result, the amplitude of the source signals is no longer constant and the sources are fluctuating. This may cause a failure in the identification and

tracking of the source signals. DOA estimation techniques that are capable of handling such problems are required, especially for mobile communication systems.

The objective of this thesis is to develop new compressive sensing based schemes, both in element-space and beamspace, capable of identifying correlated and closely-spaced sources under low and very low SNR conditions and yielding a performance superior to that of the existing schemes. The proposed techniques are aimed at employing as few snapshots as possible for the DOA estimation so as to make them suitable for real-time applications.

1.4 Thesis Organization

The thesis is organized as follows.

In Chapter 2, background material necessary for the understanding and development of the research work undertaken in this thesis is presented.

In Chapter 3, a new iterative element-space compressive sensing-based technique for DOA estimation under low and very low SNR conditions is proposed. A weighted version of the least absolute shrinkage and selection operator (LASSO), the adaptable LASSO (A-LASSO), is presented. Two different initial weights are utilized for A-LASSO, namely, the ordinary least square (OLS) and the minimum variance distortionless response (MVDR) beamformer, resulting in OLS A-LASSO and MVDR A-LASSO algorithms, respectively. Extensive simulations are carried out both for non-fluctuating and fluctuating source signals. The performance of the proposed A-LASSO is investigated and compared to that of the classical DOA estimation techniques as well as that of LASSO.

In Chapter 4, a new compressive sensing-based DOA estimation technique based on the generalized correlation decomposition (GCD) technique is presented to identify source signals in unknown noise fields. As in the A-LASSO technique,

two initial weights are utilized for this DOA estimation as well. The performance of the proposed technique is extensively investigated using different noise mixtures.

In Chapter 5, the performance of the existing beamspace techniques is compared with that of the element-space based technique proposed in Chapter 3 in order to provide motivation for developing beamspace techniques for DOA estimation. Then, two new beamspace compressive sensing-based DOA estimation techniques are introduced. The full beamspace is used for the first one whereas multiple beam beamspace for the second one. The performance of the proposed beamspace-based techniques is compared with that of the element-space based technique developed in Chapter 3 using both non-fluctuating and fluctuating source signals. The capability of the proposed beamspace techniques to detect stationary and moving sources even when their trajectories intersect is studied. The computational complexity for each of the proposed techniques is also presented.

In Chapter 6, a study is conducted for the feasibility of real-time implementation of the DOA techniques proposed in this work.

Finally, some concluding remarks highlighting the contributions of the thesis and some suggestions for future work based on the schemes developed in this thesis are provided in Chapter 7.

Chapter 2

Background Material

In this chapter, we provide the necessary background material for understanding of the techniques proposed in this thesis for the direction of arrival estimation in element-space as well as beamspace. In addition, some of the mathematical tools necessary for such estimation are also presented.

2.1 Sensor Array

A sensor array consists of a number of transducers or sensors arranged in a particular configuration. Each transducer converts an electromagnetic wave into a voltage and visa-versa. For many years, systems with multiple sensors have been used to receive or send signals through a wireless channel [1]. Sensor array systems have several advantages over single sensor systems. First, they can increase the SNR up to M times that of a single sensor by appropriately processing the received signals. Second, sensor arrays can steer the transmitting or receiving beams and by doing so, they can separate multiple signals [2]. This is very useful in applications such as multi-user wireless communications which require the processing of as many signals as possible without mutual interference, or passive radar applications which need to localize signal source locations.

2.1.1 Basics of Antenna Array

An antenna array is a group of antennas used for transmitting or receiving signals. Each individual antenna is often called an array element. In a receive array, the signals received by the various array elements are combined and then processed for various applications, including DOA estimation [2, 11, 12, 53].

For illustration purposes, let us consider a three-element uniform linear array

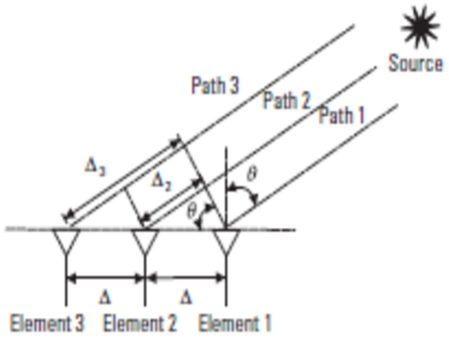

Figure 2.1: Simple Antenna Array Configuration [11]

(ULA), wherein the elements are aligned uniformly along a line as shown in Figure 2.1. The waves impinge on the array at an angle of θ. As a result, the line paths from the source to elements 2 and 3 are longer than the path to element 1 (reference element) by the extra distance of

$$\triangle_m = (m-1)\triangle . \sin\theta \qquad m = 1, 2, 3 \tag{2.1}$$

Now assume that the wave signal received by the reference element (i.e., element 1) is

$$x_1(t) = s(t) \tag{2.2}$$

without taking into account the atmospheric noise. Then the signals received by elements 2 and 3 can be written as:

$$\begin{aligned} x_2(t) &= s(t)e^{-j\beta\triangle_2} = s(t)e^{-j\frac{2\pi\triangle}{\lambda}\sin\theta} \\ x_3(t) &= s(t)e^{-j\beta\triangle_3} = s(t)e^{-j2\frac{2\pi\triangle}{\lambda}\sin\theta} \end{aligned} \tag{2.3}$$

respectively, where $k_o = \beta = \frac{2\pi}{\lambda}$ is the phase shift constant of the wave propagating in air, λ being the wavelength. The phase shift term $e^{-j\beta\triangle_m}$ is the result of the signal propagating over an extra distance $\triangle_m$ in comparison with the path to the first element[2].

In a more generalized way, the signals received by the three elements can be written as:

$$\mathbf{x} = \begin{bmatrix} x_1(t) \\ x_2(t) \\ x_3(t) \end{bmatrix} = \begin{bmatrix} 1 \\ e^{-j\frac{2\pi\triangle}{\lambda}\sin\theta} \\ e^{-j2\frac{2\pi\triangle}{\lambda}\sin\theta} \end{bmatrix} s(t) = \begin{bmatrix} 1 \\ e^{j\mu} \\ e^{-j2\mu} \end{bmatrix} s(t) = \mathbf{a}(\mu)s(t) \tag{2.4}$$

where $\mu = \frac{2\pi\triangle}{\lambda}sin\theta$ and $\mathbf{a}(\mu) = \begin{bmatrix} 1 & e^{j\mu} & e^{-j2\mu} \end{bmatrix}^T$ which is often called the array steering vector.

Even though a non-uniform linear array, which is an array wherein the spacing between neighboring elements is not the same, has certain advantages such as a lager aperture for the same number of sensors and is more suitable for actual installation, it cannot be used for many of the DOA estimation algorithms such as MUSIC [14] and ESPRIT [16] because of the manifold ambiguity problem. Therefore, in this section we will consider the simplest array, namely, ULA.

Consider a ULA as shown in Figure 2.2. Let a plane wave signal generated

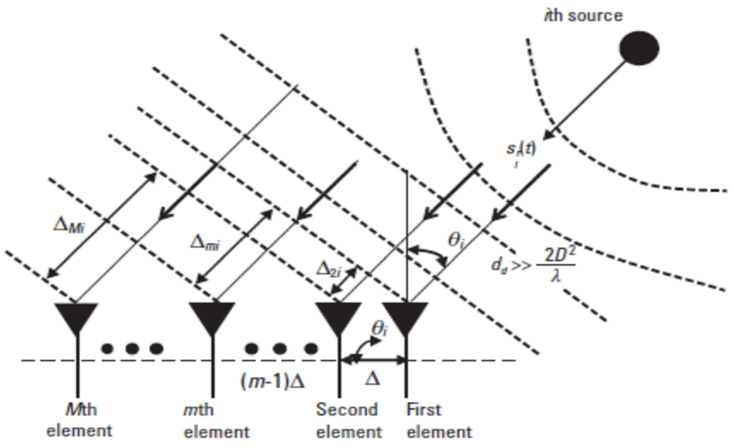

Figure 2.2: Data model for DOA using ULA [11]

by source i impinge on the array at an angle θ_i and the signal generated by source i is a narrowband signal $s_i^r(t)$; it then travels over a distance of d_d at a speed of c and reaches the first (rightmost) element. In other words, the signal received by the rightmost element is the delayed version of the $s_i^r(t)$ with a delay of $\tau_d = \frac{d_d}{c}$. That is

$$s_{i1} = s_i^r(t - \tau_d) = \alpha_i(t - \tau_d)\cos[2\pi f_c(t - \tau_d) + \beta(t - \tau_d)] = \mathrm{Re}\{s_i(t)\} \tag{2.5}$$

and in phasor form, Equation (2.5) can be written as

$$s_{i1} = \alpha_i(t - \tau_d)e^{[2\pi f_c t + \beta_i(t-\tau_d) + 2\pi f_c \tau_d]} \tag{2.6}$$

Since the array elements in a ULA are situated on a line, the signal traveling to the mth element has to travel an extra distance in comparison with the signal arriving at the rightmost element. This extra distance is given by:

$$\triangle_{mi} = (m-1)\triangle \sin\theta_i \qquad m = 1, 2, ..., M \tag{2.7}$$

Therefore, the signal arriving at the mth element will have an additional delay,

which is equal to:

$$\tau_{mi} = \frac{\triangle_{mi}}{c} = (m-1)\frac{\triangle \sin\theta_i}{c} \tag{2.8}$$

The signal received by the mth element is then the delayed version of the signal $s_{i1}(t)$ (which is received by the first element) with the additional delay of τ_{mi}:

$$\begin{aligned} s_{im}(t) &= s_{i1}(t-\tau_{mi}) = s_i^r(t-\tau_d-\tau_{mi}) \\ &= \alpha_i(t-\tau_d-\tau_{mi})\cos[2\pi f_c(t-\tau_d-\tau_{mi})+\beta(t-\tau_d-\tau_{mi})] \\ &\approx \alpha_i(t-\tau_d)\cos[2\pi f_c(t-\tau_d)+\beta_i(t-\tau_d)-(m-1)\mu_i] \\ &= \mathrm{Re}\{s_i(t)e^{j(m-1)\mu_i}\} \end{aligned} \tag{2.9}$$

where $\mu_i = -\frac{2\pi f_c}{c}\triangle \sin\theta_i = -\frac{2\pi}{\lambda}\triangle \sin\theta_i$, called the spatial frequency that is associated with the ith source that generates the signal with an incident angle θ_i, and $\lambda = \frac{c}{f_c}$ denotes the wavelength corresponding to the carrier frequency f_c.
In complex phasor form, Equation (2.9) can be written as:

$$\begin{aligned} s_{im}(t) &\approx \alpha_i(t-\tau_d)e^{j[2\pi f_c(t-\tau_d)+\beta_i(t)]}e^{j(m-1)\mu_i} \\ &= s_i(t)e^{j(m-1)\mu_i} \end{aligned} \tag{2.10}$$

Equation (2.10) shows that the signal received by the mth element from the ith source is the same as that received by the first (rightmost) element, but with an additional phase shift factor of $e^{j(m-1)\mu_i}$. This factor is dependent only on the spatial frequency μ_i and the position of the element relative to the first element.
For each incident angle θ_i that determines a source, there is a corresponding spatial frequency μ_i. Therefore, the whole objective of estimating a DOA is to extract this spatial frequency μ_i from the signals received by the array.

Now consider all the signals generated by all the d sources, $s_i(t)$, $1 \le i \le d$. Then the overall signal and noises received by the mth element at time t can be

expressed as:

$$\begin{aligned}\mathbf{x}_m(t) &= \sum_{i=1}^{d} s_i(t) + n_m(t) \\ &= \sum_{i=1}^{d} s_i(t) e^{j(m-1)\mu_i} + n_m(t) \\ &= s_i(t) \sum_{i=1}^{d} e^{j(m-1)\mu_i} + n_m(t) \qquad m = 1, 2, ..., M\end{aligned} \tag{2.11}$$

In matrix form, (2.11) can be written as:

$$\mathbf{x}(t) = \begin{bmatrix} a(\mu_1) & a(\mu_2) & ... & a(\mu_d) \end{bmatrix} \begin{bmatrix} s_1(t) \\ s_2(t) \\ \vdots \\ s_d(t) \end{bmatrix} + n(t) = \mathbf{A}\mathbf{s}(t) + \mathbf{n}(t) \tag{2.12}$$

where $\mathbf{x}(t) = \begin{bmatrix} x_1(t) & x_2(t) & ... & x_M(t) \end{bmatrix}^T$ is the data column vector received by the array, $\mathbf{s}(t) = \begin{bmatrix} s_1(t) & s_2(t) & ... & s_M(t) \end{bmatrix}^T$ is the signal column vector and $\mathbf{n}(t) = [n_1(t)$ $n_2(t)$ $\ldots n_M(t)]^T$ is a zero-mean spatially uncorrelated additive noise with spatial covariance matrix equal to $\sigma_N^2 I_M$.

The array steering column vector $a(\mu_i)$ is defined as:

$$\mathbf{a}(\mu_i) = \begin{bmatrix} 1 & e^{j\mu_i} & e^{j2\mu_i} & ... & e^{j(M-1)\mu_i} \end{bmatrix}^T \tag{2.13}$$

It is a function of the unknown spatial frequencies μ_i; these steering vectors form

the columns of the $M \times d$ steering matrix $\mathbf{A}$:

$$\begin{aligned}\mathbf{A} &= \begin{bmatrix}\mathbf{a}(\mu_1) & \dots & \mathbf{a}(\mu_i) & \dots & \mathbf{a}(\mu_d)\end{bmatrix} \\ &= \begin{bmatrix} 1 & 1 & \dots & 1 \\ e^{j\mu_1} & e^{j\mu_2} & \dots & e^{j\mu_d} \\ \vdots & \vdots & \ddots & \vdots \\ e^{j(M-1)\mu_1} & e^{j(M-1)\mu_2} & \dots & e^{j(M-1)\mu_d} \end{bmatrix}\end{aligned} \tag{2.14}$$

Depending upon the different configurations of the antenna array, different array steering matrices can be formed. However, using one-dimensional arrays, we can only estimate one source signal parameter, which is the elevation angle, θ.

2.2 Models for Fluctuating Source Signals

It is to be noted that most of DOA estimation techniques that have been studied in the literature [7, 47, 48, 54, 55, 56, 57, 58, 59, 60, 61] (and the references therein), assume that the source signals are non-fluctuating, which is unlikely in practice.

The propagation channel in urban environments contains multiple objects which randomly scatter the energy of the sources, and multiple replicas of the source signals reach the receiver [62, 63, 64, 65]. Swerling models have been proposed to describe the statistical properties of the fluctuating source signals [66, 67]. Swerling models can be classified as follows [67]:

- Swerling Case I: It is assumed that the power of the various snapshots of the signal source is constant within a single scan, but fluctuates from scan-to-scan. The signal source power varies from scan to scan according to a Chi-squared probability density function with two degrees of freedom.

- Swerling Case II: It is assumed that the fluctuations in the signal power are

independent from snapshot-to-snapshot in each scan and follows a Chi-squared distribution with two degrees of freedom.

- Swerling Case III: This is similar to case I, except that the Chi-squared distribution has 4 degrees of freedom.

- Swerling Case IV: This is similar to case II, except that the Chi-squared distribution has 4 degrees of freedom.

Denote by $s_i, i = 1, \ldots, N$, the individual snapshots, where N is the total number of snapshots, and let

$$\mathbf{s} = \sum_{i=1}^{N} s_i \tag{2.15}$$

For a fluctuating source signal, s_i and $\mathbf{s}$ are random variables; the probability density function of the integrator output is determined by the probability distribution of $\mathbf{s}$, which is determined using the joint probability distribution of $s_1, \ldots, s_N$ [68]. If $s_i, i = 1, \ldots, N$ have a chi-square distribution, the fluctuations are called wide-sense chi-square. In this case, the probability density functions of s_i is denoted by

$$w_k(s_i, \bar{s}_i) = \frac{1}{(k-1)!} \frac{k}{\bar{s}_i} \left(\frac{k s_i}{\bar{s}_i} \right) \exp\left(\frac{-k s_i}{\overline{s} \bar{s}_i} \right) \tag{2.16}$$

where w_k is the probability density function, $\bar{s}_i$ is the mean of s_i and $2k$ is the number of degrees of freedom of s_i. Table 2.1 gives the values of k corresponding to each case of the Swerling models [67]. The χ^2 probability density function distributions for $k = 1$ and $k = 2$ are shown in Figure 2.3.

Table 2.1: Various values of k corresponding to the different Swerling models

Fluctuating Source Signal Model	Value of k
Swerling Case I	1
Swerling Case II	1
Swerling Case III	2
Swerling Case IV	2

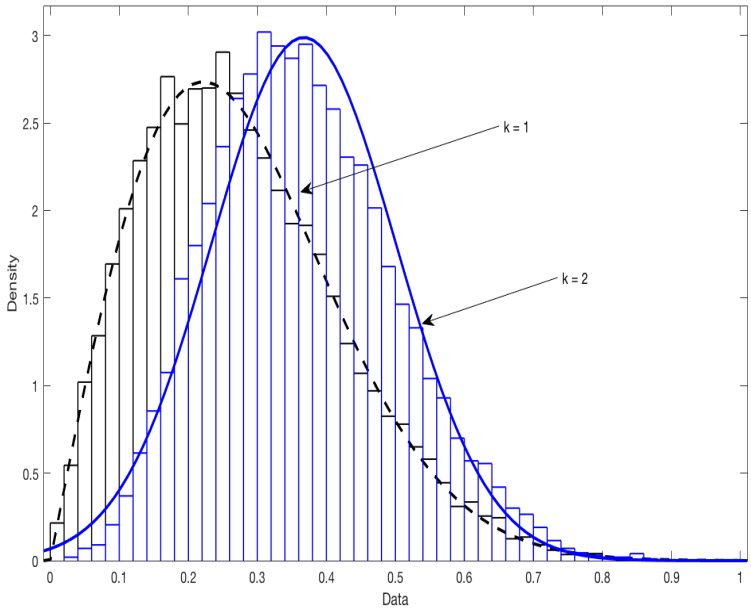

Figure 2.3: Chi-square probability density function for different values of k.

2.3 Beamforming

The basic idea behind BF techniques is to "steer" the array in one direction at a time and measure the output power. When the "steered" direction coincides with DOA of a signal, the maximum output power will be observed [11]. Given the knowledge of the array steering vector, an array can be steered electronically just as a fixed antenna can be steered mechanically. A weight vector $\mathbf{w}$ can be designed and then

used to linearly combine the data received by the array elements to form a single output signal $\mathbf{y}(t)$ [2, 11, 12],

$$\mathbf{y}(t) = \mathbf{w}^H \mathbf{x}(t) \tag{2.17}$$

The total average output power out of an array over K snapshots can be expressed as [2, 11, 12]

$$\begin{aligned} \mathbf{P}(w) &= \frac{1}{K} \sum_{k=1}^{K} \mid \mathbf{y}(t_k) \mid^2 \\ &= \mathbf{w}^H \mathbf{R}_{xx} \mathbf{w} \end{aligned} \tag{2.18}$$

2.3.1 Conventional Beamforming

In conventional beamforming (CBF), $\mathbf{w} = \mathbf{a}(\theta)$, θ being a scanning angle that is scanned over the angular region of interest. For example, for a ULA of M elements, $\mathbf{w} = \mathbf{a}(\theta)$ is defined similar to the way a steering vector is defined, but with an arbitrary scanning angle θ:

$$\mathbf{a}(\theta) = \begin{bmatrix} 1 & e^{j\mu} & e^{j2\mu} & \dots & e^{j(M-1)\mu} \end{bmatrix}^T \tag{2.19}$$

with $\mu = -\frac{2\pi f_c}{c} \triangle \sin\theta = -\frac{2\pi}{\lambda} \triangle \sin\theta$.

For each look or scanned direction θ, the average power output $\mathbf{P}(\theta)$ of the steered array is then measured or computed using Equation (2.18).

It can be shown that when $\theta = \theta_i$, the impinging angle of the signal from source i, the output power $\mathbf{P}(\theta)$ will reach a peak or maximum value. At this moment, $\mathbf{w} = \mathbf{a}(\theta$ - $\theta_i)$ aligns the phases of the signal components received by all the elements of the array, causing them to add constructively and produce maximum power.

In practical computations, $\mathbf{w} = \mathbf{a}(\theta)$ is normalized as [11, 12]

$$\mathbf{w} = \mathbf{w}_{CON} = \frac{\mathbf{a}(\theta)}{\sqrt{\mathbf{a}^H(\theta)\mathbf{a}(\theta)}} \tag{2.20}$$

By inserting the weight vector Equation (2.20) into Equation (2.18), the output power as a function of the angle of arrival, termed as spatial spectrum, is obtained as [11, 12]

$$\mathbf{P}(\theta) = \mathbf{P}_{CON}(\theta) = \frac{\mathbf{a}^H(\theta)\hat{\mathbf{R}}_{xx}\mathbf{a}(\theta)}{\mathbf{a}^H(\theta)\mathbf{a}(\theta)} \tag{2.21}$$

The weight vector in Equation (2.20) can be interpreted as a spatial filter. It is matched to the impinging spatial angles of the incoming signal to produce a peak, but it attenuates the output power for signals not coming from the angles of the incoming signals. Intuitively, it equalizes the different signal delays experienced by the array elements and maximally combines their respective contributions to form a peak in the output power at the angles of the incoming signals.

2.3.2 Capon's Beamformer

In Capon's method, the degrees of freedom used to form a beam in the look direction and at the same time null the other directions in order to reject other signals. For a particular look direction, Capon's method uses all but one of the degrees of freedom to minimize the array output power while using the remaining degrees of freedom to constrain the gain in the look direction to be unity [11, 12]:

$$\min \mathbf{P}(\mathbf{w}) \text{ subject to } \mathbf{w}^H\mathbf{a}(\theta) = 1 \tag{2.22}$$

The weight vector chosen in this way is often referred to as the MVDR beamformer. The vector is given by [11, 12]

$$\mathbf{w} = \mathbf{w}_{CAP} = \frac{\hat{\mathbf{R}}_{xx}^{-1}\mathbf{a}(\theta)}{\mathbf{a}^H(\theta)\hat{\mathbf{R}}_{xx}^{-1}\mathbf{a}(\theta)} \tag{2.23}$$

Inserting the weight vector Equation (2.23) into Equation (2.20), the output power spatial spectrum, is obtained as [11, 12]

$$\mathbf{P}(\theta) = \mathbf{P}_{CAP}(\theta) = \frac{1}{\mathbf{a}^H(\theta)\hat{\mathbf{R}}_{xx}^{-1}\mathbf{a}(\theta)} \tag{2.24}$$

2.4 Beamspace Processing

For any sensor array, increasing the number of elements leads to an improvement of the DOA estimation algorithms. However, the computational requirements are directly related to the dimensions of the received data; consequently, the burden increases rapidly with the number of the elements used in the array. In many applications, such as in radar applications, the antenna array is composed of hundreds of sensors. For such applications, a large number of phase-shifters, analog to digital converters, and frequency converters are required to process the data which may be prohibitive in case of element-space (ES) processing [69]. As mentioned in Section 1.2, ES processing is to process the observation (output) of each element of the sensor array at the same time. In order to reduce the dimension of the observation vector of the sensor array, beamspace (BS) processing is mandatory.

As mentioned above, in BS processing, the received data (the ES data), which is of higher dimension, is first projected into a subspace of lower dimension to produce BS data. Then the BS data is processed in the resultant lower dimensional BS, thus reducing the computational complexity. The BS processing can be broadly classified into two types: full beamspace (FBS) and reduced-dimension beamspace

(RBS) [12]. In FBS, we process the output of a sensor array containing M elements to produce M orthogonal beams whose center beam is a conventional beam pointed at the broadside ($\theta_c = 90°$). If a sector of interest that contains all the source signals is known *a priori* then RBS could be used. By selecting the appropriate beams suitable for the area to be covered, the resulting processing could be notably reduced. Finally, multiple beams may be combined together so that multiple sectors could be scanned at the same time.

2.4.1 Full-dimension Beamspace

For an array with M sensors, the FBS beams can be calculated using [12]

$$B_m(u) = \frac{1}{M} \frac{\sin\left[M\frac{\pi}{2}(u - \frac{2m}{M})\right]}{\sin\left[\frac{\pi}{2}(u - \frac{2m}{M})\right]}, \quad m = \begin{cases} -\frac{M-1}{2}, \ldots, \frac{M-1}{2} & \text{if } M \text{ is odd} \\ -\frac{M}{2} + 1, \ldots, \frac{M}{2} & \text{if } M \text{ is even} \end{cases} \tag{2.25}$$

where the direction cosines u_x, u_y and u_z with respect to each of the axes are given by

$$u_x = \sin\theta\cos\phi, \quad u_y = \sin\theta\sin\phi, \quad u_z = \cos\theta \tag{2.26}$$

Consider an example for FBS using a ULA containing $M = 7$ sensors. In such a case, there are 7 beams centered at $2m/M$, with $m = -3, -2, -1, 0, 1, 2, 3$. The center beam is located at $u_z = 0$ ($\theta_c = 90°$). Fig. 4.8(a) shows the seven beams centered at the seven values of m.

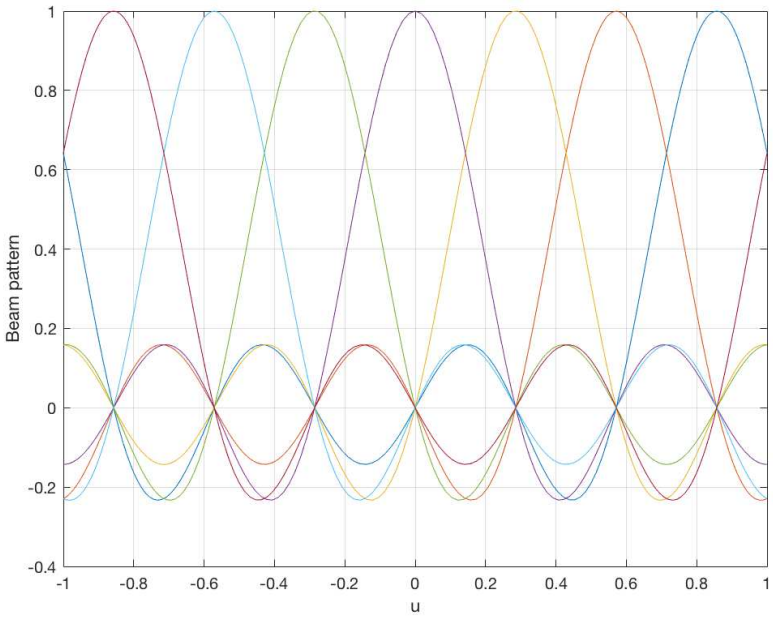

(a) u-space

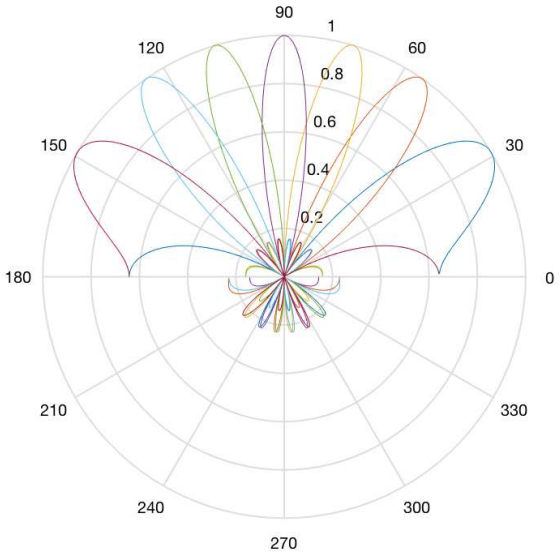

(b) θ-space

Figure 2.4: Beam pattern, full-dimension BS. (a) u-space and (b) θ-space.

2.4.2 Reduced-Dimension Beamspace

In reduced-dimension beamspace (RBS), a beam fan composed of N_{bs} beams is produced. The RBS beams can be calculated using [12]

$$\left[\mathbf{b}_{bs,m}^{H}\right] = \frac{1}{\sqrt{M}} \exp\left[-j(m - \frac{M-1}{2})(\psi_c - (n_{bs} - 4)\frac{2\pi}{M})\right], \quad m = 0, \ldots, M-1, \quad n_{bs} = 1, \ldots, N_{bs} \tag{2.27}$$

where the center beam is pointed at $\psi_c = \frac{2\pi}{\lambda} d \cos\theta_c$, λ being the wavelength, d the enter-element spacing, and θ_c is the center beam angle. We now consider an example using a ULA with 21 elements and a fan beam consisting of $N_{bs} = 5$. Hence, $m = 0, 1, \ldots, 20$ and $m_{bs} = 1, \ldots, 5$. Figures 2.5(a) and 2.6(a) show the beam patterns in the u-space when $u_z = 0.5$ ($\theta_c = 60°$) and $u_z = -0.5$ ($\theta_c = 120°$), respectively. The corresponding beam patterns in the θ-space are shown in Fig. 2.5(b) and 2.6(b), respectively.

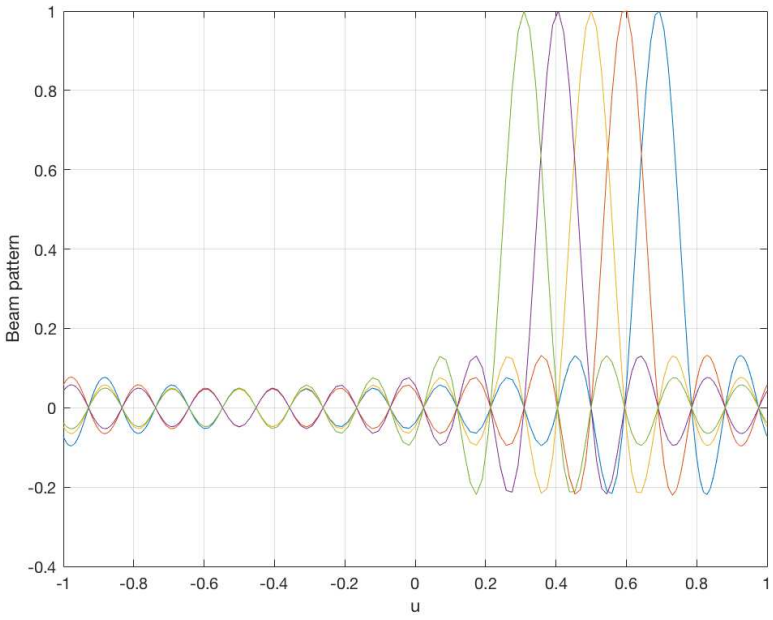

(a) u-space, $u_z = 0.5$

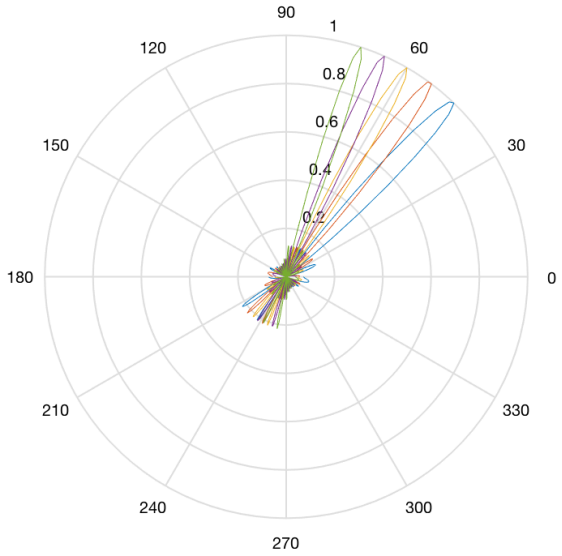

(b) θ-space, $\theta = 60°$

Figure 2.5: Beam pattern, reduced-dimension BS, $M = 21$ sensor, $N_{bs} = 5$, $u = 0.5$ ($\theta_c = 60°$).

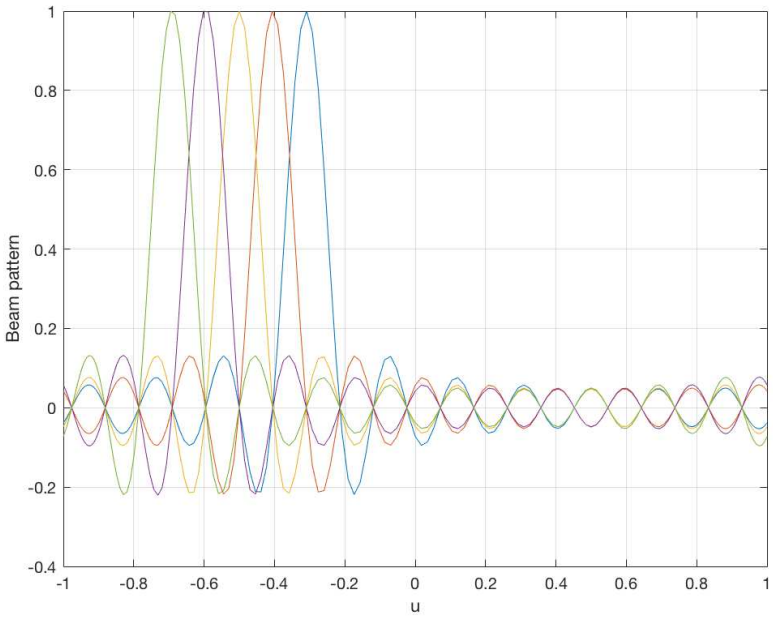

(a) u-space, $u_z = -0.5$

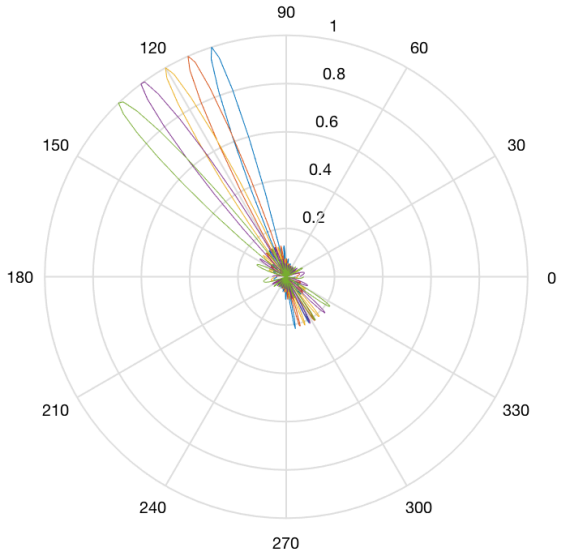

(b) θ-space, $\theta = 120°$

Figure 2.6: Beam pattern, reduced-dimension BS, $M = 21$ sensor, $N_{bs} = 5$, $u = -0.5$ ($\theta_c = 120°$).

2.5 Ill-posed inverse problems and regularization

An inverse problem is a mathematical framework that is used to obtain information about a physical object or system from observed measurements [70, 71, 72, 73]. Let $\mathbf{y} = \Phi(\mathbf{x})$ where $\mathbf{x}$ is the unknown, $\mathbf{y}$ is the vector of observations or measurements and Φ is a known linear operator; then for a noise-free scenario

$$\mathbf{y} = \Phi\mathbf{x},\ \mathbf{y} \in \mathbb{C}^M,\ \mathbf{x} \in \mathbb{C}^N,\ \Phi \in \mathbb{C}^{M\times N} \tag{2.28}$$

Lack of solution means that $\mathbf{y}$ does not lie in the range of Φ, and lack of uniqueness means that the nullspace of Φ is not trivial. A direct way to solve such a problem is by taking the Moore-Penrose pseudo-inverse of Φ. Taking the SVD

$$\Phi = \mathbf{U}\Sigma\mathbf{V}^H = \sum_{i=1}^{\min(M,N)} \mathbf{u}_i\sigma_i\mathbf{v}_i^H \tag{2.29}$$

where $\mathbf{U}$ is an $M \times M$ unitary matrix whose columns are left-singular vectors $\mathbf{u}_i$ for the corresponding singular values σ_i, Σ is a diagonal $M \times N$ matrix with the singular values σ_i on the diagonal (namely, the singular values of Φ) and $\mathbf{V}$ is an $N \times N$ unitary matrix whose columns are right-singular vectors $\mathbf{v}_i$ for the corresponding singular values , and $\mathbf{V}^H$ represents the Hermitian transpose of $\mathbf{V}$.

Let $K = \text{rank}(\Phi)$. Then the Moore-Penrose pseudo-inverse of Φ is

$$\Phi^\dagger = \sum_{i=1}^{K} \mathbf{v}_i\sigma_i^{-1}\mathbf{u}_i^H \tag{2.30}$$

By applying the pseudo-inverse we find the minimum-norm least squares solution

and the reconstruction is given by

$$\begin{aligned}\hat{\mathbf{x}} = \Phi^{\dagger}\mathbf{y} &= \left(\sum_{i=1}^{K}\mathbf{v}_i\sigma_i^{-1}\mathbf{u}_i^H\right)\mathbf{y} = \sum_{i=1}^{K}\mathbf{v}_i\sigma_i^{-1}\mathbf{u}_i^H\sum_{j=1}^{\min(M,N)}\mathbf{u}_j\sigma_j\mathbf{v}_j^H \\ &= \sum_{i=1}^{K}\sum_{j=1}^{\min(M,N)}\frac{\sigma_j}{\sigma_i}\mathbf{v}_i\mathbf{u}_i^H\mathbf{u}_j\mathbf{v}_j^H\mathbf{x} = \sum_{i=1}^{K}\mathbf{v}_i\mathbf{v}_i^H\mathbf{x} \\ &= \left(\mathbf{I}_N - \sum_{i=K+1}^{N}\mathbf{v}_i\mathbf{v}_i^H\right)\mathbf{x}\end{aligned} \tag{2.31}$$

where $\mathbf{I}$ is an $N\times N$ identity matrix. Assuming that $K < N$, the estimated vector $\hat{\mathbf{x}}$ is an an approximation of $\mathbf{x}$. It should be noted that $\Phi^{\dagger}$ chooses the min-norm solution so that the components of $\mathbf{x}$ that lie in the null space of Φ are set to zero. Since $\Phi^{\dagger}$ is a linear function in a finite dimensional space, then it is necessarily continuous. However, in some applications $\Phi^{\dagger}$ may be very large, making the pseudo-inverse discontinuous.

Now, for a noisy measurement case, (2.28) will be

$$\mathbf{y} = \Phi\mathbf{x} + \mathbf{n} \tag{2.32}$$

where $\mathbf{n}$ is the noise term. It is noted that the addition of the noise, even if it is a small amount, may corrupt the solution as follows

$$\begin{aligned}\hat{\mathbf{x}} = \Phi^{\dagger}\mathbf{y} &= \Phi^{\dagger}\left(\Phi\mathbf{x} + \mathbf{n}\right) \\ &= \hat{\mathbf{x}}_{(2.31)} + \sum_{i=1}^{K}\mathbf{v}_i\sigma_i^{-1}\mathbf{u}_i^H\mathbf{n}\end{aligned} \tag{2.33}$$

where $\hat{\mathbf{x}}_{(2.31)}$ is the term on the right hand side of (2.31). It is seen from (2.33) that the noise components are multiplied by σ_i^{-1}, the last few of which are very large since Φ is ill-conditioned. Consequently, the noise components will dominate the solution, and the signal component of interest becomes hidden under the noise floor.

So $\Phi^{\dagger}$ should be replaced by a good approximation which is much less sensitive to noise.

Regularization is used to solve such ill-posed problems by incorporating *a priori* knowledge about the signal of interest to provide reasonable and useful solutions. The problem now is to minimize some measure $F_1(\mathbf{x})$ related to $\mathbf{y}$, as well as to satisfy as much as possible the *a priori* information about $\mathbf{x}$, by minimizing some appropriate measure $F_2(\mathbf{x})$. However, these two objectives cannot be met simultaneously, and hence we look for a trade-off between them by taking a linear combination of the two as follows

$$F(\mathbf{x}) = F_1(\mathbf{x}) + \tau F_2(\mathbf{x}) \tag{2.34}$$

where τ is the a regularization parameter which brings a compromise between fidelity to the data, $F_1(\mathbf{x})$, and fidelity to the prior information, $F_2(\mathbf{x})$. A special case of (2.34) is the non-regularized (least squares) solution when $\tau = 0$. Selecting an appropriate regularization parameter is required for the success of the regularization problem, as will be discussed in Section 3.5.

2.5.1 Regularization Methods

Tikhonov approach [74] is one of the well known approaches to solve ill-posed inverse problems. The method assumes that the norm of the solution should be small, which limits the amount of amplification due to small eigenvalues as follows

$$F(x) = \|\Phi\mathbf{x} - \mathbf{y}\|_2^2 + \tau \|\mathbf{x}\|_2^2 \tag{2.35}$$

where $\|.\|_2^2$ is the ℓ_2-norm. The first term (the residual) is the data-fidelity term, $F_1(x)$, and the second serves as $F_2(x)$. The Tikhonov function has a closed-form

solution given by

$$\hat{\mathbf{x}} = \sum_{i=1}^{K} \left(\frac{\sigma_i^2}{\sigma_i^2 + \tau} \right) \frac{\mathbf{u}_i^H \mathbf{y}}{\sigma_i} \mathbf{v}_i \tag{2.36}$$

The truncated or damped SVD regularization methods have a similar solution [75]

$$\hat{\mathbf{x}} = \sum_{i=1}^{K} w_i \, \frac{\mathbf{u}_i^H \mathbf{y}}{\sigma_i} \mathbf{v}_i \tag{2.37}$$

They can be regarded as a weighted version of the pseudo inverses with the weight, w_i. In this case, Tikhonov method can be considered as a special case with

$$w_i = \frac{\sigma_i^2}{\sigma_i^2 + \tau} \tag{2.38}$$

The idea behind all of these methods is to leave the large singular values almost unchanged, and to limit the effects of the inverses of small singular values.

One of the approaches to solve the regularization problem is to consider the cost function to be [76, 77, 78, 79]

$$F(x) = \|\Phi \mathbf{x} - \mathbf{y}\|_2^2 + \tau \, \|\mathbf{x}\|_p^p \tag{2.39}$$

where $\|.\|_p^p$ is the ℓ_p-norm and $0 < p \leq 1$. A special case of this when $p = 1$ is the well-known LASSO regularization method [50], and the corresponding cost function is given by [50]

$$F(x) = \|\Phi \mathbf{x} - \mathbf{y}\|_2^2 + \tau \, \|\mathbf{x}\|_1 \tag{2.40}$$

where $\|.\|_1$ is the ℓ_1-norm. The ℓ_1-norm penalty of the LASSO regularization favors sparse values of $\mathbf{x}$. But, it does not have an analytical solution. However, there exists an efficient algorithm, namely, the least angle regression (LARS) algorithm, which can be utilized to obtain an approximate solution to the LASSO problem given by (2.40).

2.6 Summary

In this chapter, a brief account of the background material necessary for the development of the work undertaken in this thesis has been presented. To start with, the one-dimension uniform linear array model has been introduced and a mathematical representation for the steering vector and the received data discussed. A brief description of fluctuating sources is given along with mathematical representation of such sources. Next, the concepts of beamforming and beamspace processing are then discussed along with the benefits of beamspace processing.

An exact solution for the ill-posed inverse problem in a noise-free scenario has been briefly discussed. Further, regularization methods to overcome the problem associated with the ill-conditioned inverse problem in the case of noisy environment is presented.

Chapter 3

Compressive Sensing-Based DOA Estimation In Element-Space

3.1 Introduction

Array signal processing plays an important role in many applications, including sonar, radar, seismology and radio astronomy. DOA deals with the problem of determining the number and locations of multiple sources using an antenna array. Many of the recent algorithms deal with DOA estimation of spatiotemporal electromagnetic waves emanating from multiple sources.

Increasing the number of sensor array elements leads to an enhancement in the array gain and directivity, thus improving the array's overall performance. On the other hand, increasing the number of array elements increases the complexity of the feeding network and the time needed to process the received data. Researchers have focused recently on the pursuit of light weight, small sized and compact antenna arrays to satisfy the requirements of present day applications like the IoT and unmanned vehicles. Physically increasing the number of antenna array elements is therefore not an option. Recent literature investigating the virtual array concept

has shown it to enhance the performance of a sensor array [41, 43, 80, 81, 82].

MRAs and ACM have been investigated for virtually extending the sensor array aperture by increasing the available degrees of freedom [28, 29, 30]. However, there is no closed form expression for the locations of the sensors in the virtual array and for the number of achievable degrees of freedom. Furthermore, ACM is not positive semi-definite for a finite number of snapshots, and a transformation was suggested in [31] to overcome this problem. Higher order cumulants were used to increase the available degrees of freedom and consequently extend the array aperture. However, using the fourth order cumulants, Gaussian source signals cannot be estimated. The KR product was suggested for the DOA estimation of quasi-stationary source signals in [41, 82].

Co-prime arrays have been proposed in the literature [83, 84, 85, 86] to increase the degrees of freedom in the array. For these arrays, the number of the degrees of freedom can be determined, and closed-form expressions for the locations of the sensors in the corresponding virtual arrays can be obtained. However, the corresponding virtual arrays are not uniform. Nested arrays have been investigated for the first time in [43]. These arrays, in addition to all of the advantages provided by the co-prime arrays, result in virtual arrays that are uniform and provide degrees of freedom that are even higher [83]. For example, using six elements, the nested array provides 23 degrees of freedom in contrast to only 17 provided by the co-prime array.

compressive sensing (CS) has evolved rapidly in recent years and has found multiple applications in various fields, such as medicine [87], ultrasound imaging [44] and radar detection [46]. Malioutov et al. [47] investigated the DOA estimation performance using CS with respect to the SNR, the number of sources and the coherence of the sources' signals. Xenaki et al. [49] studied the DOA estimation using CS with coherent arrivals, single-snapshot data and different array geometries.

It has been proven in [49] that CS does not require the arrivals to be incoherent. Furthermore, single or multiple snapshots can be used. In terms of resolution, the performance of the CS-based DOA is superior to that of the MVDR [88].

In this chapter, we propose a new algorithm for DOA estimation, the adaptable LASSO (A-LASSO), which combines the benefits of the virtual array concept for extended array aperture along with CS [61]. Extensive simulations are carried out to examine the performance of the proposed A-LASSO for non-fluctuating as well as fluctuating signals.

3.2 Difference Co-Array

Consider a linear array (LA), uniform or non-uniform, consisting of M elements. Let d_i denote the i-th element position in the array. Let us assume that there are L narrowband, far-field sources with angles of arrival (AOA) (θ_l) and powers (σ_l^2), $l = 1, 2, \ldots, L$. It is also assumed that the source signals are uncorrelated with one another. Let $\mathbf{a}(\theta_l) \in \mathbb{C}^{M\times 1}$ be the steering vector corresponding to AOA (θ_l), whose i-th element is $e^{-jk_o d_i \cos(\theta_l)}$, where $k_o = 2\pi/\lambda$ is the wavenumber and λ is the wavelength of the propagating waves. Let the vector $\mathbf{s}(t) = [s_1(t)\ s_2(t)\ \ldots\ s_L(t)]^T$, where $\mathbf{s} \in \mathbb{C}^{L\times 1}$ represent the source signals. Then, the output of LA can be written as:

$$\mathbf{x}(t) = \mathbf{A}\mathbf{s}(t) + \mathbf{n}(t) \tag{3.1}$$

where $\mathbf{A} = [\mathbf{a}(\theta_1)\ \mathbf{a}(\theta_2)\ \ldots\ \mathbf{a}(\theta_L)]$, $\mathbf{A} \in \mathbb{C}^{M\times L}$ is the array manifold matrix and $\mathbf{n}(t) \in \mathbb{C}^{M\times 1}$ is an AWGN that is uncorrelated with the source signals. One can

obtain the covariance matrix of the received signals as [12]:

$$\begin{aligned}\mathbf{R}_{xx} &= E[\mathbf{x}\mathbf{x}^H] \\ &= \mathbf{A}\mathbf{R}_{ss}\mathbf{A}^H + \sigma_n^2\mathbf{I} \\ &= \mathbf{A}\begin{bmatrix} \sigma_1^2 & & & & \\ & \ddots & & & \\ & & \sigma_l^2 & & \\ & & & \ddots & \\ & & & & \sigma_L^2 \end{bmatrix}\mathbf{A}^H + \sigma_n^2\mathbf{I}\end{aligned} \tag{3.2}$$

where $\sigma_l^2, \quad l = 1, \ldots, L$, correspond to the power of the source signals, $\mathbf{I}$ is the identity matrix of size $(M \times M)$ and σ_n^2 is the noise power. One can now vectorize $\mathbf{R}_{xx} \in \mathbb{C}^{M\times M}$ as [41, 82]:

$$\begin{aligned}\mathbf{V} = \text{vec}(\mathbf{R}_{xx}) &= \text{vec}\left[\sum_{l=1}^{L}\sigma_l^2(\mathbf{a}(\theta_l)\mathbf{a}^H(\theta_l))\right] + \sigma_n^2\mathbf{1} \\ &= (\mathbf{A}^* \odot \mathbf{A})\mathbf{p} + \sigma_n^2\mathbf{1}\end{aligned} \tag{3.3}$$

where $\mathbf{p} \in \mathbb{C}^{L\times 1} = [\sigma_1^2 \ \sigma_2^2 \ \ldots \ \sigma_L^2]^T$ and $\mathbf{1} \in \mathbb{C}^{M\times M} = [\mathbf{e}_1^T \ \mathbf{e}_2^T \ \ldots \ \mathbf{e}_M^T]^T$ with $\mathbf{e}_i \in \mathbb{C}^{M\times 1}$ being a column vector of zeros except for a one at the i-th position. Comparing Equations (3.3) and (3.1), we can see that $\mathbf{V} \in \mathbb{C}^{M^2\times 1}$ in Equation (3.3) can be considered as the output of an array with a manifold $(\mathbf{A}^*\odot\mathbf{A})$, $\mathbf{p}$ representing the equivalent source signals and the noise given by $\sigma_n^2\mathbf{1}$ being deterministic. The distinct rows of $(\mathbf{A}^*\odot\mathbf{A})$ form the virtual array (VA); the locations of whose distinct elements are given by the set:

$$D = \{d_i - d_j\}, \quad \forall i, j = 1, 2, \ldots, M \tag{3.4}$$

where d_i is the position vector of the i-th sensor in the original array. This array is known as the difference co-array [43].

We now assume that the original array is a two-level nested array [43] for which M is even, and each level contains $M/2$ sensor elements. In such a case, the VA is a ULA consisting of $\bar{M}$ sensors, $\bar{M} = (M^2/2 + M - 1)$, which are located from $-(\bar{M}-1)d/2$ to $(\bar{M}-1)d/2$, where d is the distance between two adjacent sensors [43]. Detailed information about the number of sensor in each level, the distinct sensors in the *difference co-array*, $\bar{M}$, and the maximum number of source signals to be estimated for odd and even M sensors, are as shown in Table 3.1. In each case, the virtual array is a ULA consisting of $\bar{M}$ sensors which are located from $-(\bar{M}-1)d/2$ to $(\bar{M}-1)d/2$ [43].

Table 3.1: Sensors distribution for a two-level nested array.

M	1^{st} level	2^{nd} level	$\bar{M}$	Max L
Odd	$(M-1)/2$	$(M+1)/2$	$(M^2-1)/2 + M$	$((M^2-1)/2 + M - 1)/2$
Even	$M/2$	$M/2$	$M^2/2 + M - 1$	$(M^2/2 + M - 2)/2$

It should be noted that the equivalent source signal vector $\mathbf{p}$ (for the difference co-array) contains the power of the sources σ_l^2, $l = 1, \ldots, L$. Therefore, they act like fully-correlated sources. A spatial smoothing technique was suggested by Pal et al. [43] to overcome this problem of correlated sources. However, by using the CS technique, we will no longer need spatial smoothing or any preprocessing scheme, and CS will be able to detect the source signals.

3.3 Compressive Sensing Framework

Since the sources are assumed to be located in the far field, they can be considered as point sources; hence, the sources become sparse in space. Let Ω denote the set of all

possible source locations, $\{\bar{\theta}_n\}_{n=1}^{N}$, N denoting a grid that covers Ω, with $N \gg L$. Let:

$$\bar{\mathbf{s}}(t) = [\bar{\sigma}_1 \ \bar{\sigma}_2 \ \dots \ \bar{\sigma}_n \ \dots \ \bar{\sigma}_N]^T \tag{3.5}$$

where $\bar{\mathbf{s}} \in \mathbb{C}^{N\times 1}$, and:

$$\begin{aligned}\Phi &= [\bar{\mathbf{a}}(\bar{\theta}_1) \ \bar{\mathbf{a}}(\bar{\theta}_2) \ \dots \ \bar{\mathbf{a}}(\bar{\theta}_n) \ \dots \ \bar{\mathbf{a}}(\bar{\theta}_N)] \\ &= \begin{bmatrix} e^{jk_o d(-(\bar{M}-1)/2)\cos\bar{\theta}_1} & e^{jk_o d(-(\bar{M}-1)/2)\cos\bar{\theta}_2} & \dots & e^{jk_o d(-(\bar{M}-1)/2)\cos\bar{\theta}_N} \\ \vdots & \vdots & & \vdots \\ 1 & 1 & \ddots & 1 \\ \vdots & \vdots & & \vdots \\ e^{jk_o d((\bar{M}-1)/2)\cos\bar{\theta}_1} & e^{jk_o d((\bar{M}-1)/2)\cos\bar{\theta}_2} & \dots & e^{jk_o d((\bar{M}-1)/2)\cos\bar{\theta}_N} \end{bmatrix}\end{aligned} \tag{3.6}$$

where $\Phi \in \mathbb{C}^{\bar{M}\times N}$ and $\bar{\mathbf{a}}(\bar{\theta}_n) \in \mathbb{C}^{\bar{M}\times 1}$ is the steering vector of the VA corresponding to the AOA $(\bar{\theta}_n)$. Then, the received signal at the $\bar{m}$-th sensor is:

$$y_{\bar{m}}(t) = \phi_{\bar{m}}\bar{\mathbf{s}}(t) + \bar{n}_{\bar{m}}(t), \quad \bar{m} = 1, 2, \dots, \bar{M} \tag{3.7}$$

where $\phi_{\bar{m}}$ is the $\bar{m}$-th row of Φ. The n-th element of $\bar{\mathbf{s}}(t)$, $\bar{s}_n(t)$, is nonzero only if $(\bar{\theta}_n = \theta_l)$, and in that case, $\bar{\sigma}_n = \sigma_l$. Then, Equation (3.7) can be rewritten as:

$$\mathbf{y}(t) = \Phi\bar{\mathbf{s}}(t) + \bar{\mathbf{n}}(t) \tag{3.8}$$

where $\mathbf{y} \in \mathbb{C}^{\bar{M}\times 1}$ and $\bar{\mathbf{n}} \in \mathbb{C}^{\bar{M}\times 1}$. In accordance with conventional DOA estimation, the technique is to estimate the signal energy as a function of the source location showing peaks corresponding to the source locations. Since the sources are point sources and their number is small, the spatial spectrum is sparse. Hence, we can solve this problem by regularizing it to favour sparse signal fields using LASSO [50].

The LASSO minimization is defined as:

$$\min_{s} \left\| \mathbf{y} - \sum_{n=1}^{N} \phi_n \bar{s}_n \right\|^2 + \tau \sum_{n=1}^{N} |\bar{s}_n| \tag{3.9}$$

where ϕ_n is the n-th element of $\phi_{\bar{m}}$ and $\bar{s}_n$ is the n-th element of $\bar{\mathbf{s}}$. Equation (3.9) can be rewritten as:

$$\hat{\mathbf{s}}_{lasso} = \min_{s} \|\mathbf{y} - \Phi\bar{\mathbf{s}}\|_2^2 + \tau \|\bar{\mathbf{s}}\|_1 \tag{3.10}$$

where τ is a nonnegative regularization parameter. The first term in Equation (3.9) is the ℓ_2 norm, while the second is an ℓ_1 penalty function, which is very important for the success of LASSO. LASSO shrinks the coefficients toward zero, as the regularization parameter τ increases. This parameter, τ, controls the relative importance between the sparsity of the solution (ℓ_1-norm term) and the fitness to the measurements (ℓ_2-norm term). However, the ℓ_1-norm penalty associated with LASSO tends to produce biased estimates for large coefficients [89], thus degrading the estimation accuracy. Zou [51] proposed a new version of LASSO, the A-LASSO, wherein adaptable weights are used for penalizing the coefficients in the ℓ_1-norm term iteratively. Furthermore, Zou [51] suggests using the OLS solution as the initial weights to construct the adaptable weights in the A-LASSO first iteration. We shall refer to this as OLS A-LASSO. It should be mentioned that the ℓ_1 penalization approach is also known as *basis pursuit* [90].

3.4 Modified LASSO for DOA Estimation

One can notice from Equation (3.9) that the regularization parameter, τ, penalizes the coefficients equally in the ℓ_1-norm term. Therefore, the LASSO estimates could be biased [89] and result in reducing the solution accuracy. In order to overcome this deficiency, we apply the A-LASSO in the DOA estimation problem for the first

time. Hence, the A-LASSO minimizes:

$$\|\mathbf{y} - \Phi\bar{\mathbf{s}}\|_2^2 + \tau \sum_{n=1}^{N} w_n |\bar{s}_n| \tag{3.11}$$

where w_n is the n-th element of the weight vector, $\mathbf{w} \in \mathbb{C}^{N\times 1}$. Let, $\hat{\mathbf{s}}$ be the initial estimate for $\bar{\mathbf{s}}$. Now, choosing any weight factor, γ, where $\gamma > 0$, and defining the weight vector as $\hat{\mathbf{w}} = [\hat{w}_1 \hat{w}_2 \dots \hat{w}_N]^T$, where:

$$\hat{w}_n = \frac{1}{|\hat{s}_n|^\gamma} \quad n = 1, 2, \dots, N \tag{3.12}$$

the A-LASSO is given by:

$$\hat{\mathbf{s}}^{(k)} = \min_{s} \|\mathbf{y} - \Phi\bar{\mathbf{s}}\|_2^2 + \tau_k \sum_{n=1}^{N} \hat{w}_n |\bar{s}_n| \tag{3.13}$$

where k is the iteration number and $\hat{w}_n$ is the n-th element of the weight vector, $\hat{\mathbf{w}}$. The minimization in Equation (3.13) corresponds to a convex optimization problem; it does not have multiple local minima, and its global minimizer can easily be found. The A-LASSO is ℓ_1 penalized, so any efficient algorithm that can solve the conventional LASSO should also be able to solve the adaptable version. The least angle regression (LARS) algorithm [91] is utilized to solve the A-LASSO as illustrated in Algorithm 3.1

The steps from 2 to 5 are repeated until convergence to a predefined residual, R, is obtained or when the chosen number of iterations is reached. The computational cost is of the order $O(KN^2)$, where K is the total number of iterations, which is of the same order as the computation of a single OLS minimization. Figure 3.1 summaries the above steps from 1 to 5. The efficient path algorithm makes the A-LASSO an attractive method for practical applications [51].

Algorithm 3.1 The A-LASSO technique.

1: Let the initial estimate for $\bar{\mathbf{s}}$ be $\hat{\mathbf{s}}$.
2: Find $\hat{\mathbf{w}}$, where the n-th element of $\hat{\mathbf{w}}$, $\hat{w}_n$, is given by $\hat{w}_n = \frac{1}{|\hat{s}_n|^\gamma}$, $n = 1, 2, \ldots, N$.
3: Define $\bar{M} \times N$ matrix Φ^*, such that its $(\bar{m}, n)$-th element is given by $\phi_{\bar{m}n}/\hat{w}_n$, where $\bar{m} = 1, 2, \ldots, \bar{M}$ and $n = 1, 2, \ldots, N$.
4: **for** $k = 1, 2, \ldots, K$ iterations **do**

Solve the LASSO problem as:

$$\hat{\mathbf{s}}^* = \min_{s} \|\mathbf{y} - \Phi^* \bar{\mathbf{s}}\|_2^2 + \tau_k \|\bar{\mathbf{s}}\|_1$$

Calculate $\hat{s}^{(k)} = \hat{s}_n^*/\hat{w}_n, \quad n = 1, 2, \ldots, N.$

5: **end for**
6: Find the final DOA estimation.

For the uniqueness of the sparse solution, the spark of matrix Φ, defined as the smallest number of columns from Φ that are linearly dependent [92], must be investigated. Hence, the above algorithm can identify a unique L-sparse solution only if $L < Spark[\Phi]/2$, $Spark[.]$ denoting the spark of a matrix [92]. Since any set of $(M^2/2 + M - 1)$ columns of Φ is linearly independent, $Spark(\Phi) = (M^2/2 + M)$. Hence, the algorithm can identify L-sparse solutions only if $L < Spark(\Phi)/2$. That is, our algorithm can detect up to $(M^2/2 + M - 2)/2$ sources using an array of M sensors.

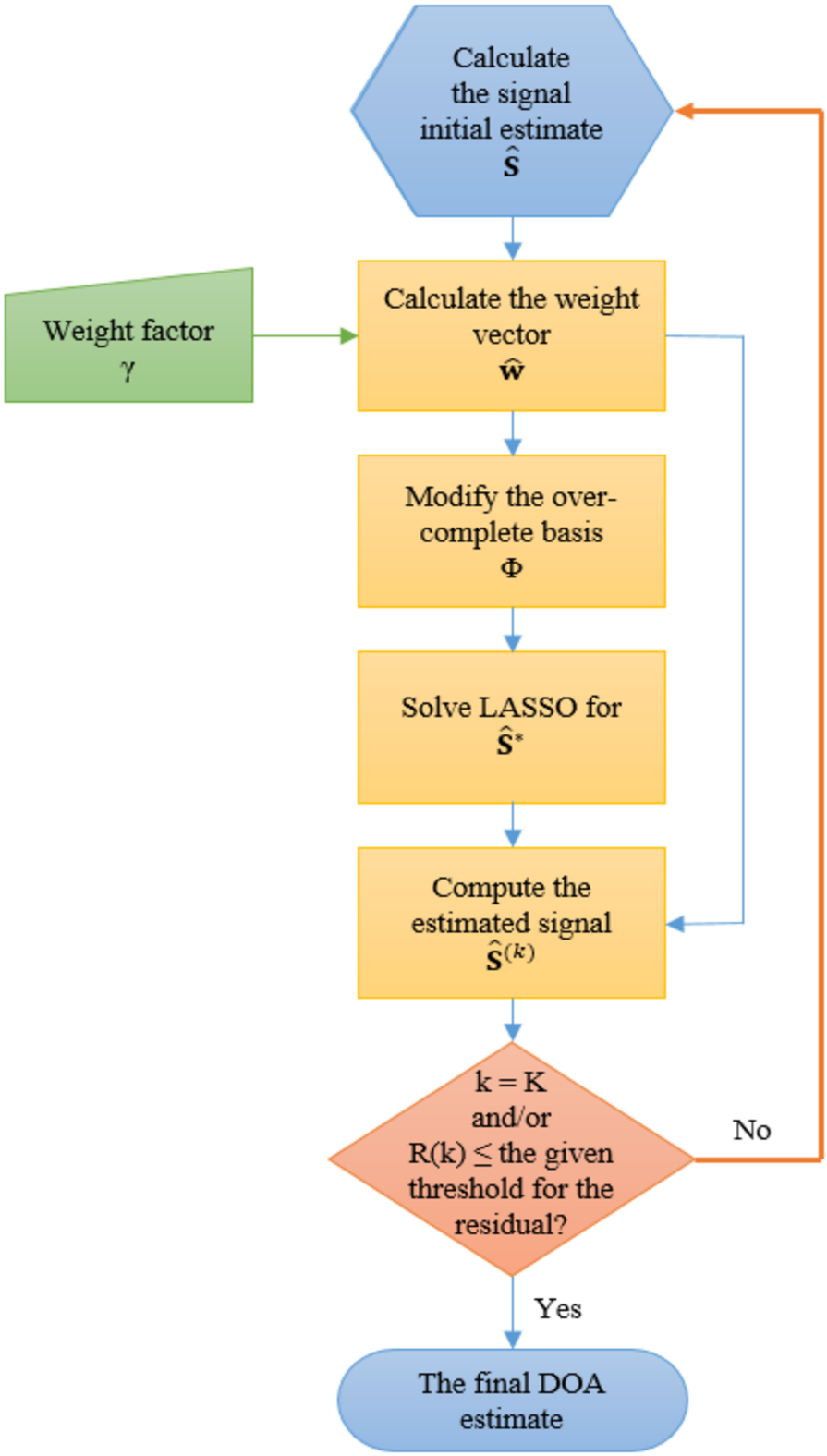

Figure 3.1: A flowchart of the algorithm for A-LASSO-based DOA estimation.

3.4.1 OLS A-LASSO

Previously, a vector of ones is assumed as the initial signal estimate for $\bar{\mathbf{s}}$. However, as proven from the simulations, a vector of ones is not the appropriate guess for the signal to be estimated, especially since there is no relation between the vector of ones and the signal to be estimated. Furthermore, multiplying that vector by a factor, β, will affect the regularized solution (the same effect as that of changing τ, the regularization parameter). Even more, if we try to push the algorithm to the limits (by choosing a small β), we find spurious peaks along with the genuine peaks. Therefore, we will use the OLS solution as the initial signal estimate for $\bar{\mathbf{s}}$, with the expectation that this modification leads to better results and that the OLS A-LASSO solution converges faster than that of the A-LASSO.

We assume replacing $\hat{s}_n$ in Equation (3.12) with $\hat{s}_{OLSn}$, where $\hat{s}_{OLSn}$ is the n-th element of $\hat{\mathbf{s}}_{OLS} \in \mathbb{C}^{N\times 1}$ and is given by:

$$\hat{\mathbf{s}}_{OLS} = \min_{s} \|\mathbf{y} - \Phi\bar{\mathbf{s}}\|_2^2 \tag{3.14}$$

The minimization in Equation (3.14) is known as the ordinary least square minimization. The computational cost for Equation (3.14) is of order $O(N^2)$. It should be mentioned that the number of source signals is not required to be known in advance for OLS A-LASSO. However, we do not use OLS for DOA estimation. We use it in OLS A-LASSO only as an initial guess for the signal to be estimated (not a stand-alone DOA estimation technique). Furthermore, OLS gives nonzero estimates to all of the coefficients (compared to LASSO minimization) and does not favor sparse signals as in the case of LASSO minimization.

3.4.2 MVDR A-LASSO

The MVDR technique uses the available degrees of freedom to form a beam in the look direction and, at the same time, nulling the output in all of the other directions. Thus, for a particular DOA, MVDR uses all, but one of the degrees of freedom to minimize the array output while using the remaining ones to constrain a unity gain in the look direction according to the following optimization [11]:

$$\min_{\mathbf{z}} \mathbf{z}^H \mathbf{R}_{ss} \mathbf{z}, \quad \text{subject to} \quad \mathbf{z}^H \mathbf{a}_1(\bar{\theta}) = 1 \tag{3.15}$$

where $\mathbf{z} \in \mathbb{C}^{(M^2/4+M/2)\times 1}$ is the MVDR beamformer weight vector, $\mathbf{R}_{ss}$ is the spatially-smoothed (SS) covariance matrix, which we will now obtain, and $\mathbf{a}_1 \in \mathbb{C}^{(M^2/4+M/2)\times 1}$ is the steering vector of the array whose SS covariance matrix is $\mathbf{R}_{ss}$. It should be noted that we are not able to use the covariance matrix $\mathbf{R}_{xx}$ in Equation (3.2), since this contains information only about the real sensor array. Furthermore, the received source signals are represented as the deterministic vector $\mathbf{p}$ in Equation (3.3). Therefore, we are not able to use $\mathbf{V}$ of Equation (3.3) directly for MVDR, since the resultant covariance matrix is rank defective. However, in our case, it is required to construct the covariance matrix of the virtual array. Hence, we perform spatial smoothing on $\mathbf{V}$ to construct a full rank covariance matrix for the virtual array. Assuming a two-level nested array containing M even sensors, the distinct elements of vector $\mathbf{V}$ in Equation (3.3), $\bar{\mathbf{V}} \in \mathbb{C}^{\bar{M}\times 1}$ can be rewritten as:

$$\bar{\mathbf{V}} = [\bar{v}_1 \ \bar{v}_2 \ \ldots \ \bar{v}_{\bar{m}} \ \ldots \ \bar{v}_{\bar{M}}]^T, \quad \bar{M} = (M^2/2 + M - 1) \tag{3.16}$$

Then, the covariance matrix of the virtual array can be obtained as follows.

Let $\mathbf{R}$ be the Toeplitz matrix:

$$\mathbf{R} = \begin{bmatrix} \bar{v}_{\frac{(\bar{M}-1)}{2}+1} & \bar{v}_{\frac{(\bar{M}-1)}{2}+2} & \cdots & \bar{v}_{\bar{M}} \\ \bar{v}_{\frac{(\bar{M}-1)}{2}} & \bar{v}_{\frac{(\bar{M}-1)}{2}+1} & \cdots & \bar{v}_{\bar{M}-1} \\ \vdots & \vdots & \ddots & \vdots \\ \bar{v}_1 & \bar{v}_2 & \cdots & \bar{v}_{\frac{(\bar{M}-1)}{2}+1} \end{bmatrix} \tag{3.17}$$

where $\mathbf{R} \in \mathbb{C}^{M^2/4+M/2 \times M^2/4+M/2}$. forward-backward (FB) SS [12] is applied to $\mathbf{R}$ to obtain the spatial smoothed covariance matrix, $\mathbf{R}_{ss}$. It should be noted that FBSS is used here only in establishing a full rank covariance matrix. The resulting n-th element of the weight vector $\mathbf{w}_{MVDR} \in \mathbb{C}^{N\times 1}$ is given by [11]:

$$w(\bar{\theta}_n) = \frac{1}{\mathbf{a}_1^H(\bar{\theta}_n)\mathbf{R}_{ss}^{-1}\mathbf{a}_1(\bar{\theta}_n)}, \quad n = 1, 2, \ldots, N \tag{3.18}$$

which is also known as the scalar output power for a single steering direction [93]. The computational complexity of the MVDR algorithm [94] is as shown in Table 3.2. It is noted that the MVDR-based DOA estimation technique does not require the number of the source signals to be known in advance. Furthermore, the MVDR DOA estimation method performance is better than that of the CBF. In addition, assuming that ($N \gg \bar{M}$), the computational complexity of obtaining the MVDR weights is less than that of obtaining the OLS one.

Table 3.2: Computational complexity of the MVDR algorithm.

Operation	**Computation**	**Cost**
Inverse Covariance Matrix	$\mathbf{R}_{ss}^{-1}$	$O(\bar{M}^3)$
Beamformer Weight	$z = \frac{\mathbf{R}_{ss}^{-1}\mathbf{a}_1(\bar{\theta}_n)}{\mathbf{a}_1^H(\bar{\theta}_n)\mathbf{R}_{ss}^{-1}\mathbf{a}_1(\bar{\theta}_n)}$	$O(2\bar{M}^2 + 3\bar{M})$
Beamformer Sum	$w(\bar{\theta}_n) = [\mathbf{a}_1^H(\bar{\theta}_n)\mathbf{R}_{ss}^{-1}\mathbf{a}_1(\bar{\theta}_n)]^{-1}$	$O(\bar{M}N)$

It should be noted that our proposed algorithm does not depend on the orthogonality of the signal subspaces nor on implementing SVD on the sensor array data. Therefore, it can perform DOA estimation without knowing the number of source signals in advance. On the other hand, subspace-based techniques, such as MUSIC and ESPRIT, cannot estimate the DOA without a priori knowledge of the number of source signals. Furthermore, it is known from the literature that the MUSIC algorithm is superior to the ESPRIT algorithm [95, 96, 97]. However, for the sake of evaluating our proposed algorithm in comparison with MUSIC, we assume that the number of signal source is to be known a priori.

3.5 Selecting the Regularization Parameter

Choosing the regularization parameter, τ, is an important issue for the success of LASSO minimization Equation (3.10). The regularization parameter controls the trade-off between the data fidelity ($\|\mathbf{y} - \Phi\bar{\mathbf{s}}\|_2^2$) and the prior information ($\|\bar{\mathbf{s}}\|_1$). The discrepancy principle (DP), cross-validation (CV), generalized cross-validation (GCV) and L-curve method are some of the existing regularization parameter selection methods. The regularization parameter in DP is chosen so that the sum of squares of the weighted residuals is equal to the mean of a chi-square distribution [71, 98, 99]. CV selects the regularization parameter that minimizes the mean square error, while GCV selects the value of the regularization parameter that minimizes the GCV function, which is a leave-one-out CV function for large-scale problems [71, 100]. The L-curve criterion is based on a log-log plot of the corresponding values of the solution norms and the residuals for a range of values of the regularization parameter [88, 101, 102]. From Figures 3.2(a) and 3.3(a), it is seen that as the value of the regularization parameter τ is increased, the significance of the A-LASSO estimates shifts from large non-sparse estimates to smaller sparse estimates. In other

words, a small value of τ leads to an under-regularized estimate, whereas a large value results into an over-regularized estimate. Therefore, suitable values of τ are those lying in the knee of the L-curve. We consider the beginning of the knee to correspond the value of τ at which the solution norm starts to decrease and the end of the knee to correspond to the value of τ at which the residual norm does not significantly change. These are the two red stars on the L-curve. We empirically determine a segment of this knee corresponding to which all of the τ values provide satisfactory estimates. We have chosen the value of the regularization parameter τ to be the midpoint of this segment. It should be mentioned that there are different methods to select a suitable value for the regularization parameter in the literature [71, 98, 99, 100]. However, it has been shown in [103] that the L-curve [88, 101, 102] method gives a good estimation of the regularization parameter. In order to illustrate how τ is chosen, we consider two source signals from DOAs of 60° and 120° to be impinging a six-sensor two-level nested array with the sampling grid being uniform from 1° to 180°, in increments of 1°, and an SNR of 10 dB; the corresponding L-curve plot is as shown in Figure 3.2(a). Selecting τ to be between 1.39 and 2.19, the resulting DOA estimation is as shown in Figure 3.2(b). Lowering the SNR to be 0 dB, the results for the same specifications are shown in Figure 3.3. In this case, a suitable value for τ is between 1.86 and 2.58. From Figure 3.2(b), it can be seen that we are able to identify correctly the two source signals, even at low SNR conditions.

3.6 Simulation Results for non-Fluctuating Source Signals

Consider a sparse linear two-level nested array, for which M is even, consisting of $M = 6$ elements, as shown in Figure 3.4. Investigating the array output by applying

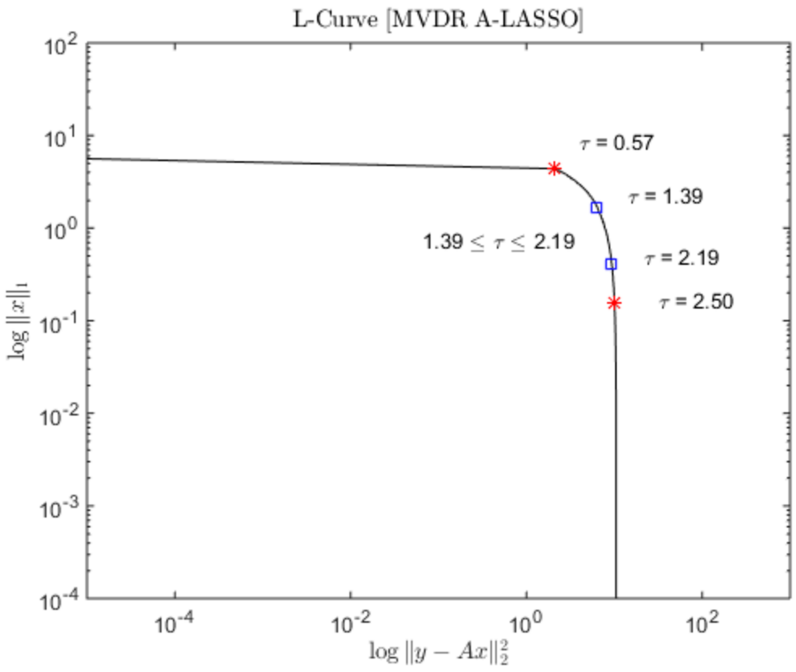

(a)

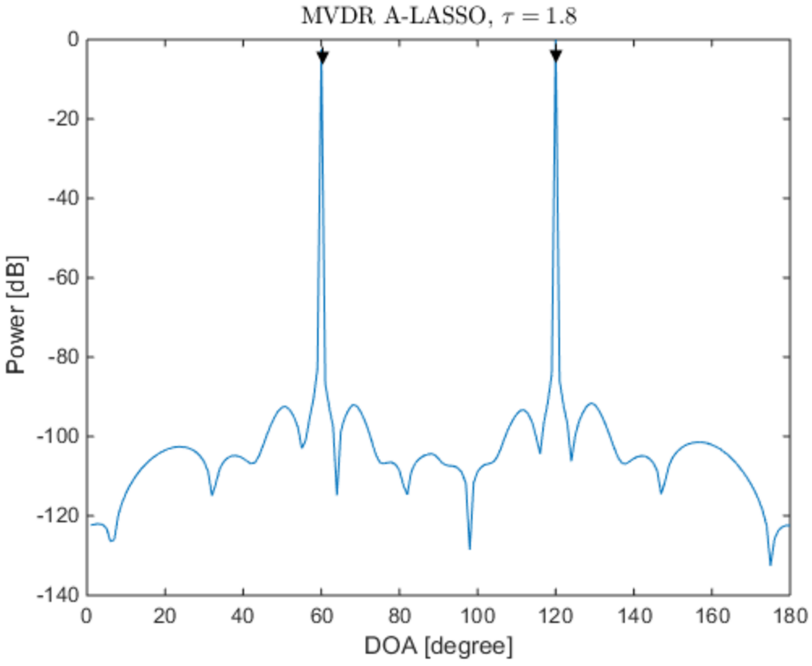

(b)

Figure 3.2: (a) The data residual $\|\mathbf{y} - \Phi^* \bar{\mathbf{s}}\|_2^2$ versus the solution ℓ_1-norm linear scale on a log-log scale (L-curve); (b) DOA estimation for two source signals; τ was selected using L-curve, in the MVDR A-LASSO problem (SNR = 10 dB).

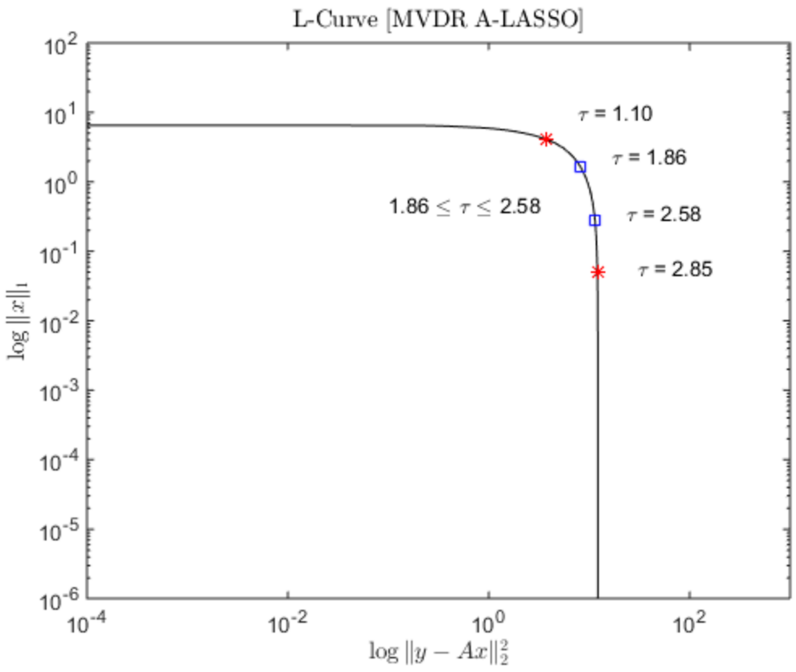

(a)

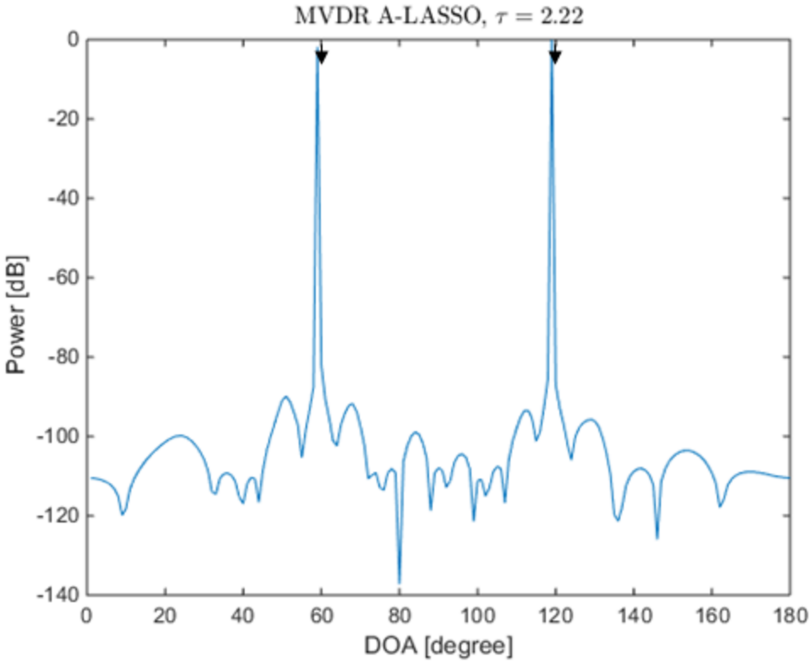

(b)

Figure 3.3: (a) The data residual $\|\mathbf{y} - \Phi^* \bar{\mathbf{s}}\|_2^2$ versus the solution ℓ_1-norm linear scale on a log-log scale (L-curve); (b) DOA estimation for two source signals; τ was selected using L-curve, in the MVDR A-LASSO problem (SNR = 0 dB).

Equations (3.1) to (3.3) and extracting the equivalent distinct virtual elements from the virtual array manifold ($\mathbf{A}^* \odot \mathbf{A}$), one can see that the virtual ULA contains $\bar{M} = 23$ elements, as shown in Figure 3.4. It should be noted that the resultant virtual is a ULA [43]. The sampling grid $\bar{\theta}_n \in [1^\circ : 180^\circ]$ that covers Ω is chosen to be of 1° step, except for the twelfth simulation and $d = \lambda/2$, where λ is the wavelength of the propagating waves.

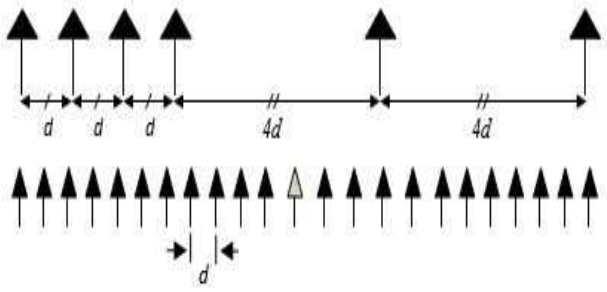

Figure 3.4: The proposed sparse (**upper**) and the virtual co-array (**lower**).

All of the simulated source signals are assumed to be equi-power and uncorrelated with one another or with the noise, except in the fifth experiment, where the sources are assumed to be correlated. The weight parameter, γ, is set to 0.5 in all of the simulations, except for the eleventh experiment. The total number of simulations, N_{sim}, is set to $N_{sim} = 100$ for each observation point except in the case of the eleventh simulation, where it is set to 10. For each experiment, the regularization parameter, τ, is selected based on the idea of the L-curve [88, 101, 102].

The CVX toolbox [104, 105] for convex optimization that is available within the MATLAB environment is used for examining the performance of the proposed A-LASSO algorithms. It uses semi-definite quadratic-linear programming (SDPT3) [106] to obtain the global solution for the optimization problem.

The RMSE is used as the performance measure:

$$RMSE = \frac{1}{L}\sum_{l=1}^{L}\sqrt{\frac{1}{N_{sim}}\sum_{n=1}^{N_{sim}}(\widehat{\theta}_{l,n} - \theta_l)^2} \tag{3.19}$$

where $\widehat{\theta}_{l,n}$ is the estimate of the DOA angle θ_l of the n-th Monte Carlo trial.

In the first experiment, we study the effect of the initial vectors on the performance of the three LASSO algorithms, namely classical LASSO (for which $\gamma = 0$), OLS A-LASSO and MVDR A-LASSO. For the latter two, we assume $\gamma = 0.5$. We consider two source signals impinging on the sparse array from the DOA of 60° and 120°. For SNR of 0 dB, 10 snapshots and one iteration, the results are as shown in Figure 3.5. It can be seen that the MVDR A-LASSO yields a performance better than that of the classical LASSO, as well as that of the OLS A-LASSO. It may be mentioned that by increasing the number of iterations, OLS A-LASSO can be made to yield a performance similar to that of MVDR A-LASSO. This superior performance of the MVDR A-LASSO can be attributed to the initial weights used, compared to the least square weights used for the OLS A-LASSO, as will be seen later in Simulation 6. It should be noted that classical LASSO uses equal initial weights and has the poorest performance.

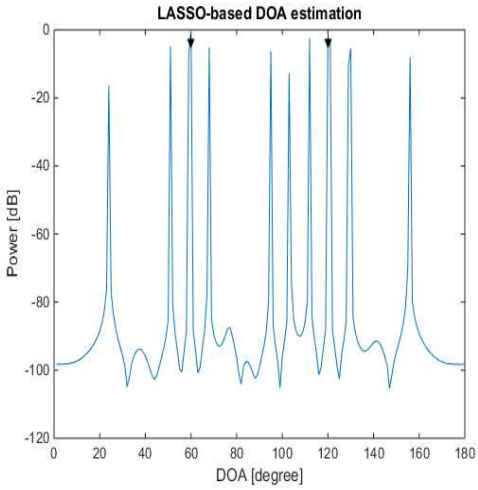

(a) LASSO

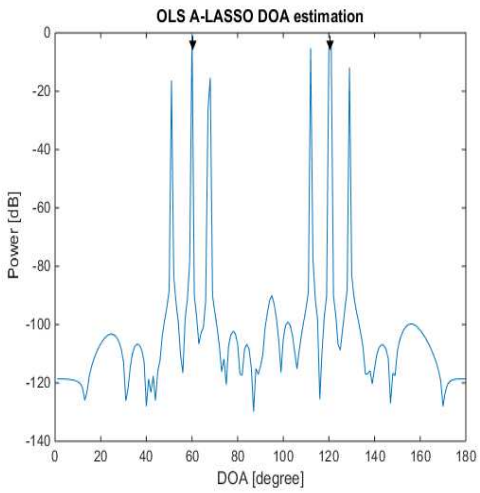

(b) OLS A-LASSO

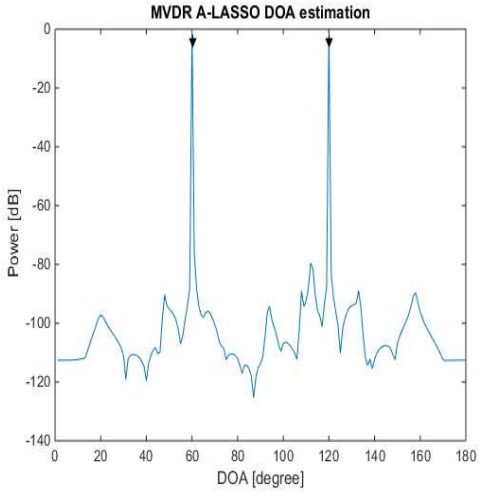

(c) MVDR A-LASSO

Figure 3.5: Performance of LASSO, OLS A-LASSO and MVDR A-LASSO, for two source signals at DOAs 60° and 120°, 10 snapshots, SNR = 0 dB and one iteration. (a) LASSO; (b) OLS A-LASSO; and (c) MVDR A-LASSO.

In the second experiment, we investigate the performance of the proposed MVDR A-LASSO algorithm as we vary SNR and compare it with that of LASSO and OLS A-LASSO. Two source signals are assumed to impinge on the sparse array from DOA of 60° and 120°. The performances of the proposed MVDR A-LASSO algorithm, along with that of the conventional LASSO and OLS A-LASSO are shown

in Figure 3.6. It is clear from this figure that the MVDR A-LASSO algorithm outperforms both the LASSO and OLS A-LASSO algorithms for all SNR.

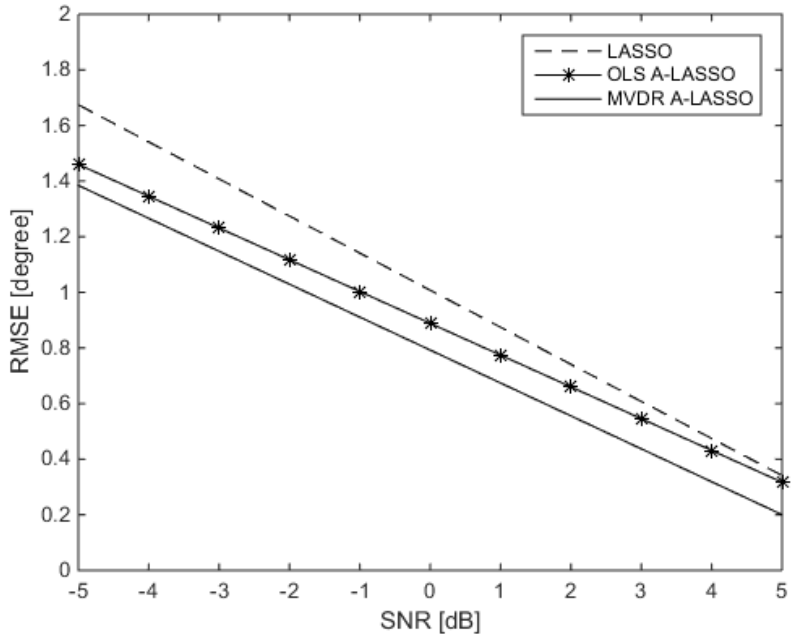

Figure 3.6: Performance of the three LASSO algorithms versus SNR, for two source signals at DOAs 60° and 120°, 10 snapshots and after one iteration of the MVDR A-LASSO and OLS A-LASSO algorithms.

Assuming now that L (the number of source signals) is known, we compare the performance of the LASSO algorithms with that of the MVDR algorithm and that of MUSIC. For that purpose, two ULAs, one consisting of six elements and another consisting of 23 elements, are used to evaluate the performance of MUSIC, while only the ULA with six elements is considered for the MVDR algorithm. However, for the three LASSO algorithms, the real array used is as shown in Figure 3.4, namely with six elements. The performance of the various algorithms as SNR is varied is shown in Figure 3.7. It is observed from the figure that all three LASSO algorithms outperform the MUSIC algorithm, as well as the MVDR algorithm, even when 23 elements are used in the array.

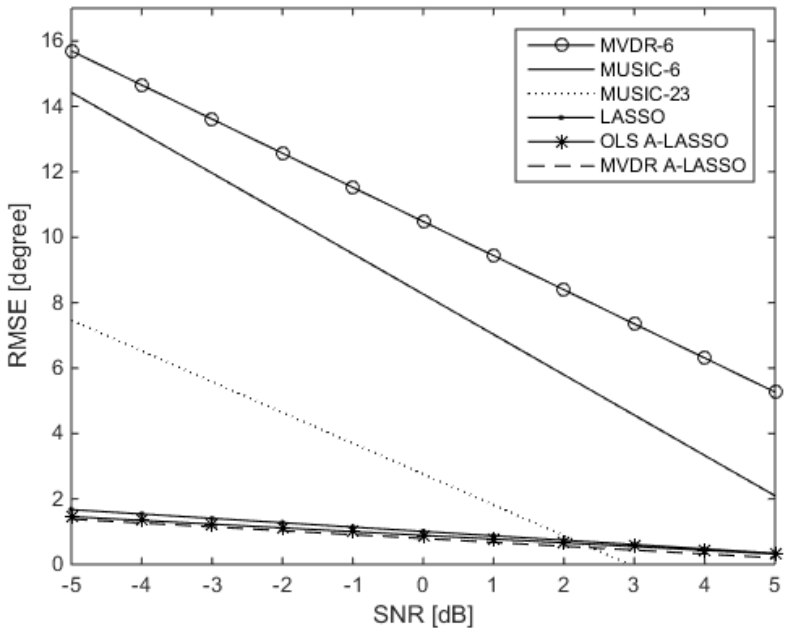

Figure 3.7: Performance of the LASSO algorithms as SNR is varied in comparison with that of MVDR and MUSIC algorithms, for two source signals at DOAs 60° and 120°, 10 snapshots and after one iteration of the MVDR A-LASSO and OLS A-LASSO algorithms.

We investigate, in the third experiment, the capabilities of the proposed algorithms in detecting the sources even when the number of sources exceeds the number of physical array elements. In other words, the proposed algorithm is for an underdetermined DOA scenario. For that purpose, two ULAs, one consisting of six elements and another consisting of 23 elements, are used to evaluate the performance of MVDR, while only the ULA with 23 elements is considered for the MUSIC algorithm. However, for the three LASSO algorithms, the real array used is as shown in Figure 3.4, namely with six elements. Let 11 source signals impinge the array from uniformly-distributed DOAs over $\theta = [30°, 150°]$. The snapshots number is chosen to be 70, and SNR is set to be -5 dB. All of the LASSO algorithms can easily identify 11 peaks (even after just one iteration of the MVDR A-LASSO and OLS A-LASSO algorithms), as seen from Figures 3.8,3.9, and 3.10, while MVDR and MUSIC fail to identify the source signals.

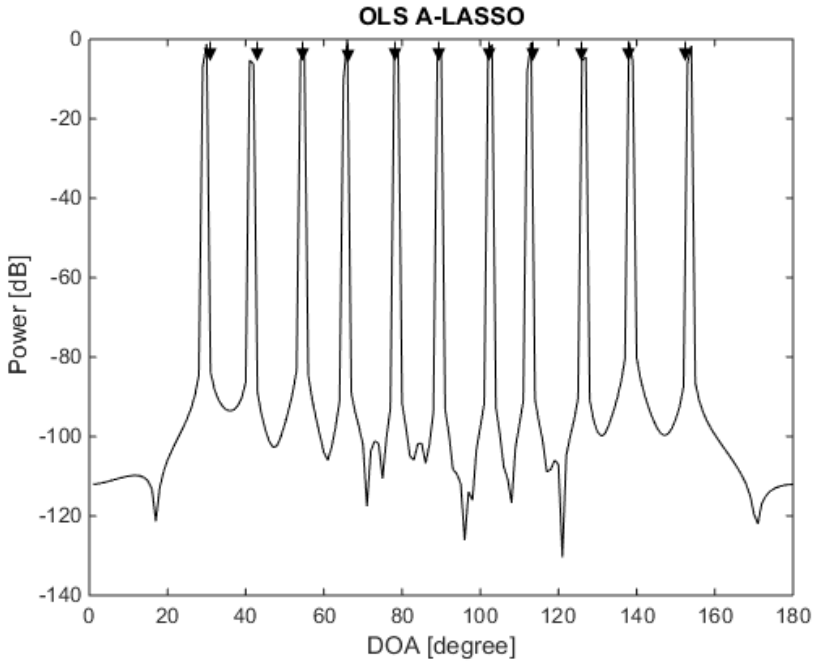

(a)

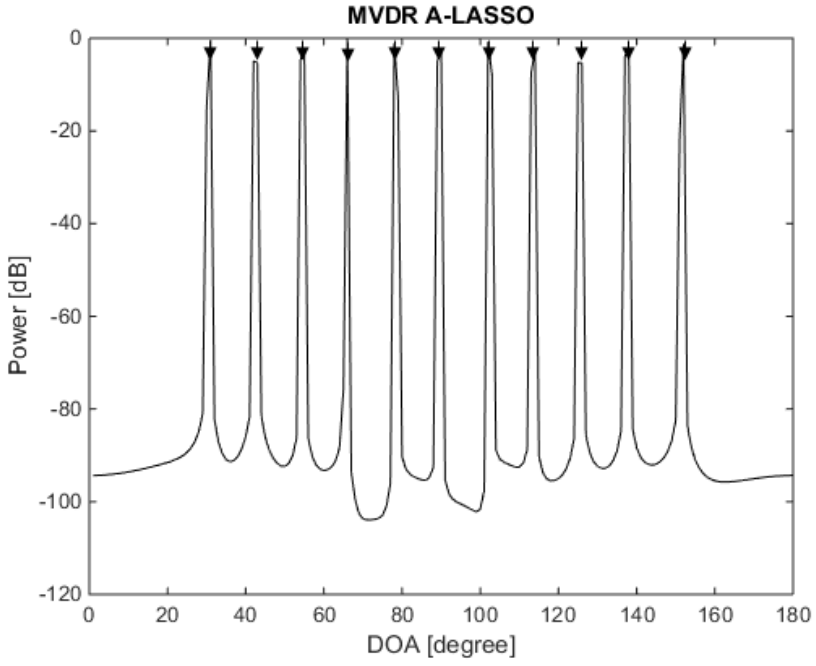

(b)

Figure 3.8: DOA estimation when the number of sources is more than the number of sensors: (a) After one iteration of OLS A-LASSO and (b) After one iteration of MVDR A-LASSO.

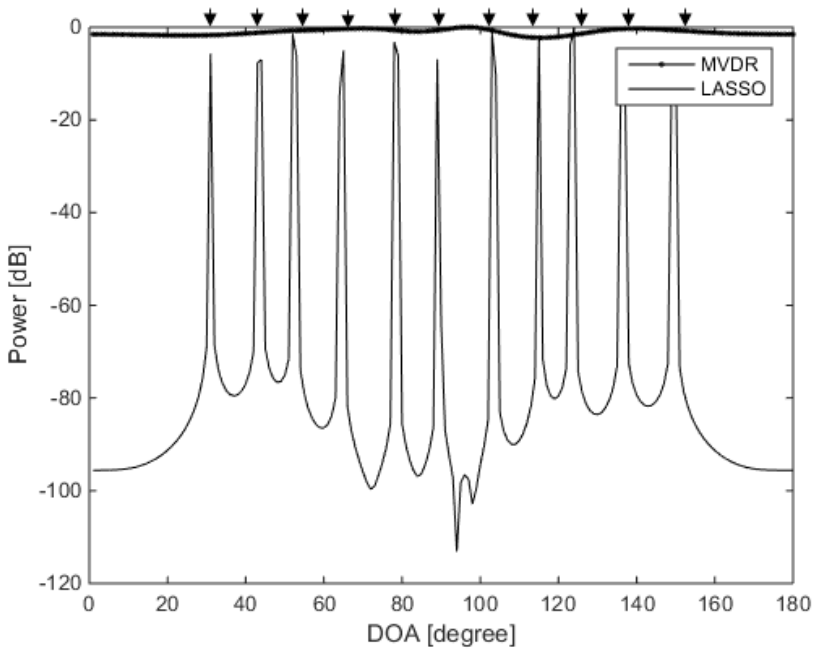

(a)

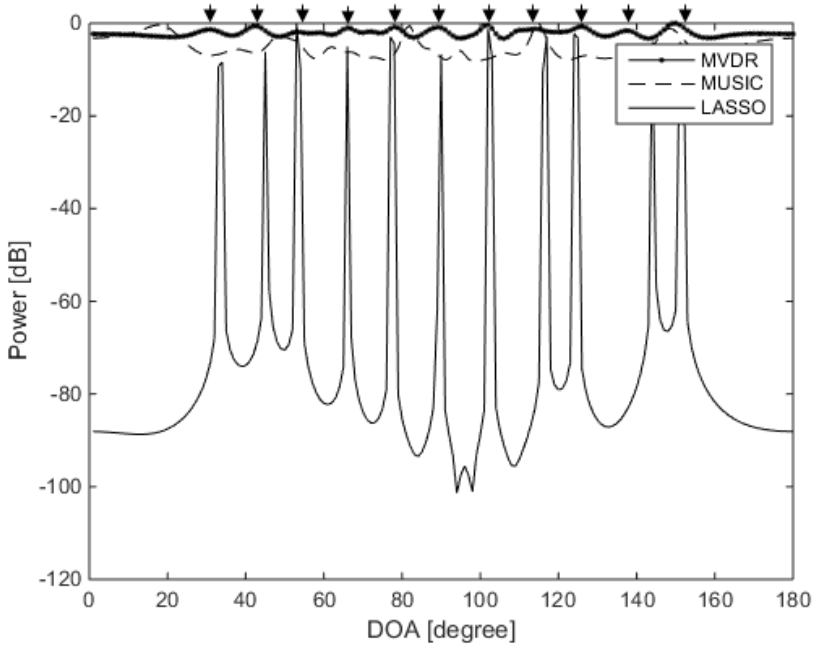

(b)

Figure 3.9: DOA estimation when the number of sources is more than the number of sensors: (a) Classical LASSO and MVDR using a six-element array; (b) Classical LASSO, MVDR and MUSIC using a 23-element array.

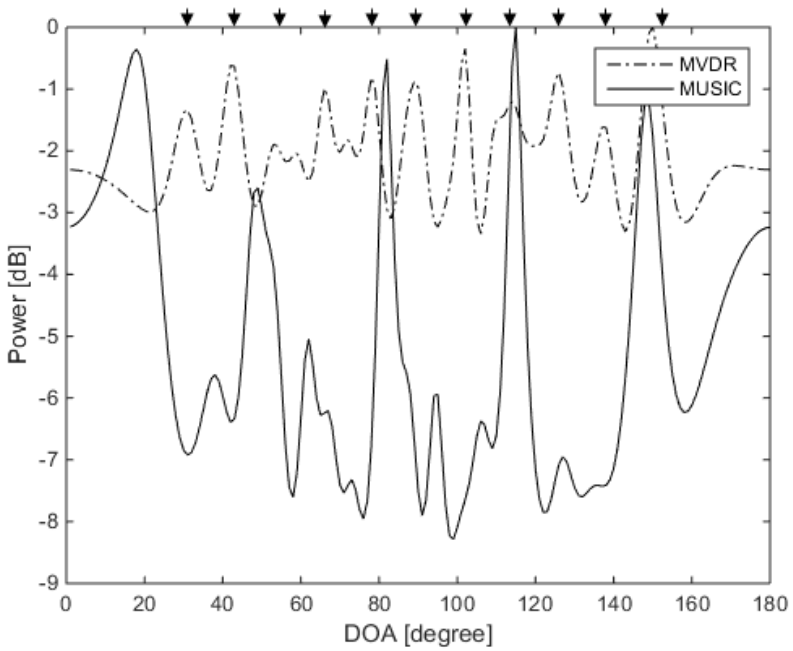

Figure 3.10: DOA estimation when the number of sources is more than the number of sensors: MVDR and MUSIC using a 23-element array.

In the fourth experiment, we examine the resolution of the proposed adaptive algorithms in comparison with that of MVDR and MUSIC. Two spatially-correlated equi-power signals are assumed to impinge on the array from the DOAs of 85° and 95°. The SNR is set to 15 dB. Figure 3.11 illustrates the results. Two peaks can easily be identified in the case of the three LASSO algorithms, while in the case of MVDR and MUSIC algorithms, the two peaks are merged into one.

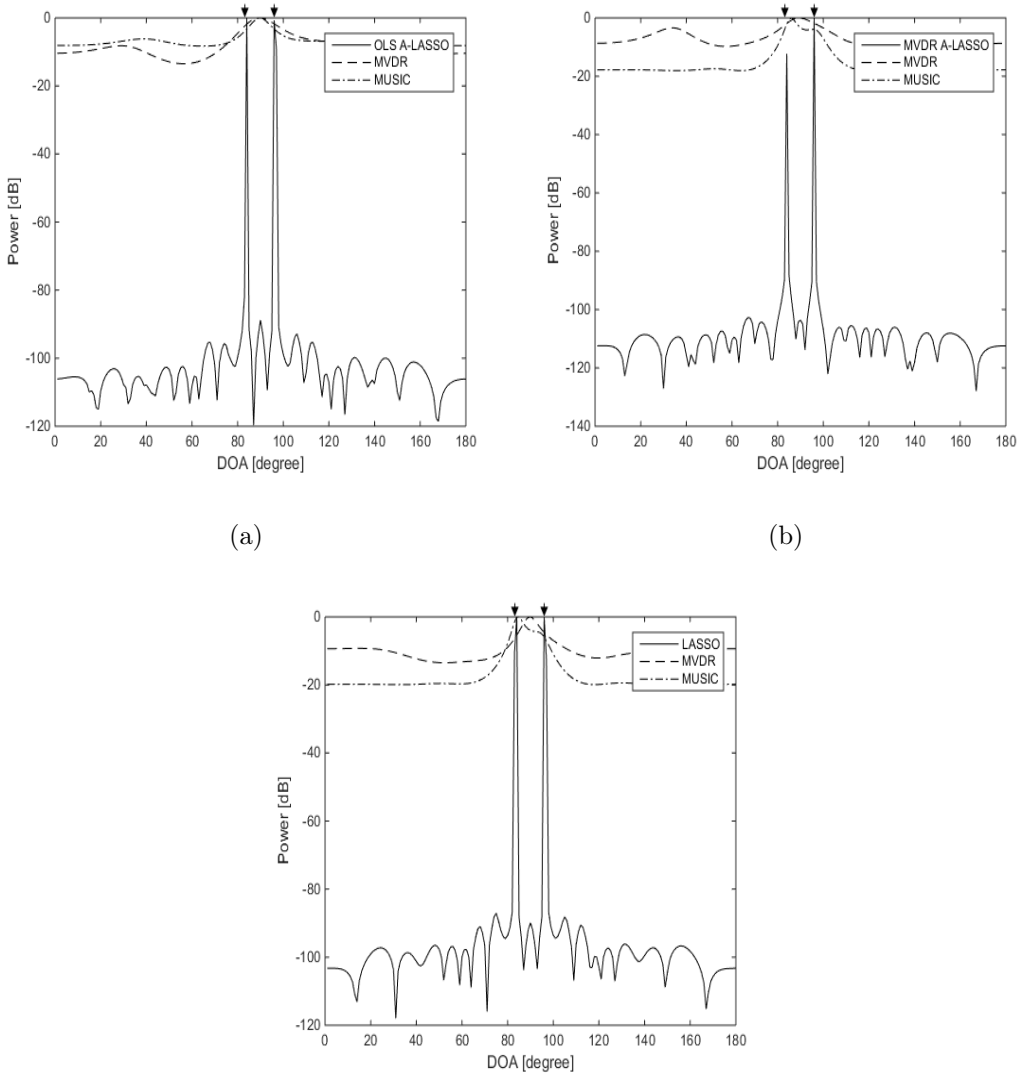

Figure 3.11: DOA estimation for spatially-closed two-source signals using LASSO algorithms, for two source signals at DOAs 85° and 95°, 10 snapshots, SNR = 15 dB and one iteration of the MVDR A-LASSO and OLS A-LASSO algorithms. (a) OLS A-LASSO after the first iteration; (b) MVDR A-LASSO after the first iteration; and (c) the classical LASSO algorithm.

In the fifth experiment, we examine the performance of our proposed algorithms for the detection of correlated source signals. Two fully-correlated (coherent) source signals are assumed to impinge on the array from directions of 60° and 100° with SNR set to 15 dB. Figure 3.12 shows that the three LASSO algorithms can

resolve the two sources, revealing the capability of the algorithms in detecting correlated source signals. It is also clear that MVDR and MUSIC fail to distinguish the two sources.

From the above experiments, it is seen that the performance of the A-LASSO-based DOA estimation is superior to that of the MVDR (for which L is not required to be known) and that of MUSIC (for which L must be known in advance). Further, we also conclude that the performance of the classical LASSO is inferior to that of the two A-LASSO schemes, even though it exhibits a performance better than that of MVDR and MUSIC. In view of these results, we will not consider MVDR, MUSIC or the classical LASSO algorithm further in our study.

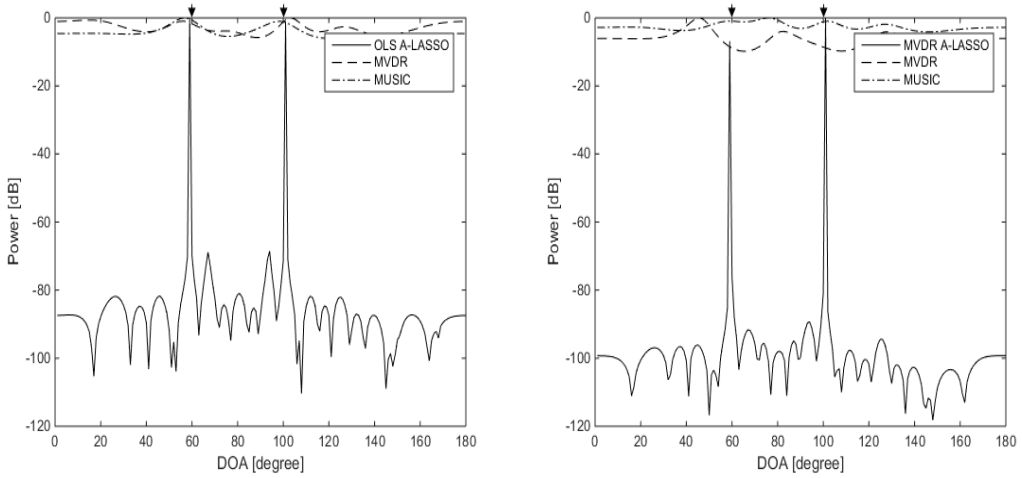

(a)

(b)

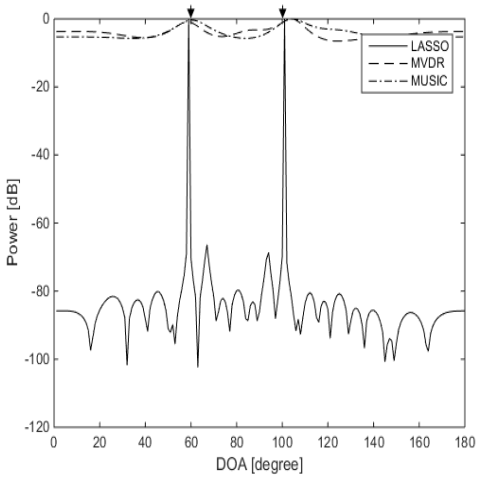

(c)

Figure 3.12: DOA estimation for two correlated source signals using LASSO algorithms, for two source signals at DOAs 60° and 100°, 10 snapshots, SNR = 15 dB and one iteration of the MVDR A-LASSO and OLS A-LASSO algorithms. (a) OLS A-LASSO after the first iteration; (b) MVDR A-LASSO after the first iteration; and (c) the classical LASSO algorithm.

In the sixth experiment, we test the performance of the OLS A-LASSO and MVDR A-LASSO algorithms in a low SNR situation. For this purpose, we consider two source signals with DOAs of 60° and 120°, set SNR to 0 dB and snapshots to 10. The results for the two A-LASSO algorithms are shown in Figure 3.13. It can be seen

from this figure that MVDR A-LASSO can detect the source signals after the first iteration itself, while OLS A-LASSO needs more iterations to be able to eliminate all of the false peaks. This can be explained by looking at the initial weights for both the OLS A-LASSO and MVDR A-LASSO algorithms. Figure 3.13(d) illustrates the initial weights for OLS A-LASSO and MVDR A-LASSO; it can be seen that the weights using the MVDR A-LASSO algorithm are relatively smooth compared to those of OLS A-LASSO. Furthermore, it can be seen that the OLS A-LASSO weight consists of many peaks that affect its performance and lead to false source signal peaks.

The DOA performance is investigated after five and 15 iterations for both the OLS A-LASSO and MVDR A-LASSO in the seventh experiment. Two signal sources are assumed to be impinging the array from DOAs of 60° and 120°, while the SNR changes. The snapshot number is chosen to be 10; the results are shown in Figure 3.14. It can be seen from the figure that, in terms of RMSE, MVDR A-LASSO outperforms the OLS A-LASSO algorithms.

Based on the results of the previous experiments (Figures 3.5, 3.6, 3.13 and 3.14), it is clear that MVDR A-LASSO outperforms OLS A-LASSO. Hence, OLS A-LASSO will not be considered in the rest of this chapter.

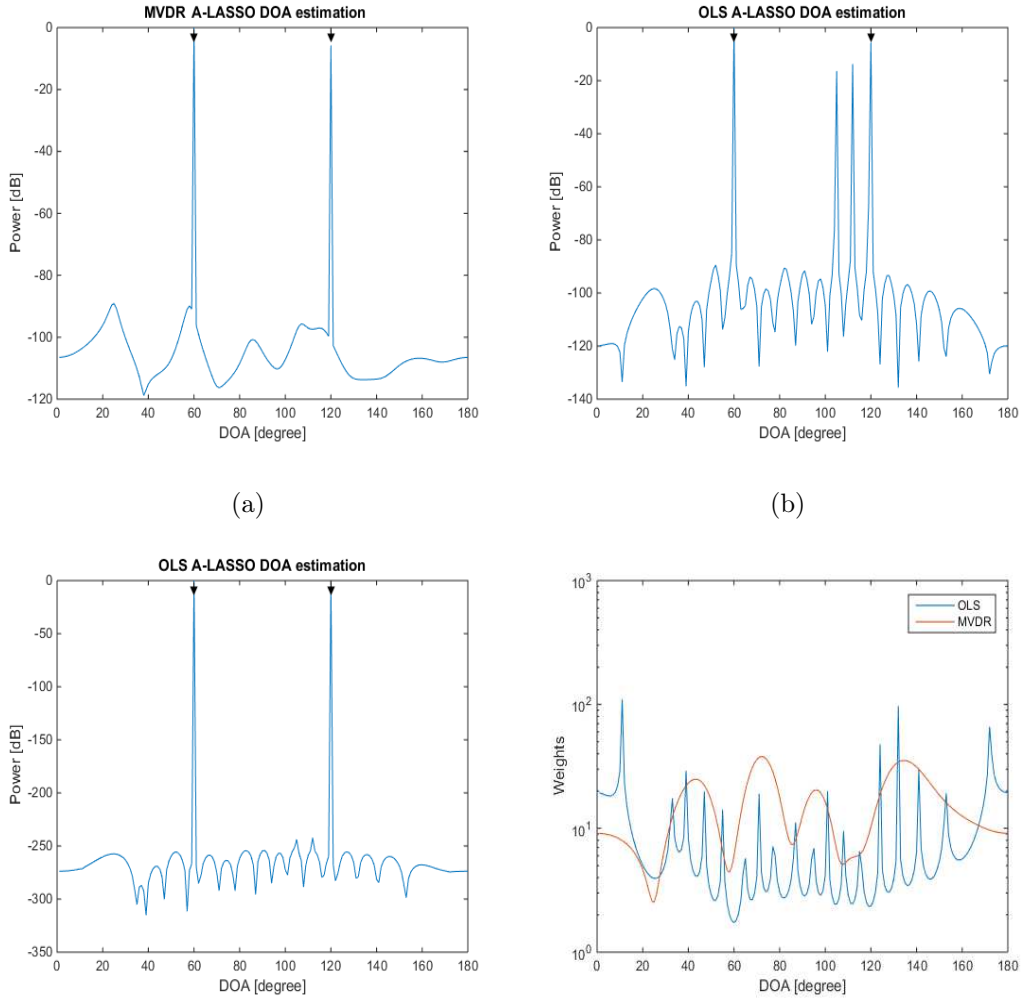

Figure 3.13: DOA estimation using A-LASSO algorithms, for two source signals at DOAs 60° and 120°, 10 snapshots, SNR = 0 dB. (a) MVDR A-LASSO after the first iteration; (b) OLS A-LASSO after the first iteration; (c) OLS A-LASSO after five iterations; and (d) initial weights of the two algorithms.

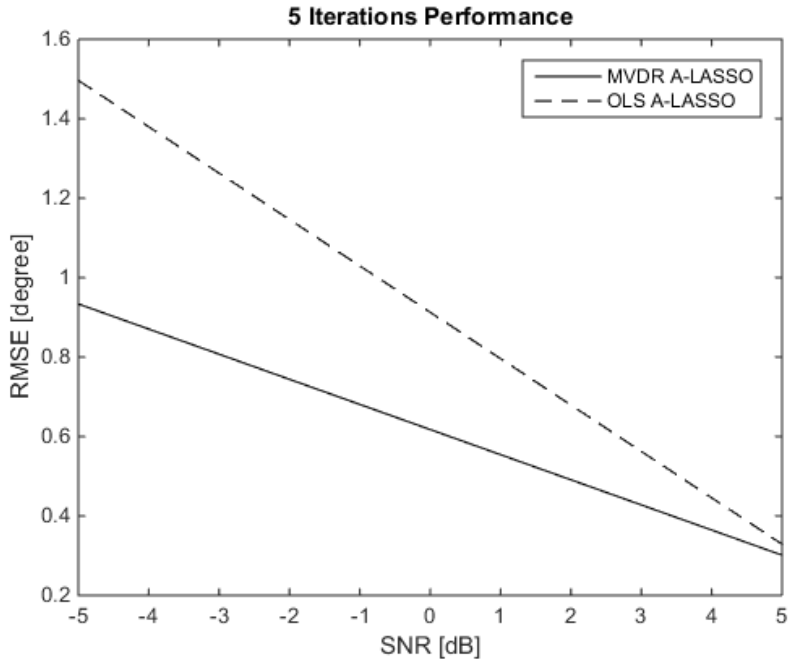

(a)

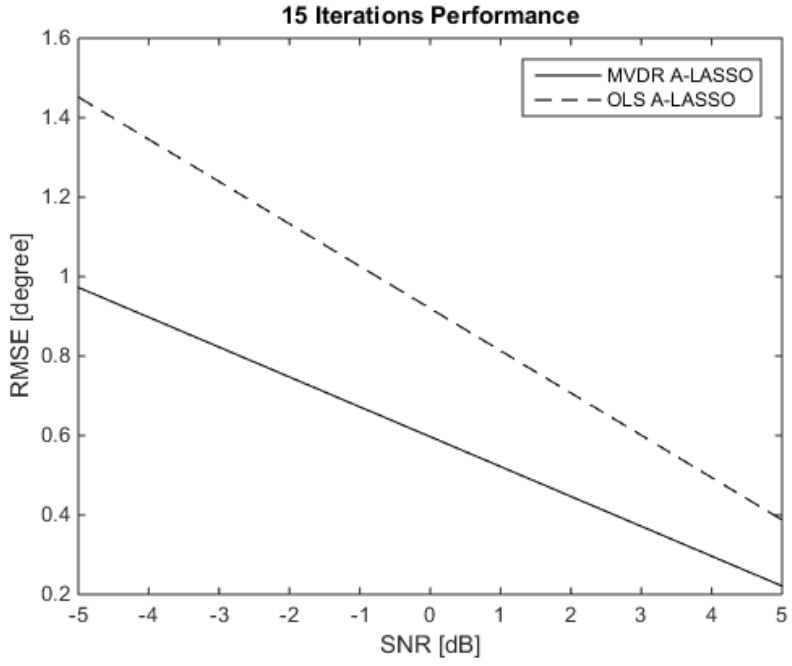

(b)

Figure 3.14: DOA estimation of two source signals at DOAs 60° and 120°, and 10 snapshots (a) after five iterations and (b) after 15 iterations, using the A-LASSO algorithms.

The eighth experiment investigates the DOA estimation using MVDR A-LASSO as we increase the number of iterations. Let two source signals with DOAs of 60° and 120° impinge on the array, and let the SNR be -5 dB and 50 snapshots be used. The results for the first five iterations are shown in Figure 3.15. It is seen from the figure that, after the first iteration, fake source signal peaks appear. As the algorithm runs, the weights corresponding to the fake source signals become very large, whereas those of the actual source signals remain constant. Hence, the weights corresponding to the false source signals damp the false peaks, while those of the real source signals remain constant. As a consequence, as the number of iterations increases, it is clear that only the real source signal peaks remain. Furthermore, it can be observed that the sidelobe ratio (SLR) after the fifth iteration is more than twice that after the first iteration.

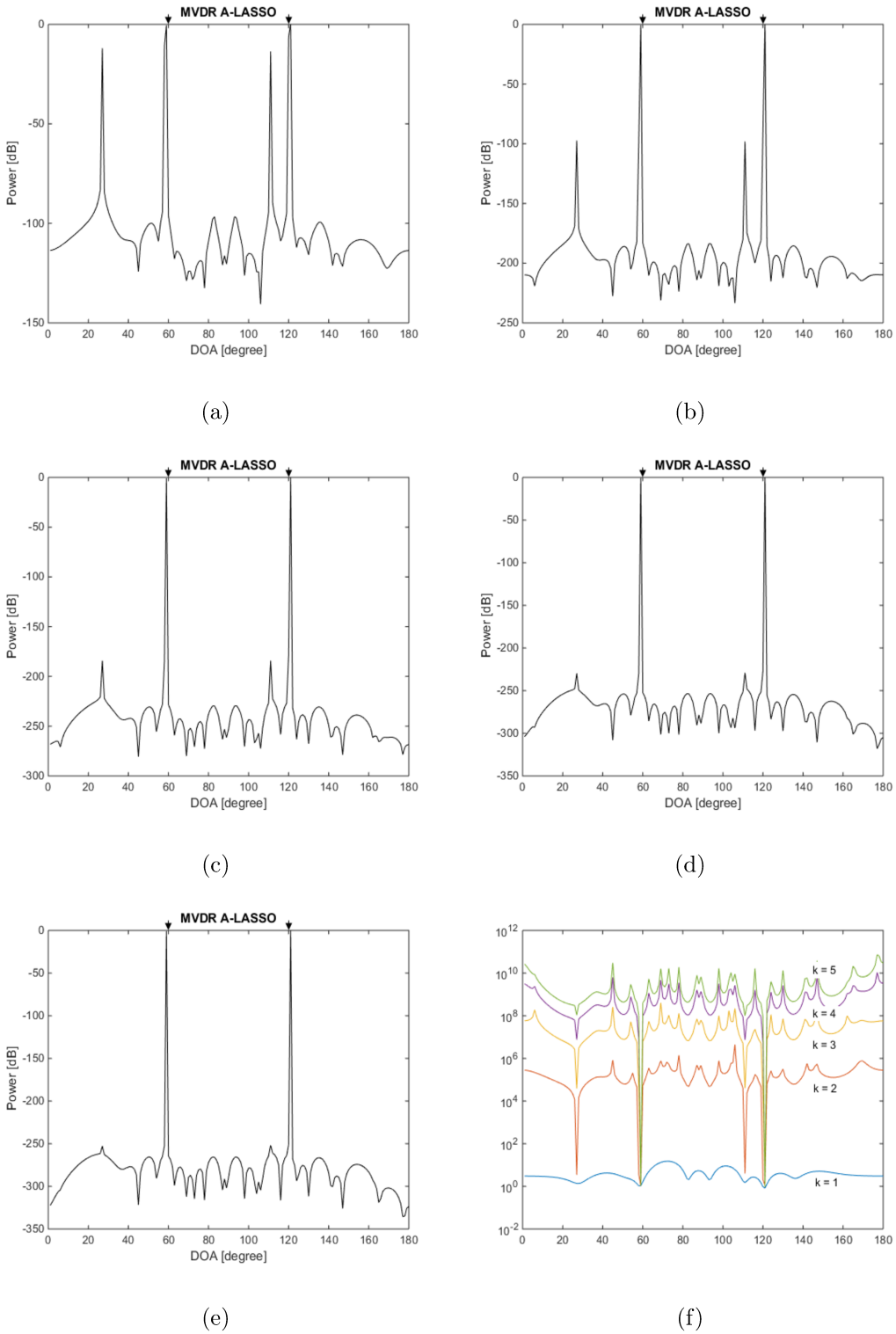

Figure 3.15: DOA estimation in the case of two source signals at DOAs 60° and 120°, SNR = −5 dB, 50 snapshots using MVDR A-LASSO algorithm. (a–e) after $1-5$ iterations; and (f) MVDR A-LASSO weights as the number of iterations k varies.

We now examine the performance of the proposed MVDR A-LASSO algorithm at low and very low SNR situations in the ninth experiment. The same settings as in the previous experiment are used, except that the SNR is set to -10 dB and -15 dB. The snapshot number is set to 150 for the first case and 200 for the second one. The results are as shown in Figure 3.16 for SNR of -10 dB and Figure 3.17 for that of SNR set to be -15 dB. It can be seen from Figures 3.16 and 3.17 that the two signals can be identified after only five iterations, even for very low SNR conditions. However, more snapshots are needed in this situation. Thus, it is a trade-off between SNR and the number of snapshots required so that the DOA of the source signals can be correctly identified. It is further observed that even after three iterations, we are able to identify the two source signals.

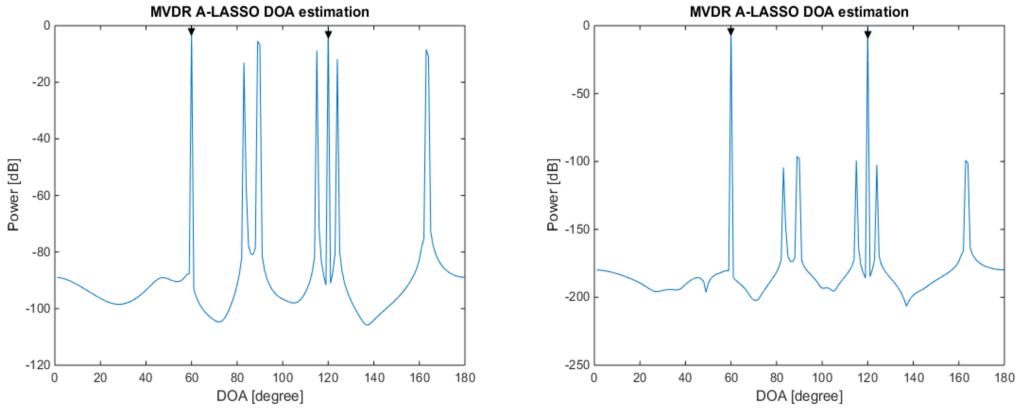

(a) 1st iteration

(b) 2nd iteration

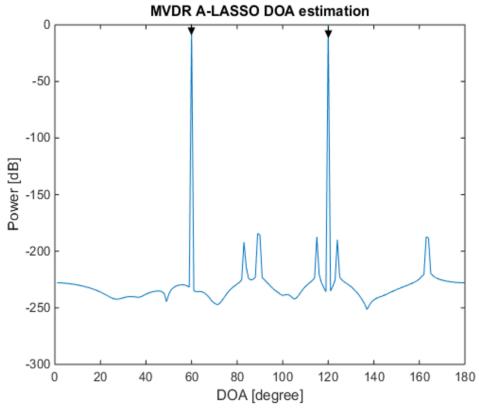

(c) 3rd iteration

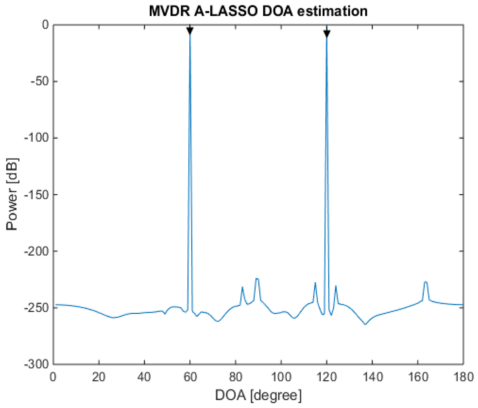

(d) 4th iteration

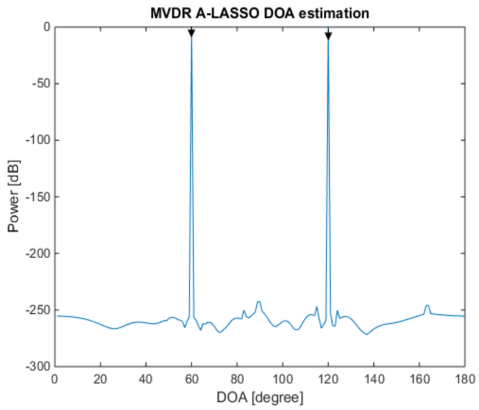

(e) 5th iteration

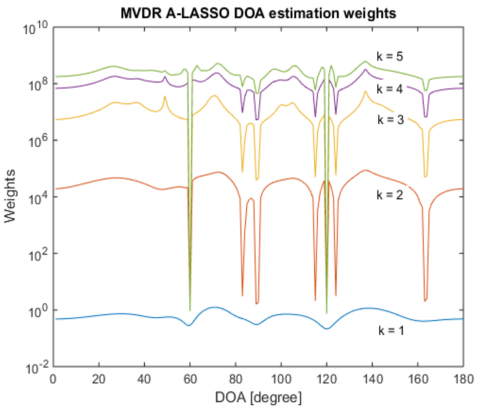

(f) MVDR A-LASSO weights

Figure 3.16: DOA estimation in the case of two source signals at DOAs 60° and 120°, SNR = −10 dB, 150 snapshots, using the MVDR A-LASSO algorithm. (a–e), after one to five iterations; and (f) MVDR A-LASSO weights as the number of iterations k varies.

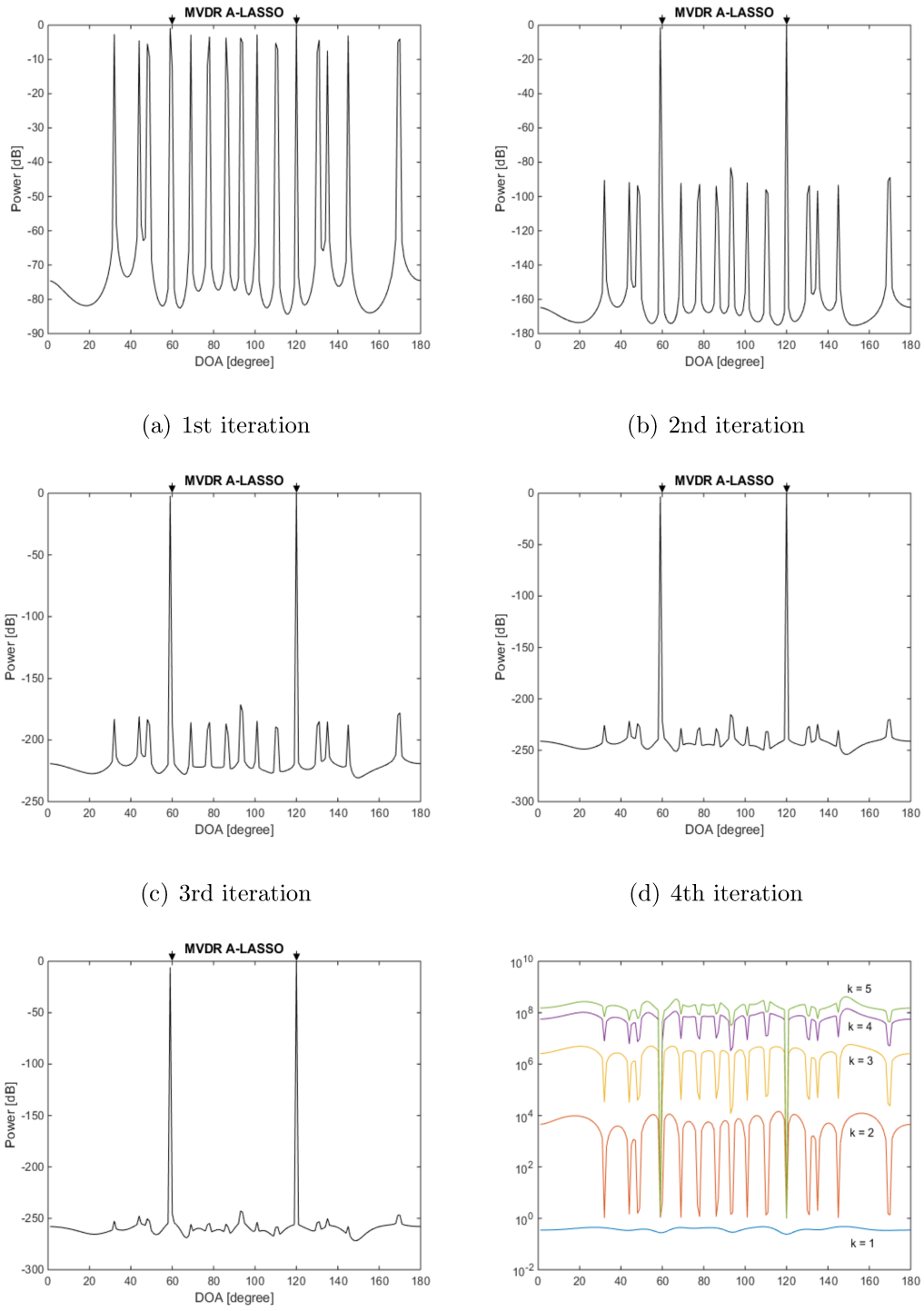

(a) 1st iteration

(b) 2nd iteration

(c) 3rd iteration

(d) 4th iteration

(e) 5th iteration

(f) MVDR A-LASSO weights

Figure 3.17: DOA estimation, two source signals at DOAs 60° and 120°, SNR = −15 dB, 200 snapshots, using the MVDR A-LASSOalgorithm. (a–e) after one to five iterations; and (f) MVDR A-LASSO weights as the number of iterations k varies.

In the tenth experiment, we study the effect of changing the number of snapshots on the performance of MVDR A-LASSO. We consider two source signals arriving from DOAs of 60° and 120° with SNR changing from −5 dB to 5 dB. The results are shown in Figure 3.18. It can be observed from this figure that increasing the number of snapshots leads to an enhancement in the performance, in terms of RMSE. In other words, it is a trade-off between the number of snapshots and the RMSE. For low and very low SNR, the number of snapshots has to be increased, for better performance.

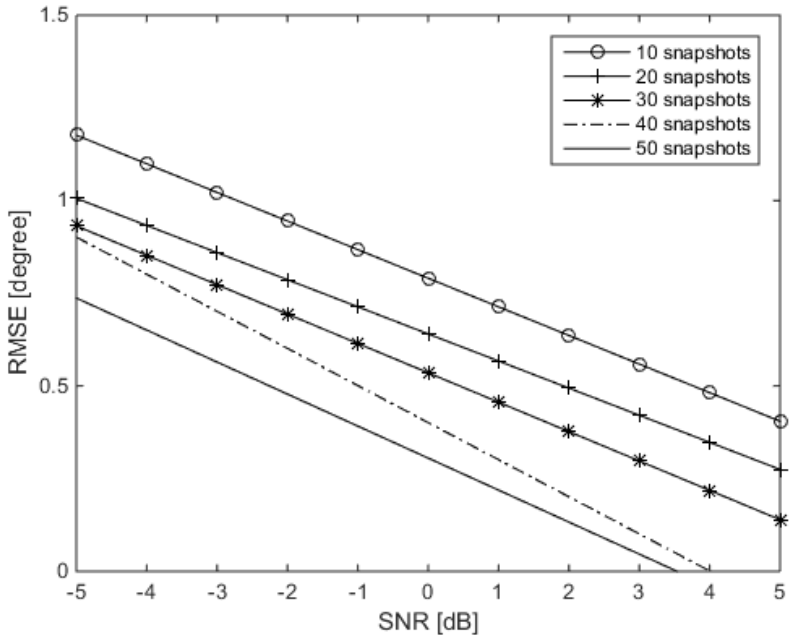

Figure 3.18: MVDR A-LASSO DOA estimation performance versus the number of snapshots, two source signals with DOAs 60° and 120°, $\gamma = 0.5$.

The eleventh experiment involves the investigation of the effect of changing γ. Two source signals impinging the array from DOAs of 60° and 120° are considered, the SNR being set to −5 dB while changing γ. Figure 3.19 shows the residual, R, in terms of the absolute value of ($\|\mathbf{y} - \Phi\bar{\mathbf{s}}_{k+1}\|_2^2 - \|\mathbf{y} - \Phi\bar{\mathbf{s}}_k\|_2^2$), where k is the iteration number, for 10 simulations. From this figure, it is clear that increasing the number of snapshots decreases the residuals for all three cases of $\gamma = 0.25, 0.5$ and

0.75. Furthermore, the residual after the end of the first iteration using $\gamma = 0.5$ is smaller than when $\gamma = 0.25$ or 0.75, even when the number of snapshots is increased. From Figure 3.19b, it can be seen that, at the end of the second iteration, the residual corresponding to $\gamma = 0.25$ is smaller than that corresponding to $\gamma = 0.5$ or $\gamma = 0.75$. However, for none of these values of γ have we achieved convergence by the end of the second iteration. At the end of Iteration 3, the convergence of the residual is achieved only for the weight factor $\gamma = 0.5$. However, since the residual for $\gamma = 0.5$ at the end of the first iteration is less than that of $\gamma = 0.25$, the signal sources are identified at the end of the first iteration (Figure 3.13e), while that of $\gamma = 0.25$ needs more iterations (Figure 3.13a–c). The effect of γ on the DOA estimation, using the same previous source signals, with SNR chosen to be -5 dB is shown in Figure 3.20. In this case, 50 snapshots are used, while γ assumes values of $0.25, 0.50$ and 0.75. It can be seen from this figure that $\gamma = 0.5$ provides the right signal sources at the end of the first iteration with a smaller residual than for $\gamma = 0.25$ or 0.75. On the other hand, selecting $\gamma = 0.25$ leads to more fake source signals being detected, and as a consequence, more iterations are needed to identify the real sources, while using $\gamma = 0.75$ leads to misidentifying one of the source signals.

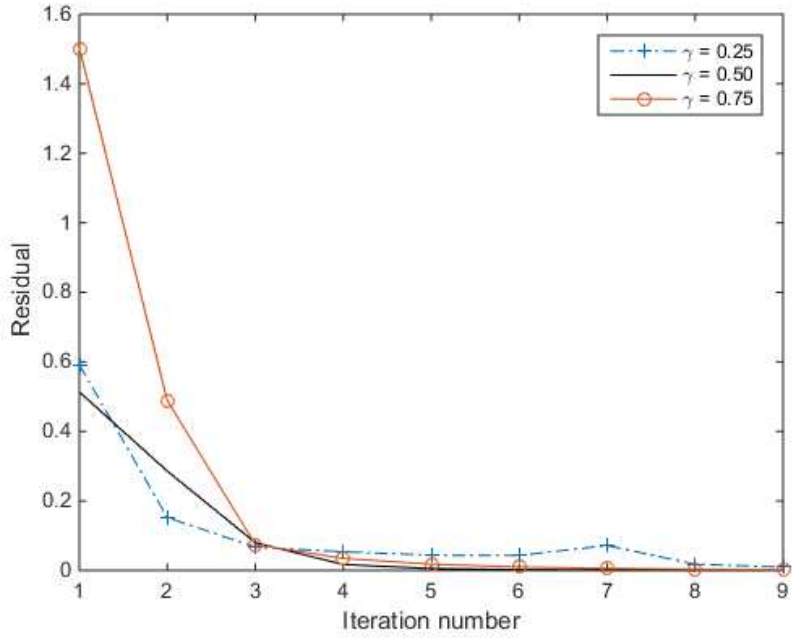

(a)

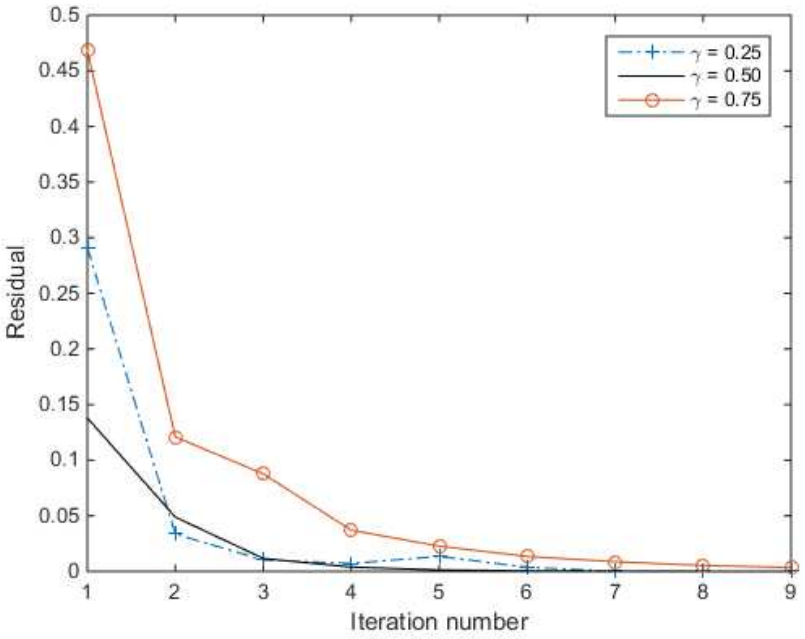

(b)

Figure 3.19: The residual for two source signals at DOAs 60° and 120°, with $\gamma = 0.25, 0.5$ and 0.75, 10 iterations, SNR $= -5$ dB using the MVDR A-LASSO algorithm, (a) 10 snapshots and (b) 50 snapshots.

The twelfth experiment involves the investigation of the effect of varying the angular separation between the source signals. Consider two source signals, the first one held fixed at DOA of 60°, while the second one with DOA ranging from 61° to 100° with steps of 1°. The SNR is set to be 10 dB; 10 snapshots are considered for the simulation; 100 trials for each point; and a sampling grid $\bar{\theta}_n \in [1^\circ : 180^\circ]$ chosen to be of 0.1° steps. Figure 3.21 illustrates the DOA estimation error as a function of the angular separation between the two source signals. It can be seen from this figure that the DOA estimation error is less than 2° for an angular separation $< 5^\circ$. This DOA estimation error is reduced to $< 0.4^\circ$ for an angular separation $\geq 6^\circ$.

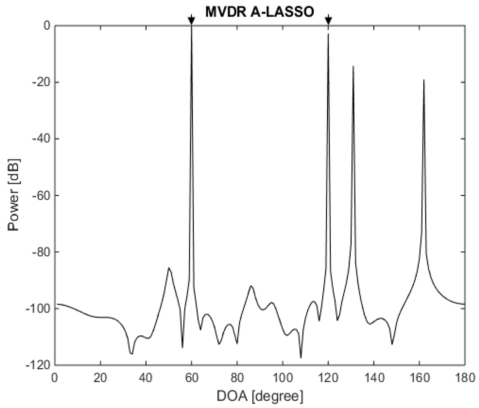

(a) $\gamma = 0.25$, 1st iteration

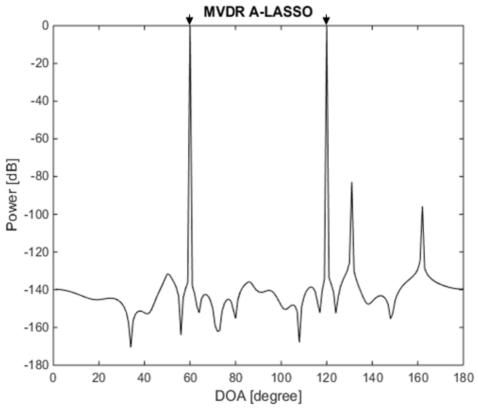

(b) $\gamma = 0.25$, 2nd iteration

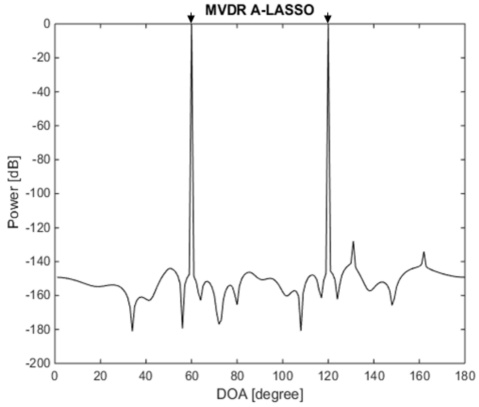

(c) $\gamma = 0.25$, 3rd iteration

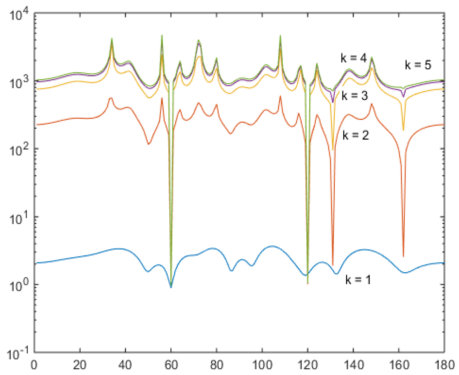

(d) $\gamma = 0.25$, weights

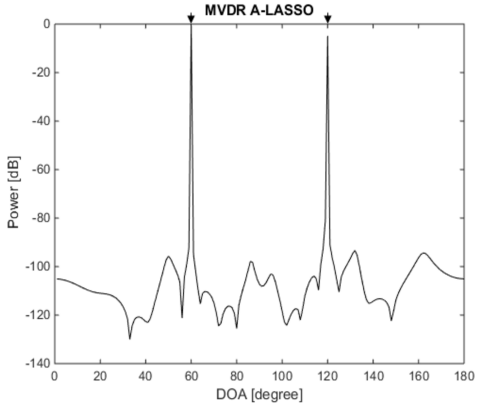

(e) $\gamma = 0.50$, 1st iteration

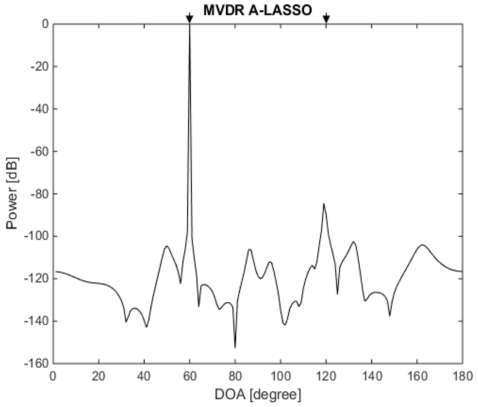

(f) $\gamma = 0.75$, 1st iteration

Figure 3.20: DOA estimation of two source signals at DOAs 60° and 120°, 50 snapshot, SNR $= -5$ dB, using the MVDR A-LASSO algorithm, (a)–(d) $\gamma = 0.25$; (e) $\gamma = 0.50$; and (f) $\gamma = 0.75$.

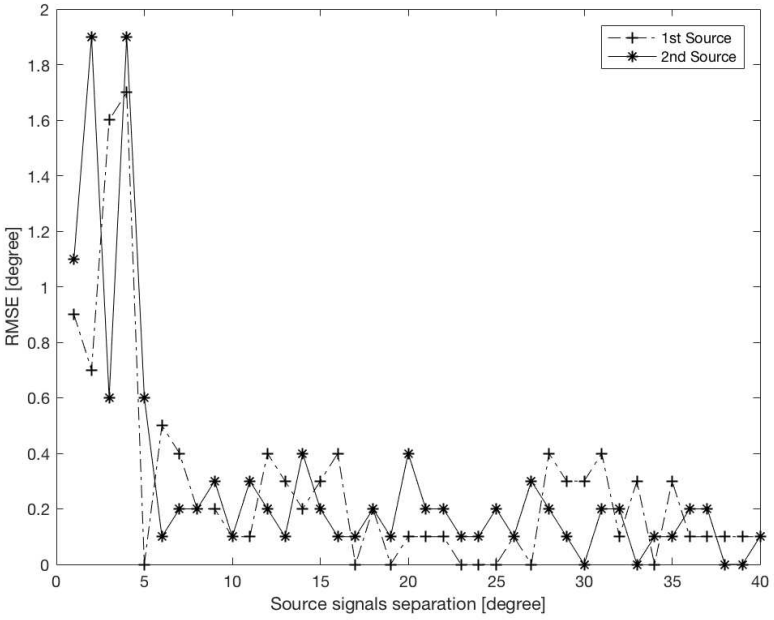

Figure 3.21: RMSE for each of the signals as a function of the separation between two sources, SNR = 10 dB, 10 snapshots and one iteration of MVDR A-LASSO.

3.7 Simulation Results for Fluctuating Signal Sources

Consider a sparse linear two-level nested array, for which M is odd, consisting of $M = 7$ elements, three of which are in the first level, and four in the second level. Investigating the array output by applying Equations (3.1) to (3.3) and extracting the equivalent distinct virtual elements from the virtual array manifold ($\mathbf{A}^* \odot \mathbf{A}$), one obtains a virtual ULA containing $\bar{M} = 31$ elements. The sampling grid $\bar{\theta}_n \in [1^\circ : 180^\circ]$ that covers Ω is chosen to be in steps of 1° and $d = \lambda/2$, where λ is the wavelength of the propagating waves.

The power of the fluctuating simulated source signals is assumed to follow the Chi-squared distribution as given in Section 2.2 and the sources are assumed to be uncorrelated with one another or with noise. The signal sources are modeled as $e^{j2\pi f_d t}$ where f_d is the Doppler frequency. For Swerling sources of type I as well as III, each scan is assumed to contain 10 snapshots.

In the first experiment, we investigate the performance of the MVDR A-LASSO estimation technique in terms of RMSE given by Equation (3.19), as we vary SNR. Two fluctuating source signals of the same type are assumed to impinge on the nested array from fixed DOA of 60° and 120°. The SNR is varied from −5 dB to 10 dB. The number of snapshots is set to be 10 and 50. The DOA estimation error for non-fluctuating source signal is also included in the figures as a reference, where again the number of snapshots is set to 10 and 50. These numbers correspond respectively to 1 and 5 scans for Swerling source types I and III.

The simulations results are as shown Fig. 3.22. From this figure, it can be seen that the non-fluctuating sources have the lowest RMSE, as expected. It is noted that the performance can be improved by increasing the number of snapshots. It is seen from the figure that by increasing the number of snapshots to 50 from 10, the DOA estimation error for sources can be reduced by at least 40%.

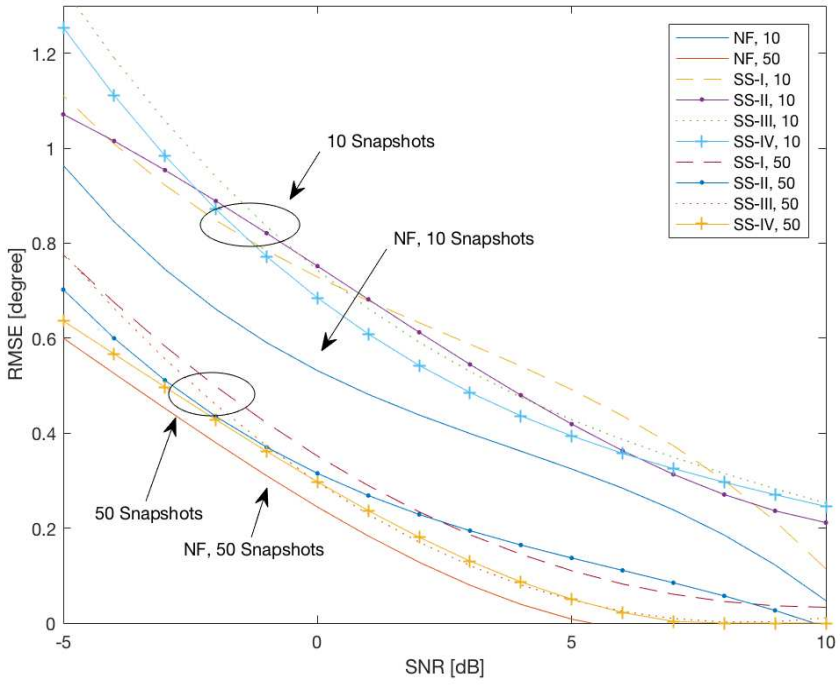

Figure 3.22: Performance of MVDR A-LASSO as SNR is varied, for two fluctuating source signals at DOAs 60° and 120°, using different Swerling source signals models.

In the second experiment, we investigate the effect of varying the angular separation between the Swerling source signals. Consider two fluctuating source signals, the first one with a fixed DOA of 60° while the DOA of the second ranges from 65° to 110° in steps of 5°. The SNR is set 0 dB, 10 snapshots are considered for the simulation and 100 trials for each observation point.

Fig. 3.23 illustrates the RMSE versus the angular separation for the different Swerling sources. Results for RMSE for non-fluctuating source signals is also included for reference. The same number of snapshots is used for the non-fluctuating sources as for the fluctuating sources. It is noted that for angular separation of 5° or less, the two source signals cannot be identified as separate signals. Hence, the results are presented starting with a 10° separation.

From this figure, it is seen that the DOA estimation error for non-fluctuating sources is the lowest. Further, the errors for Swerling types II and IV are lower than that for types I and III. The DOA estimation errors can be reduced by increasing the number of snapshots (see previous experiments).

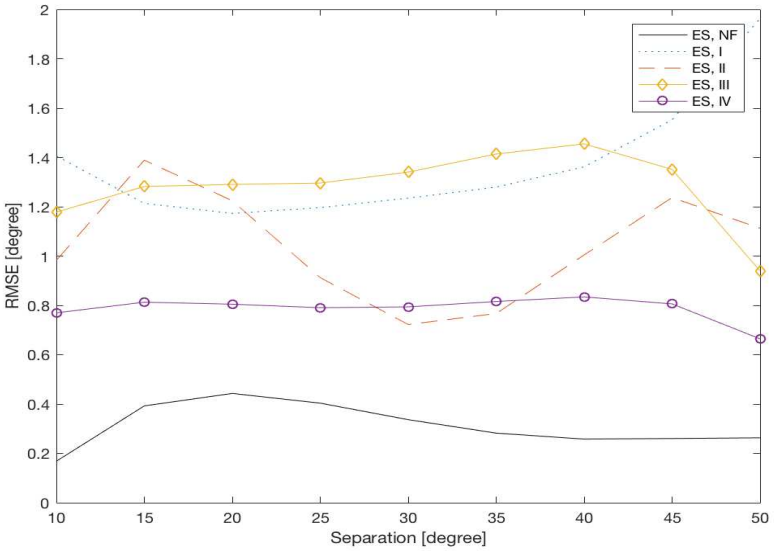

Figure 3.23: RMSE for two sources as a function of separation between the DOAs of the sources, SNR = 0 dB, 10 snapshots using MVDR A-LASSO.

In the third experiment, we investigate the probability of detection (POD) of the different Swerling source signals using the MVDR A-LASSO DOA estimation technique. For this purpose, let two fluctuating source signals impinge the sensor array from fixed DOAs of 60° and 120°. The POD measuring scenario is as follows: for each trial, the height of the peaks of the estimated source signals is measured. If the height is ≥ 0.5 (using normalized power scale), the peak is considered to correspond to the detection of a possible source signal; otherwise, the peak is considered no to correspond to a source signal. This operation is repeated 100 times for various values of SNR.

The POD corresponding to the different Swerling source signals using only 10 snapshots for non-fluctuating and Swerling source types II and IV, and $10, 50$ and 100 snapshots for Swerling source types I and III, are shown in Fig. 3.24. It is seen from Fig. 3.24(a) that the POD for non-fluctuating sources and Swerling source types II and IV are greater than 0.99. Further, it is observed from fig. 3.24(b) that the Swerling source types I and III need more number of snapshots than that required for types II and IV, in order to achieve an acceptable detection probability similar to that of types II and IV.

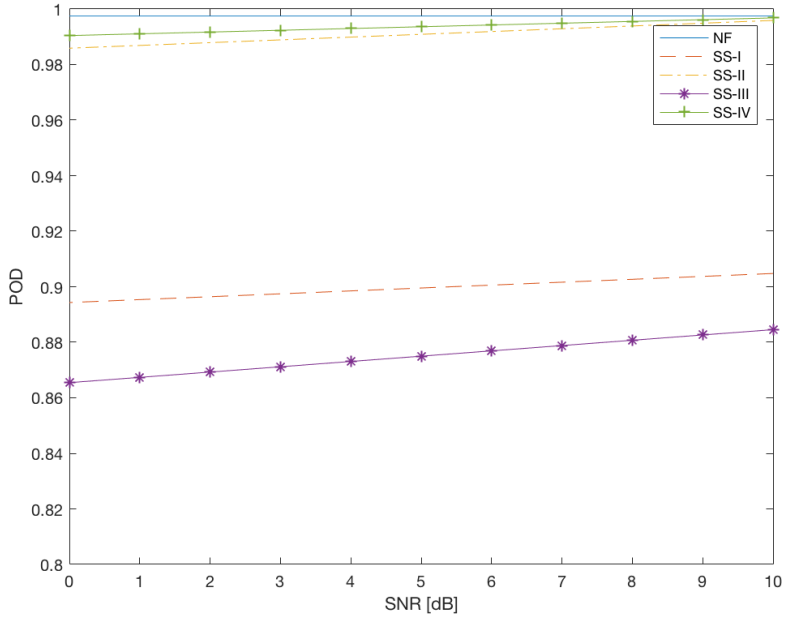

(a) 10 snapshots

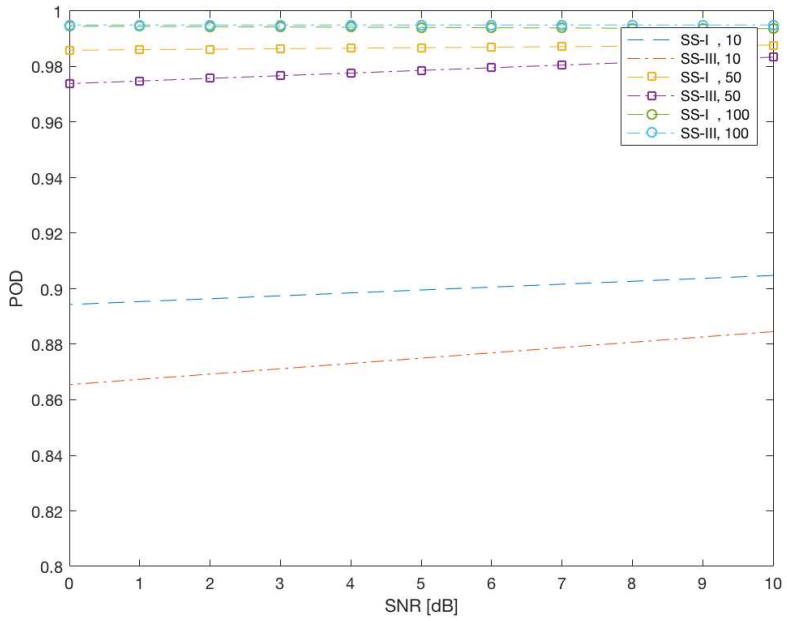

(b) 50 and 100 snapshots

Figure 3.24: Probability of detection of different Swerling source signals, two source signals with DOA of 60° and 120° using MVDR A-LASSO. (a) 10 snapshots and (b) 50 and 100 snapshots.

The following experiments are now conducted to investigate the capability of the proposed method to track the various sources along different trajectories. For this purpose, three different scenarios are considered for the simulations using two uncorrelated source signals. In the first one, the two sources are assumed to be moving in phase, which is designated as "*in phase*" scenario. In the second scenario, the two source signals are moving in opposite phases, which will be designated as "*opp-phase*" scenario. In the last scenario, one of the source signals has a fixed DOA, while DOA of the other is changing, and this scenario is designated as "*fixed vs. moving*".

Furthermore, the trajectory of a source signal is divided into four sections. In the first section, the source signal follows a sinusoidal trajectory while in the second section the direction of the source DOA is fixed. In the last two sections, the source follows a linear trajectory with positive and negative slopes, respectively. The proposed source signal trajectories are shown in Fig. 3.25.

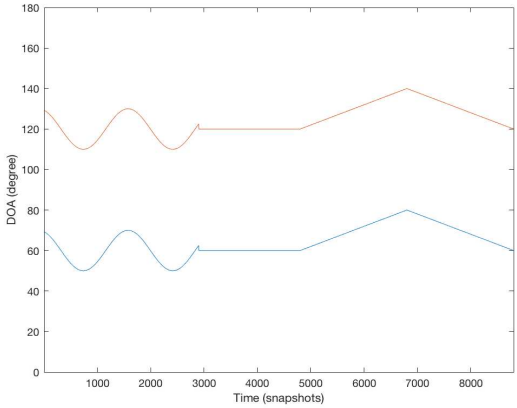

(a) In pahse

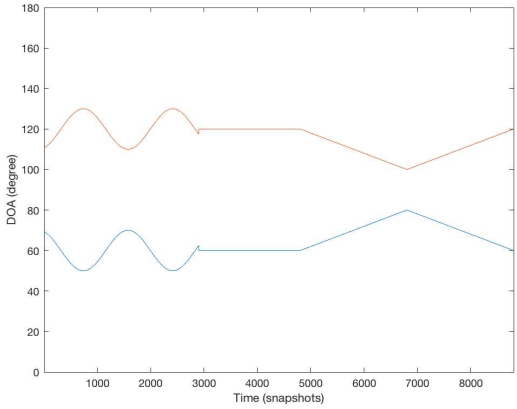

(b) Opp-phase

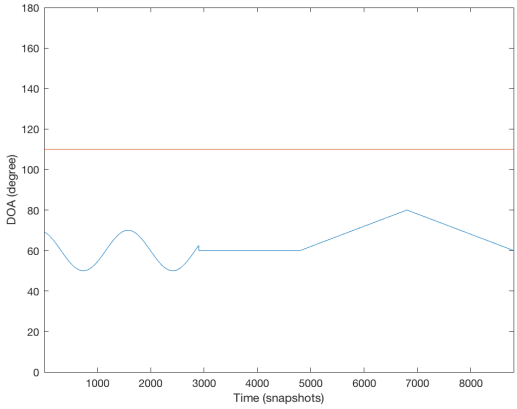

(c) Fixed vs. moving

Figure 3.25: The proposed ideal source signals trajectories where in the sources DOA are following (a) the same direction, (b) opposite directions, and (c) one source DOA is being fixed while the other is changing.

In the last experiment, the three different scenarios explained above are used with SNR being set to 10 dB. Based on the results of the third experiment (see Fig. 3.24) and in order to obtain an acceptable POD, the total number of snapshots is chosen to be 10 for non-fluctuating as well as for Swerling source types II and IV, while this number is set to 100 for Swerling source types I and III. Figures 3.26, 3.27, 3.28, 3.29 and 3.30 show the results of tracking the various signals using MVDR A-LASSO. From these figures, it can be seen that the MVDR A-LASSO technique is able to detect and track properly not only non-fluctuating but also fluctuating source signals.

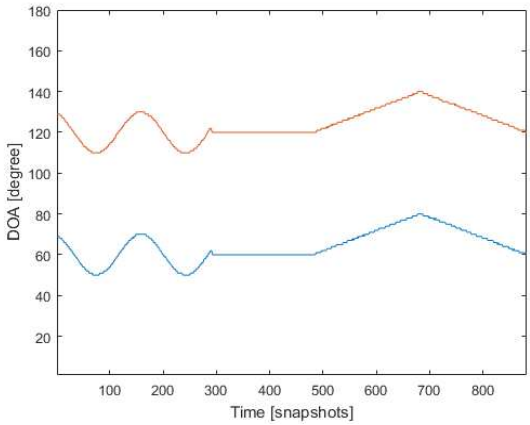

(a)

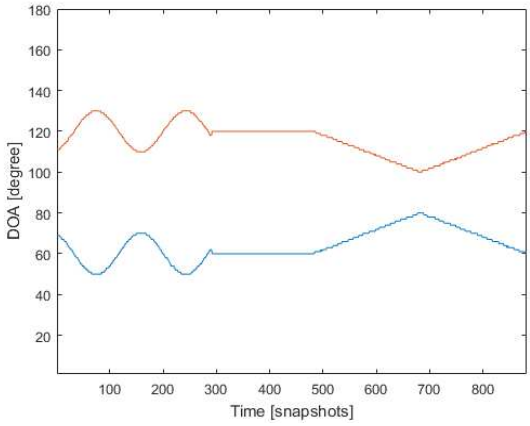

(b)

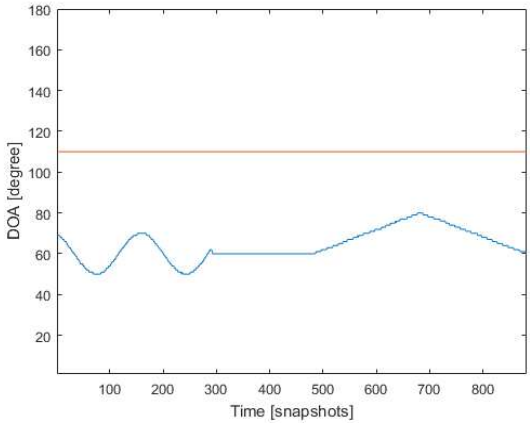

(c)

Figure 3.26: Trajectory of two non-fluctuating source signals using MVDR A-LASSO, SNR = 10 dB using 10 snapshots.

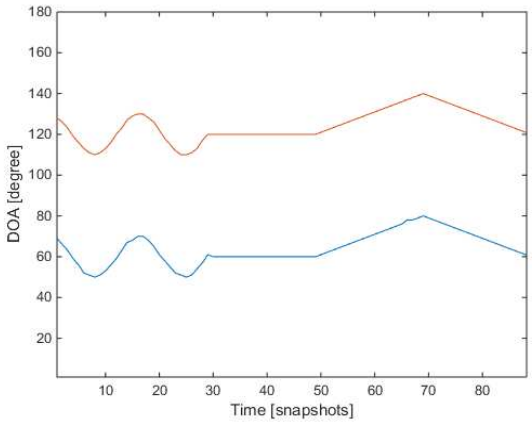

(a)

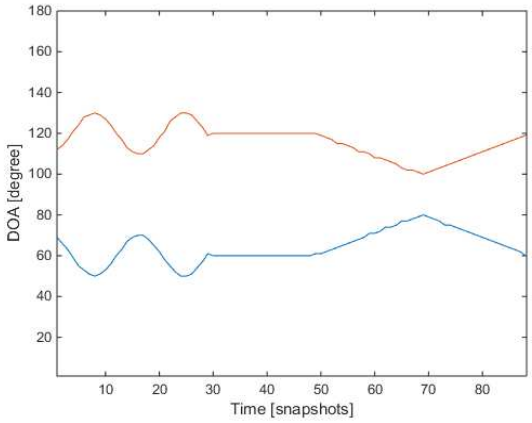

(b)

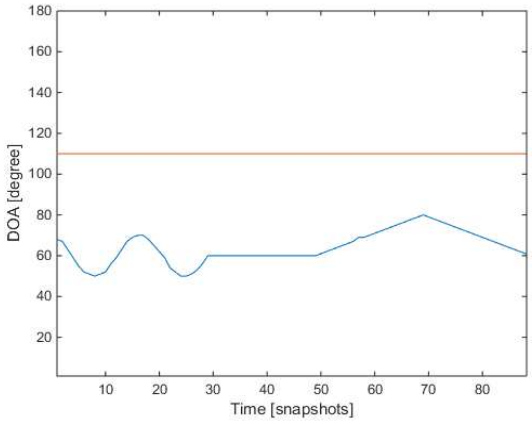

(c)

Figure 3.27: Trajectory of two fluctuating source signals using MVDR A-LASSO, SNR = 10 dB. (a,b, and c) Swerling-I, 100 snapshots.

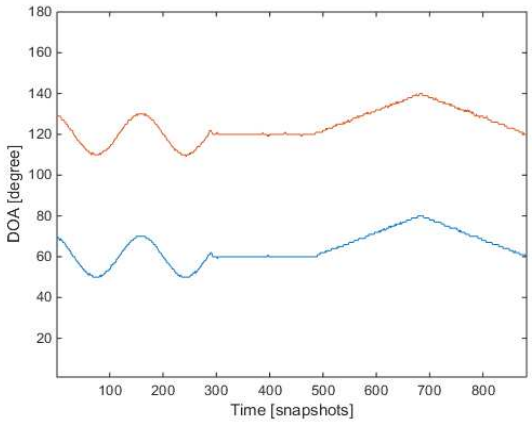

(a)

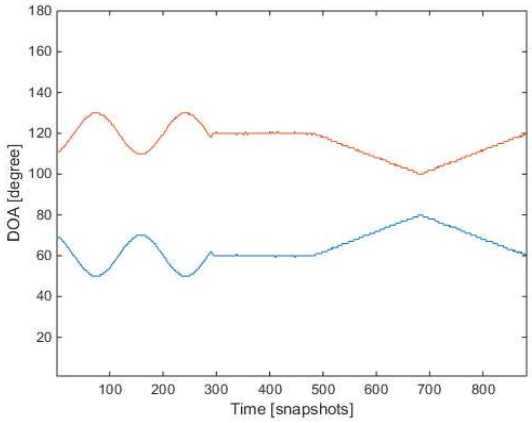

(b)

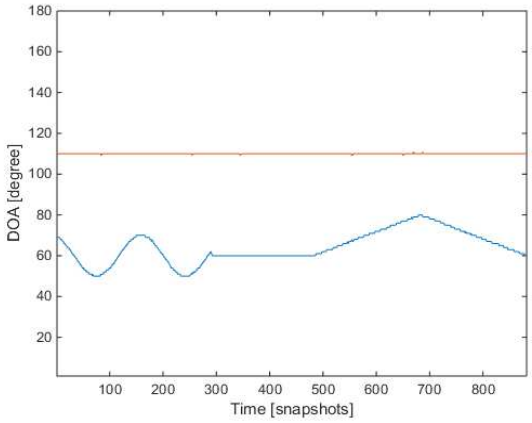

(c)

Figure 3.28: Trajectory of two fluctuating source signals using MVDR A-LASSO, SNR = 10 dB. (a,b, and c) Swerling-II, 10 snapshots.

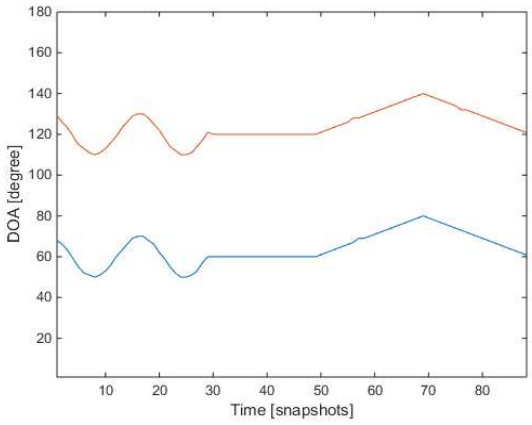

(a)

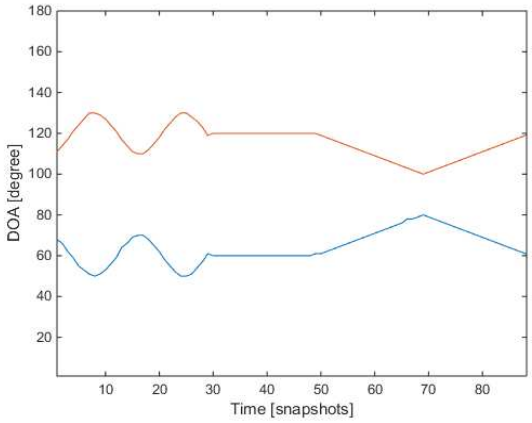

(b)

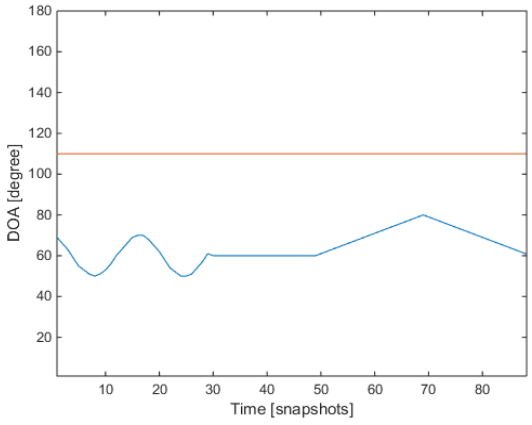

(c)

Figure 3.29: Trajectory of two fluctuating source signals using MVDR A-LASSO, SNR = 10 dB. (a,b, and c) Swerling-III, 100 snapshots.

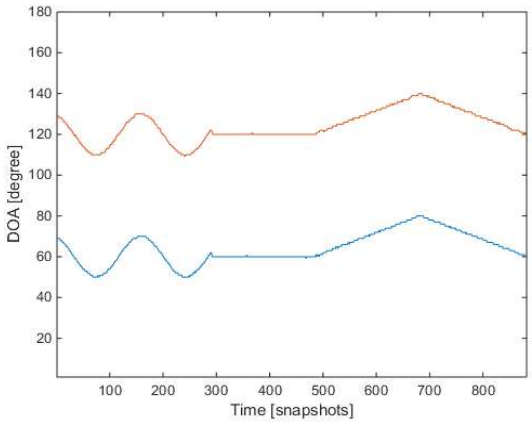

(a)

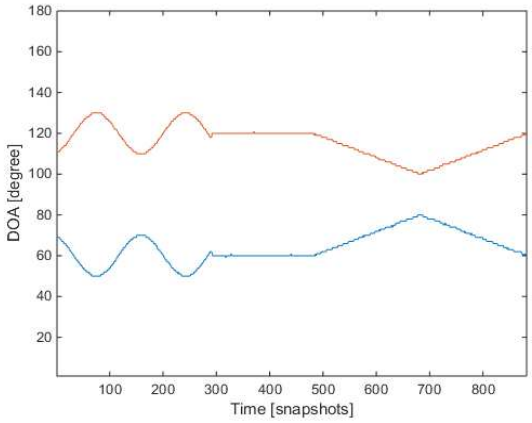

(b)

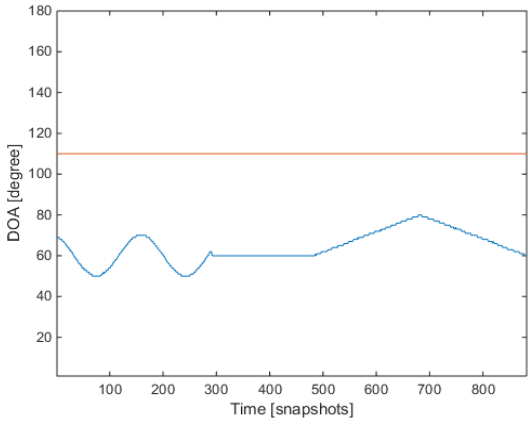

(c)

Figure 3.30: Trajectory of two fluctuating source signals using MVDR A-LASSO, SNR = 10 dB. (a,b, and c) Swerling-IV, 10 snapshots.

3.8 Summary

In this chapter, we have presented a novel technique in compressive sensing framework for estimating DOAs of signals using a linear array. We have proposed a new A-LASSO algorithm, the MVDR A-LASSO, for the DOA estimation problem. The proposed A-LASSO algorithm outperforms the classical LASSO, as well as the classical DOA estimation techniques. It does not require any a priori knowledge about the number of source signals.

The proposed algorithm is able to perform DOA estimation using a small number of snapshots and is able to estimate correlated source signals as well as spatially-close source signals. Our proposed algorithm can identify $((M^2-2)/2 + M-1)/2$ source signals using M sensors and has a high resolution. Using the proposed technique, we are able to eliminate any spurious peaks and identify only those that corresponds to actual sources. Further, it has been shown that, using the proposed MVDR A-LASSO, the source signals can be identified with a lesser number of iterations than that using OLS A-LASSO. Thus lowering the computational cost of the MVDR A-LASSO with respect to that of the OLS A-LASSO.

The simulation results have shown that MVDR A-LASSO is also able to detect fluctuating source signals. Furthermore, it is able to detect and track signals moving with certain types of trajectories.

Chapter 4

Compressive Sensing-Based DOA Estimation For Unknown Noise Fields In Element-Space

4.1 Introduction

Many of the DOA techniques that have been proposed assume spatially white noise [107, 108, 109, 110]. Hence, the array noise covariance matrix is related to the noise power through an identity matrix. However, the assumption of spatially white noise is not realistic in many practical applications [111, 112, 113, 114, 115, 116, 117], where the noise fields are spatially colored. The colored noise significantly degrades the performance of the DOA estimator. Furthermore, estimating the number of signal sources becomes a problem. In addition, some of the peaks due to the non-white noise background may be identified as source signals.

To overcome this degradation, certain constraints are imposed on the signal or on the colored noise. In [109], the signal is assumed to be partially known as a linear combination of a set of basis functions, while in [118] the noise is modeled

as an autoregressive process. However, these assumptions are still not realistic, and furthermore, if they are not satisfied, then the DOA performance will be highly degraded. In [82], an underdetermined KR based technique using a ULA was proposed for DOA estimation in unknown spatial noise covariance. However, the source signals are assumed to be quasi-stationary. Iterative methods using ULAs for DOA estimation in nonuniform noise were proposed in [119]. These methods are based on estimating the signal subspace and noise covariance matrices simultaneously. Yet, the number of sources to be estimated is assumed to be known in advance and the methods are computationally intensive.

Sparse arrays are used to avoid the above unrealistic assumptions for DOA estimation in the presence of spatially colored noise [115, 120]. In [120], the separation between the sub-arrays is chosen such that the noise is uncorrelated between the sub-arrays. In this situation, the noise covariance matrix has a block-diagonal structure, which allows the DOA estimation to be done accurately. In [115], the DOA estimation was explored using two separated sub-arrays and based on the generalized correlation (GC) analysis, a new method for DOA estimation in unknown noise (UN) fields known as, UN-MUSIC, is proposed for DOA estimation in the case of unknown correlated noises. However, two separate ULAs are used for the DOA estimation and in order to be able to decompose the received signal into its unique subspaces a long procedure is required. In [116], a maximum likelihood (ML) technique on a sparse sensor array is proposed for DOA estimation in the presence of spatially colored noise. However, the technique requires a large number of snapshots. Furthermore, the algorithm is based on the ML technique, which is computationally the most intensive amongst the DOA estimation methods [11] and further, the number of sources to be estimated is assumed to be known a priori [121].

In this chapter, using a single sparse linear array, we propose a new CS-based DOA estimation technique, called the GCD A-LASSO technique, that is capable

of performing DOA estimation for source signals in the presence of unknown noise fields [122].

4.2 GCD A-LASSO for DOA Estimation in Unknown Noise Fields

Taking into account that the source signals are far-field sources, they can be considered as point sources and consequently become sparse in space. Hence, the output of the sensor array, $\mathbf{y} \in \mathbb{C}^{\bar{M}\times 1}$, can be expressed as

$$\mathbf{y}(t) = \Phi\bar{\mathbf{s}}(t) + \bar{\mathbf{n}}(t) \tag{4.1}$$

where $\Phi \in \mathbb{C}^{\bar{M}\times N}$ is the overcomplete steering matrix and is given by

$$\begin{aligned}\Phi &= [\mathbf{a}'(\bar{\theta}_1)\ \mathbf{a}'(\bar{\theta}_2)\ \ldots\ \mathbf{a}'(\bar{\theta}_n)\ \ldots\ \mathbf{a}'(\bar{\theta}_N)] \\ &= \begin{bmatrix} e^{jk_o d(-(\bar{M}-1)/2)\cos\bar{\theta}_1} & e^{jk_o d(-(\bar{M}-1)/2)\cos\bar{\theta}_2} & \ldots & e^{jk_o d(-(\bar{M}-1)/2)\cos\bar{\theta}_N} \\ \vdots & \vdots & & \vdots \\ 1 & 1 & \ddots & 1 \\ \vdots & \vdots & & \vdots \\ e^{jk_o d((\bar{M}-1)/2)\cos\bar{\theta}_1} & e^{jk_o d((\bar{M}-1)/2)\cos\bar{\theta}_2} & \ldots & e^{jk_o d((\bar{M}-1)/2)\cos\bar{\theta}_N} \end{bmatrix}\end{aligned} \tag{4.2}$$

and $\bar{\mathbf{n}} \in \mathbb{C}^{\bar{M}\times 1}$ is an AWGN. Denoting $\mathbf{a}'(\bar{\theta}_n) \in \mathbb{C}^{\bar{M}\times 1}$ as the steering vector of the virtual array corresponding to AOA of $(\bar{\theta}_n)$, where $\{\bar{\theta}_n\}_{n=1}^{N}$ denotes a grid that covers the set of all possible locations, Ω and $N \gg L$. In this case, the source signal vector $\bar{\mathbf{s}} \in \mathbb{C}^{N\times 1}$ is given by

$$\bar{\mathbf{s}}(t) = [\bar{\sigma}_1\ \bar{\sigma}_2\ \ldots\ \bar{\sigma}_n\ \ldots\ \bar{\sigma}_N]^T \tag{4.3}$$

where the nth element of $\bar{\mathbf{s}}(t)$, $\bar{s}_n(t)$, is nonzero only if $(\bar{\theta}_n = \theta_l)$ and, in that case, $\bar{\sigma}_n = \sigma_l$. The compressive sensing (CS) technique is to estimate the signal energy as a function of the source signal locations given the sensor array output, $\mathbf{y}$. In a noise free scenario, a direct way to investigate the sparsity on $\bar{\mathbf{s}}$ is by minimizing the ℓ_0-norm, which counts the number of nonzero elements in the vector $\bar{\mathbf{s}}$, as follows

$$\min_{\bar{\mathbf{s}}} \|\bar{\mathbf{s}}\|_0 \text{ subject to } \mathbf{y} = \Phi\bar{\mathbf{s}} \tag{4.4}$$

However, this minimization is an NP-hard problem [123], which becomes, even for a moderate dimensional problem, computationally intractable. For that reason, different alternative approaches to approximate the solution of ℓ_0-norm problems were presented in [123, 124, 125, 126]. It has been proven that, for sufficiently sparse signals and sensing matrices with sufficiently incoherent columns [127, 128], the ℓ_0-norm problem is equivalent to the ℓ_1-norm one [129, 130, 131], where ℓ_1 minimization is given by

$$\min_{\bar{\mathbf{s}}} \|\bar{\mathbf{s}}\|_1 \text{ subject to } \mathbf{y} = \Phi\bar{\mathbf{s}} \tag{4.5}$$

Furthermore, ℓ_2-norm could be used as an alternative approach to solve ℓ_0-norm problem by relaxing ℓ_0-norm into ℓ_2-norm as follows

$$\min_{\bar{\mathbf{s}}} \|\bar{\mathbf{s}}\|_2 \text{ subject to } \mathbf{y} = \Phi\bar{\mathbf{s}} \tag{4.6}$$

which is a convex problem and has an analytic solution given by

$$\hat{\bar{\mathbf{s}}} = \Phi^H(\Phi\Phi^H)^{-1}\mathbf{y} \tag{4.7}$$

However, ℓ_1-norm problem favors sparse signals than the ℓ_2-norm. Furthermore, ℓ_1-norm relaxation is the closest convex optimization to that of the ℓ_0-norm

and it converges to the global minimum [49]. In practice, CS can be extended to noisy measurement scenarios. The ℓ_1-norm problem for a noisy measurement can written as

$$\min_{\bar{\mathbf{s}}} \|\bar{\mathbf{s}}\|_1 \text{ subject to } \|\Phi\bar{\mathbf{s}} - \mathbf{y}\|_2 \leq \beta \tag{4.8}$$

where β is an error tolerance parameter ($\beta > 0$). The ℓ_2-norm used for evaluating the error $\Phi\bar{\mathbf{s}} - \mathbf{y}$ can be replaced by any other norm, such as ℓ_∞ or ℓ_p, $0 < p < 1$. Proper choice of β is an important issue for the success of minimization in (4.8) [75, 98]. An ℓ_1-norm constrained form of (4.8) is known as LASSO [50]. The LASSO minimization problem can be written as

$$\min_{\bar{\mathbf{s}}} \|\mathbf{y} - \Phi\bar{\mathbf{s}}\|_2^2 + \tau \|\bar{\mathbf{s}}\|_1 \tag{4.9}$$

where τ is a nonnegative regularization parameter. The ℓ_1 penalization approach is also known as the *basis pursuit* [90]. Two iterative versions of LASSO, namely, the OLS A-LASSO and MVDR A-LASSO, were introduced in [61]. It was shown that the performance of these A-LASSO techniques is superior to that of the classical DOA estimation techniques and LASSO-based DOA estimation. The A-LASSO is given by [61]

$$\hat{\bar{\mathbf{s}}}^{(k)} = \min_{\bar{\mathbf{s}}} \|\mathbf{y} - \Phi\bar{\mathbf{s}}\|_2^2 + \tau_k \sum_{n=1}^{N} \hat{w}_n |\bar{s}_n| \tag{4.10}$$

where k is the iteration number and $\hat{w}_n$ is the n-th element of the weight vector, $\hat{\mathbf{w}}$ which is given by OLS or MVDR in the first iteration, $k = 1$.

It should be pointed out that in most of the CS-based DOA estimation techniques, the noise covariance structure is known in advance; it is assumed to be AWGN (see [7] and the references therein). However, in practice, this assumption does not hold and the noise covariance structure is probably unknown. Thus, the DOA estimator performance is highly degraded when the noise covariance is not known. Further, in such scenarios, more false source signal peaks could appear due

to the background noise.

In order to overcome the above mentioned problem, we adopt the following technique for signal source DOA estimation in unknown correlated noise fields [115]. Consider two ULAs whose output vectors can be written as

$$\begin{aligned} \mathbf{x}_1(t) &= \mathbf{A}_1\mathbf{s}_1(t) + \mathbf{n}_1(t) \\ \mathbf{x}_2(t) &= \mathbf{A}_2\mathbf{s}_2(t) + \mathbf{n}_2(t) \end{aligned} \tag{4.11}$$

where $\mathbf{x}_1(t)$ and $\mathbf{x}_2(t)$ are the data vectors of dimensions M_1 and M_2, respectively, $\mathbf{A}_1 \in \mathbb{C}^{M_1 \times L}$ and $\mathbf{A}_2 \in \mathbb{C}^{M_2 \times L}$ are the steering matrices of the arrays and $\mathbf{s}_1(t)$ and $\mathbf{s}_2(t)$ are the signal vectors. The outputs of the two sub-arrays can be considered to be the same, but one is a delayed version of the other. The noise vectors $\mathbf{n}_1(t)$ and $\mathbf{n}_2(t)$ are assumed to be stationary, zero-mean, Gaussian with the joint covariance, $\mathbf{J}$, given by

$$\mathbf{J} = \left\{ \begin{bmatrix} \mathbf{n}_1 \\ \mathbf{n}_2 \end{bmatrix} \begin{bmatrix} \mathbf{n}_1^H & \mathbf{n}_2^H \end{bmatrix} \right\} = \begin{bmatrix} \mathbf{R}_{nn_1} & 0 \\ 0 & \mathbf{R}_{nn_2} \end{bmatrix} \tag{4.12}$$

$\mathbf{R}_{nn_1}$ and $\mathbf{R}_{nn_2}$ are unknown covariance matrices of the noise of the two sub-arrays. The joint covariance matrix of the received data from the two sub-arrays, $\Sigma \in \mathbb{C}^{2(M_1+M_2)\times 2(M_1+M_2)}$, can be written as [115]

$$\Sigma = \left\{ \begin{bmatrix} \mathbf{x}_1 \\ \mathbf{x}_2 \end{bmatrix} \begin{bmatrix} \mathbf{x}_1^H & \mathbf{x}_2^H \end{bmatrix} \right\} = \begin{bmatrix} \mathbf{R}_{11} & \mathbf{R}_{12} \\ \mathbf{R}_{21} & \mathbf{R}_{22} \end{bmatrix} \tag{4.13}$$

where

$$\begin{aligned} \mathbf{R}_{ii} &= \mathbf{A}_i\mathbf{R}_{ss_i}\mathbf{A}_i^H + \sigma_n^2\mathbf{R}_{nn_i}, \quad i = 1, 2 \\ \mathbf{R}_{12} &= \mathbf{R}_{21}^H = \mathbf{A}_1\mathbf{R}_{ss_{12}}\mathbf{A}_2^H \end{aligned} \tag{4.14}$$

where $\mathbf{R}_{ss_i}$ is the auto-correlation and $\mathbf{R}_{ss_{12}}$ is the cross-correlation of the signals

such that

$$\begin{aligned} \mathbf{R}_{ss_i} &= \mathrm{E}\left\{\mathbf{s}_i\mathbf{s}_i^H\right\}, \quad i = 1, 2 \\ \mathbf{R}_{ss_{12}} &= \mathrm{E}\left\{\mathbf{s}_1\mathbf{s}_2^H\right\} \end{aligned} \tag{4.15}$$

and both are assumed to be of full rank. In practice, we do not know the true value of Σ, and therefore, we use the average of the outer products of the output data as an estimate of Σ such that

$$\widehat{\Sigma} = \frac{1}{T}\sum_{n=1}^{N}\begin{bmatrix}\mathbf{x}_1(n)\\ \mathbf{x}_2(n)\end{bmatrix}\left[\mathbf{x}_1^H(n)\ \mathbf{x}_2^H(n)\right] = \begin{bmatrix}\hat{\mathbf{R}}_{11} & \hat{\mathbf{R}}_{12}\\ \hat{\mathbf{R}}_{21} & \hat{\mathbf{R}}_{22}\end{bmatrix} \tag{4.16}$$

where T is the snapshot number. It should be noted that $\mathbf{R}_{12}$ and $\mathbf{R}_{21}$ contain noiseless DOA information. So, we can proceed using any technique such as MUSIC [14] to estimate the DOA. However, the signal subspace estimation from $\hat{\mathbf{R}}_{12}$ is not unique. To uniquely estimate the signal subspace from $\hat{\mathbf{R}}_{12}$, the GCD is used to develop the UN-MUSIC algorithm in [115].

Consider now a two-level nested array containing an odd number of sensors, M; the resulting virtual array will contain $\bar{M}$ virtual sensors, as given in Table 3.1. Assume that the first sub-array contains the virtual sensors from the first virtual sensor to the $(\bar{M}-Q)$-th sensor and the second sub-array contains the sensors from $(Q+1)$-th to the last virtual sensor, so that the total number of sensors in each of the sub-arrays is $\bar{M}-Q$. It should be pointed out that the maximum number of sources to be estimated will be affected by Q and is given by $(\bar{M}-Q-1)/2$. Due to the overlapping of the two sub-arrays and because the source signals are assumed to be located in the far-field, the steering matrices $\mathbf{A}_1$ and $\mathbf{A}_2$ of the two sub-arrays could be assumed to be the same, that is $\mathbf{A}_1 = \mathbf{A}_2 = \bar{\mathbf{A}}$, where $\bar{\mathbf{A}}$ is the steering matrix of the sensor array for which the total number of sensors is $\bar{M}-Q$ and is given by

$$\bar{\mathbf{A}} = \left[\bar{\mathbf{a}}(\bar{\theta}_1)\ \bar{\mathbf{a}}(\bar{\theta}_2)\ \ldots\ \bar{\mathbf{a}}(\bar{\theta}_N)\right] \tag{4.17}$$

where $\bar{\mathbf{a}}(\bar{\theta}_n) \in \mathbb{C}^{(\bar{M}-Q)\times 1}$ as the steering vector of the sensor array whose $\bar{m}$th element can be written as

$$\bar{a}_{\bar{m}}(\bar{\theta}_n) = e^{jk_o d\bar{m}\cos\bar{\theta}_n}, \quad \bar{m} = \begin{cases} -\frac{\bar{M}-Q-1}{2}, \ldots, \frac{\bar{M}-Q-1}{2} & \text{if } Q \text{ is even} \\ -\frac{\bar{M}-Q}{2}+1, \ldots, \frac{\bar{M}-Q}{2} & \text{if } Q \text{ is odd} \end{cases} \tag{4.18}$$

Consider extracting $\hat{\mathbf{R}}_{12} \in \mathbb{C}^{\bar{M}-Q\times\bar{M}-Q}$ from (4.16) which can be written as

$$\hat{\mathbf{R}}_{12} = \mathbf{A}_1\mathbf{R}_{ss_{12}}\mathbf{A}_2^H = \bar{\mathbf{A}}\mathbf{R}_{ss_{12}}\bar{\mathbf{A}}^H \tag{4.19}$$

Following linear algebra theory, each column (vector) of $\hat{\mathbf{R}}_{12}$ can be linearly represented by any complete basis in the $(\bar{M}-Q)$-dimensional complex vector space [48]. The qth column of $\hat{\mathbf{R}}_{12}$ can be written as

$$\hat{\mathbf{r}}_q = \Phi^*\mathbf{b}_q, \quad q = 1, \ldots, \bar{M}-Q \tag{4.20}$$

where $\mathbf{b}_q$ is the representation coefficient vector in terms of the overcomplete steering matrix, Φ^* and $\Phi^* \in \mathbb{C}^{(\bar{M}-Q)\times N}$ is the overcomplete steering matrix for the sensor array for which the total number of sensors is $\bar{M}-Q$. In matrix from, (4.20) can be written as

$$\hat{\mathbf{R}}_{12} = \Phi\mathbf{B} \tag{4.21}$$

where $\mathbf{B} = [\mathbf{b}_1, \ldots, \mathbf{b}_q, \ldots, \mathbf{b}_{\bar{M}-Q}]$. It should be noted that $\{\mathbf{b}_q\}_{q=1}^{\bar{M}-Q}$ have the same sparsity structure, i.e., the non-zero elements of each vector of $\mathbf{B}$ appear in the same index [48]. Based on (4.20), DOA estimation is the same as seeking the sparsity of $\mathbf{b}_q$, which has the same structure as that of the signal to be estimated. Using (4.20),

the DOA estimation problem can be reformulated using A-LASSO [61] as follows:

$$\mathbf{b}_q^{(k)} = \min_{\mathbf{b}_q} \|\hat{\mathbf{r}}_q - \Phi \mathbf{b}_q\|_2^2 + \tau_k \sum_{n=1}^{N} \hat{w}_n |b_{q_n}| \tag{4.22}$$

We denote (4.22) as GCD A-LASSO. Algorithm 4.1 illustrates single iteration of the GCD A-LASSO technique. Following [61], two initial weights are considered for the first iteration ($k = 1$) of the GCD A-LASSO algorithm, these initial weights are given by OLS or MVDR. Depending on whether OLS or MVDR weights are used as initial weights, the algorithm will be known as GCD OLS A-LASSO or GCD MVDR A-LASSO, respectively.

Algorithm 4.1 GCD A-LASSO

1: Collect T snapshots of the received signals, $\mathbf{x}(t)$.
2: Calculate the covariance matrix, $\mathbf{R}_{xx}$.
3: Vectorize $\mathbf{R}_{xx}$ and construct the virtual sensor array output as given in Section 3.2.
4: Divide the virtual array into two equal uniform linear sub-array with $\bar{M} - Q$ virtual sensor in each sub-array.
5: Calculate the joint covariance matrix, Σ, from (4.16) and extract $\hat{\mathbf{R}}_{12}$ from the result.
6: Select q-th column of $\hat{\mathbf{R}}_{12}$ where $q = 1, \ldots, \bar{M} - Q$.
7: Compute the initial estimate for the signal, $\bar{s}$, using OLS or MVDR as initial weights.
8: Find $\hat{\mathbf{w}}$, where the n-th element of $\hat{\mathbf{w}}$, $\hat{w}_n$, is given by $\hat{w}_n = 1/|\hat{s}_n|^{\gamma}, \quad n = 1, \ldots, N$.
9: Define $\Phi' \in \mathbb{C}^{(\bar{M}-Q)\times N}$ matrix, such that its (q, n)-th element is given by $\phi_{qn}/\hat{w}_n$, where $q = 1, \ldots, \bar{M} - Q$ and $n = 1, \ldots, N$.
10: **for** $k = 1, 2, \ldots, K$ iterations **do**

Solve the LASSO problem as:

$$\mathbf{b}_q^* = \min_{\mathbf{b}_q} \|\hat{\mathbf{r}}_q - \Phi' \mathbf{b}_q\|_2^2 + \tau_k \|\mathbf{b}_q\|_1$$

Calculate $b^{(k)} = b_n^*/\hat{w}_n$, $n = 1, 2, \ldots, N$.

11: **end for**
12: Find the final DOA estimation.

4.3 Simulation Results

Consider a sparse linear two-level nested array, for which M is odd, consisting of three elements in the first level and with four elements in the second level. Thus, the total number of sensors is $M = 7$, as shown in Fig. 4.1. Investigating the array output by applying (3.1) - (3.3), and extracting the equivalent distinct virtual elements from the virtual array manifold $(\mathbf{A}^* \odot \mathbf{A})$, one can see that the virtual array is a uniform linear array containing $\bar{M} = 31$ elements. The number of sensors in each of the two sub-arrays of the virtual array is chosen to be 29, that is, $Q = 2$. As a sequence, we see from (4.18) that $\bar{m} = (-14, \ldots, 14)$. We shall call such an array of antennas as array #1. The sampling grid $\bar{\theta}_n \in [1^\circ : 180^\circ]$ that covers Ω is chosen to be of 1° step. The received signals are assumed to be contaminated by a mixture of correlated noise and AWGN in all the simulations.

The signal sources are modeled as $e^{j2\pi f_d t}$ where f_d is the Doppler frequency and 10 snapshots are assumed for the simulations, except in the first simulation. A single iteration A-LASSO [61] is considered for all the simulations. All the simulated source signals are assumed to be equi-power and uncorrelated with one another or with the noise except in the third simulation, where the sources are assumed to be correlated with each other. The total number of trials, N_{sim}, is set to 100 for each observation point. For each experiment, the regularization parameter, τ, is selected based on the idea of the L-Curve [101, 102] and following the same procedure as given in [61].

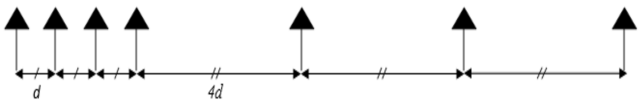

Figure 4.1: Two level nested array with 7 elements.

The CVX toolbox [104, 105] for convex optimization that is available within the MATLAB environment is used for examining the performance of the proposed

algorithms.

We investigate, in the first experiment, the capabilities of the proposed algorithm in detecting the sources even when the number of sources exceeds the number of physical array elements in the presence of unknown noise fields. In other words, the proposed algorithm is for an underdetermined DOA scenario. For that purpose, let 14 fixed source signals impinge the array from uniformly distributed DOAs over $\theta = [38^\circ, 142^\circ]$. The number of snapshots is set to 100, SNR is set to 0 dB and the noise is a mixture of AWGN and pink noise.

For UN-MUSIC simulations, two different scenarios are assumed. In the first scenario, two separate ULAs are considered for the simulation and the number of sensors in each one of them is chosen to be 7, that is, $M_1 = M_2 = 7$ (the same number of sensors as that of the two-level nested array). Such an array will be denoted as array #2. However, using this scenario, we cannot identify the 14 source signals because the maximum number of sources that can be estimated using UN-MUSIC is upper limited by the number of the used sensors, that is, $L_{max} < \{M_1, M_2\}$ [115]. Hence, one can detect only up to 6 source signals using UN-MUSIC. Furthermore, the number of sources to be estimated is assumed to be known in advance in the UN-MUSIC technique.

We therefore assume, in the second scenario, for UN-MUSIC technique, two separate ULAs each containing 15 elements, that is, $M_1 = M_2 = 15$. Therefore, the maximum number of sources that can be estimated using this array, which we shall call array #3, is 14 sources [115].

Simulations are carried out on array #1 using both of the proposed techniques, namely, GCD OLS A-LASSO and GCD MVDR A-LASSO, as well as array #3 using the UN-MUSIC technique to identify the 14 sources. The results are as shown in Figs. 4.2 and 4.3. Figs. 4.2(a) and 4.2(b), show that all of the 14 source signals are identified correctly by both the GCD OLS A-LASSO and GCD MVDR A-LASSO,

even in the presence of unknown noise, whereas even when we use 15 sensors and theoretically the maximum number of sources that can be identified is 14, UN-MUSIC has identified only 6 source signals, see Fig. 4.3(a). However, increasing the number of snapshots to be at least 10^5 snapshots, UN-MUSIC is able to identify the 14 sources as shown in Fig. 4.3(b). This clearly shows the capability of the proposed techniques in being able to identify all the sources $((\bar{M}-Q-1)/2)$, which is exactly the maximum number of sources that our method is supposed to be able to identify. It should be mentioned that, in order to uniquely calculate the signal and the noise subspaces for the UN-MUSIC technique, a long procedure is followed. Increasing the number of snapshots will increase the computational load of the DOA estimation technique. Consequently, UN-MUSIC will not be suitable for real-time applications. On the other hand, the proposed techniques are able to identify the maximum number sources that they suppose to detect using a fewer number of snapshots comparing to that of used for the UN-MUSIC technique, even for low SNR scenario. In view of this result, for the succeeding experiments we assume the number of sources to be three, except in the last one where we assume only 2 sources.

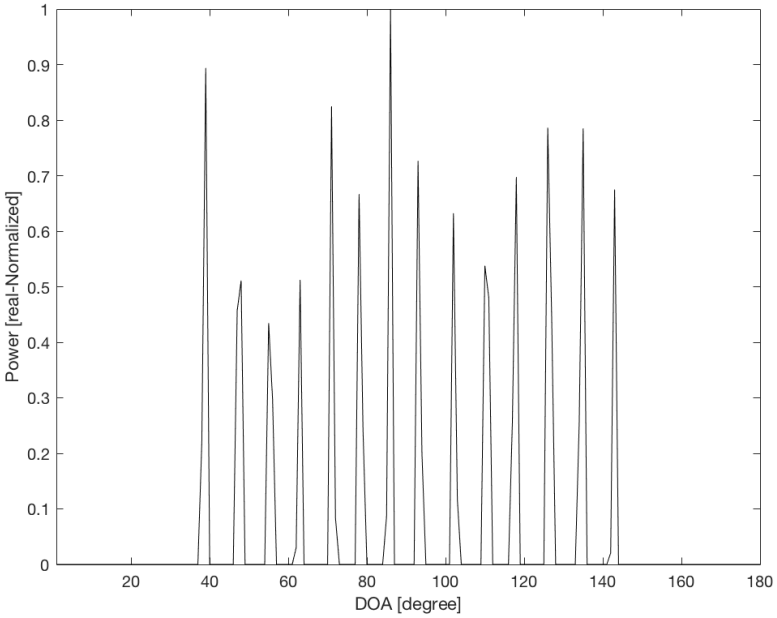

(a) GCD MVDR A-LASSO, array #1, 100 snapshots

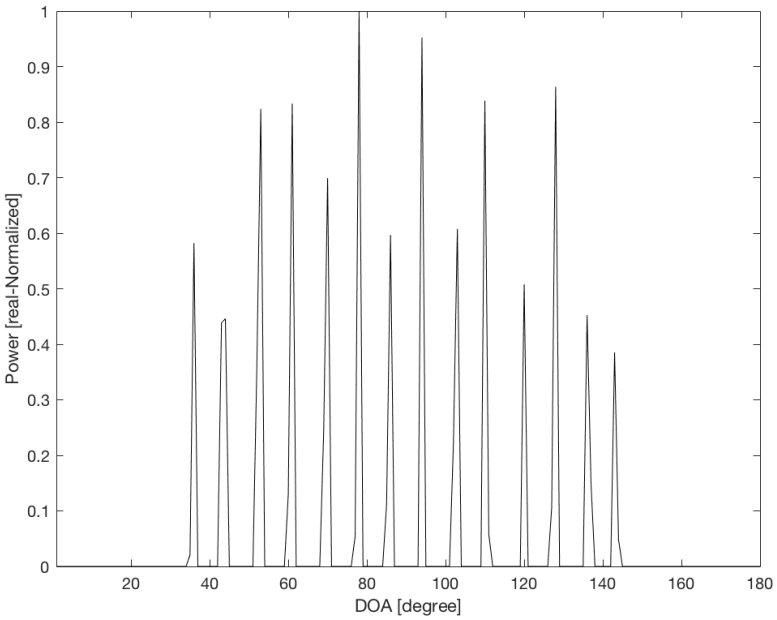

(b) GCD OLS A-LASSO, array #1, 100 snapshots

Figure 4.2: DOA estimation when the number of sources is more than the number of sensors, 100 snapshots, SNR = 0 dB, using array #1.

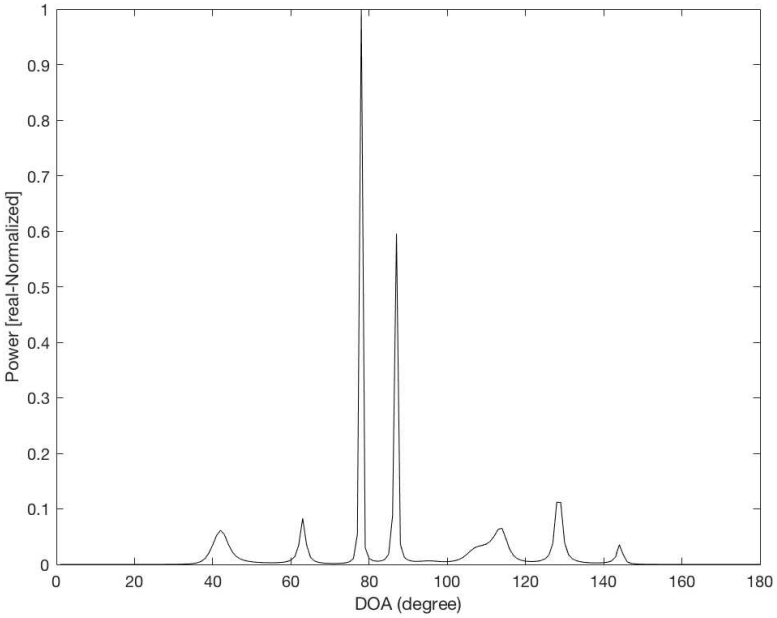

(a) UN-MUSIC, array #3, 100 snapshots

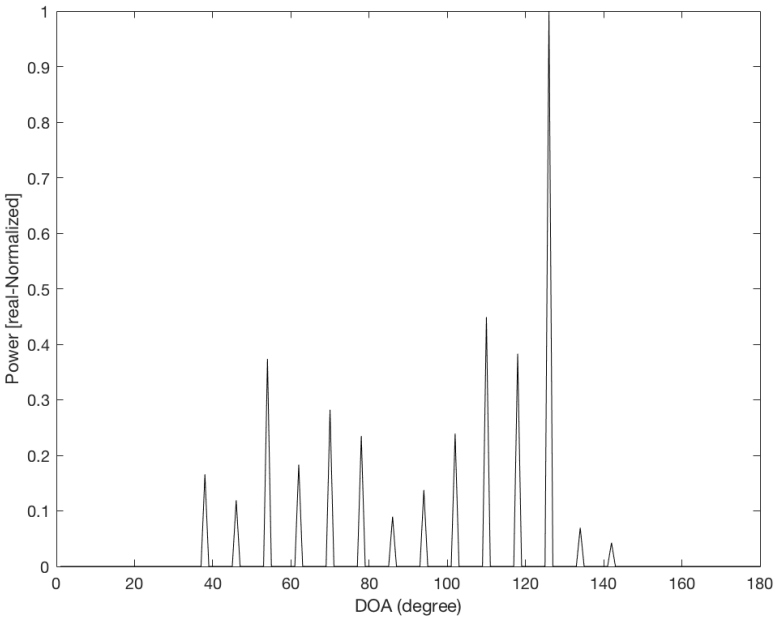

(b) UN-MUSIC, array #3, 10^5 snapshots

Figure 4.3: DOA estimation when the number of sources is more than the number of sensors, SNR = 0 dB, using (a) array #3 and 100 snapshots, and (b) array #3 and 10^5 snapshots.

In the second experiment, we consider two cases: (a) three uncorrelated signals impinging on array #1 and 2 at $40°, 60°$ and $160°$, and (b) three signals impinging at the same angles, but with the first two signals being fully correlated (coherent). The received signal is assumed to be contaminated by pink noise and AWGN with SNR set to 0 dB and only 10 snapshots are employed. Figs. 4.4 and 4.5 show that all the three techniques namely, the two proposed and the UN-MUSIC, are able to identify the three signals when they are uncorrelated. However, when two of the sources are correlated, Figs. 4.6 and 4.7 show that all the source signals are correctly identified by the two proposed techniques, whereas UN-MUSIC is not able to do so even with furthermore number of snapshots even when more number of snapshots is used. In fact, UN-MUSIC is unable to identify correlated signals.

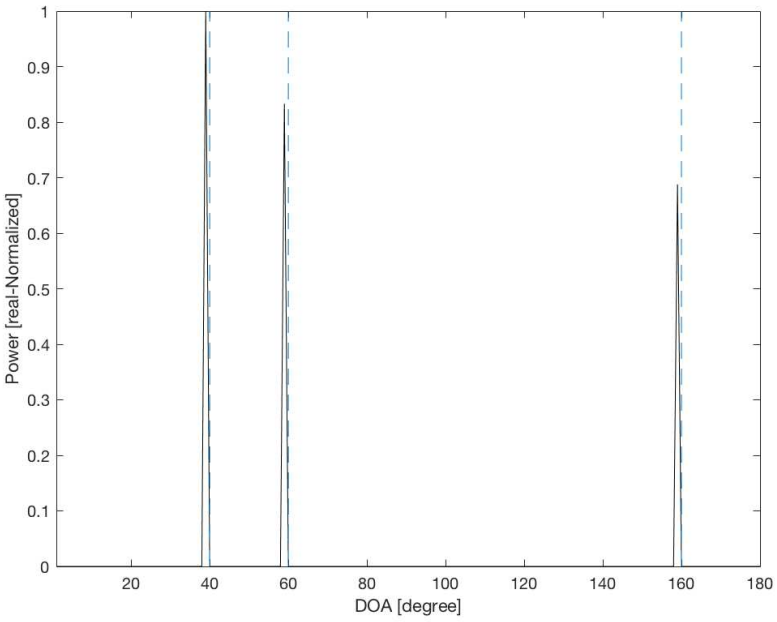

(a) GCD MVDR A-LASSO

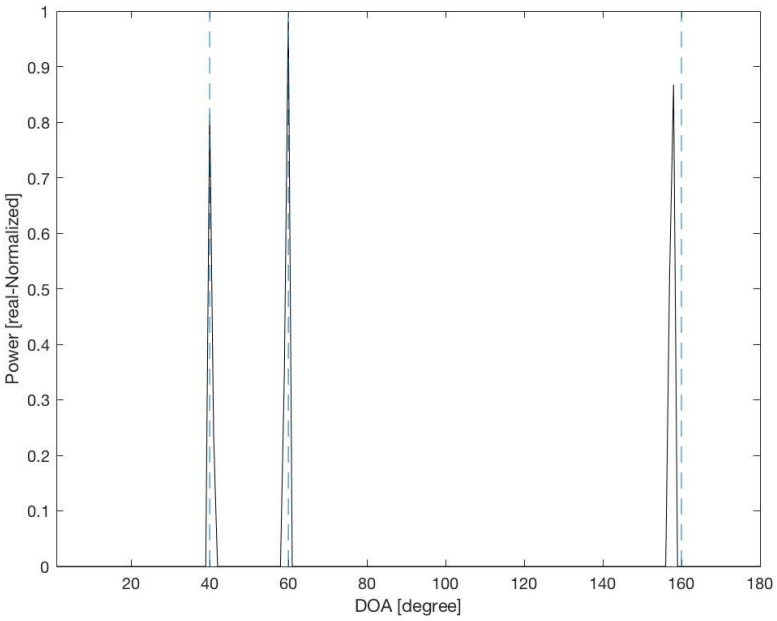

(b) GCD OLS A-LASSO

Figure 4.4: DOA estimation for 3 source signals with DOAs $40°, 60°$ and $160°$, uncorrelated sources, 10 snapshots, and pink noise and AWGN with SNR = 0 dB, using (a) GCD MVDR A-LASSO and (b) GCD OLS A-LASSO.

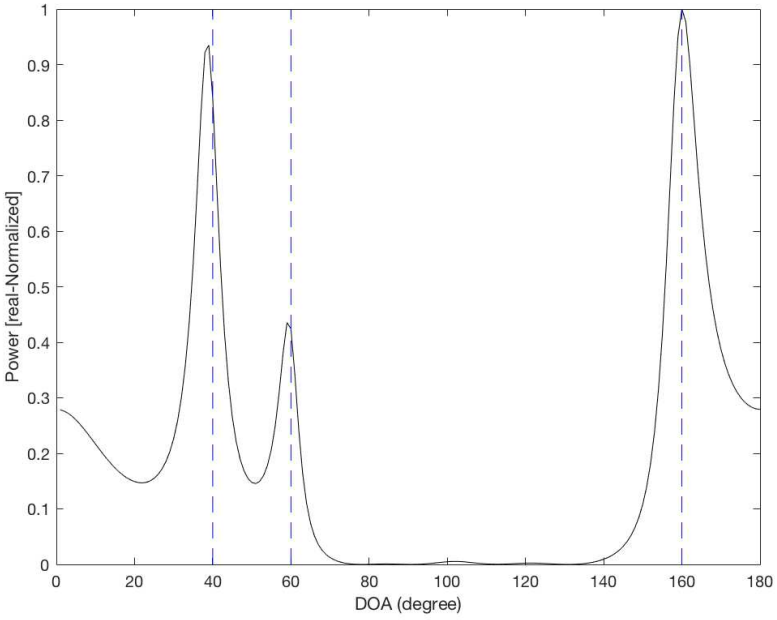

(a) UN-MUSIC

Figure 4.5: DOA estimation for 3 source signals with DOAs $40°, 60°$ and $160°$, uncorrelated sources, 10 snapshots, and pink noise and AWGN with SNR = 0 dB, using UN-MUSIC.

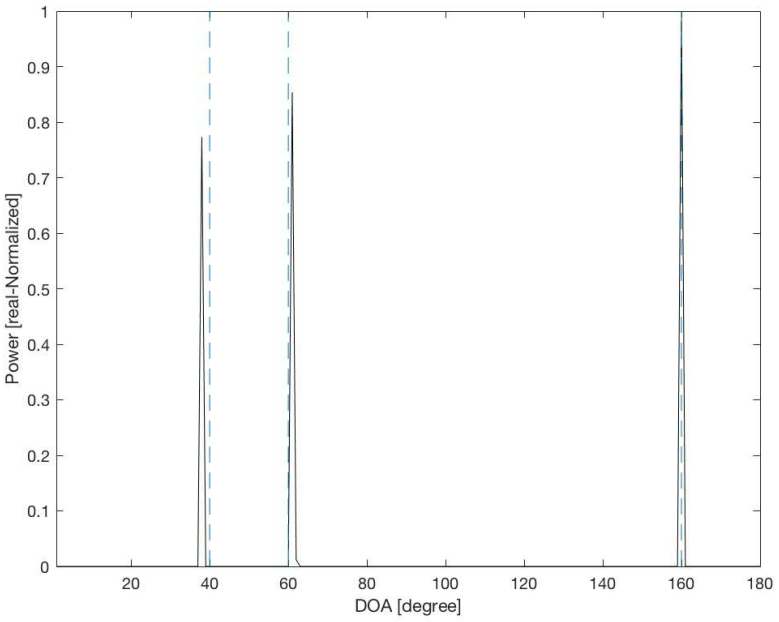

(a) GCD MVDR A-LASSO

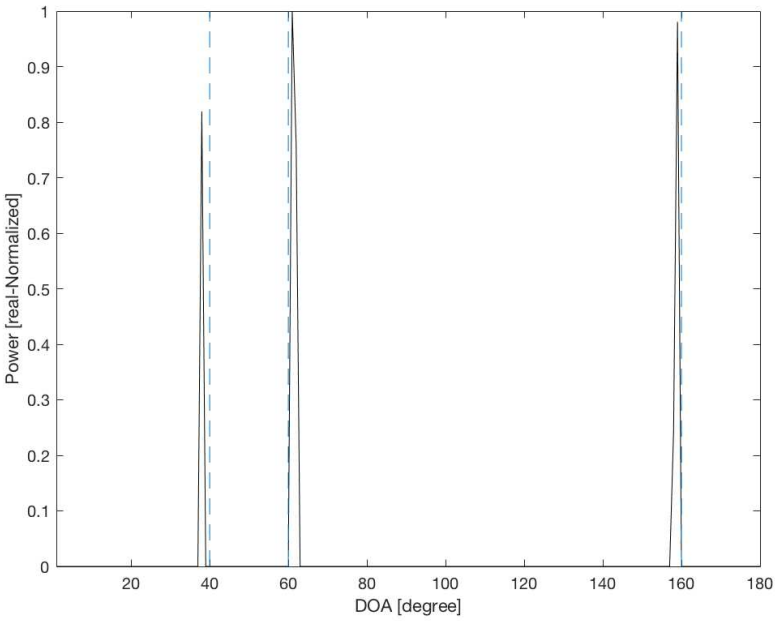

(b) GCD OLS A-LASSO

Figure 4.6: DOA estimation for 3 source signals with DOAs $40°, 60°$ and $160°$, where the first 2 source signals are fully correlated, 10 snapshots, and pink noise and AWGN with SNR = 0 dB, using (a) GCD MVDR A-LASSO and (b) GCD OLS A-LASSO.

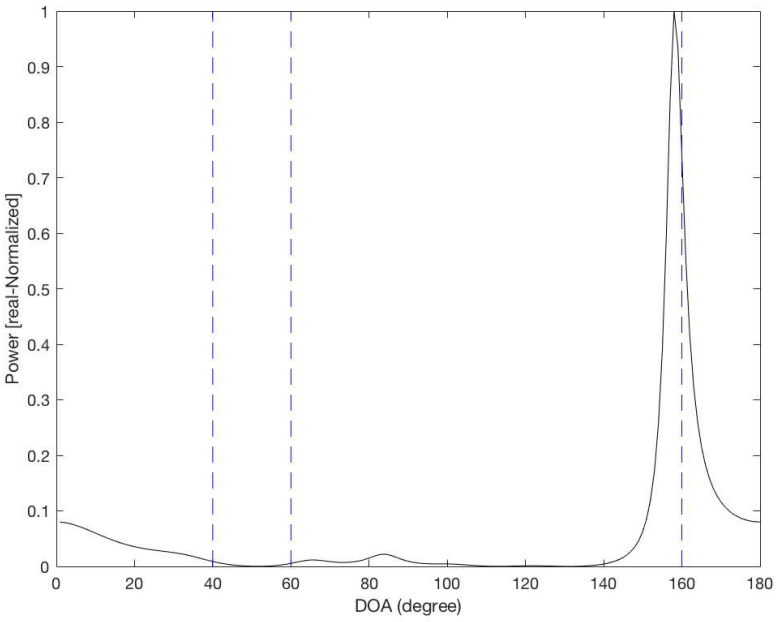

(a) UN-MUSIC, 10 snapshots

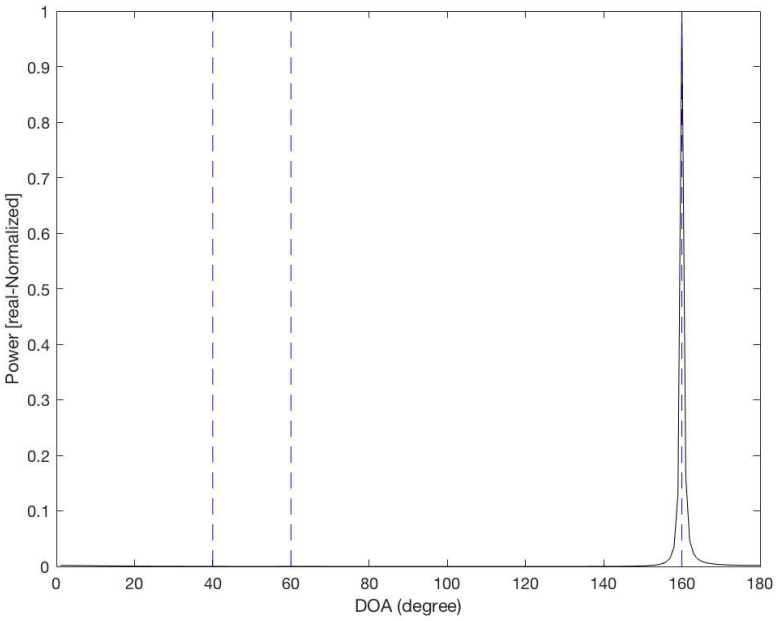

(b) UN-MUSIC, 10^4 snapshots

Figure 4.7: DOA estimation for 3 source signals with DOAs $40°, 60°$ and $160°$, where the first 2 source signals are fully correlated, 10 snapshots, and pink noise and AWGN with SNR = 0 dB, using (a) UN-MUSIC, 10 snapshots, and (b) UN-MUSIC, 10^4 snapshots.

In the third experiment, we examine the capability of the proposed techniques in identifying closely-spaced sources. For this purpose, let three sources impinge arrays #1 and 2 form DOAs of 55°, 60°, and 170°. The received signal sources are assumed to be contaminated with pink noise with SNR is set to 0 dB, and 10 snapshots of the received data are used. The simulations results are shown in Figs. 4.8 and 4.9. From these figures, three peaks can easily be identified using GCD OLS A-LASSO and GCD MVDR A-LASSO, thus identifying the three sources. However, UN-MUSIC is not able to identify the sources properly; and the two closely-spaced sources are identified as a single source. However, increasing the number of snapshots to be at least 2×10^4 snapshots, UN-MUSIC is hardly able to discriminate the sources. Yet, Even with more number of snapshots, UN-MUSIC is not able to clearly discriminate the closely-spaced sources as that of GCD OLS A-LASSO as well as GCD MVDR A-LASSO are able to clearly identify using only 10 snapshots.

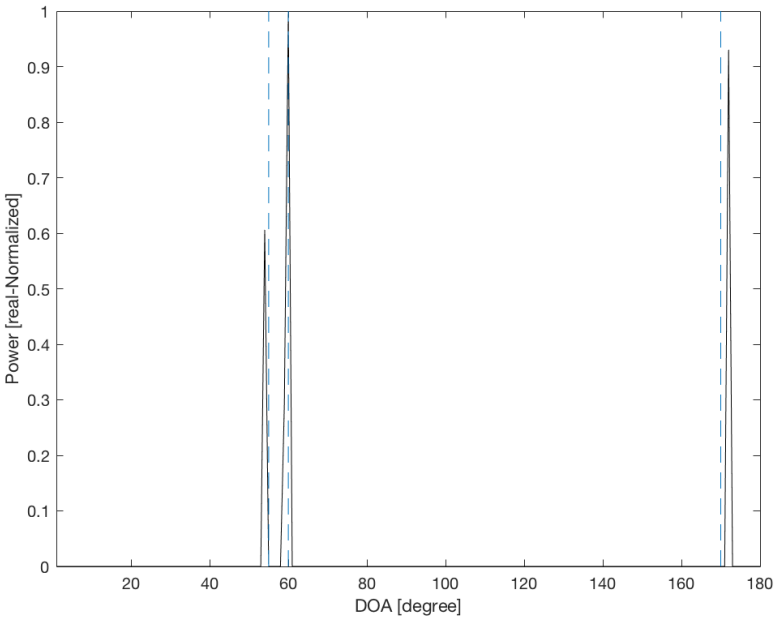

(a) GCD MVDR A-LASSO, 10 snapshots

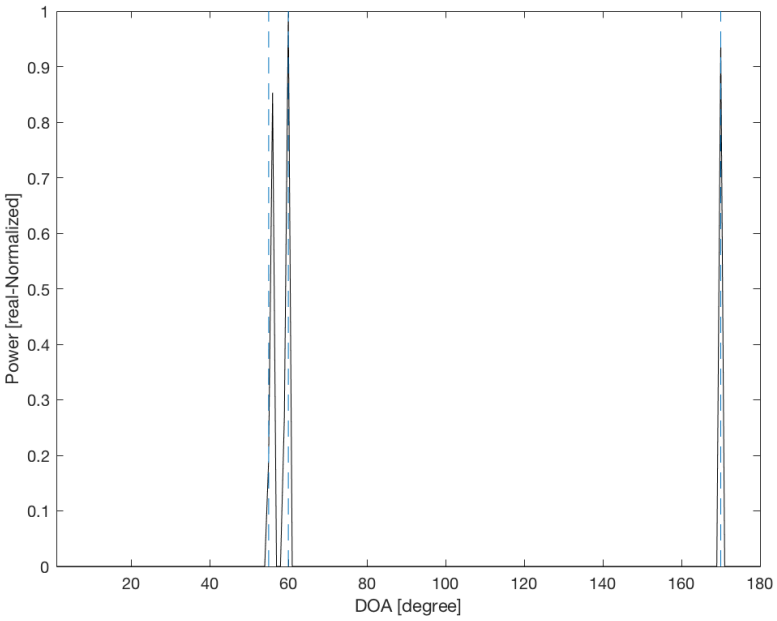

(b) GCD OLS A-LASSO, 10 snapshots

Figure 4.8: DOA estimation for spatially closed two source signals, pink Noise with SNR = 0 dB, two source signals at DOAs 60° and 64°, 10 snapshots, using (a) GCD MVDR A-LASSO and (b) GCD OLS A-LASSO.

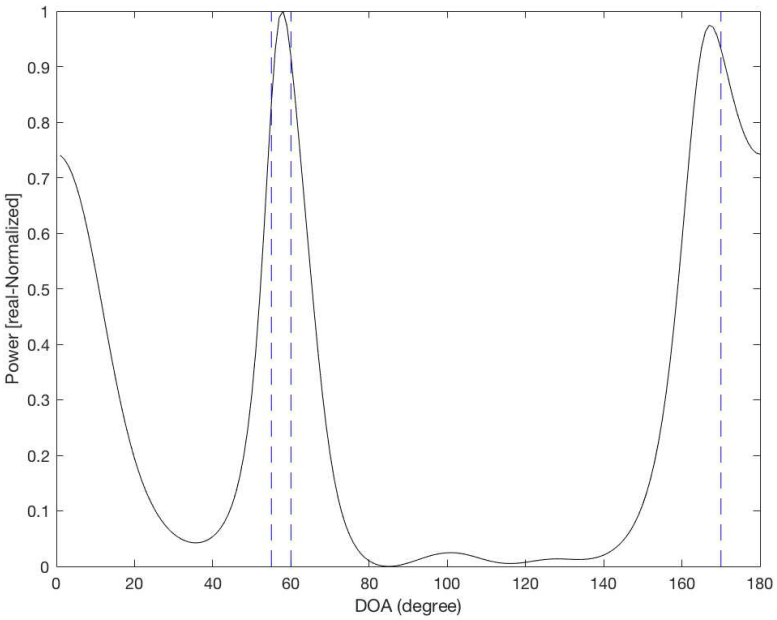

(a) UN-MUSIC, 10 snapshots

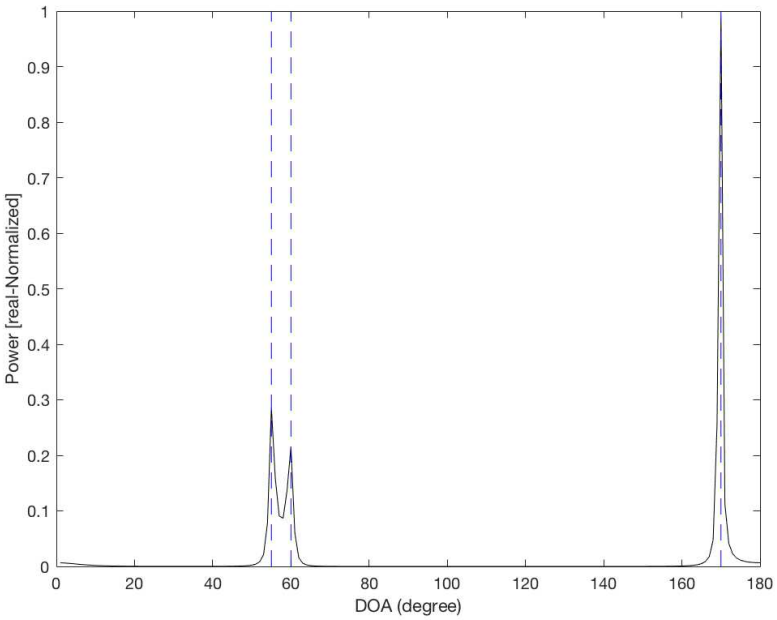

(b) UN-MUSIC, 2×10^4 snapshots

Figure 4.9: DOA estimation for spatially closed two source signals, pink Noise with SNR = 0 dB, two source signals at DOAs 60° and 64°, 10 snapshots, using (a) and (b) UN-MUSIC.

In the next two experiment, the RMSE is used as the performance measure, which is given by

$$\text{RMSE} = \frac{1}{L}\sum_{l=1}^{L}\sqrt{\frac{1}{N_{sim}}\sum_{n=1}^{N_{sim}}(\widehat{\theta}_{l,n}-\theta_l)^2} \tag{4.23}$$

where $\widehat{\theta}_{l,n}$ is the estimate of the DOA angle θ_l of the n-th Monte Carlo trial.

In the fourth experiment, we investigate the performance of the GCD OLS A-LASSO, GCD MVDR A-LASSO, and UN-MUSIC algorithms as we vary SNR. For this purpose, let three source signals impinge on the arrays from DOA of $60°, 70°$ and $120°$. For UN-MUSIC, as before two separated ULAs are used wherein each ULA contains 7 sensors ($M_1 = M_2 = 7$). The performance of the various algorithms as SNR is varied is shown in Figs. 4.10 and 4.11. It is observed from the figures that both GCD OLS A-LASSO and GCD MVDR A-LASSO outperform UN-MUSIC algorithm for the four assumed different noise mixtures. Furthermore, GCD MVDR A-LASSO performs better than GCD OLS A-LASSO for all the different noise mixtures.

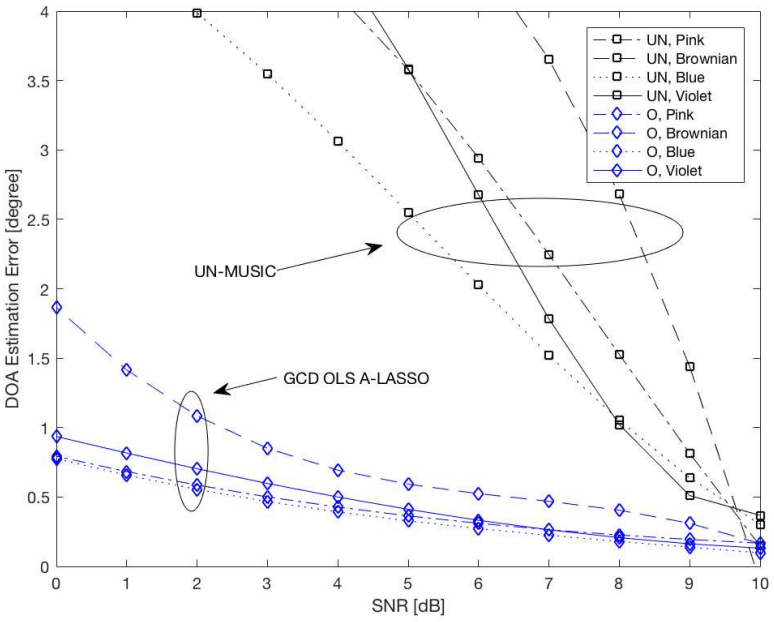

(a) UN-MUSIC VS. GCD OLS A-LASSO

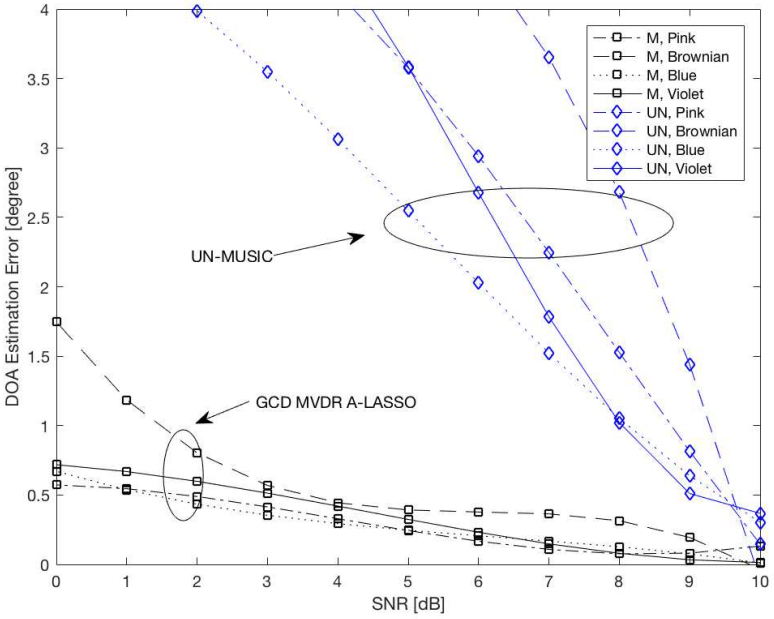

(b) UN-MUSIC VS. GCD MVDR A-LASSO

Figure 4.10: Performance comparison of the different algorithms as SNR is varied using UN-MUSIC, GCD OLS A-LASSO (single iteration), and GCD MVDR A-LASSO (single iteration). (a) UN-MUSIC vs. GCD OLS A-LASSO and (b) UN-MUSIC vs. GCD MVDR A-LASSO

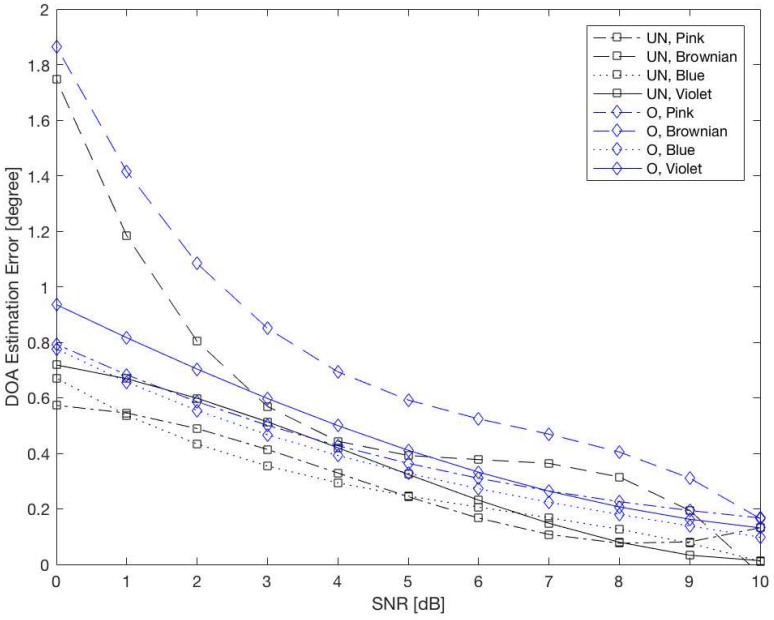

Figure 4.11: Performance comparison of the different algorithms as SNR is varied using GCD OLS A-LASSO (single iteration), and GCD MVDR A-LASSO (single iteration).

The final experiment involves the investigation of the effect of varying the angular separation between the source signals. Consider two source signals, the first being held fixed at DOA of 60°, while for the second one the DOA ranges from 62° to 90° in steps of 2°. The SNR is set to be 5 dB, 10 snapshots are considered for the simulation, 100 trials for each observation point, and a sampling grid varying from 1° to 180° with 1° steps. In UN-MUSIC, for source signals with separation $\leq 10°$, the DOA estimation error is high. Hence, the simulations for the UN-MUSIC are conducted starting form a source signal separation $> 10°$. Fig. 4.12 illustrates the DOA estimation error as a function of the angular separation between the two source signals using the proposed DOA estimation techniques. It can be seen from this figure that, the performance of GCD OLS A-LASSO and GCD MVDR A-LASSO are superior to that of the UN-MUSIC technique. Moreover, The DOA estimation error for of the GCD MVDR A-LASSO technique is always less than that of the

GCD OLS A-LASSO; in fact the DOA of GCD MVDR A-LASSO estimation error is $< 0.2^\circ$ for an angular separation of $\geq 8^\circ$.

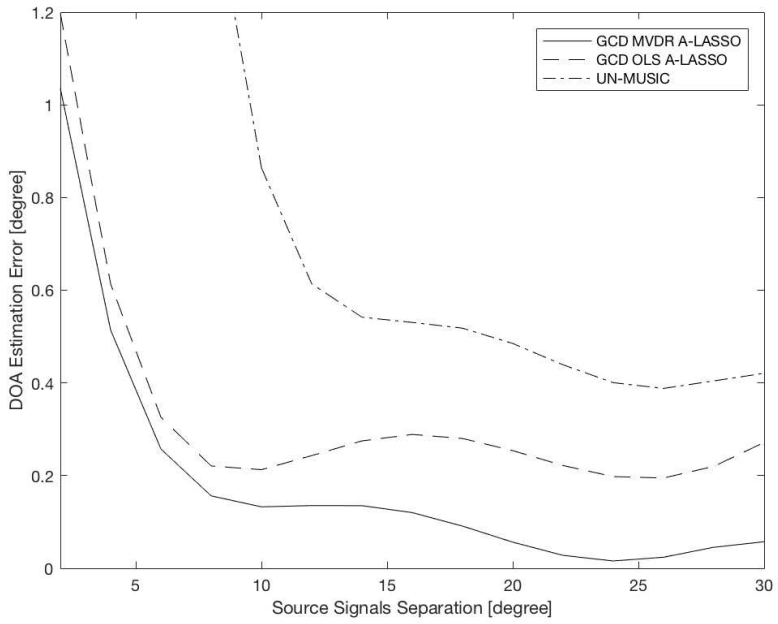

Figure 4.12: DOA estimation error for two sources as a function of separation between the two sources, SNR = 5 dB, 10 snapshots.

4.4 Summary

This chapter has presented two novel techniques using the compressive sensing framework on a sparse linear array for DOA estimation in the presence of unknown noise; based on the generalized correlation decomposition (GCD); these have referred to as GCD OLS A-LASSO and GCD MVDR A-LASSO, depending on whether ordinary least squares or minimum variance distortionless response is used as the initial weights. The performance of the proposed techniques is studied and compared with that of the UN-MUSIC technique. Neither of the proposed techniques require a priori knowledge about the number of source signals.

The proposed algorithms are able to perform the DOA estimation using a small number of snapshots and are able to estimate correlated source signals and

closely-spaced source signals in the presence of unknown noise using a fewer number of snapshots. The proposed algorithms can identify source signals of order $O(M^2)$ using an array of order $O(M)$ sensor, with high resolution.

For UN-MUSIC, even when the number of antennas is more than the number of sources, it is not able to distinguish source signals that are close to one another nor able to identify coherent sources. Even when the sources are not correlated, the UN-MUSIC technique requires more number of snapshots than that required by the proposed techniques in order to identify the sources but not necessarily all of them. Furthermore, since UN-MUSIC procedure itself is a long one, increasing the number of snapshots will dramatically increase the computational burden of the DOA estimation technique which will make it not suitable for real-time applications. On the other hand, both of the proposed techniques are able to fulfill the DOA estimation task, even in low SNR scenario, using a much lower number of snapshots than that used for UN-MUSIC.

It has been shown that the DOA estimation performance using the proposed techniques is superior to that of the UN-MUSIC; further, the performance of GCD MVDR A-LASSO is better than that of GCD OLS A-LASSO.

Chapter 5

Beamspace Compressive Sensing-Based DOA Estimation

5.1 Introduction

We would like to recall that the CS-based DOA estimation algorithms proposed in Chapters 3 and 4 are in element-space. In order to reduce the computational burden of the DOA estimation techniques, especially for sensor arrays with a high number of elements which are used for applications such as radar, BS-processing is proposed [12]. As already explained in Chapter 2, in a BS processor, the high dimensional data received in ES is first projected into a subspace with reduced dimensions to produce the BS data. This BS data is then processed in the resultant reduced dimensional space. BS processing schemes could be categorized into two main methods, full beamspace (FBS) and reduced-dimension beamspace (RBS), as explained in Sections 2.4.1 and 2.4.2, respectively.

It has been shown in Chapter 3 that the performances of CS-based DOA estimation algorithms, namely, ES OLS A-LASSO and ES MVDR A-LASSO, are vastly superior to that of the other ES-based methods. We will show in this chapter

that the performances of the CS-based algorithms are superior to that of the existing BS-based techniques, such as BS MVDR, BS MUSIC and BS ESPRIT.

This has motivated us to extend the CS-based techniques to BS to take advantage of the lower computational burden of BS processing. In order to do so, we first give a brief review of the existing BS methods and then compare the performance of existing BS methods with that of ES A-LASSO techniques proposed in Chapter 3. Finally, we propose CS-based techniques in BS and compare the performance with that of CS-based MVDR techniques in ES [132].

5.2 A Brief Review of BS Methods

In this subsection, we give a brief review of the existing BS methods, namely, BS MVDR [12, 133, 134], BS MUSIC [135, 136], and BS ESPRIT [11, 12, 137, 138]. It should be mentioned that the current BS-based DOA estimation techniques are developed using the FBS processing scheme.

5.2.1 BS MVDR

The sensor array output is given by (3.1) which is reproduced below

$$\mathbf{x}(t) = \mathbf{A}\mathbf{s}(t) + \mathbf{n}(t) \tag{5.1}$$

As discussed in Section 3.4, MVDR considers the following minimization problem:

$$\min_{\mathbf{w}} \mathbf{w}^H \mathbf{R}_{xx} \mathbf{w}, \quad \text{subject to} \quad \mathbf{w}^H \mathbf{a}(\theta) = 1 \tag{5.2}$$

where $\mathbf{w}$ is the MVDR beamformer weight vector, $\mathbf{R}_{xx}$ is the covariance matrix and $\mathbf{a}(\theta)$ is the sensor array steering vector corresponding to the DOA given by angle θ.

The MVDR weight vector $\mathbf{w}$ is given by [11, 12]:

$$\mathbf{w}_{ES} = \frac{\mathbf{R}_{xx}^{-1}\mathbf{a}(\theta)}{\mathbf{a}^H(\theta)\mathbf{R}_{xx}^{-1}\mathbf{a}(\theta)} \tag{5.3}$$

and the MVDR beamformer output is given by [11, 12]

$$\mathbf{P}_{ES} = \frac{1}{\mathbf{a}^H(\theta)\mathbf{R}_{xx}^{-1}\mathbf{a}(\theta)} \tag{5.4}$$

Using the FBS transformation matrix, $\mathbf{B}$, given by Equation (2.25), the sensor array output is transformed from ES to FBS by the transformation [12, 133, 134]

$$\mathbf{y}(t) = \mathbf{B}^H\mathbf{x}(t) \tag{5.5}$$

Denoting the FBS steering vector as $\mathbf{b}(\theta) = \mathbf{B}^H\mathbf{a}(\theta)$, the associated beamspace covariance matrix is given by $\mathbf{R}_{yy} = \mathbf{B}^H\mathbf{R}_{xx}\mathbf{B}$. Hence, the BS MVDR weight vector is given by [133, 134]

$$\mathbf{w}_{BS} = \frac{\mathbf{R}_{yy}^{-1}\mathbf{b}(\theta)}{\mathbf{b}^H(\theta)\mathbf{R}_{yy}^{-1}\mathbf{b}(\theta)} \tag{5.6}$$

and the BS MVDR sensor array output is given by [133, 134]

$$\mathbf{P}_{BS} = \frac{1}{\mathbf{a}^H(\theta)\mathbf{B}\mathbf{R}_{yy}^{-1}\mathbf{B}^H\mathbf{a}(\theta)} \tag{5.7}$$

5.2.2 BS MUSIC

Given an M-element sensor array output as in Equation (5.1), the ES covariance matrix, $\mathbf{R}_{xx}$ is given by [12]

$$\mathbf{R}_{xx} = \mathrm{E}[\mathbf{x}(t)\mathbf{x}^H(t)] = \mathbf{A}\mathbf{R}_{ss}\mathbf{A}^H + \sigma^2\mathbf{I} \tag{5.8}$$

where $\mathbf{R}_{ss}$ is the signal covariance matrix, $\mathbf{E}$ denotes the statistical expectation, σ^2 and $\mathbf{I}$ are the noise variance and identity matrix, respectively. The subspace decomposition of the covariance matrix, $\mathbf{R}_{xx}$, is [12]

$$\mathbf{R}_{xx} = \sum_{i=1}^{M} \lambda_i e_i e_i^H = \mathbf{E}_s \Lambda_s \mathbf{E}_s^H + \mathbf{E}_n \Lambda_n \mathbf{E}_n^H \tag{5.9}$$

where $\lambda_1 \cdots \geq \lambda_L \geq \ldots \lambda_M$ are the eigenvalues of $\mathbf{R}_{xx}$ and e_i are the corresponding orthonormal eigenvectors. $\mathbf{E}_s = [e_1 \ldots e_L]$ is the signal subspace with rank L (the number of sources) and $\mathbf{E}_n = [e_L + 1 \ldots e_M]$ is the noise subspace. Λ_s and Λ_n are diagonal matrices, with the corresponding eigenvalues. The MUSIC spectrum is given as follows [11, 12, 135, 136]

$$\mathbf{P}_{ES-MUSIC} = \frac{\mathbf{a}^H(\theta)\mathbf{a}(\theta)}{\mathbf{a}^H(\theta)\mathbf{E}_n\mathbf{E}_n^H\mathbf{a}(\theta)} \tag{5.10}$$

where $\mathbf{a}(\theta)$ is the sensor array steering vector corresponding to the DOA given by angle θ. Using the FBS transformation matrix, $\mathbf{B}$, given by Equation (2.25) and utilizing Equation (5.5), the BS MUSIC spatial spectrum can be described as [11, 12, 135, 136]

$$\mathbf{P}_{BS-MUSIC} = \frac{\mathbf{a}^H(\theta)\mathbf{B}\mathbf{B}^H\mathbf{a}(\theta)}{\mathbf{a}^H(\theta)\mathbf{B}\mathbf{E}_{n,bs}\mathbf{E}_{n,bs}^H\mathbf{B}^H\mathbf{a}(\theta)} \tag{5.11}$$

where $\mathbf{E}_{n,bs}$ is the BS noise subspace eigenvector matrix calculated from the SVD of the BS covariance matrix, $\mathbf{R}_{yy} = \mathbf{B}^H\mathbf{R}_{xx}\mathbf{B}$.

5.2.3 BS ESPRIT

As explained in the previous subsections, one can calculate the BS array output using Equation (5.5). Following the square-root approach, the signal subspace, $\mathbf{E}_s$

is computed as the L dominant left singular vectors of

$$[\mathrm{Re}(\mathbf{y})\mathrm{Im}(\mathbf{y})] \quad \text{with} \quad \mathbf{y}(t) = \mathbf{B}^H \mathbf{x}(t) \tag{5.12}$$

where Re and Im correspond to the real and the imaginary parts, respectively. Let the L singular vectors corresponding to the L largest singular values of (5.12) be denoted by $\mathbf{E}_s$ (the signal subspace). Asymptotically, the real-valued matrices $\mathbf{E}_s$ and $\mathbf{B}$ span the same L-dimensional signal subspace, so there is a nonsingular matrix $\mathbf{T}_A$ such that [11]

$$\mathbf{B} = \mathbf{E}_s \mathbf{T}_A \tag{5.13}$$

Then the real-valued invariance equation is [11]

$$\Gamma_1 \mathbf{E}_s \mathbf{Y} = \Gamma_2 \tag{5.14}$$

where Γ_1 and Γ_2 are the selection matrices [11] and

$$\mathbf{Y} = \mathbf{T}_A \Psi \mathbf{T}_A^{-1} \tag{5.15}$$

Ψ being a real-valued diagonal matrix containing the desired DOA information as

$$\Psi = \mathrm{diag}[\tan(\frac{\mu_1}{2}), \ldots, \tan(\frac{\mu_l}{2}), \ldots, \tan(\frac{\mu_L}{2})] \tag{5.16}$$

In the above equation, $\mu_l = \frac{2\pi}{\lambda} d \cos(\theta_l)$, d being the inter-element spacing, λ denotes the wavelength and θ_l is the DOA of the lth source signal. Equation (5.15) is used to solve for Ψ by using either the least square or trilinear least square. Then the desired DOA information, namely, the angles θ_l, $l = 1, \ldots, L$ are obtained using Equation (5.16).

5.3 Performance Comparison of existing Beamspace techniques with that of Element-space A-LASSO methods

In this section, we investigate the performance of the existing BS-based techniques in comparison with that of the ES-based techniques, namely, ES OLS A-LASSO and ES MVDR A-LASSO proposed in Chapter 3.

For this purpose, we conduct a number of experiments to examine the capability of the BS MVDR and BS MUSIC algorithms, as well as the ES A-LASSO algorithms to detect the number of source signals that they are supposed to be able to identify, theoretically. For that purpose, we consider a ULA containing M elements. For such a scenario, all the algorithms are supposed to be able to identify up to L_{max} source signals, where $L_{max} \leq (M-1)$. It should be mentioned that the number of source signals to be estimated is assumed to be known in advance in the BS MUSIC and BS ESPRIT DOA estimation techniques, whereas no such assumption is needed for ES-based A-LASSO techniques. Further, the BS-based techniques are covariance matrix dependent. Hence, it is not possible to estimate the covariance matrix correctly, by using a single snapshot. In view of this, in the BS-based DOA estimation techniques, we consider at least 10 snapshots. However, only a single snapshot along with only one iteration is employed for the ES OLS A-LASSO and ES MVDR A-LASSO simulations.

We now evaluate the performance with regard to estimating the DOA using a ULA with $M = 7$. Hence, it should be possible to identify up to 6 sources. Let us assume that there are 6 sources impinging on the array with DOAs being uniformly distributed over $\theta = [40^\circ, 140^\circ]$. Let us also assume that the noise is AWGN and SNR $= 0$ dB.

Simulations are carried out using ES OLS A-LASSO and ES MVDR A-LASSO,

as well as the BS MVDR and BS MUSIC DOA estimation techniques to identify the 6 sources. The results are as shown in Figs. 5.1, 5.2 and 5.3. Fig. 5.1 shows that all of the 6 source signals are identified correctly using the ES OLS A-LASSO or ES MVDR A-LASSO technique with only a single snapshot of the received data. However, even when we use 7 sensors and theoretically the maximum number of sources that can be identified is 6, neither BS MVDR nor BS MUSIC is able to clearly identify the source signals using 10 snapshots (Figs. 5.2(a) and 5.3(a)). BS MVDR is unable to identify properly even when the number of snapshots is increased to 200 (Fig. 5.2(b)). Also, it is seen from Fig. 5.3(b) that even with 200 snapshots, BS MUSIC is hardly able to identify the 6 source signals. Thus, it is seen that with a single snapshot, both the ES OLS A-LASSO and ES MVDR A-LASSO techniques are able to identify the 6 sources properly, while neither BS MVDR nor BS MUSIC is able to identify the sources with 10 snapshots and require a large number of snapshots to be able to barely identify all the sources. It should be noted that increasing the number of snapshots will lead to increased computational complexity of the DOA estimation algorithms, thus making them unsuitable for real-time applications.

Since even with 200 snapshots, neither BS MVDR nor BS MUSIC is able to identify properly all the source signals, we now reduce the number of sources to only three to see if BS-based methods can correctly identify the sources using a reasonable number of snapshots.

Fig. 5.4 illustrates the DOA estimation of 3 source signals impinging on the the 7 element ULA from DOAs of $60°, 75°$ and $120°$. In this case, we set SNR to be 0 dB and use 10 snapshots for the BS-based techniques, while only a single snapshot along with only one iteration is considered for ES OLS A-LASSO as well as ES MVDR A-LASSO. From this figure, it is clear that all the DOA estimation techniques are able to identify the three sources correctly. Even though the results

are shown only for specific case of $\theta = 60°, 75°$ and $120°$, similar results have been obtained for various values of SNR and values of θ, assuming only 3 sources and keeping the angles to be not very close to one another.

In view of the results obtained by the above experiments, for the remaining experiments, we assume that there are only 3 signal sources, so that we can utilize a reasonable number of snapshots for the BS-based methods.

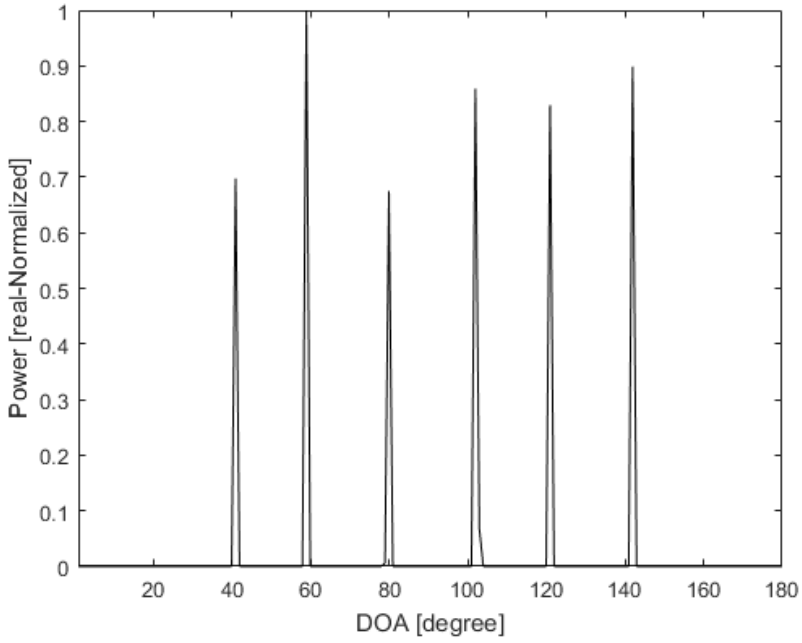

(a) ES MVDR A-LASSO, single snapshot

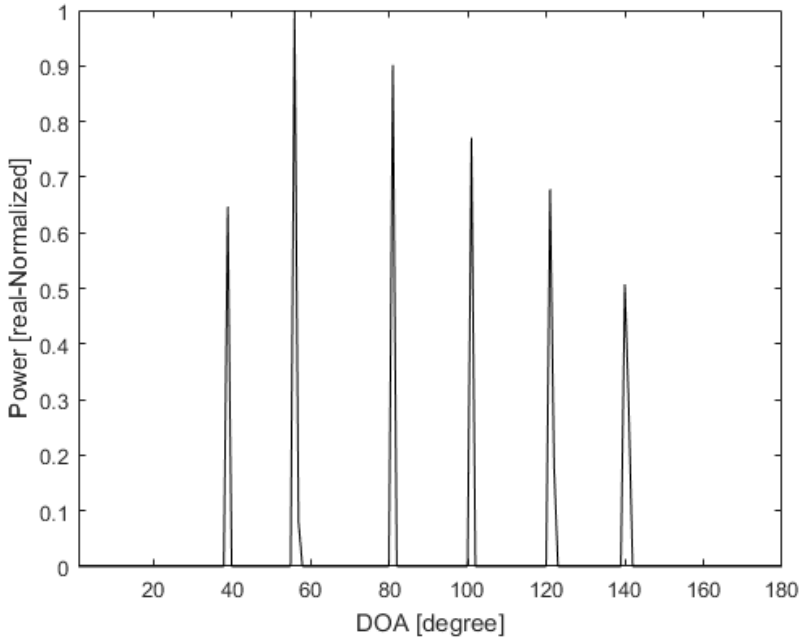

(b) ES OLS A-LASSO, single snapshot

Figure 5.1: DOA estimation of 6 sources using a ULA containing 7 elements, single snapshot, single iteration, SNR = 0 dB, using (a) ES MVDR A-LASSO and (b) ES OLS A-LASSO.

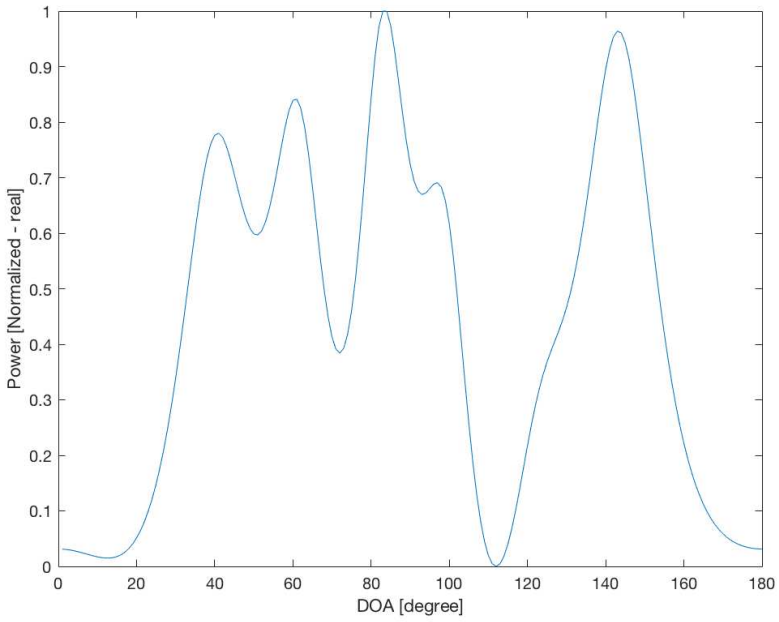

(a) BS MVDR, 10 snapshots

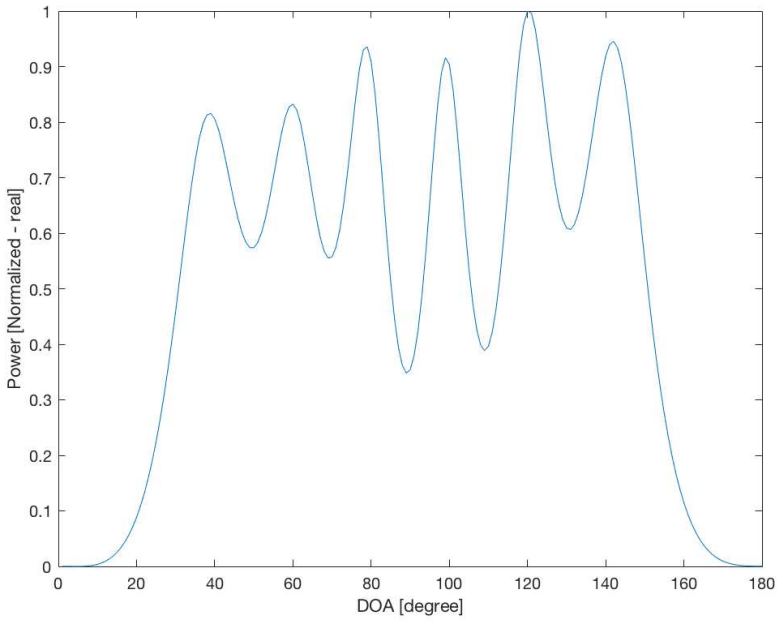

(b) BS MVDR, 200 snapshots

Figure 5.2: BS MVDR DOA estimation of 6 sources using a ULA containing 7 elements, SNR = 0 dB, using (a) 10 snapshots and (b) 200 snapshots.

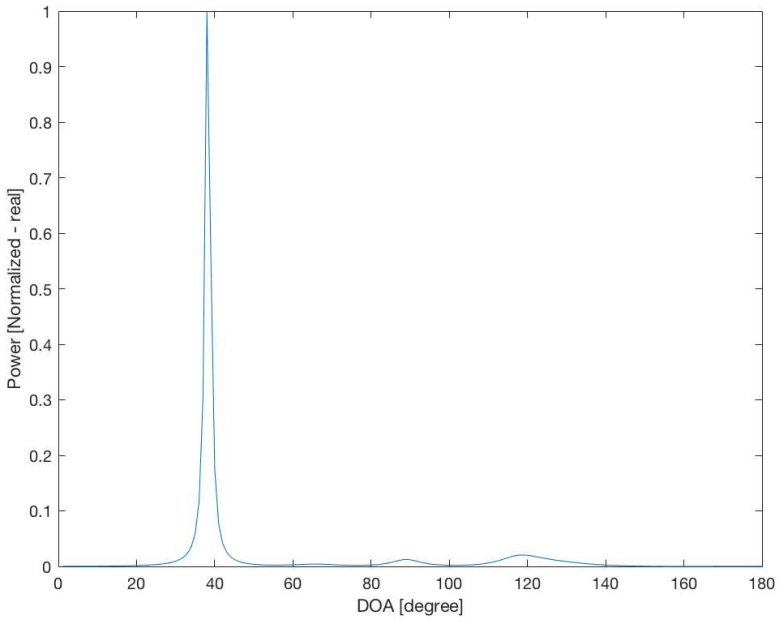

(a) BS MUSIC, 10 snapshots

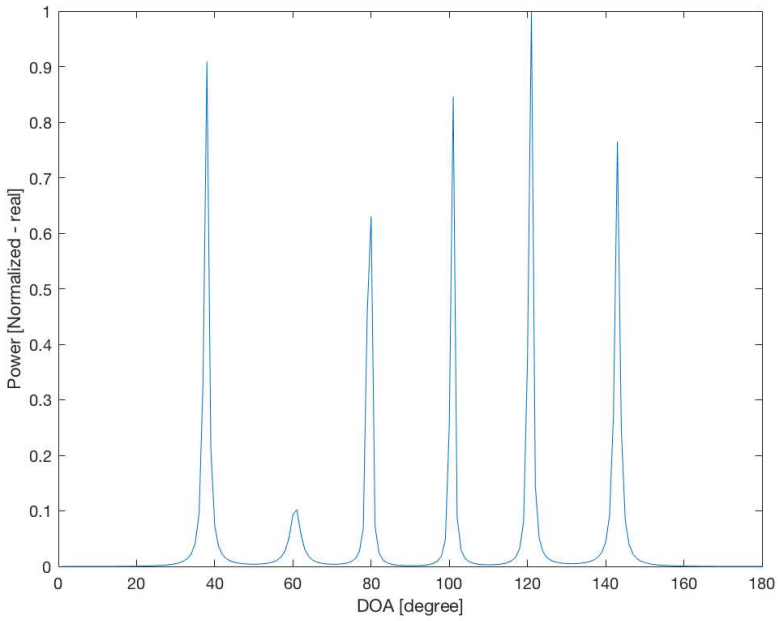

(b) BS MUSIC, 200 snapshots

Figure 5.3: BS MUSIC DOA estimation of 6 sources using a ULA containing 7 elements, SNR = 0 dB, using (a) 10 snapshots and (b) 200 snapshots.

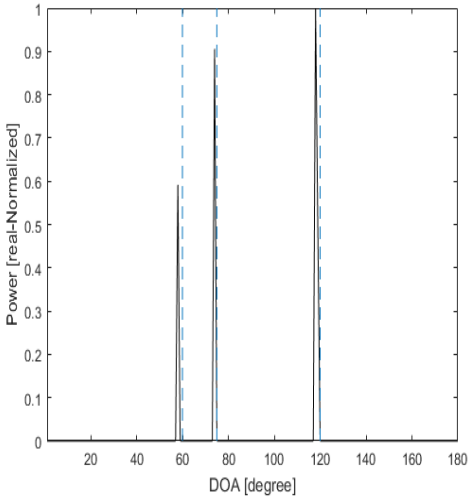

(a) ES MVDR A-LASSO

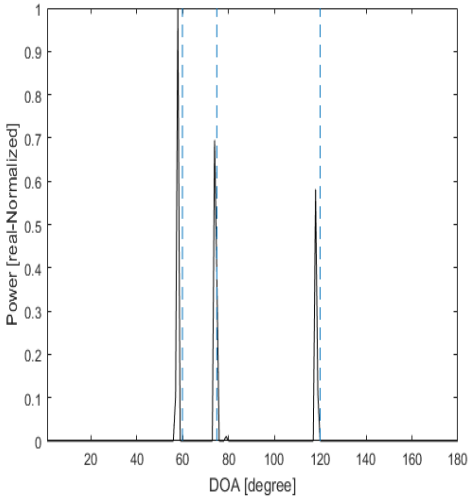

(b) ES OLS A-LASSO

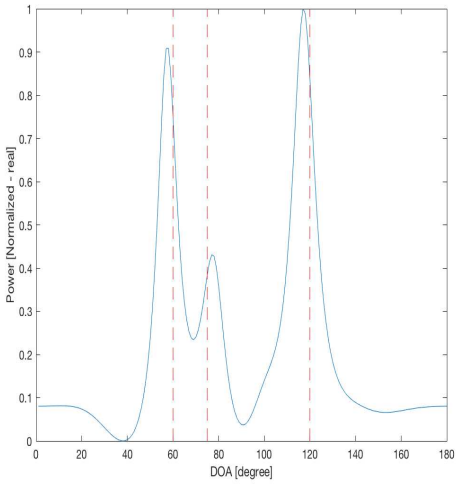

(c) BS MVDR

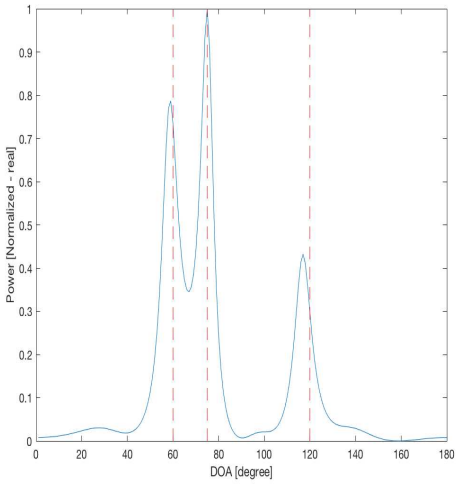

(d) BS MUSIC

Figure 5.4: DOA estimation of 3 sources using a ULA containing 7 elements, SNR = 0 dB, using (a) ES MVDR A-LASSO, (b) ES OLS A-LASSO, (c) BS MVDR, and (d) BS MUSIC.

The purpose of the second experiment is to investigate as to whether the two BS-based algorithms can identify correlated sources. From Chapter 3, we know that the ES-based A-LASSO algorithms can in fact identify such correlated sources. For this experiment, we again assume a ULA of 7 elements, and consider two cases: (a) three uncorrelated signals impinging on the array from DOAs of $40°, 60°$ and $160°$, and (b) three signals impinging from the same angles, but with the first two signals being fully correlated (coherent). The received signal is assumed to be contaminated by AWGN with SNR set to 0 dB. A single snapshot with a single iteration is considered for ES OLS A-LASSO and ES MVDR A-LASSO techniques and 10 snapshots are employed for BS-based methods. Figs. 5.5(a), 5.6(a), 5.7(a), 5.7(b), 5.8(a) and 5.8(b) show that all the DOA estimation techniques are able to identify the source signals when they are uncorrelated, even though the BS-based techniques require a very large number of snapshots.

Even with a number of snapshots as large as 10^4, when two of the sources are correlated, Figs. 5.7(c) and (d) and Figs. 5.8(c) and (d) show that neither BS MVDR nor BS MUSIC is able to detect the coherent sources. In fact, the BS-based techniques will not be able to identify correlated sources.

However, even with a single snapshot along with just one iteration, both ES OLS A-LASSO and ES MVDR A-LASSO techniques are able to identify properly uncorrelated as well as correlated sources.

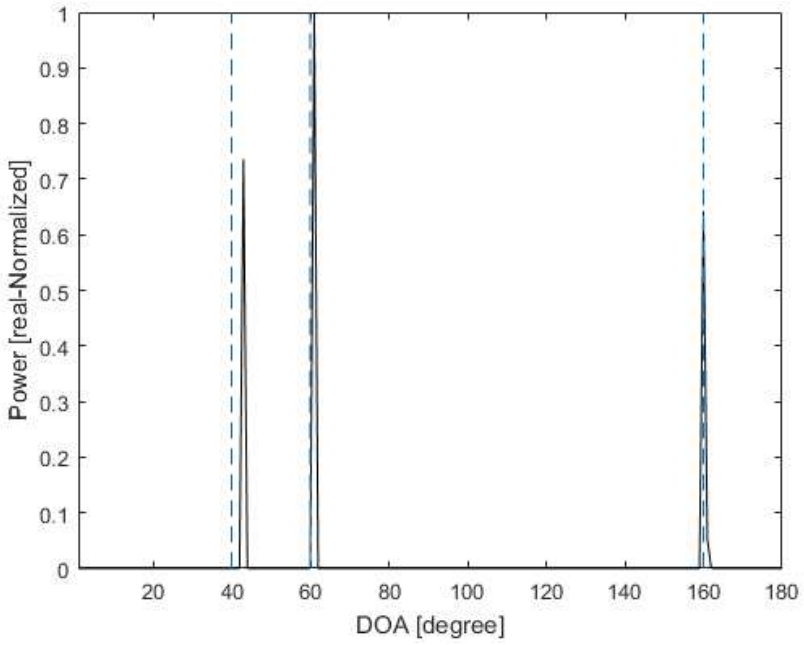

(a) ES MVDR A-LASSO, uncorrelated sources

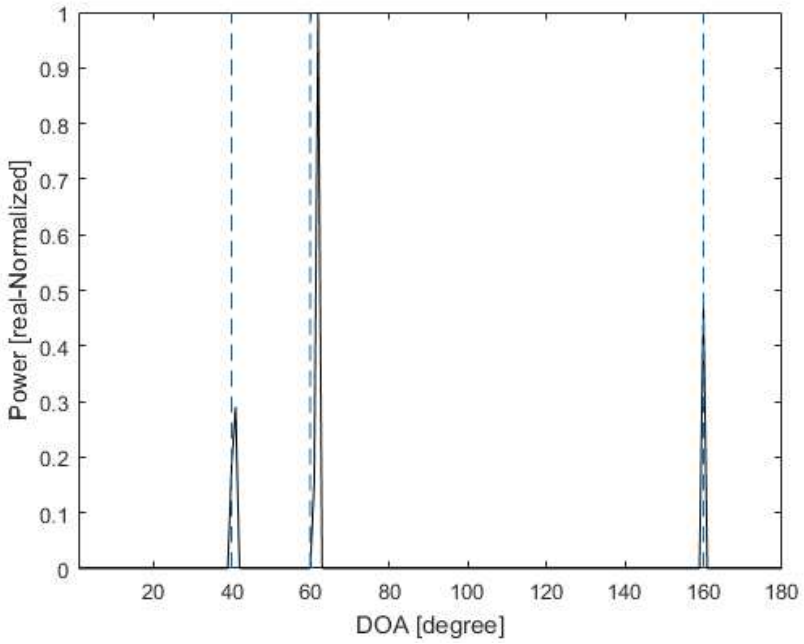

(b) ES MVDR A-LASSO, correlated sources

Figure 5.5: DOA estimation for 3 source signals with DOAs $40°, 60°$ and $160°$, single snapshot and single iteration and AWGN with SNR = 0 dB, using ES MVDR A-LASSO. (a) Uncorrelated sources and (b) two of the sources being correlated.

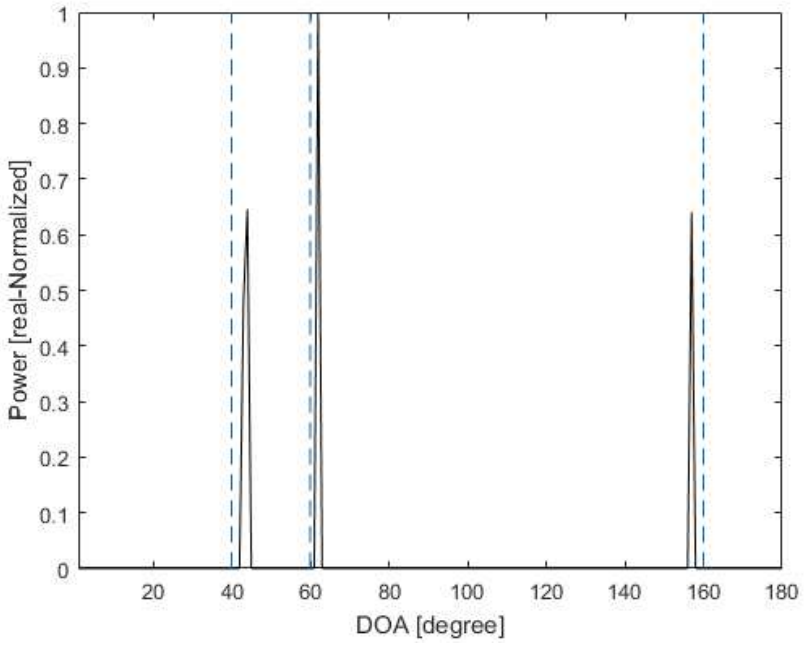

(a) ES OLS A-LASSO, uncorrelated sources

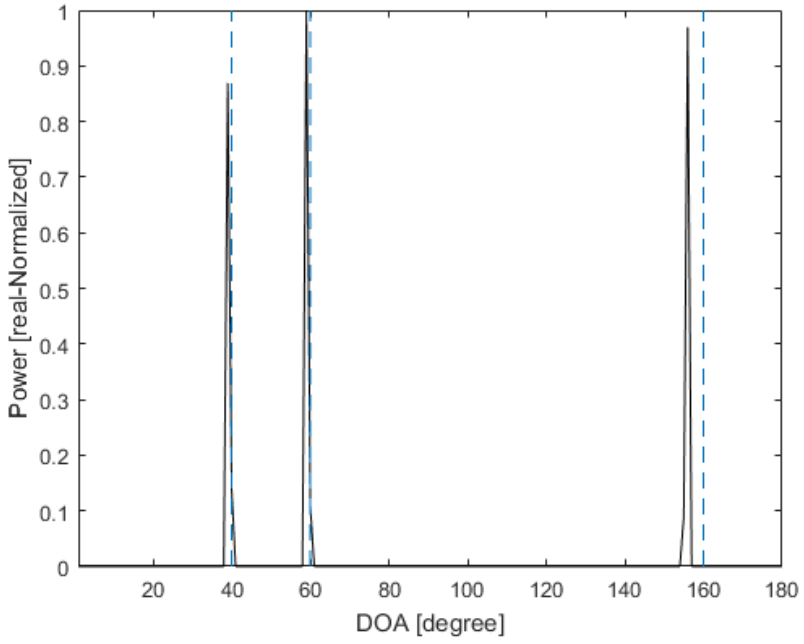

(b) ES OLS A-LASSO, correlated sources

Figure 5.6: DOA estimation for 3 source signals with DOAs $40°, 60°$ and $160°$, single snapshot and single iteration and AWGN with SNR = 0 dB, using ES OLS A-LASSO. (a) Uncorrelated sources and (b) two of the sources being correlated.

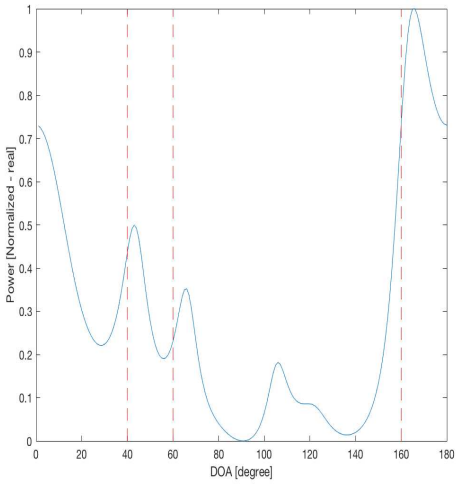

(a) BS MVDR, 10 snapshots

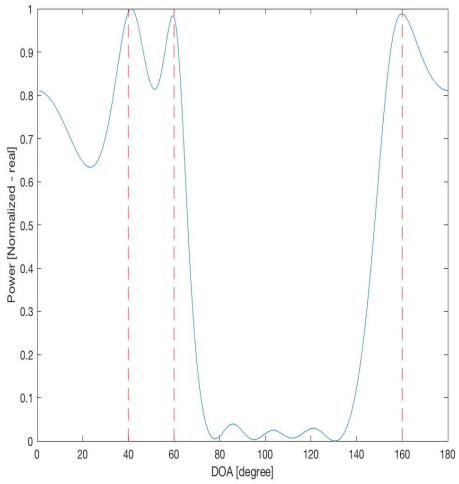

(b) BS MVDR, 10^4 snapshots

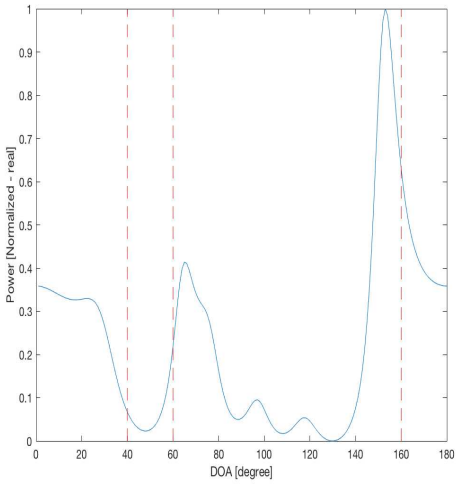

(c) BS MVDR, 10 snapshots

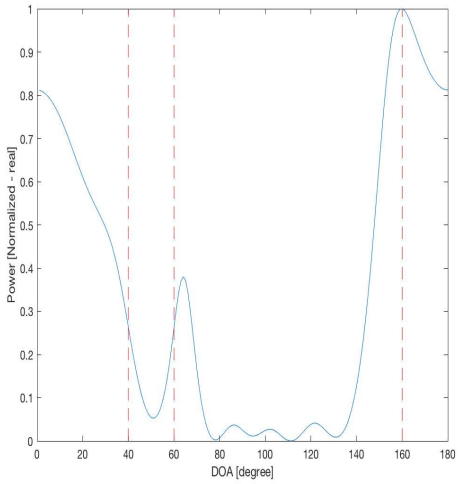

(d) BS MVDR, 10^4 snapshots

Figure 5.7: DOA estimation for 3 source signals with DOAs $40°, 60°$ and $160°$, SNR = 0 dB, using BS MVDR. (a)and (b) uncorrelated sources, (c) and (d) two of the sources being correlated.

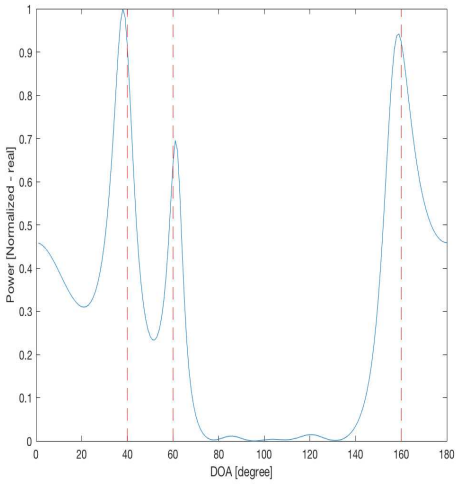

(a) BS MUSIC, 10 snapshots

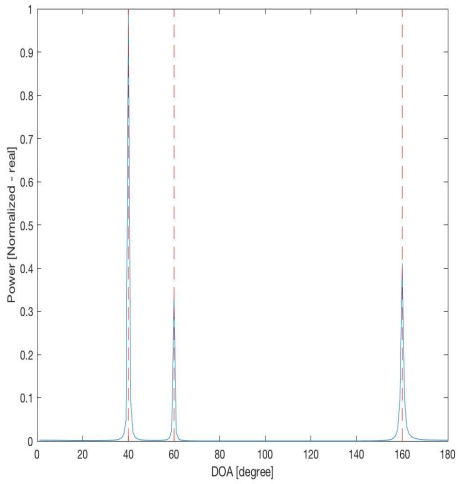

(b) BS MUSIC, 10^4 snapshots

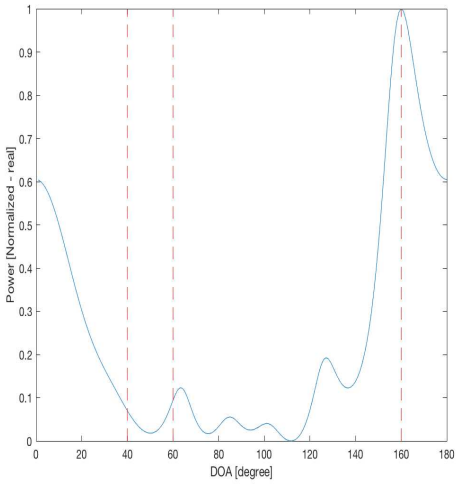

(c) BS MUSIC, 10 snapshots

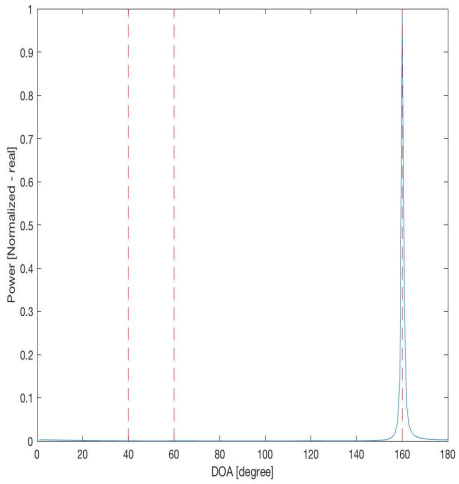

(d) BS MUSIC, 10^4 snapshots

Figure 5.8: DOA estimation for 3 source signals with DOAs $40°, 60°$ and $160°$, SNR = 0 dB, using BS MUSIC. (a) and (b) uncorrelated sources, (c) and (d) two of the sources being correlated.

In the third experiment, we examine the capability of the proposed techniques in identifying closely-spaced sources. For this purpose, let three sources impinge the array form DOAs of 50°, 60°, and 170°. The received signal is assumed to be contaminated with AWGN with SNR set to 0 dB. Single snapshot with single iteration is considered for the ES-based DOA estimation techniques and 10 or more snapshots of the received data are used for BS-based DOA estimation methods. The simulations results are shown in Figs. 5.9, 5.10 and 5.11. From these figures, three peaks can easily be identified using ES MVDR A-LASSO and ES OLS A-LASSO, thus identifying the three sources.

Using 10 snapshots, neither BS MVDR nor BS MUSIC is able to identify the two closely-spaced sources, and these two source signals are identified as a single one. Furthermore, even with number of snapshots as large as 10^6, BS MVDR is not able to identify the two closely-spaced sources.

Even with 7×10^2 snapshots, BS MUSIC is hardly able to discriminate the sources. On the other hand, as mentioned earlier, increasing the number of snapshots will lead to increased computational load, and consequently, these BS-based estimation techniques will not be suitable for real-time application.

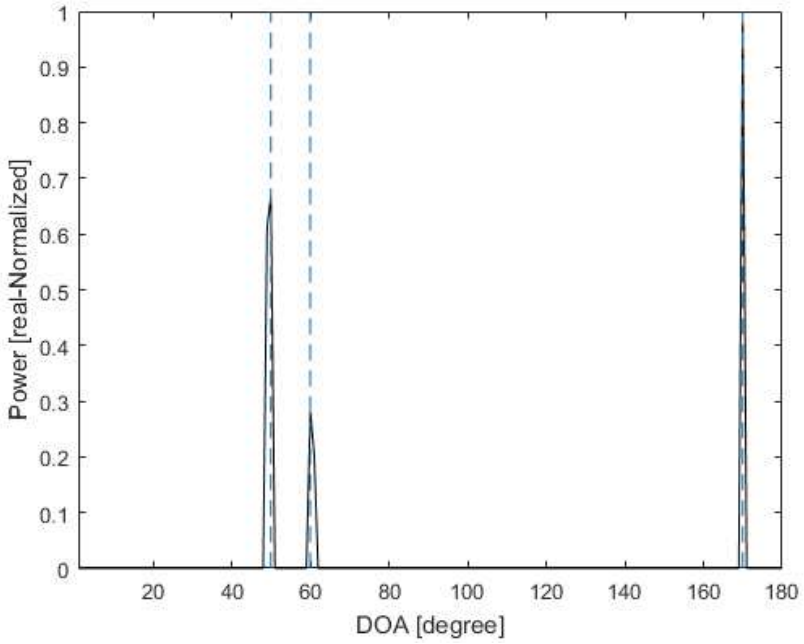

(a) ES MVDR A-LASSO

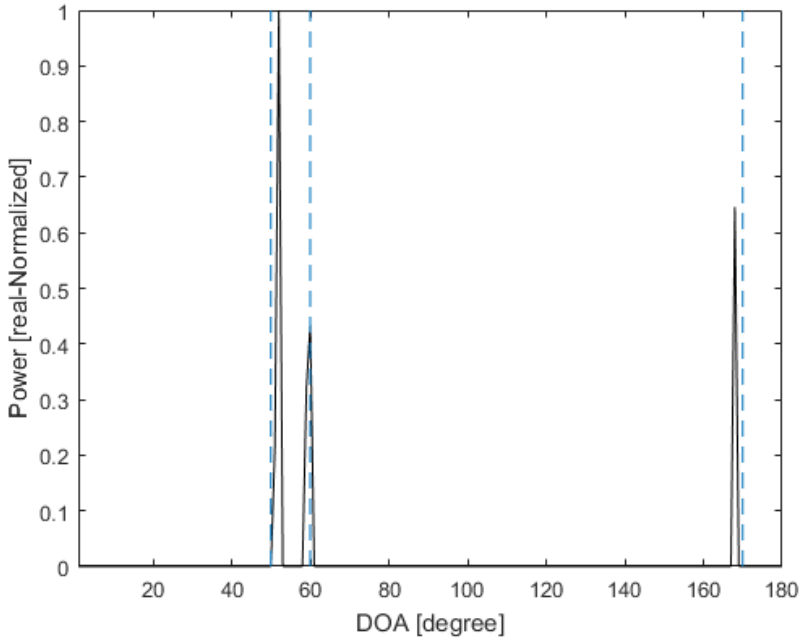

(b) ES OLS A-LASSO

Figure 5.9: DOA estimation for 3 source signals with DOAs $50°, 60°$ and $170°$, uncorrelated sources, single snapshot, single iteration and AWGN with SNR = 0 dB, using (a) ES MVDR A-LASSO and (b) ES OLS A-LASSO.

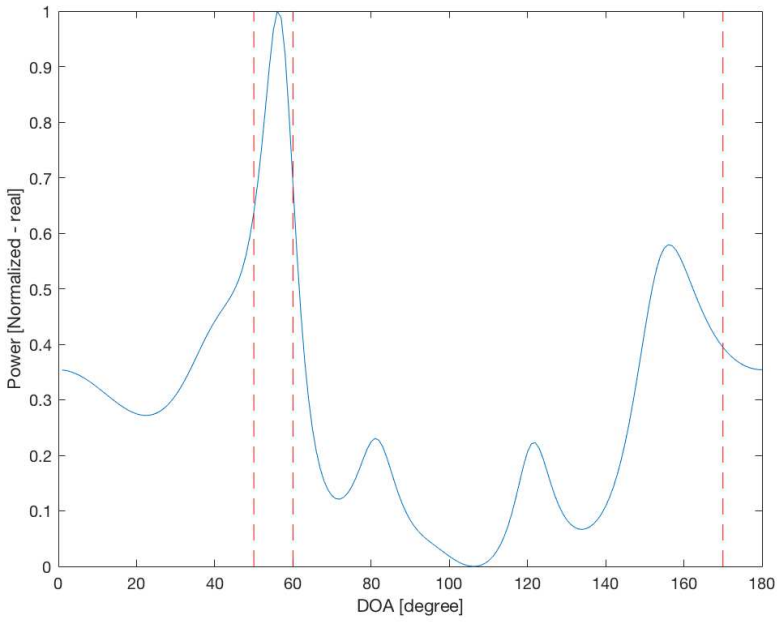

(a) BS MVDR, 10 snapshots

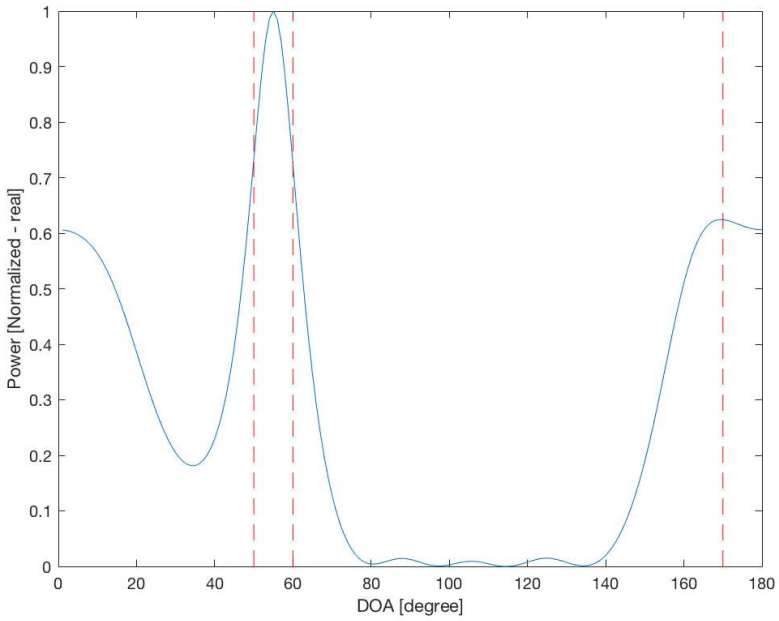

(b) BS MVDR, 10^6 snapshots

Figure 5.10: DOA estimation for 3 source signals with DOAs $50°, 60°$ and $170°$, SNR $= 0$ dB, using BS MVDR.

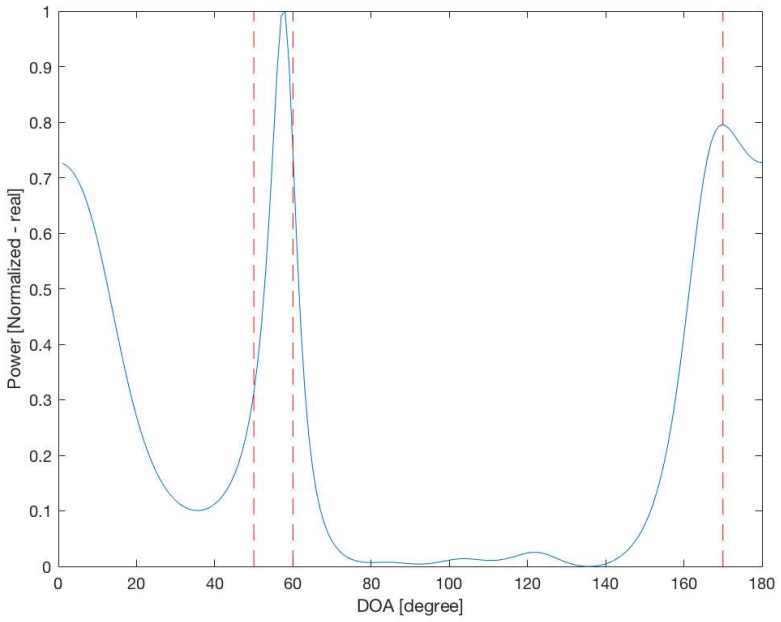

(a) BS MUSIC, 10 snapshots

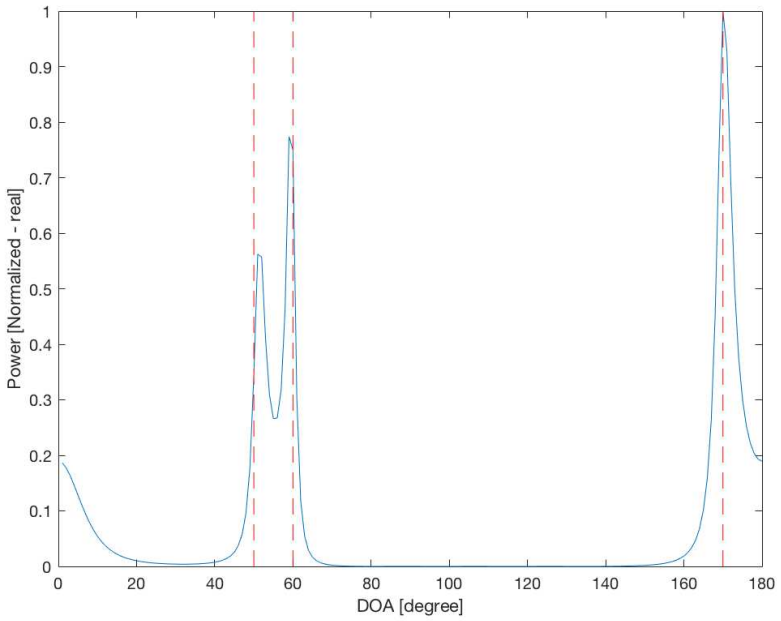

(b) BS MUSIC, 7×10^2 snapshots

Figure 5.11: DOA estimation for 3 source signals with DOAs $50°, 60°$ and $170°$, SNR $= 0$ dB, using BS MUSIC.

In the final experiment, we investigate the performance of the BS MVDR, BS MUSIC, BS ESPRIT, ES OLS A-LASSO and ES MVDR A-LASSO as we vary SNR by using RMSE as the performance measure, where RMSE is given by [139]

$$\text{RMSE} = \frac{1}{L}\sum_{l=1}^{L}\sqrt{\frac{1}{N_{sim}}\sum_{n=1}^{N_{sim}}(\widehat{\theta}_{l,n}-\theta_l)^2} \tag{5.17}$$

$\widehat{\theta}_{l,n}$ being the estimate of the DOA angle θ_l of the n-th Monte Carlo trial.

For this purpose, let three non-fluctuating source signals impinge on the array from DOA of 60°, 75° and 120°. For BS MVDR, BS MUSIC as well as BS ESPRIT, 10 snapshots are considered. A single snapshot with a single iteration is considered for ES MVDR A-LASSO and ES OLS A-LASSO techniques.

The performance of the various algorithms as SNR is varied is shown in Fig. 5.12. It is observed from the figure that, even with a single snapshot along with only one iteration, the performance of the ES-based DOA estimation techniques, namely, ES OLS A-LASSO and ES MVDR A-LASSO, is superior to that of any of the BS-based methods irrespective of SNR. Further, it is noted that the performance of ES MVDR A-LASSO is superior to that of the ES OLS A-LASSO. Similar results have been obtained for other values of DOA angle θ.

Based on the results of the previous experiments, it is very clear that neither BS MVDR nor BS MUSIC is able to detect $(M-1)$ source signals even though they are theoretically supposed to be able to do so, unless a very large number of snapshots is employed. Furthermore, in order to estimate the closely-spaced source signals, they again require a large number of snapshots to be used, which means a tremendous increase in the computational load. Moreover, neither one of them is able to discriminate coherent sources. On the other hand, even with a single snapshot and with only one iteration, both of the ES-based DOA estimation techniques, namely, ES OLS A-LASSO and ES MVDR A-LASSO, are able to detect all the

$(M-1)$ source signals, identify closely-spaced source signals as well as coherent sources. Finally, the performance of the ES-based A-LASSO techniques is way superior to that of the BS-based methods in terms of the RMSE irrespective of SNR.

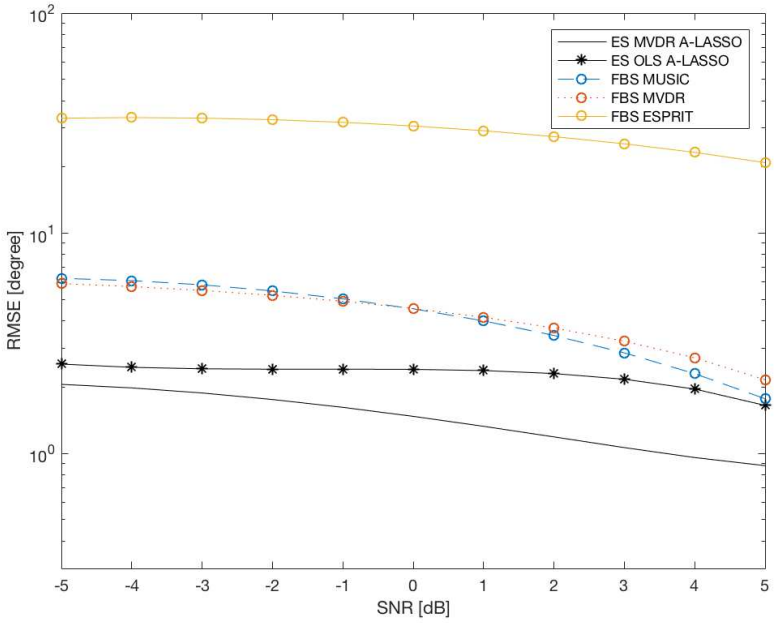

Figure 5.12: Performance comparison of the different algorithms as SNR is varied using BS MVDR, BS MUSIC, BS ESPRIT, ES OLS A-LASSO (single iteration) and ES MVDR A-LASSO (single iteration).

Thus, it is clear that the ES-based DOA estimation techniques proposed in Chapter 3 are superior to that of the existing BS-based DOA estimation methods. This motivate us to extend compressive sensing to beamspace and propose new BS-based CS DOA estimation techniques. For this purpose, we first present a new BS-processor for which more than one sector of interest is covered at the same time. Then we extend the work presented in Chapter 3 using the ES A-LASSO DOA estimation technique to produce a new BS-based one which we shall refer as BS A-LASSO.

5.4 Beamspace Compressive Sensing DOA Estimation

In contrast to the ES processing, where the signals derived from each sensor are weighted and summed to produce the array output, the BS processing is a two-stage scheme where the first stage takes the sensor array signals as input and produces a set of multiple outputs, which are then weighted and combined to produce the BS sensor array multiple beams. The processing done at the first stage is by fixed weighting of the array signals and amounts to producing multiple beams steered in different directions. The weighted sum of these beams is utilized to obtain the array output and the weights applied to the different beam outputs are then optimized to meet a specific optimization criterion. In general, for an M-element array, a FBS processor consists of a main beam steered in the signal direction and a set of not more than $M-1$ secondary beams.

5.4.1 Multiple-Beam Beamspace

It is possible to combine together multiple beams so that multiple sectors could be scanned. Assuming that it is required to provide Q fan beams and each fan beam contains $N_{bs,q},\ q=1,\ldots,Q$ beams, multiple beams could be produced using the output of the reduced-dimensional BS, described in Section 2.4.2, where for each sector of interest, $N_{bs,q}$ and $\theta_{c,q}$ must be determined a priori. Then the reduced-dimensional BS matrices, $\mathbf{b}_{bs,q}^H,\ q=1,\ldots,Q$, are combined together to compute the final BS transformation matrix, $\mathbf{B}_{bs}^H$, as follows

$$\left[\mathbf{B}_{bs}^H\right] = \left[\mathbf{b}_{bs,1}^H \ldots \mathbf{b}_{bs,q}^H \ldots \mathbf{b}_{bs,Q}^H\right] \tag{5.18}$$

Fig. 5.13 shows an example for a multiple fan beam where $Q = 2$ and each fan consists of $N_{bs,1} = N_{bs,2} = 3$ beams using an array for which $M = 31$.

It should be noted that the columns of the BS matrix are not orthogonal. To guarantee the orthogonality of the BS matrix columns, so that a source signal impinging on a beam does not corrupt the output of the other beams, the following step must be added. Let the original BS matrix to be $\mathbf{B}_{no}$ where *no* stands for "not orthogonal", then the final BS matrix, $\mathbf{B}_{bs}$, for which the columns are orthogonal, is given by [12]

$$\mathbf{B}_{bs} = \mathbf{B}_{no} \left[\mathbf{B}_{no}^H \mathbf{B}_{no}\right]^{-\frac{1}{2}} \tag{5.19}$$

so that, $\mathbf{B}_{bs}^H \mathbf{B}_{bs} = I$ holds.

5.4.2 Beamspace A-LASSO

The BS matrix given by Equation (5.19) is used to transfer the ES array output, $\mathbf{y}$, and the ES over-complete sensing matrix, Φ, into BS output, $\mathbf{y}_{bs}$, and BS over-complete sensing matrix, Φ_{bs}, respectively, as follows

$$\mathbf{y}_{bs} \in \mathbb{R}^{N_{bs} \times 1} = \mathbf{B}_{bs}^H \mathbf{y}, \quad \Phi_{bs} \in \mathbb{R}^{N_{bs} \times N} = \mathbf{B}_{bs}^H \Phi \tag{5.20}$$

Thus, the matrix $\mathbf{B}_{bs}$ is used to transfer the DOA estimation problem from ES to BS. Since the transformation matrix, $\mathbf{B}_{bs}$, is left Π-real, the resultant $\mathbf{y}_{bs}$ given by (5.20) is real [11]. Thus, the BS processing consists of two steps, projecting the received high dimensional complex ES sensor array data into lower dimension real data in BS and then processing this real lower-dimensional BS data, thus reducing the computational load of the processing scheme.

We now propose a new BS-based CS DOA estimation technique, namely, BS

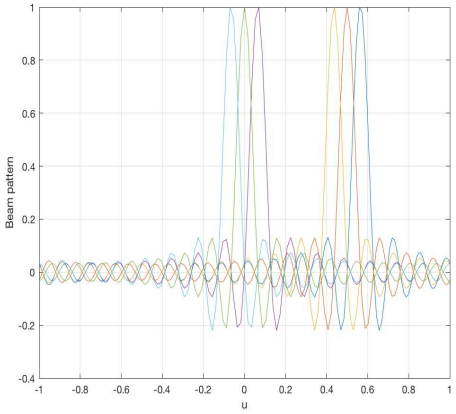

(a) u-space

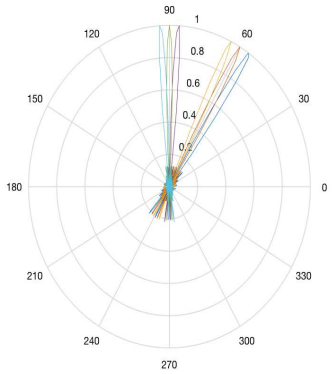

(b) θ-space

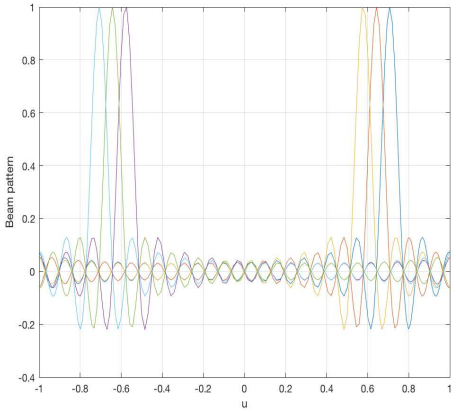

(c) u-space

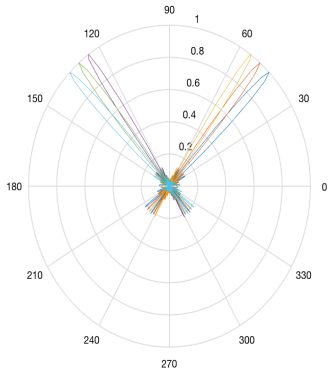

(d) θ-space

Figure 5.13: Beam pattern, multiple beam, $M = 31$, $N_{bs,1} = N_{bs,2} = 3$, (a) $\theta_{c1} = 60°, \theta_{c2} = 90°$ and (b) $\theta_{c1} = 50°, \theta_{c2} = 130°$.

A-LASSO. Given the BS output of the sensor array, which can be written as

$$\mathbf{y}_{bs}(t) = \Phi_{bs}\bar{\mathbf{s}}(t) + \mathbf{n}(t) \tag{5.21}$$

the BS A-LASSO consists of solving

$$\hat{\bar{\mathbf{s}}}^{(k)} = \min_{\bar{\mathbf{s}}} \|\mathbf{y}_{bs} - \Phi_{bs}\bar{\mathbf{s}}\|_2^2 + \tau_k \sum_{n=1}^{N} \hat{w}_n |\bar{s}_n| \tag{5.22}$$

where two different initial weights could be used in the first iteration ($k = 1$). The initial weights utilized for the first iteration of the BS A-LASSO could be OLS or MVDR and the corresponding algorithm is refereed to as BS OLS A-LASSO and BS MVDR A-LASSO, respectively. The LARS algorithm [91] is utilized to solve the above BS A-LASSO and the details are given in Algorithm 5.1.

Algorithm 5.1 The BS A-LASSO technique.

1: *Initialization*

Let the initial estimate for $\bar{\mathbf{s}}$ be $\hat{\mathbf{s}}$.

Find $\hat{\mathbf{w}}$, where the n-th element of $\hat{\mathbf{w}}$, $\hat{w}_n$, is given by $\hat{w}_n = 1/\left|\hat{s}_n\right|^{\gamma}, \quad n = 1, \ldots, N$.

Define $\Phi^* \in \mathbb{C}^{M \times N}$ matrix, such that its $(\bar{m}, n)$-th element is given by $\phi_{\bar{m}n}/\hat{w}_n$, where $\bar{m} = 1, \ldots, M$ and $n = 1, \ldots, N$.

2: *BS transformation matrix*

Select the number of the fan beams to be as that of the estimated sources, that is, $Q = L$.

Chose the number of beams in each fan beam, $N_{bs,q}, \quad q = 1, \ldots, Q$.

For each one of the fan beams, set $\theta_{c,q}(k) = \hat{\theta}_l(k-1), \quad q = 1, \ldots, Q, \quad l = 1, \ldots, L$.

Compute the BS transformation matrix, $\mathbf{B}_{bs}$.

3: *BS transformation*

$$\Phi' = \mathbf{B}_{bs}^H \Phi^* \quad (\Phi' \in \mathbb{R}^{N_{bs} \times N}) \tag{5.23a}$$

$$\mathbf{y}_{bs} = \mathbf{B}_{bs}^H \mathbf{y} \quad (\mathbf{y}_{bs} \in \mathbb{R}^{N_{bs} \times 1}) \tag{5.23b}$$

4: **for** $k = 1, 2, \ldots, K$ iterations **do**

Solve the LASSO problem as:

$$\hat{\mathbf{s}}^* = \min_{s} \left\|\mathbf{y}_{bs} - \Phi' \bar{\mathbf{s}}\right\|_2^2 + \tau_k \left\|\bar{\mathbf{s}}\right\|_1$$

Calculate $\hat{s}^{(k)} = \hat{s}_n^*/\hat{w}_n, \quad n = 1, 2, \ldots, N$.

5: **end for**

6: Estimate the DOA angles $\hat{\theta}_l, \quad l = 1, \ldots, L$.

5.5 Simulation Results

In this section, first, we investigate the performance of the BS MVDR A-LASSO techniques, namely, FBS MVDR A-LASSO and MBS MVDR A-LASSO. For this purpose, we conduct a number of experiments to examine the capability of these techniques to detect the number of source signals that they are supposed to be able to identify using a single snapshot along with a single iteration. Moreover, we examine the capability of the techniques to detect uncorrelated as well as correlated sources and spatially-close source signals.

Next, we investigate the performance of the BS MVDR A-LASSO techniques, namely, FBS MVDR A-LASSO and MBS MVDR A-LASSO in comparison with that of the ES MVDR A-LASSO technique.

5.5.1 Investigation of BS MVDR A-LASSO Techniques

In this section, we investigate the performance of the proposed BS-based techniques, namely, FBS MVDR A-LASSO and MBS MVDR A-LASSO, with regard to identifying the maximum number of sources for an antenna array of M elements as well as there ability to estimate the DOA of closely-spaced sources as well as coherent sources. Only a single snapshot along with only one iteration is considered for the BS MVDR A-LASSO simulations.

Using a ULA containing M elements, one can produce M orthogonal beams, as explained in Section 2.4.1. Let us consider a 7 element ULA; then, 7 orthogonal beams are generated using Equation (2.25) for FBS MVDR A-LASSO simulations. Also, for MBS MVDR A-LASSO simulations, a single beam ($N_{bs} = 1$) is assigned for each one of the sources to be identified, as explained in Section 5.4.1. The sampling grid $\bar{\theta}_n \in [1^\circ : 180^\circ]$ that covers Ψ is chosen to be in steps of 1°. All the simulated source signals are modeled as $e^{j2\pi f_d t}$ where f_d is the Doppler frequency.

The total number of trials, N_{sim}, is set to 100 for each observation point. For each experiment, the regularization parameter, τ, is selected based on the idea of the L-Curve [101, 102] and following the same procedure given in Section 3.5.

In the first experiment, we investigate the capabilities of the proposed BS algorithm in detecting the number of source signals that it is supposed to identify, theoretically. For that purpose, assume a ULA containing 7 elements. For such a scenario, theoretically, one should be able to identify up to 6 source signals, that is, $L_{max} \leq (M-1)$. Let 6 stationary equi-power source signals impinge the array from uniformly distributed DOAs over $\theta = [40^{\circ}, 140^{\circ}]$. SNR is set to 0 dB and the noise is AWGN.

Simulations are carried out using the FBS MVDR A-LASSO as well as MBS MVDR A-LASSO techniques to identify the 6 sources. The results are as shown in Fig. 5.14. It is seen from this figure that all of the 6 source signals are identified correctly using either FBS MVDR A-LASSO or MBS MVDR A-LASSO technique employing only a single snapshot of the received data.

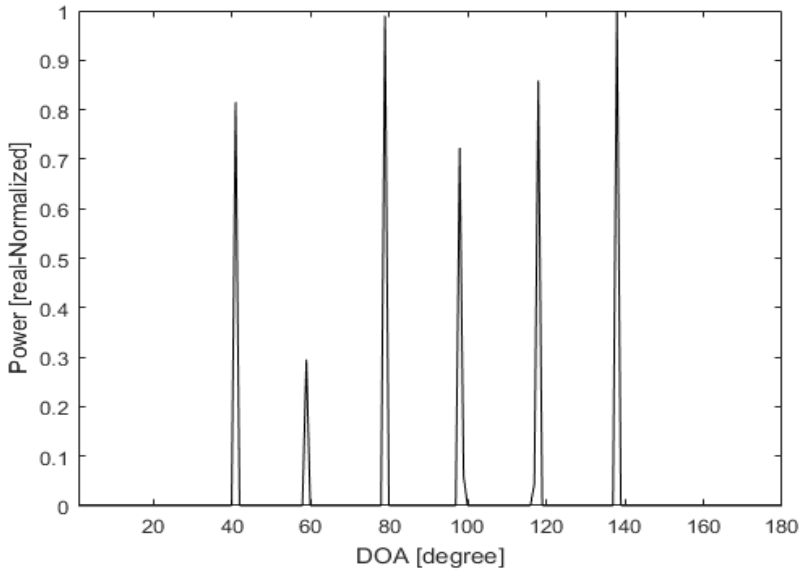

(a) FBS MVDR A-LASSO, single snapshot

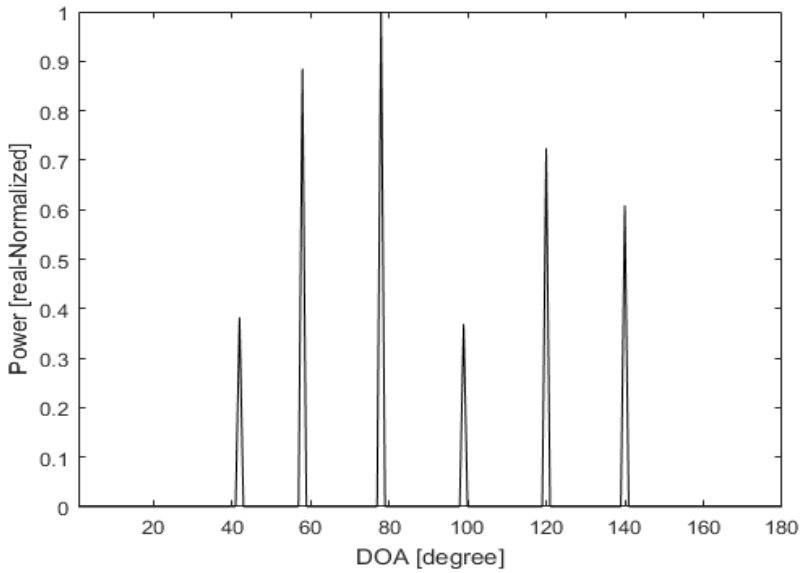

(b) MBS MVDR A-LASSO, single snapshot

Figure 5.14: DOA estimation of 6 sources using a ULA containing 7 elements, single snapshot, single iteration, SNR = 0 dB, using (a) FBS MVDR A-LASSO and (b) MBS MVDR A-LASSO.

In the second experiment, we consider two cases: (a) three uncorrelated signals impinging on the array from DOAs of $40°, 60°$ and $160°$, and (b) three signals

impinging from the same angles, but with the first two signals being fully correlated (coherent). The received signal is assumed to be contaminated by AWGN with SNR set to 0 dB. It is seen from Fig. 5.5 shows that both of the BS MVDR A-LASSO DOA estimation techniques are able to identify the source signals when they are uncorrelated as well as correlated.

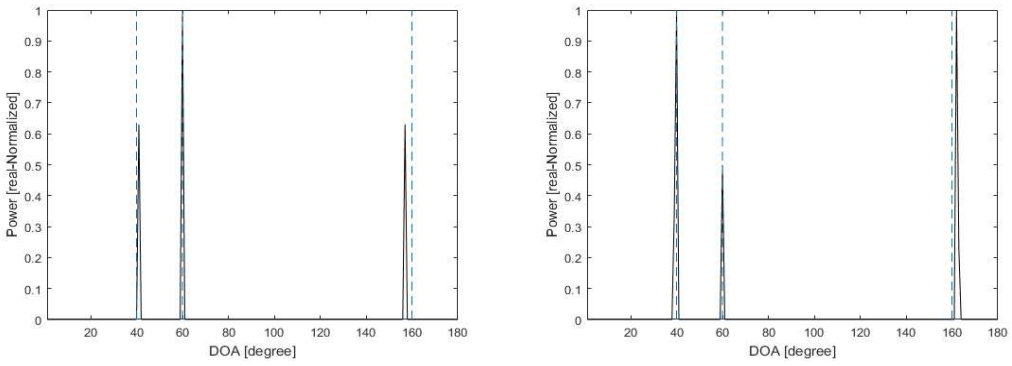

(a) FBS MVDR A-LASSO, single snapshot, non-coherent

(b) FBS MVDR A-LASSO, single snapshot, coherent

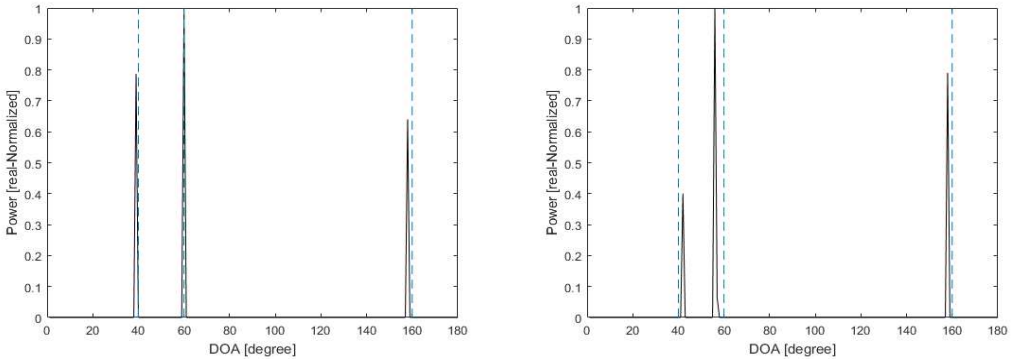

(c) MBS MVDR A-LASSO, single snapshot, non-coherent

(d) MBS MVDR A-LASSO, single snapshot, coherent

Figure 5.15: DOA estimation for 3 source signals with DOAs $40°, 60°$ and $160°$, uncorrelated sources, single snapshots, single iteration and AWGN with SNR = 0 dB, using (a, b) FBS MVDR A-LASSO and (c ,d) MBS MVDR A-LASSO. (a, c) Uncorrelated sources and (b, d) correlated sources.

In the third experiment, we examine the capability of the proposed techniques in identifying closely-spaced sources. For this purpose, let three sources impinge

the array form DOAs of 50°, 60°, and 170°. The received signal is assumed to be contaminated with AWGN with SNR set to 0 dB.

The simulations results are shown in Fig. 5.16. Three peaks can easily be identified in this figure using either FBS MVDR A-LASSO or MBS MVDR A-LASSO, thus identifying the three sources.

It should be mentioned that the same results would be obtained using either FBS OLS A-LASSO or MBS OLS A-LASSO. However, based on the results of Chapter 3 and Section 5.3, it is clear that the performance of the A-LASSO technique, for which MVDR is employed as the initial weight, is superior to that of the OLS one. Hence, BS OLS A-LASSO will not be considered further, and the performance of only BS MVDR A-LASSO will be studied in detail in comparison with that of ES MVDR A-LASSO.

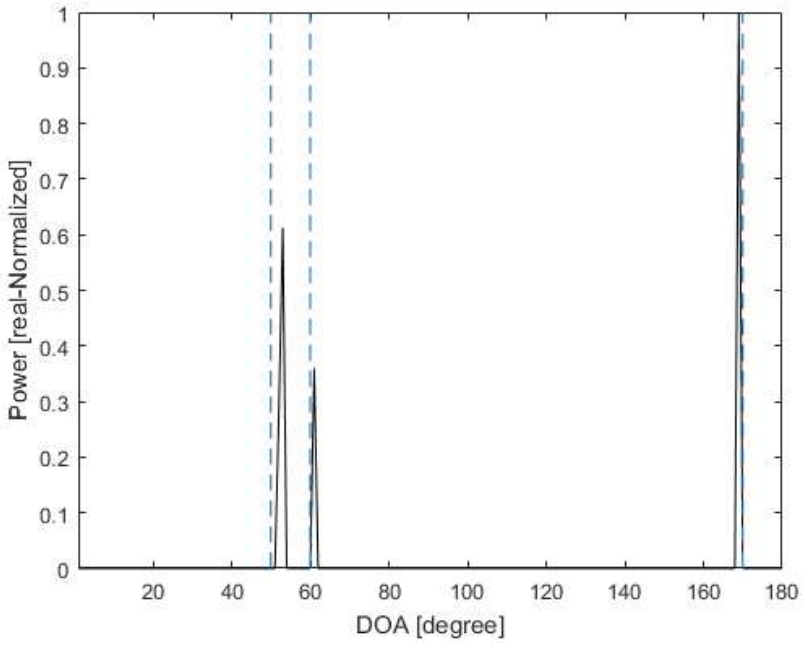

(a) FBS MVDR A-LASSO, single snapshot

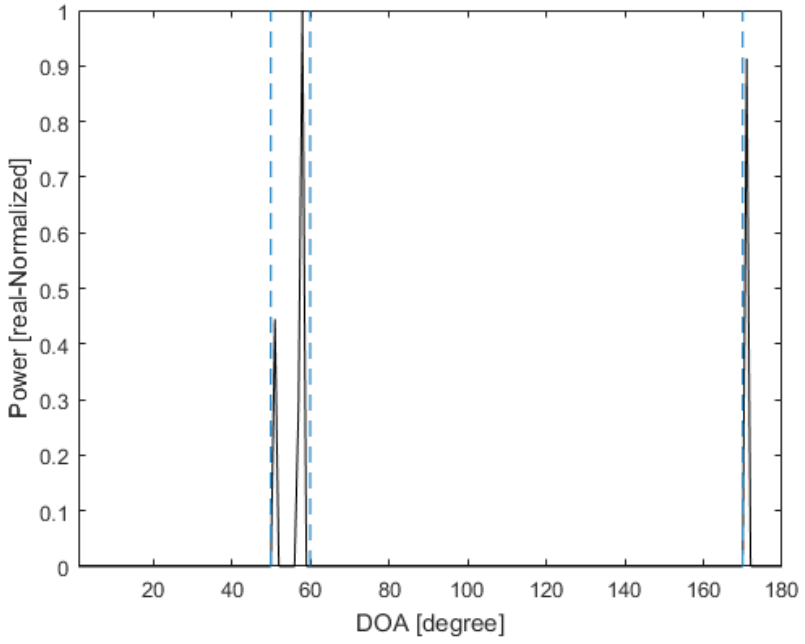

(b) MBS MVDR A-LASSO, single snapshot

Figure 5.16: DOA estimation for 3 source signals with DOAs $50°, 60°$ and $170°$, uncorrelated sources, single snapshots, single iteration and AWGN with SNR = 0 dB, using (a) FBS MVDR A-LASSO and (b) MBS MVDR A-LASSO.

5.5.2 Comparison of the BS MVDR A-LASSO techniques with that of ES MVDR A-LASSO

Consider a sparse linear two-level nested array, for which M is odd, consisting of $M = 7$ elements, three of whose elements are in the first level and four in the second level. Investigating the array output by applying Equations (3.1) to (3.3) and extracting the equivalent distinct virtual elements from the virtual array manifold $(\mathbf{A}^* \odot \mathbf{A})$, one can see that the virtual ULA contains $\bar{M} = 31$ elements. The sampling grid $\bar{\theta}_n \in [1^\circ : 180^\circ]$ that covers Ω is chosen to be in steps of 1° and $d = \lambda/2$, where λ is the wavelength of the propagating waves.

The power of the simulated fluctuating source signals is assumed to follow the Chi-squared distribution as given in Section 2.2 and the sources are assumed to be uncorrelated either with one another or with the noise. All the four different Swerling source signal models (see Table 2.1) are considered for the following experiments. For Swerling source of type I as well as type III, each scan is assumed to contain 10 snapshots.

Using a ULA containing M elements, M orthogonal beams can be generated using FBS processing, as explained in Section 2.4.1. That is, using a virtual ULA containing 31 elements, 31 orthogonal beams are generated for FBS MVDR A-LASSO simulations. On the other hand, in MBS MVDR A-LASSO simulations, a fan beam containing 3 orthogonal beams ($N_{bs} = 3$) is assigned for each one of the sources to be identified and tracked, following Equation (5.18), given in Section 5.4.1.

In the first experiment, we examine the performance of the BS MVDR A-LASSO DOA estimation techniques, namely, FBS MVDR A-LASSO and MBS MVDR A-LASSO using RMSE, given by Equation (5.17), as the performance measure, as we vary SNR using non-fluctuating as well as fluctuating sources. Let two equi-power or fluctuating source signals impinge the sensor array from fixed DOAs

of 60° and 120°. Let SNR vary from −5 to 10 dB in 1 dB steps and let the number of snapshots used be 10 and 50. These numbers correspond respectively to 1 and 5 scans for Swerling source types I and III.

Simulations are carried out using the proposed BS-based techniques, namely, FBS MVDR A-LASSO and MBS MVDR A-LASSO as well as ES MVDR A-LASSO to identify the sources. The performance of the BS MVDR A-LASSO DOA estimation techniques are as shown in Figs. 5.17, 5.18 and 5.19. From these figures, it is clear that increasing the number of snapshots to 50 from 10 reduces the DOA estimation error by at least 40% for both fluctuating and non-fluctuating signals using the different techniques. Furthermore, it can be seen from Fig. 5.17 that for non-fluctuating sources, the performance of MBS MVDR A-LASSO is superior to that of ES MVDR A-LASSO as well as that of FBS MVDR A-LASSO irrespective of the value of SNR, whether 10 or 50 snapshots are used. Also, as expected, RMSE for non-fluctuating sources, whether ES, FBS or MBS MVDR A-LASSO is used, is lower than that for fluctuating sources irrespective of the number of snapshots used for all values of SNR. Moreover, RMSE for all the types of sources can be reduced substantially by increasing the number of snapshots. In such a case, MBS will yield the lowest error.

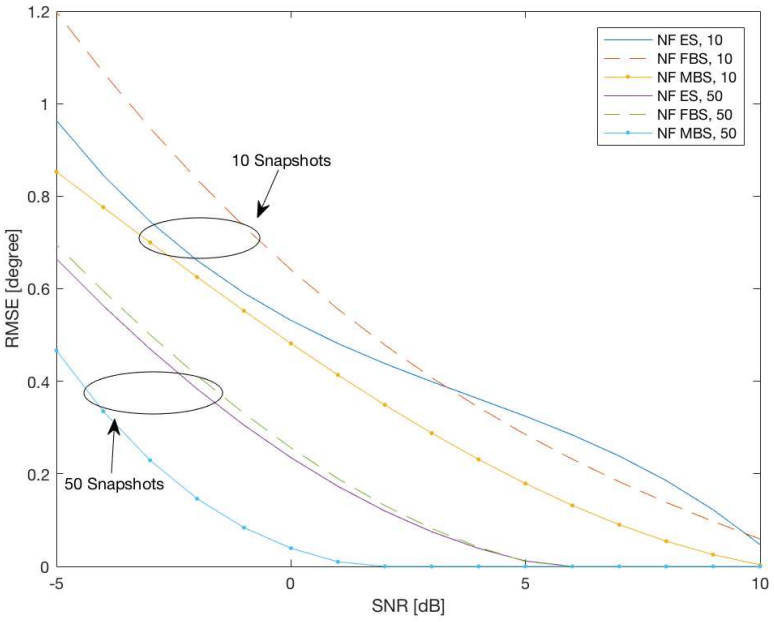

(a) NF Sources, 10 and 50 snapshots

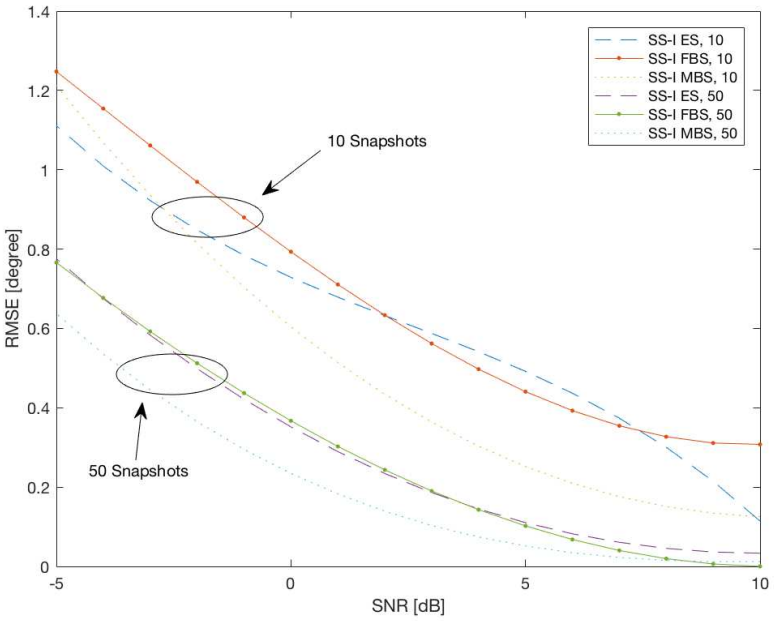

(b) Type I Sources, 10 and 50 snapshots

Figure 5.17: Performance of the various CS-based DOA estimation techniques as SNR is varied, for two source signals at DOAs 60° and 120° using 10 and 50 snapshots. (a) NF sources and (b) Type I sources.

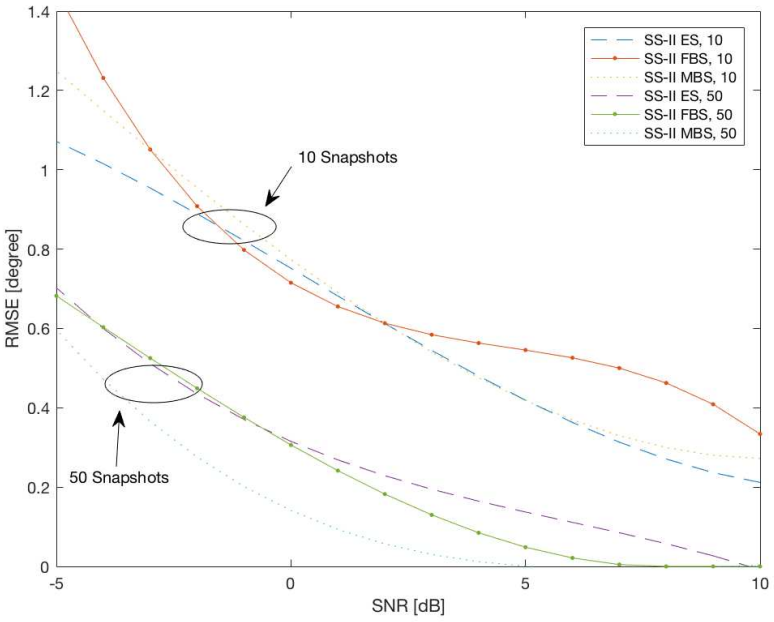

(a) Type II Sources, 10 and 50 snapshots

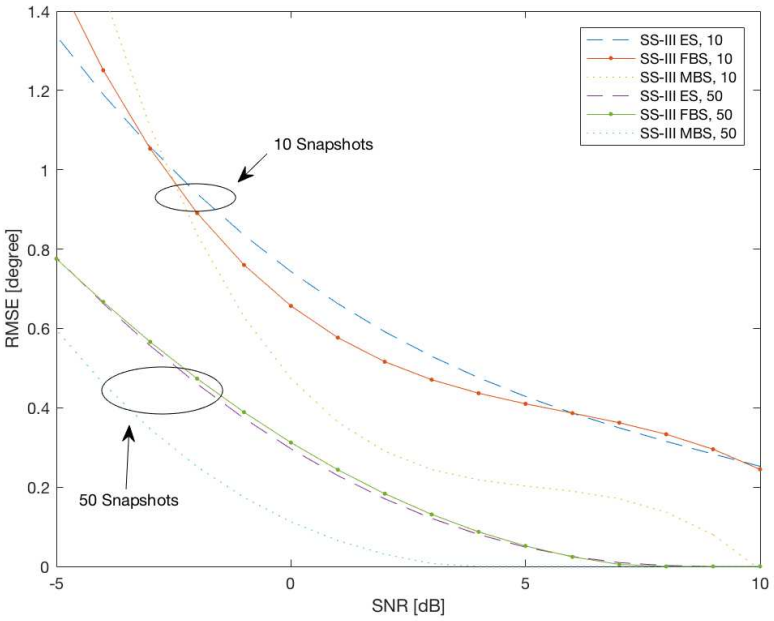

(b) Type III Sources, 10 and 50 snapshots

Figure 5.18: Performance of the various CS-based DOA estimation techniques as SNR is varied, for two fluctuating source signals at DOAs 60° and 120° using 10 and 50 snapshots. (a) Type II sources and (b) Type III sources.

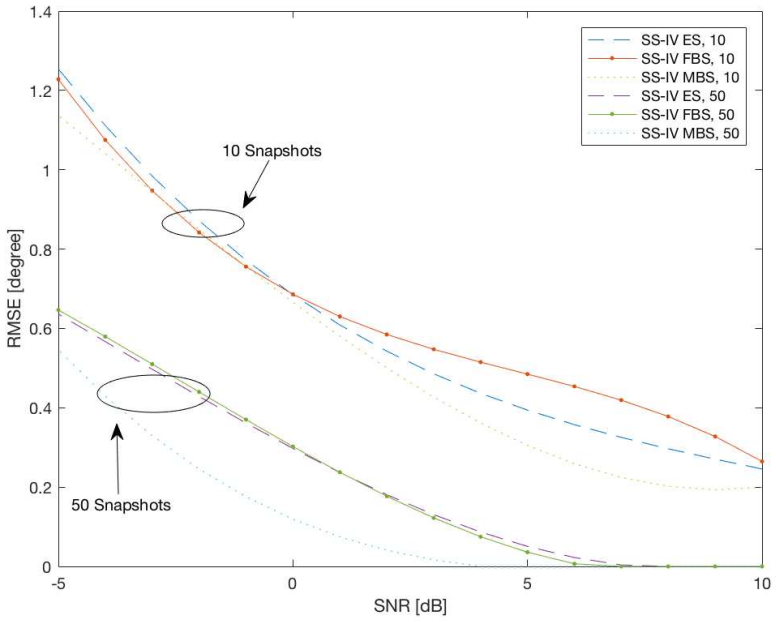

(a) Type IV Sources, 10 and 50 snapshots

Figure 5.19: Performance of the various CS-based DOA estimation techniques as SNR is varied, for two fluctuating source signals at DOAs 60° and 120° using 10 and 50 snapshots. (a) Type IV sources.

In the second experiment, we investigate the effect of varying the angular separation between the Swerling source signals. Consider two fluctuating source signals, the first one with a fixed DOA of 60° while the DOA of the second ranges from 65° to 110° in steps of 5°. The SNR is set 0 dB, 10 snapshots are considered for the simulation and 100 trials for each observation point.

Fig. 5.20 illustrates RMSE versus the angular separation for the different Swerling sources. Results for RMSE for non-fluctuating source signals is also included for reference. The same number of snapshots is used for the non-fluctuating sources as for the fluctuating sources. It is noted that for angular separation of 5° or less the two source signals cannot be identified as separate signals. Hence, the results are presented starting with a 10° separation.

From this figure, it is seen that the DOA estimation error for non-fluctuating

sources is the lowest. Further, the error for Swerling sources of types II and IV is lower than that for types I and III for an angular separation $\geq 20^\circ$ using FBS MVDR A-LASSO and MBS MVDR A-LASSO. This error could be reduced by increasing the number of snapshots (see previous experiment).

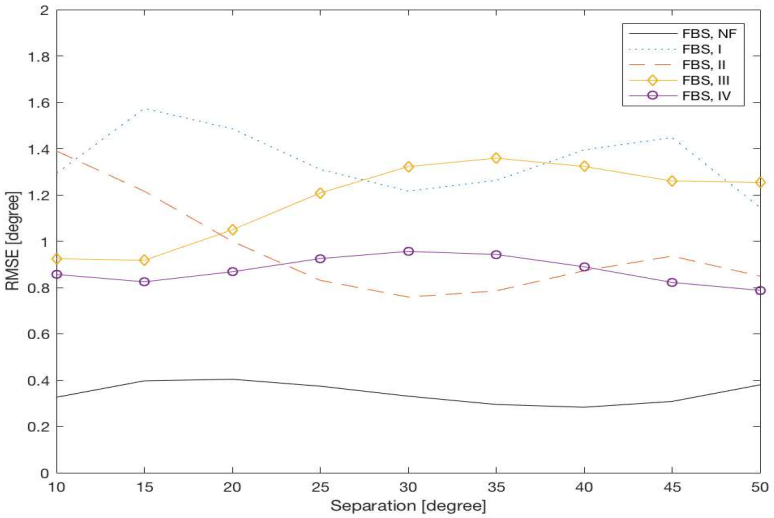

(a) FBS MVDR A-LASSO

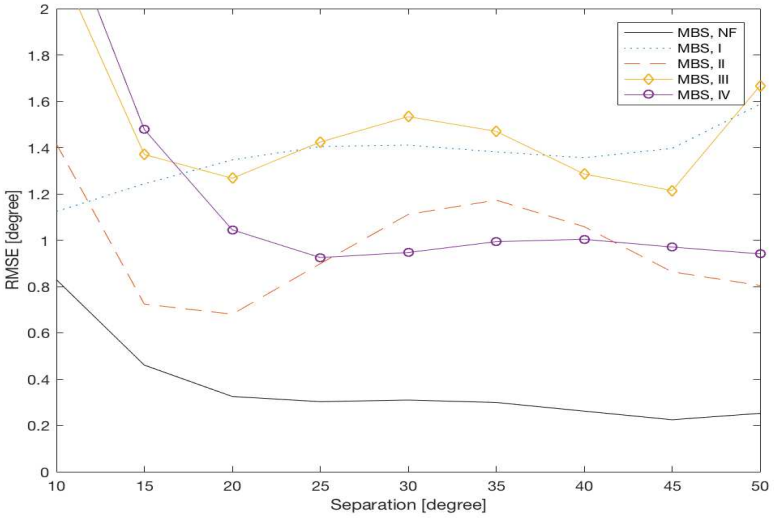

(b) MBS MVDR A-LASSO

Figure 5.20: DOA estimation error for two sources as a function of separation between the DOAs of the sources, SNR = 0 dB, 10 snapshots using (a) FBS MVDR A-LASSO and (b) MBS MVDR A-LASSO

In the third experiment, we investigate the POD of the different source signals using FBS and MBS based MVDR A-LASSO DOA estimation techniques. For this purpose, let two source signals of the same type impinge the sensor array from fixed DOAs of 60° and 120°, with varying SNR. The POD for non-fluctuating as well as fluctuating source signals, for different values of snapshots, are as shown in Figs. 5.21 and 5.22. It is seen from these figures that the POD corresponding to the non-fluctuating sources as well as to the Swerling signal types II and IV are greater than 0.99 with only 10 snapshots, while a larger number of snapshots are required for Swerling source types I and III in order to achieve an acceptable POD similar to that of types II and IV, using FBS and MBS-based DOA estimation techniques. It is noted that these results are similar to what we had obtained in Section 3.7 using the ES-based MVDR A-LASSO technique.

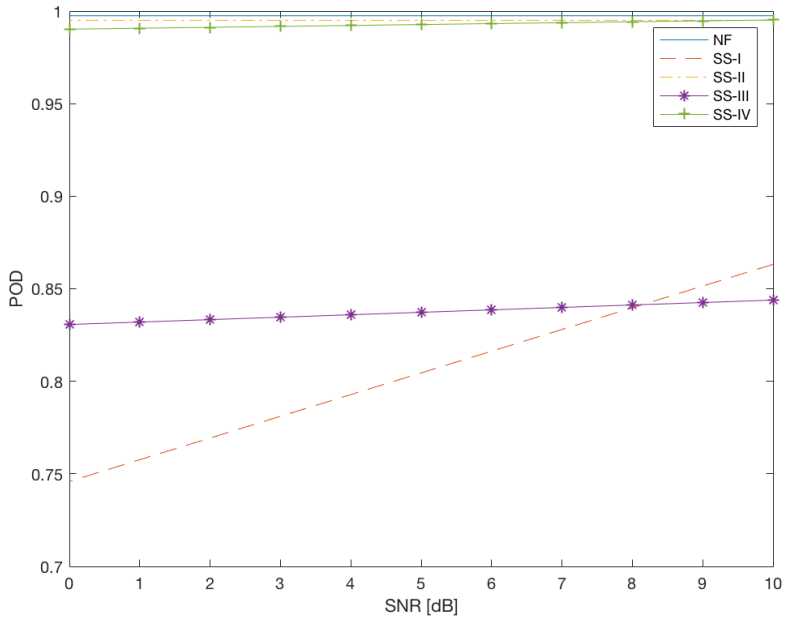

(a) FBS, 10 snapshots

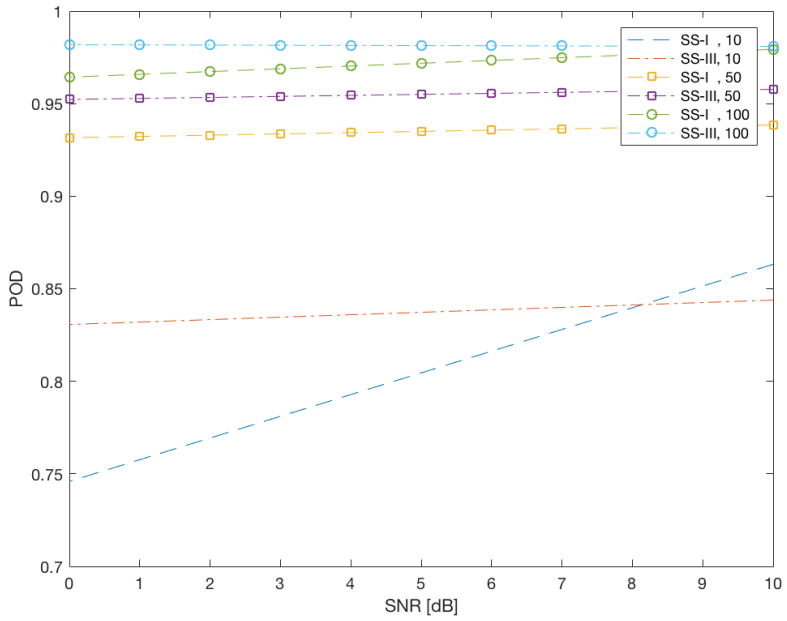

(b) FBS, ≥ 10 snapshots

Figure 5.21: Probability of detection of different Swerling source signals, two source signals with DOA of 60° and 120°, using FBS algorithm.

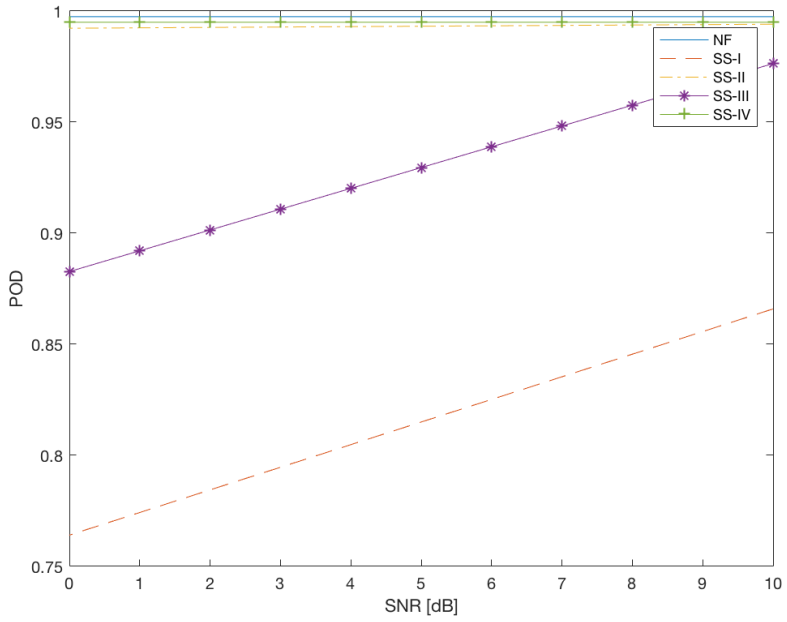

(a) MBS, 10 snapshots

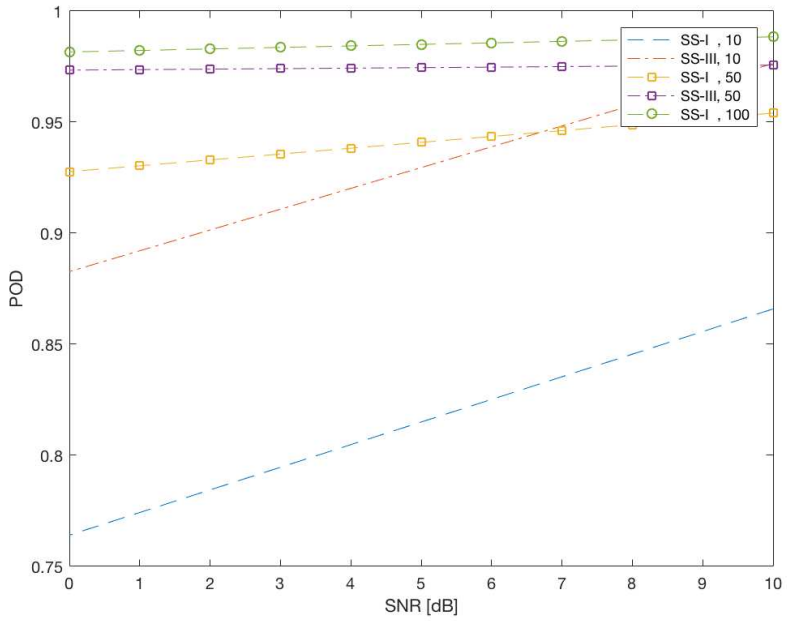

(b) MBS, $\geq$ 10 snapshots

Figure 5.22: Probability of detection of different Swerling source signals, two source signals with DOA of 60° and 120°, using MBS algorithm.

In the fourth experiment, we investigate the capability of the proposed BS-based techniques to detect and track non-fluctuating as well as fluctuating source signals. The same three scenarios assumed in Section 3.7 are used in this simulation and the following experiments. The SNR is set to 10 dB, the number of snapshots was chosen to 10 for the sources of types II and IV, while for types I and III the number of snapshots is set to 100. Fig. 5.23 illustrates the ideal trajectories considered for the simulations.

Figures from 5.24 to 5.33 illustrate the estimated trajectories for the two source signals using either FBS MVDR A-LASSO or MBS MVDR A-LASSO when non-fluctuating as well as fluctuating sources are required to be tracked. From these figures, it can be seen that the FBS and MBS-based MVDR A-LASSO DOA estimation techniques are able to detect and track the sources.

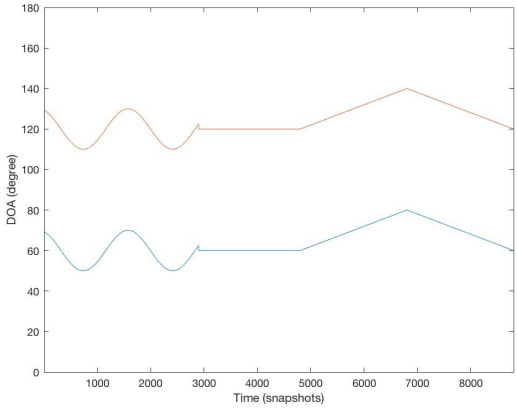

(a) In phase

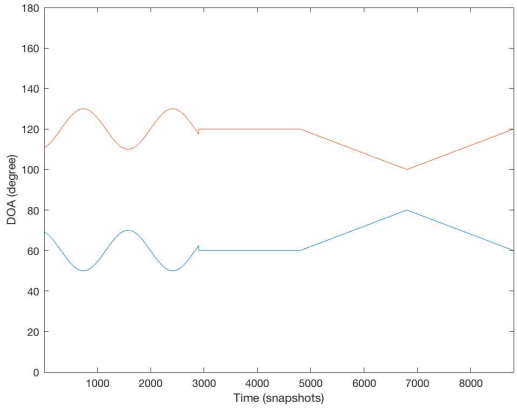

(b) Opp-phase

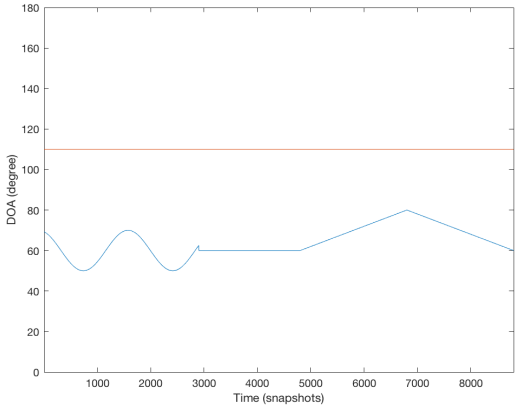

(c) Fixed vs moving

Figure 5.23: The proposed ideal source signals trajectories where in the sources DOA are following (a) the same direction, (b) opposite directions, and (c) one source DOA is being fixed while the other is changing.

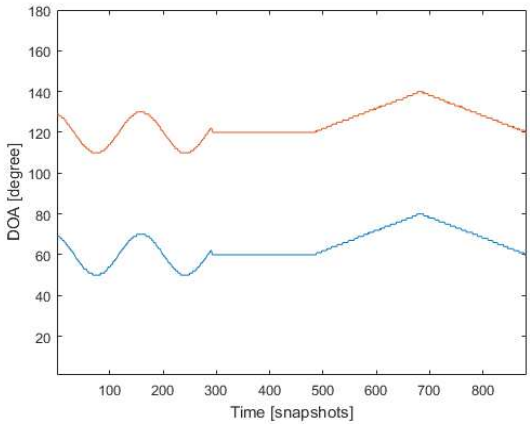

(a) In phase

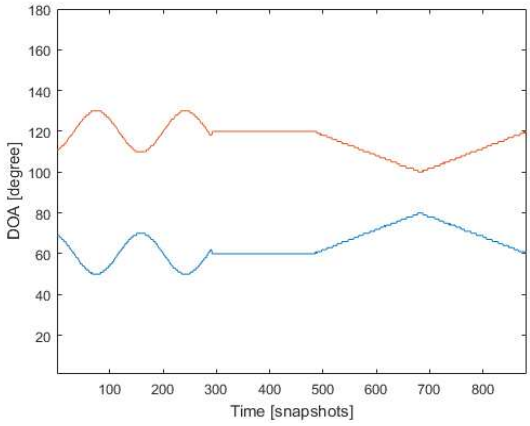

(b) Opp-phase

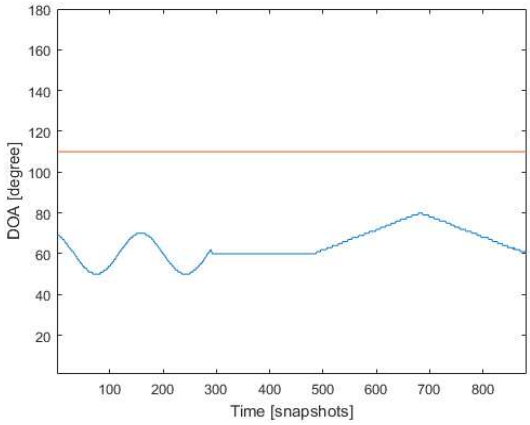

(c) Fixed vs moving

Figure 5.24: Trajectories of two source signals using FBS MVDR A-LASSO DOA estimation technique, 10 snapshots, SNR = 10 dB, non-fluctuating sources.

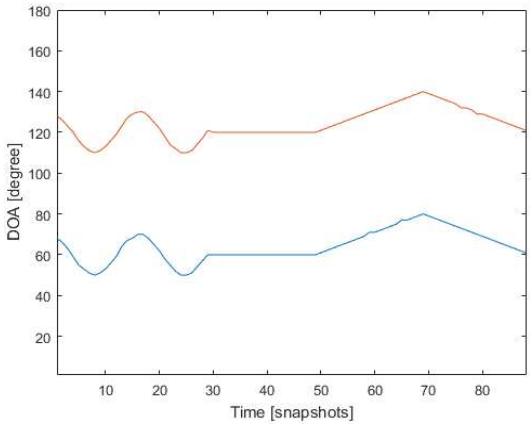

(a) In phase

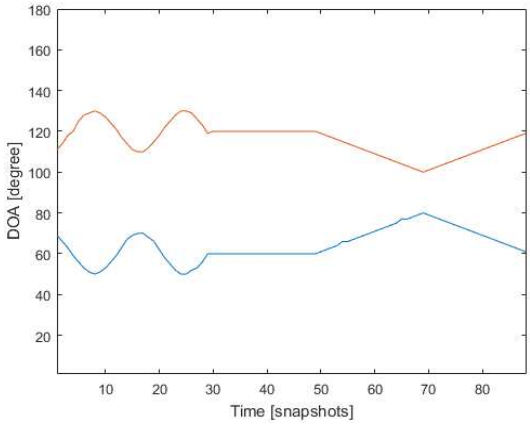

(b) Opp-phase

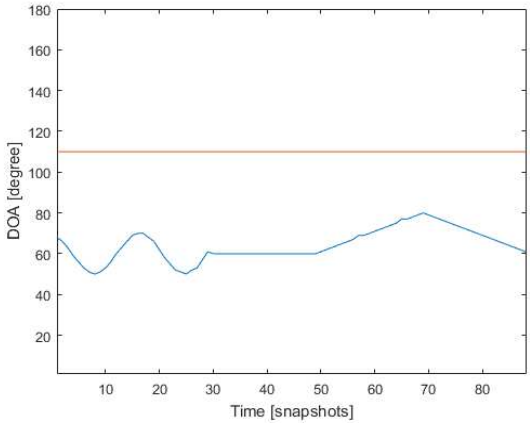

(c) Fixed vs moving

Figure 5.25: Trajectories of two source signals using FBS MVDR A-LASSO DOA estimation technique, 100 snapshots, SNR = 10 dB, type I fluctuating sources.

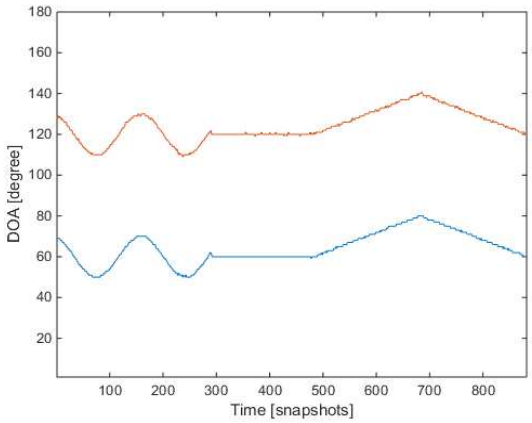

(a) In phase

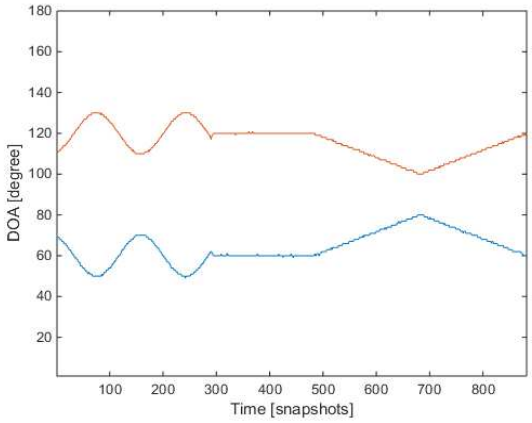

(b) Opp-phase

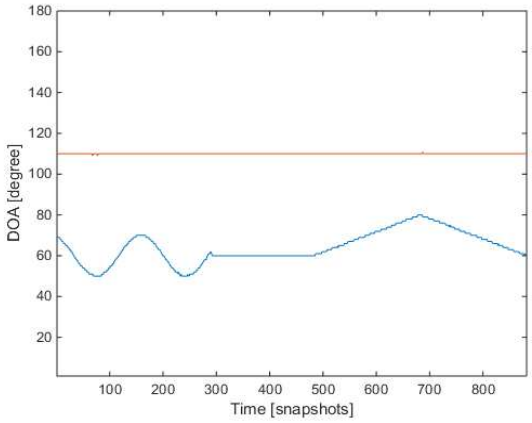

(c) Fixed vs moving

Figure 5.26: Trajectories of two source signals using FBS MVDR A-LASSO DOA estimation technique, 10 snapshots, SNR = 10 dB, type II fluctuating sources.

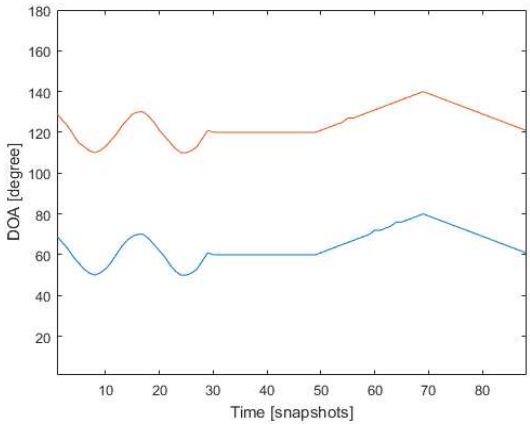

(a) In phase

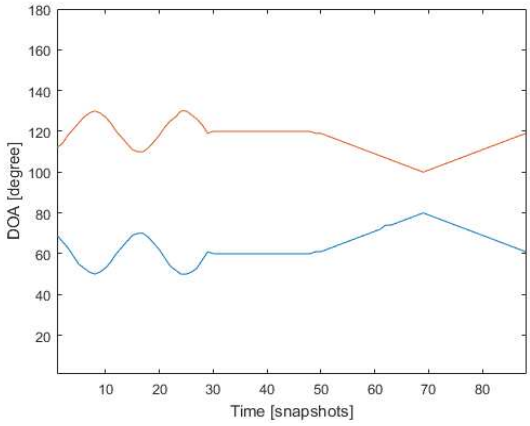

(b) Opp-phase

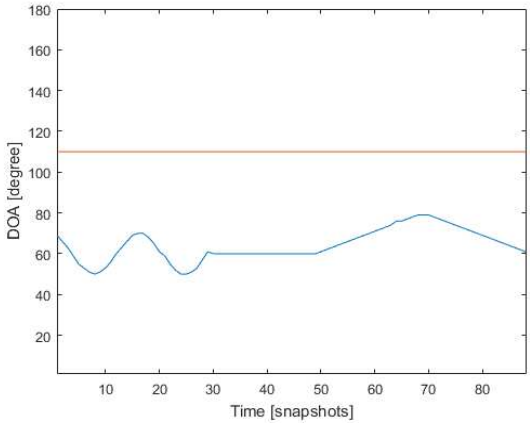

(c) Fixed vs moving

Figure 5.27: Trajectories of two source signals using FBS MVDR A-LASSO DOA estimation technique, 100 snapshots, SNR = 10 dB, type III fluctuating sources.

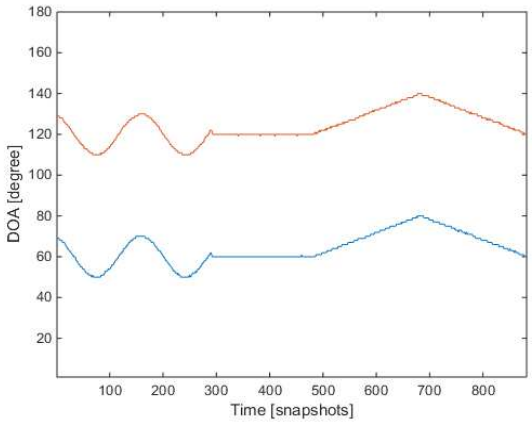

(a) In phase

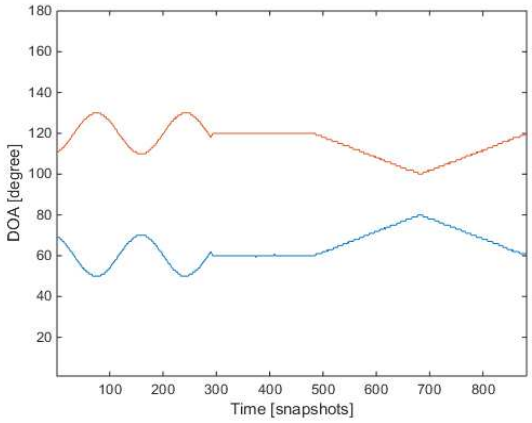

(b) Opp-phase

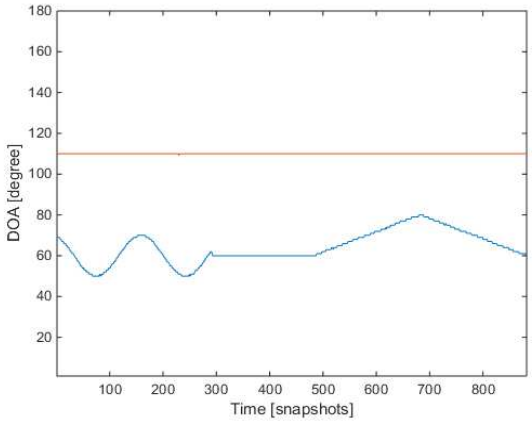

(c) Fixed vs moving

Figure 5.28: Trajectories of two source signals using FBS MVDR A-LASSO DOA estimation technique, 10 snapshots, SNR = 10 dB, type IV fluctuating sources.

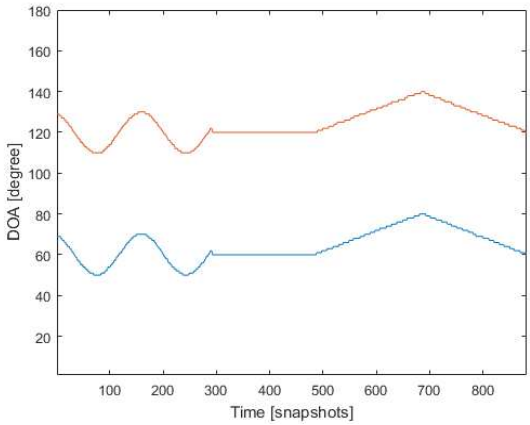

(a) In phase

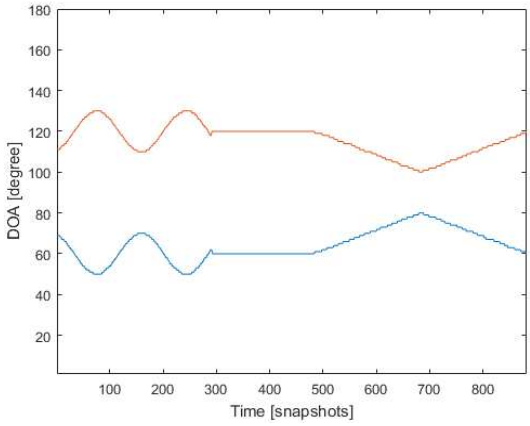

(b) Opp-phase

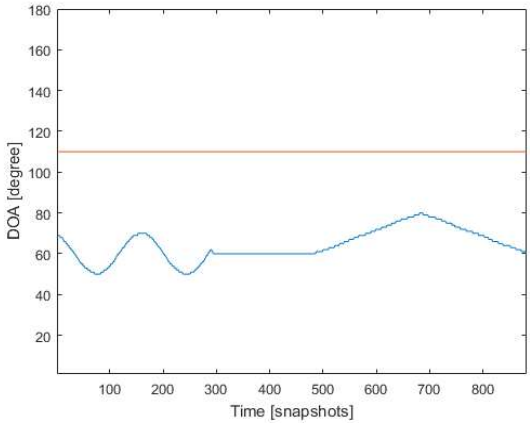

(c) Fixed vs moving

Figure 5.29: Trajectories of two source signals using MBS MVDR A-LASSO DOA estimation technique, 10 snapshots, SNR = 10 dB, non-fluctuating sources.

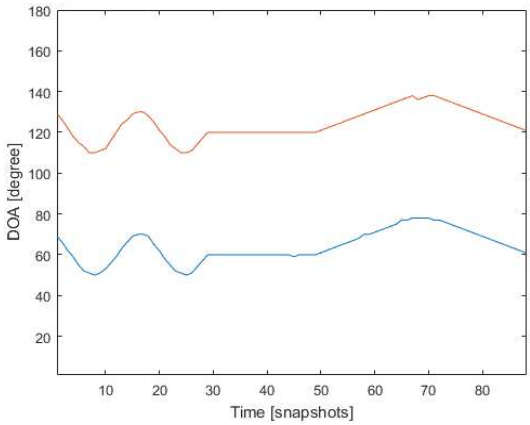

(a) In phase

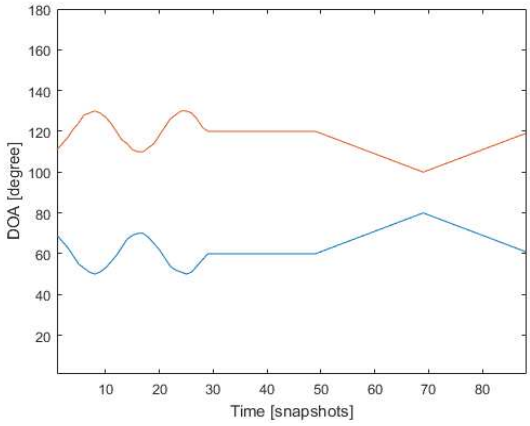

(b) Opp-phase

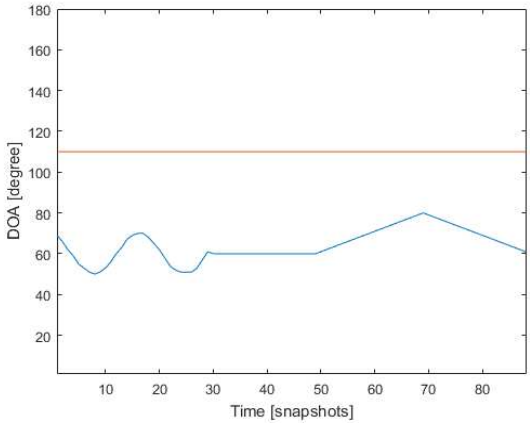

(c) Fixed vs moving

Figure 5.30: Trajectories of two source signals using MBS MVDR A-LASSO DOA estimation technique, 100 snapshots, SNR = 10 dB, type I fluctuating sources.

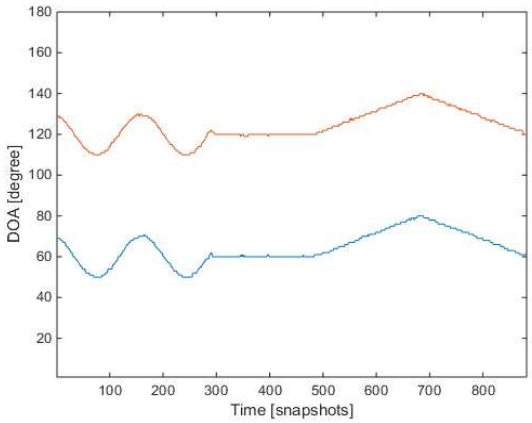

(a) In phase

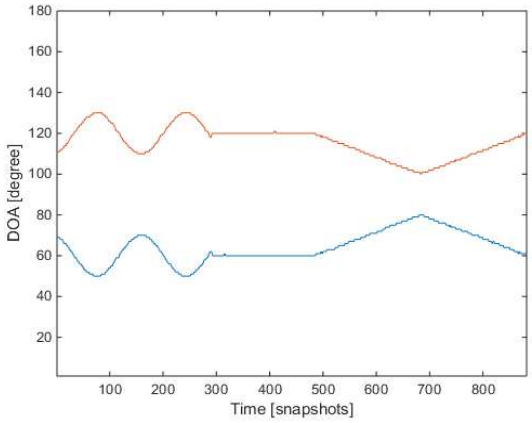

(b) Opp-phase

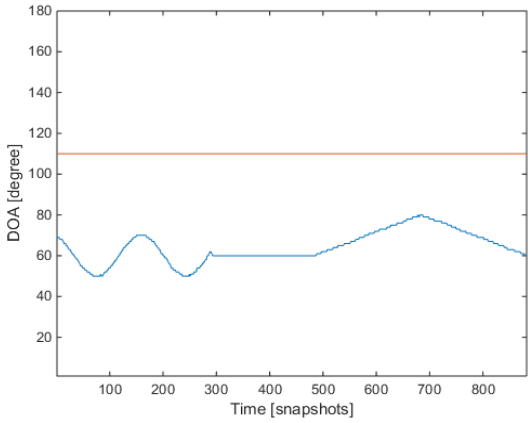

(c) Fixed vs moving

Figure 5.31: Trajectories of two source signals using MBS MVDR A-LASSO DOA estimation technique, 10 snapshots, SNR = 10 dB, type II fluctuating sources.

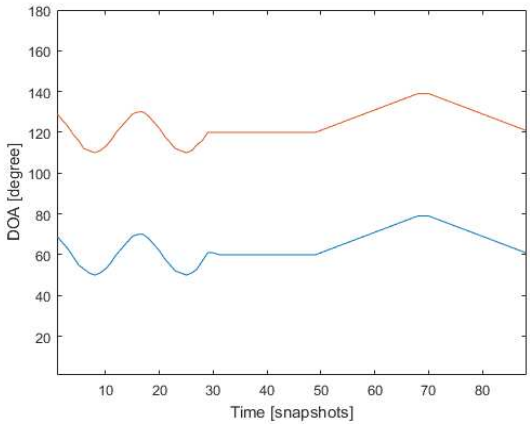

(a) In phase

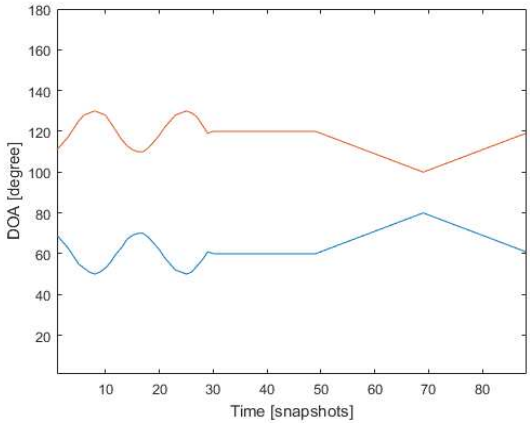

(b) Opp-phase

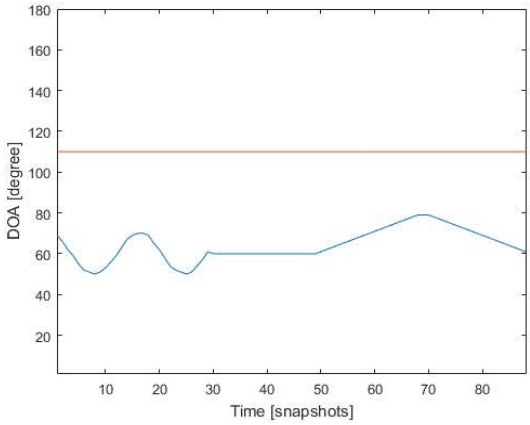

(c) Fixed vs moving

Figure 5.32: Trajectories of two source signals using MBS MVDR A-LASSO DOA estimation technique, 100 snapshots, SNR = 10 dB, type III fluctuating sources.

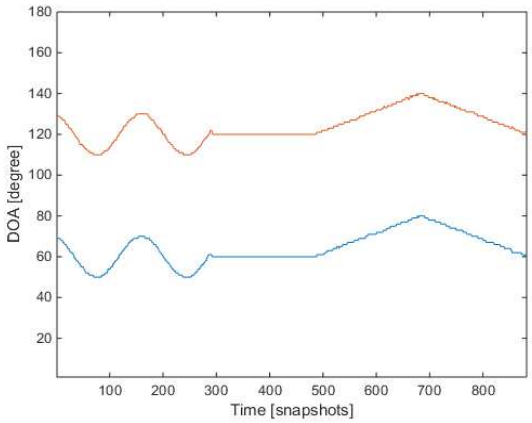

(a) In phase

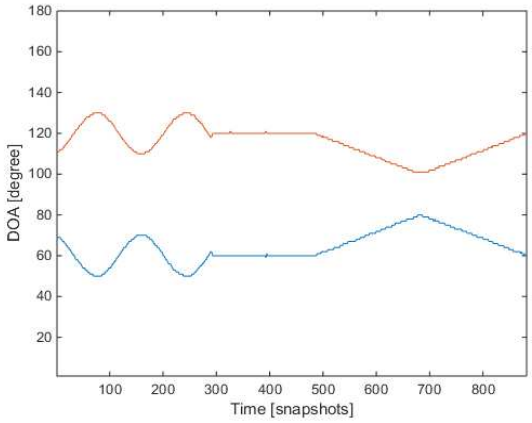

(b) Opp-phase

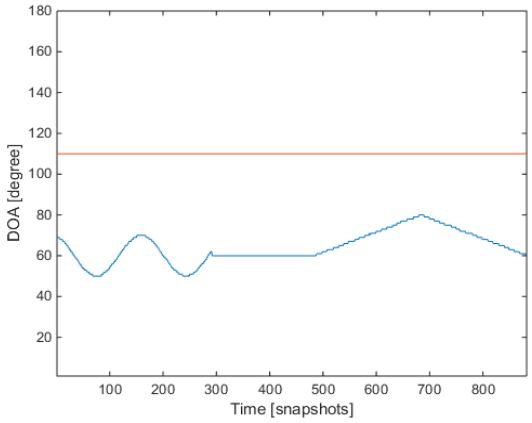

(c) Fixed vs moving

Figure 5.33: Trajectories of two source signals using MBS MVDR A-LASSO DOA estimation technique, 10 snapshots, SNR = 10 dB, type IV fluctuating sources.

In the fifth experiment, we investigate the capability of the proposed BS-based techniques to detect and track non-fluctuating source signals when their trajectories intersect with one anther. For this purpose we assume three different cases. In the first case, we assume that the DOA of one of the sources is fixed, while that of the second is changing. In the second case, we assume that the DOA of both the sources are changing. In the last case, we assume that there are three source of interest, two of them with changing DOA, while the DOA of the third is fixed. The trajectories of these three different cases are as shown in Fig. 5.34. The SNR is set to 10 dB and the number of snapshots is set to 10.

The simulations are conducted using both FBS MVDR A-LASSO and MBS MVDR A-LASSO techniques and the results are as shown in Fig. 5.35. From this figure it is clear that both of the proposed techniques are able to track the sources even when their trajectories intersect. Furthermore, it can be seen that the MBS MVDR A-LASSO technique is able to discriminate closely-spaced sources (Fig. 5.35(f)) better than FBS MVDR A-LASSO technique (Fig. 5.35(e)) can.

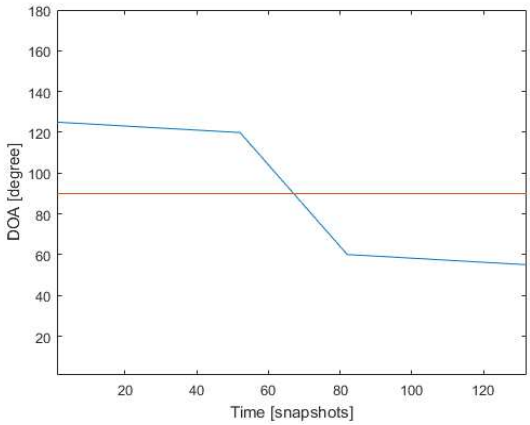

(a)

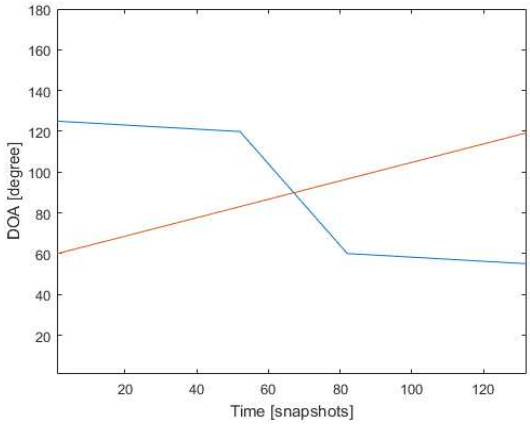

(b)

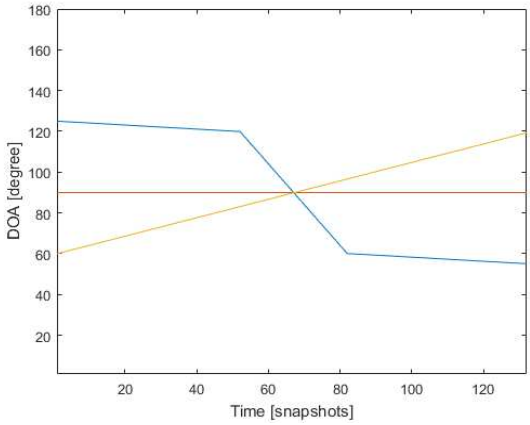

(c)

Figure 5.34: The proposed ideal source signals special trajectories with intersected paths.

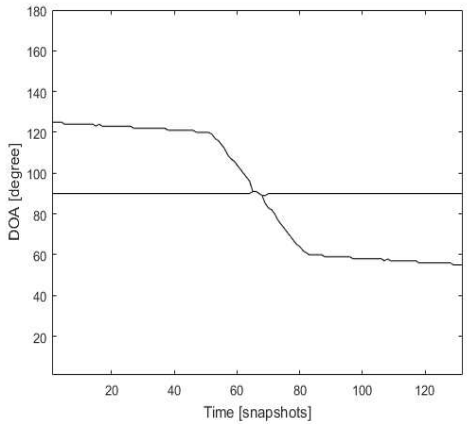

(a) FBS

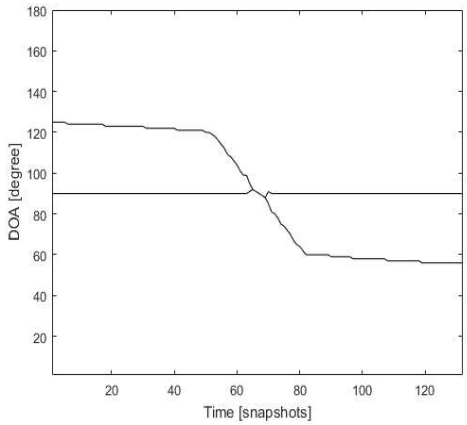

(b) MBS

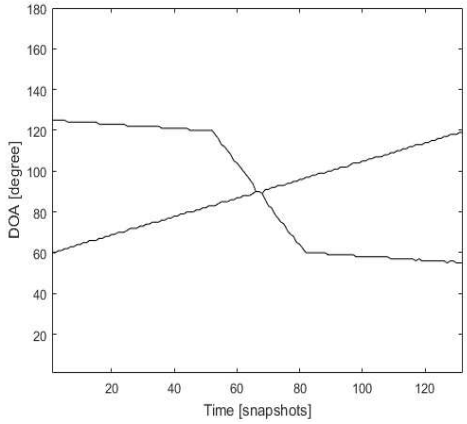

(c) FBS

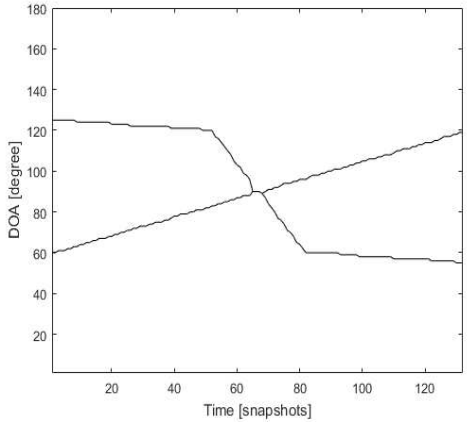

(d) MBS

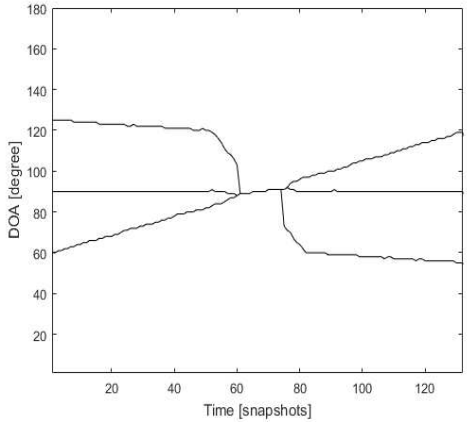

(e) FBS

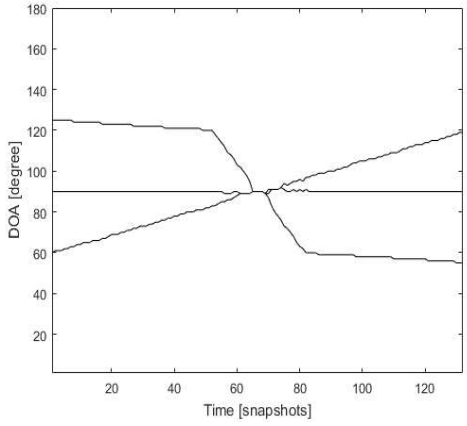

(f) MBS

Figure 5.35: The estimated source signals special trajectories with intersected paths using FBS MVDR A-LASSO and MBS MVDR A-LASSO.

In the sixth experiment, we investigate the computational complexity of the ES, FBS, and MBS MVDR A-LASSO DOA estimation techniques. The CPU time is used as the measuring tool for the computational complexity. The PC used has Intel Core i5 CPU M 430, 2.27GHz and 3GB of RAM memory. In order to calculate the CPU time corresponding to each one of the proposed techniques, we average the run times of the experiments corresponding to Figs. 3.26 to 3.30 in Section 3.7 for ES MVDR A-LASSO and the run times of the experiments corresponding to Figs. 5.24 to 5.33 in this section for FBS and MBS MVDR A-LASSO.

Fig. 5.36 illustrates the CPU time for ES, FBS, and MBS MVDR A-LASSO DOA estimation techniques. It can be seen that the BS-based DOA estimation techniques computational time is less than that of the ES-based technique by almost 35%. Furthermore, it can be seen that MBS MVDR A-LASSO has the lowest computational time.

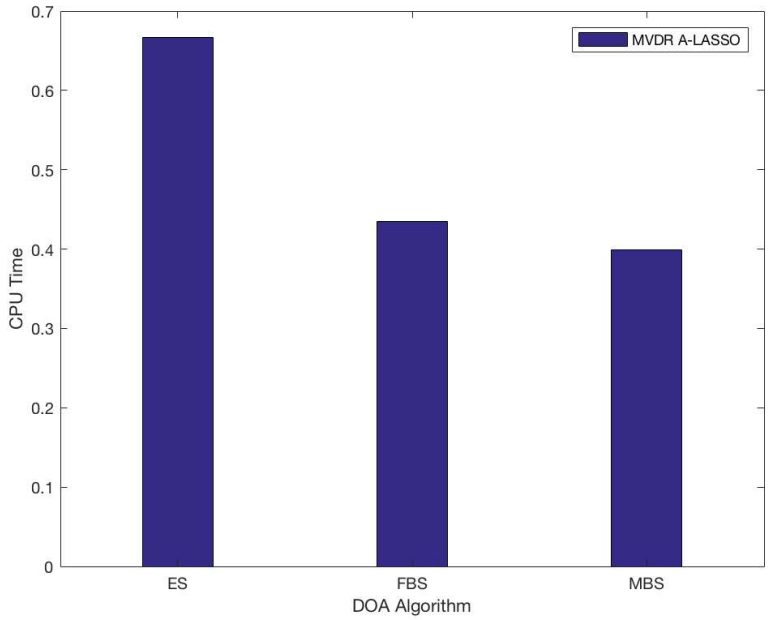

Figure 5.36: CPU time as a measure for the computational complexity of the proposed MVDR A-LASSO-based DOA estimation techniques.

5.6 Summary

It has been shown that the ES-based A-LASSO techniques are superior to that of the existing BS-based technique. Even with a single snapshot and a single iteration, the ES-based A-LASSO techniques have been shown to be able to identify the number of sources that they are supposed to identify, theoretically. Further, they are able to identify coherent source signals as well as closely-spaced sources. Moreover, in terms of RMSE, the ES-based A-LASSO techniques are superior to the existing BS-based DOA estimation methods.

Then, we developed a new BS processing scheme, namely, multiple-beam beamspace (MBS), based on the reduced-dimension BS method. The new scheme is able to scan multiple sectors of interest at the same time. Furthermore, we utilized the MBS processing scheme to transfer the ES-based CS DOA estimation problem into a BS-based one. We have proposed two new BS-based DOA estimation techniques in the CS framework, namely, full beamspace (FBS) A-LASSO and multiple-beam beamspace (MBS) A-LASSO.

Even with only a single snapshot and a single iteration, the proposed BS-based A-LASSO techniques have been shown to be able to identify the number of sources that they are supposed to identify, theoretically, as well as correlated sources and closely-spaced source signals.

Using non-fluctuating as well as fluctuating source signals, we have intensively examined the performance of the BS-based A-LASSO techniques. It has been shown that RMSE for non-fluctuating sources is the lowest irrespective of the number of snapshots employed and the estimation techniques used. Furthermore, It has been shown that Swerling source types I and III need more number of snapshots than that for non-fluctuating and Swerling II and IV, in order to achieve an acceptable POD.

Different scenarios for moving non-fluctuating and fluctuating source trajectories have been assumed and the BS-based techniques have been shown to be able to identify and track such moving sources. Moreover, different trajectories intersection scenarios are examined.

Finally, in terms of the CPU time, it has been shown that the BS-based A-LASSO techniques are superior to that of the ES-based one. Furthermore, MBS A-LASSO is superior to that of ES A-LASSO and FBS A-LASSO.

Chapter 6

Implementation of the Proposed DOA Estimation Schemes

6.1 Introduction

In this chapter, we conduct experiment using the Raspberry Pi board to study the feasibility of real-time implementation of various DOA estimation schemes proposed in this thesis.

6.2 Description of Raspberry Pi Board

Raspberry Pi is a tiny, low-cost, single-board computer that supports embedded Linux operating systems, such as Raspbian. This board contains a Broadcom system-on-a-chip (SoC), which includes an ARM processor, on board RAM, a VideoCore IV GPU, and general input/output ports. We carry out experiments with Raspberry Pi 2 Model B which is the second generation Raspberry Pi, and the specifications of this board are given in Table 6.1. Programming languages such as Python, C, C++, Java, Scratch, and Ruby are by default installed. The cost of this board is less than US $35, and is very popular in view of its features. It has been

Table 6.1: Raspberry Pi 2 Model B specification

Specs	Raspberry Pi 2 Model B
SoC	Broadcom BCM2836 (CPU, GPU, DSP, SDRAM)
CPU	900 MHz quad-core ARM Cortex A7 (ARMv7 instruction set)
GPU	Broadcom VideoCore IV @ 250 MHz
GPU info	OpenGL ES 2.0 (24 GFLOPS); 1080p30 MPEG-2 and licensed VC-1 decoder 1080p30 h.264/MPEG-4 AVC high-profile decoder and encoder
Memory	1 GB (shared with GPU)
USB ports	4
Video input	15-pin MIPI camera interface (CSI) connector
Video outputs	HDMI, composite video (PAL and NTSC) via 3.5 mm jack
Audio input	Inter-IC Sound (I^2S)
Audio outputs	Analog via 3.5 mm jack; digital via HDMI and I^2S
Storage	MicroSD
Network	10/100Mbps Ethernet
Peripherals	17 GPIO plus specific functions, and HAT ID bus
Power rating	800 mA (4.0 W)
Power source	5 V via MicroUSB or GPIO header
Size	85.60mm × 56.5mm
Weight	45g (1.6 oz)

used in a wide range of areas, including radiology [140] and robotics [141].

Because of its popularity, a support package has been introduced for Matlab versions. Using this package, we can remotely communicate with the board and use it to control, acquire, and collect data from sensors and imaging devices connected to the board. With the help of add-on Matlab signal processing toolboxes such as DSP System, Image Processing, and Computer Vision System toolboxes, one can collect, process, analyze, and visualize the data under test. Figure 6.1 illustrates

the top view of a Raspberry Pi 2 Model B.

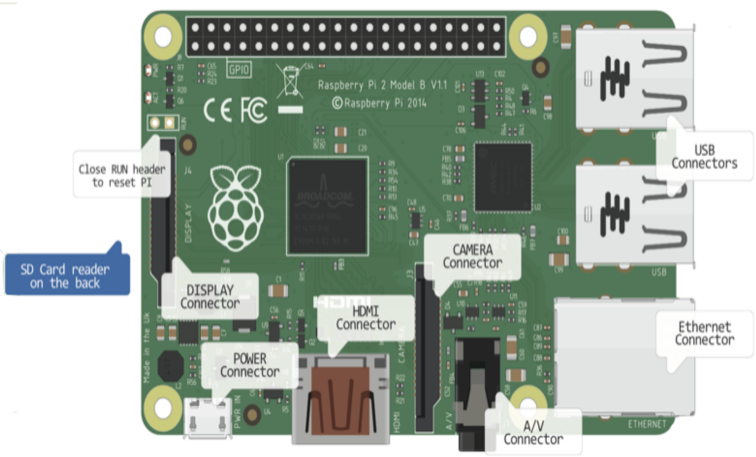

Figure 6.1: Top view of a Raspberry Pi 2 Model B.

Because of the availability of the support packages for Matlab and Simulink, we have chosen the Raspberry Pi board to test our algorithms for real-time feasibility. In order to do this, the board is connected directly to the host PC using an Ethernet cable, as shown in Fig. 6.2. Then, the Matlab codes have been reprogrammed into Simulink models. Next, these Simulink models are tested using the normal mode to check whether or not the models are ready to be used. Finally, the models are tested for real-time execution on the board remotely using the Simulink external mode.

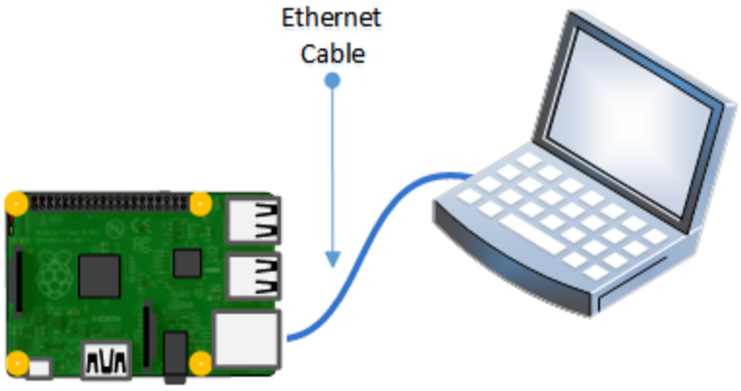

Figure 6.2: Direct connection between Raspberry Pi board and PC using Ethernet cable.

6.3 Experimental Results

In this section, we test the proposed techniques for real-time processing in the Raspberry Pi board described in the previous section. For this reason, the DOA techniques proposed in this thesis, namely, ES MVDR A-LASSO, FBS MVDR A-LASSO, and MVDR MBS A-LASSO are transfered into Simulink models in order to be compatible with the test board. Due to the absence of real data, simulated data has been generated. A sparse two-level nested array consisting of $M = 7$ elements, three elements of which are at the first level and the remaining at the second level, is considered for all the experiments. The sampling grid $\bar{\theta} \in [1^\circ : 180^\circ]$ that covers Ω is chosen to be in steps of 1° and the inter-element spacing is set to $\lambda/2$, where λ is the wavelength of the propagating waves. For each of the experiments, 10 snapshots are employed and SNR set to 0 dB.

In the first experiment, we examine the capability of the ES, FBS, and MBS MVDR A-LASSO to detect two non-fluctuating stationary sources. For this purpose, we consider two non-fluctuating fixed source signals impinging on the two-level nested array from DOAs of 60° and 120°. The noise is assumed to be AWGN. After generating the received signals, the DOAs are estimated by implementing the ES, FBS, and MBS MVDR A-LASSO DOA estimation technique remotely on the Raspberry Pi board. Fig. 6.3 illustrates the results of running the experiment on the board. From this figure, it is seen that the DOAs of the two source signals are estimated to be at 60° and 120°.

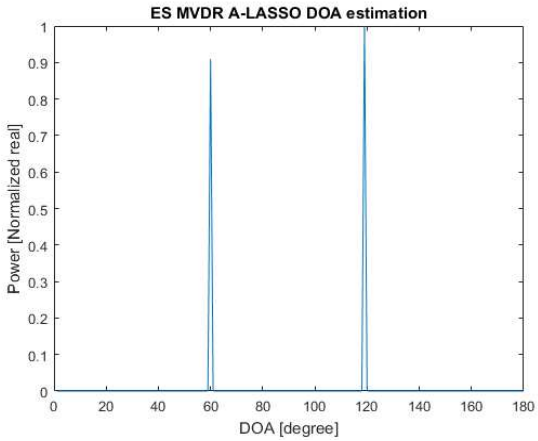

(a) ES

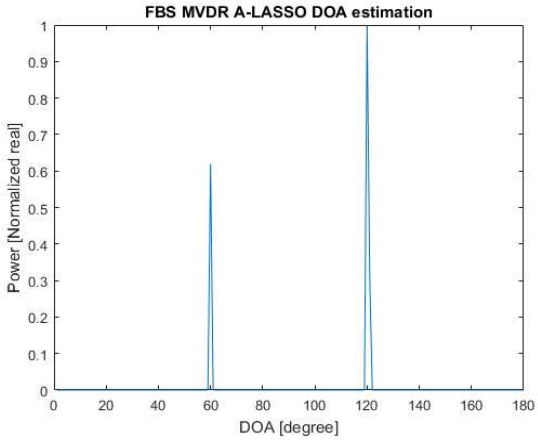

(b) FBS

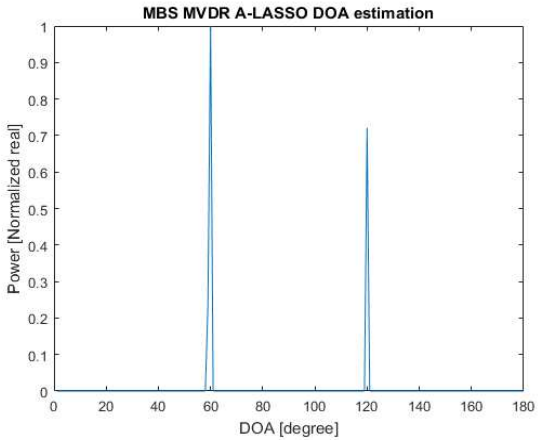

(c) MBS

Figure 6.3: Simulink-based DOA estimation for two source signals at 60° and 120°, 10 snapshots, SNR = 0 dB, External Mode, using MVDR A-LASSO (a) ES, (b) FBS, and (c) MBS.

In the second experiment, we investigate the capability of the proposed techniques to detect and track non-fluctuating source signals. The same three scenarios assumed in Section 3.7 are used in this experiment. The experiment is conducted on the board using ES, FBS, and MBS MVDR A-LASSO estimation techniques and the results are as shown in Figs. 6.4, 6.5 and 6.6. Furthermore, the execution times for the implementation of the three techniques given in Table 6.2. In order to calculate the execution time corresponding to each one of the proposed techniques, we average the run times of the experiments corresponding to Figs. 6.4, 6.5 and 6.6. As expected, the execution times for the BS-based techniques are lower than that for the ES-based technique, thus confirming the simulation results in Section 5.5.2. Moreover, the execution time of the MBS MVDR A-LASSO is the lowest.

Table 6.2: CS-based DOA estimation execution time (seconds).

Type	900 GHz Clock
ES MVDR A-LASSO	0.040
FBS MVDR A-LASSO	0.028
MBS MVDR A-LASSO	0.026

It can be concluded from the execution times given in Table 6.2 that real-time implementation of the proposed DOA estimation techniques indeed feasible.

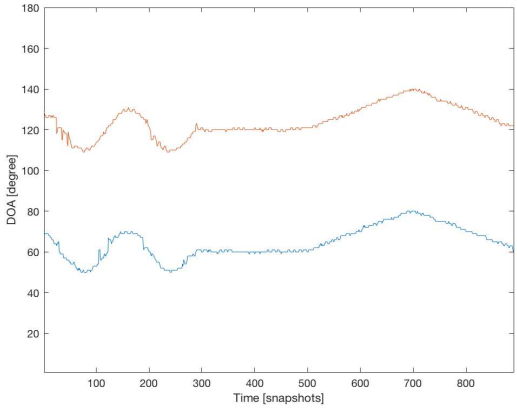

(a) In phase

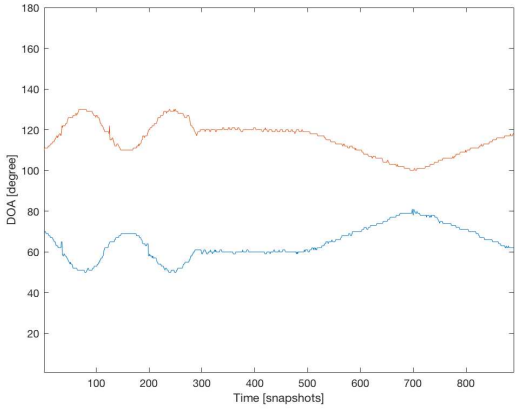

(b) Opp-phase

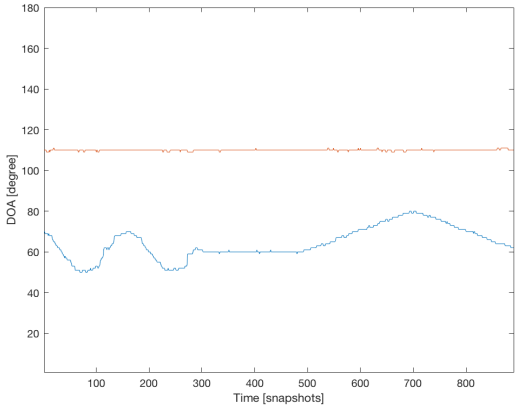

(c) Fixed vs moving

Figure 6.4: Simulink-based DOA estimation for non-fluctuating source signals, SNR = 0 dB, External Mode, using ES MVDR A-LASSO.

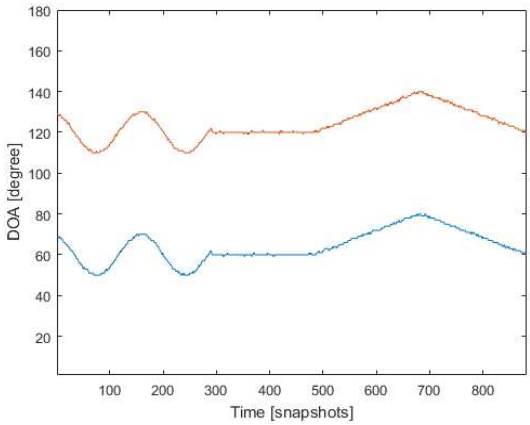

(a) In phase

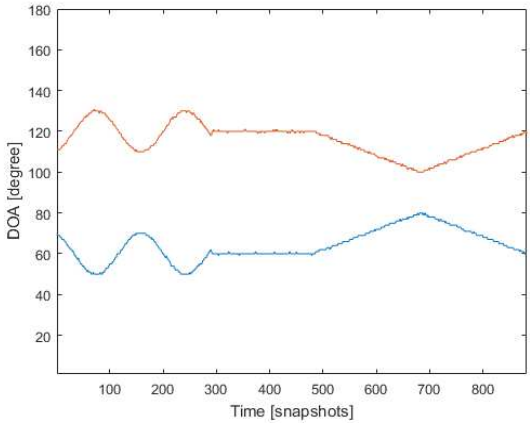

(b) Opp-phase

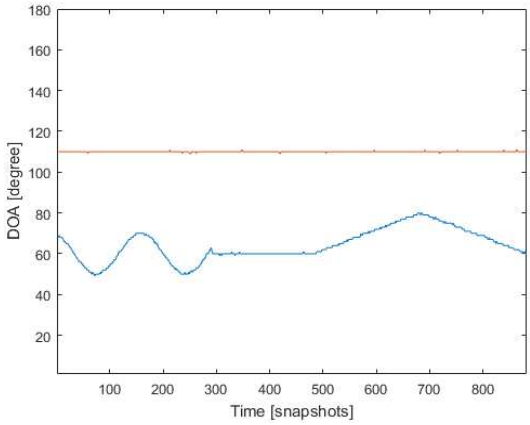

(c) Fixed vs moving

Figure 6.5: Simulink-based DOA estimation for non-fluctuating source signals, SNR = 0 dB, External Mode, using FBS MVDR A-LASSO.

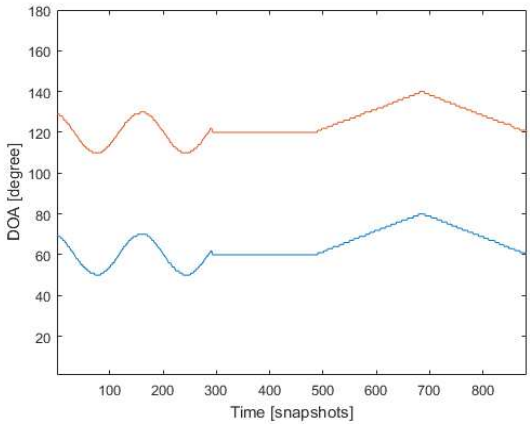

(a) In phase

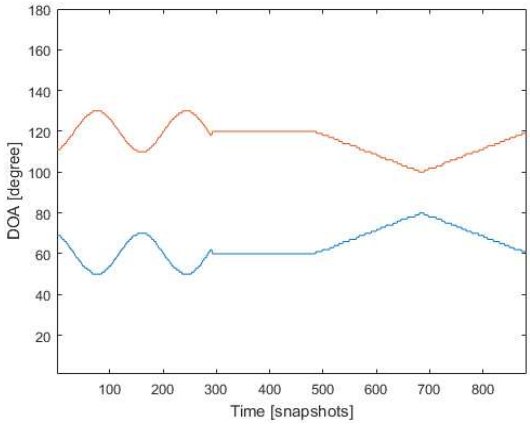

(b) Opp-phase

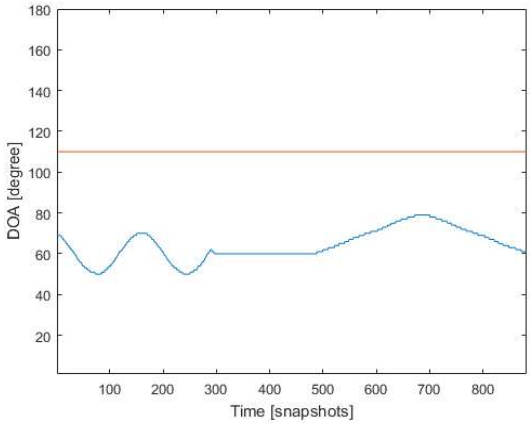

(c) Fixed vs moving

Figure 6.6: Simulink-based DOA estimation for non-fluctuating source signals, SNR = 0 dB, External Mode, using MBS MVDR A-LASSO.

6.4 Summary

In this chapter, using the Raspberry Pi board, it has been shown that all the DOA estimation techniques proposed in this thesis are feasible for real-time implementation. It can be expected that the execution time can be further reduced by reduced by realizing these techniques on a DSP board or through a custom VLSI implementation.

Chapter 7

Conclusions and Future Work

7.1 Conclusions

In this dissertation, techniques for estimation of the direction of arrival (DOA) in a compressive sensing (CS) framework have been presented for various types of source signals including fluctuating and moving sources. Three techniques have been proposed, one in the element-space, and the other two in the beamspace (BS). All these techniques have been shown to be capable of handling both non-fluctuating and fluctuating source signals as well as moving signals. They can also track moving source signals even when their trajectories intersect. Utilizing the concept of virtual arrays, all the proposed techniques are able to detect the number of source signals of the order $O(M^2)$, using a sparse linear array for which the number of sensors used is of order $O(M)$. Further, these techniques do not require an *a priori* knowledge of the number of sources to be estimated.

In element-space, an adaptable version of LASSO (A-LASSO) algorithm for the DOA estimation problem has been presented. It has been shown through a number of simulations that the proposed algorithm outperforms the classical DOA

estimation techniques as well as LASSO. The proposed algorithm is capable of performing DOA estimation using a small number of snapshots and is also capable of estimating correlated source signals as well as spatially-close sources. Further, a modified version of this algorithm has also been developed to take care of sources in unknown noise fields.

In beamspace, two techniques, one based on full beamspace (FBS) and the other on multiple beam beamspace (MBS) that has been obtained from reduced-dimension beamspace, have been developed. Just as the A-LASSO technique in element-space, these techniques are also capable of estimating correlated source signals as well as spatially-close sources using a small number of snapshots. Moreover, it has been shown that the performance of the two beamspace-based DOA estimation techniques is superior to that of the proposed element-space based technique, which already outperforms the existing beamspace-based DOA techniques. Further, the proposed beamspace-based techniques can handle both non-fluctuating and fluctuating signals as well as track moving signals.

All the techniques proposed in this thesis have been shown to be able to handle not only moving sources but even when their trajectories intersect. The three proposed DOA techniques enjoy similar characteristics of high performance; however, the beamspace-based techniques take much less time in processing than the element-space based technique does. The performance of the multiple beam beamspace based technique is shown to be superior to that of both the element-space and full beamspace based techniques for both fluctuating and non-fluctuating sources. The multiple beam beamspace based method has the lowest computational time among the three DOA techniques proposed in this thesis. Finally, by employing Raspberry Pi board, it has been shown that it is feasible to implement in real-time all the DOA estimation techniques proposed in this thesis.

7.2 Scope for Further Investigations

Based on the research carried out in this thesis, there is scope for some further work:

This thesis has proposed a compressive sensing based DOA estimation technique for the DOA estimation of sources in unknown noise fields. However, the estimation of only non-fluctuating sources has been investigated. Further investigation for fluctuating source signals can also be carried out.

All the estimation techniques presented in this thesis are for narrowband source signals. compressive sensing based DOA estimation techniques could be developed for wideband sources, which could be useful for ultra-wide band communication systems.

Compressive sensing based DOA estimation techniques have been proposed using one-dimensional sparse array. However, two-dimensional compressive sensing based DOA estimation techniques, which are required for applications such as surveillance and tracking radars, could also be developed.

Selecting an appropriate value of the regularization parameter is a very important issue in the compressive sensing framework. A bad choice of the regularization parameter could lead to an under- or over-regularized problem, and consequentially, more spurious sources could appear or even one or more source signals could be lost. In this thesis, the L-curve method has been used as a selecting tool for finding the regularization parameter. In this regard, methods for dynamically choosing the regularization parameter could be investigated.

References

[1] D. H. Johnson and D. E. Dudgeon, *Array signal processing: concepts and techniques*. New Jersey, USA: Simon & Schuster, 1992.

[2] C. A. Balanis, *Antenna theory: analysis and design*. New Jersy, USA: John Wiley & Sons, 2012.

[3] J. Kim, S. Song, and S.-C. Yu, "Denoising auto-encoder based image enhancement for high resolution sonar image," in *Proc. IEEE Underwater Technology*, Feb. 2017, pp. 1–5.

[4] X. Chen, Y. Shen, Z. Wang, W. Rhee, and Z. Wang, "A 17 mw 3-to-5 ghz duty-cycled vital sign detection radar transceiver with frequency hopping and time-domain oversampling," *IEEE Transactions on Circuits and Systems I: Regular Papers*, vol. 64, no. 4, pp. 969–980, Apr. 2017.

[5] W. Zhong, E. Dong, X. Cao, D. Zhang, Z. Huang, J. Xu, G. Li, and C. Xu, "Research on the development of heterogeneous network transmission system for seismic exploration wireless data acquisition," in *Proc. IEEE International Conference on Information Networking*, Jan. 2017, pp. 532–536.

[6] C. Granet, J. S. Kot, T. Natusch, S. Weston, and S. Gulyaev, "Design of an x-band feed system for the auckland university of technology 30m diameter warkworth radio telescope," in *Proc. IEEE European Conference on Antennas and Propagation*, Mar. 2017, pp. 3621–3625.

[7] Q. Shen, W. Liu, W. Cui, and S. Wu, "Underdetermined DOA estimation under the compressive sensing framework: A Review," *IEEE Access*, vol. 4, pp. 8865–8878, 2016.

[8] H. Krim and M. Viberg, "Two decades of array signal processing research: the parametric approach," *IEEE Signal Processing Magazine*, vol. 13, no. 4, pp. 67–94, 1996.

[9] H. Xiong, "Antenna array geometries and algorithms for direction of arrival estimation," Ph.D. dissertation, University of Nottingham, 2013.

[10] T. E. Tuncer and B. Friedlander, *Classical and modern direction-of-arrival estimation*. MA, USA: Academic Press, 2009.

[11] Z. Chen, G. Gokeda, and Y. Yu, *Introduction to Direction-of-arrival Estimation*. Artech House, 2010.

[12] H. L. Van Trees, *Detection, estimation, and modulation theory, optimum array processing*. New Yourk, USA: John Wiley & Sons, 2004.

[13] R. T. Lacoss, "Data adaptive spectral analysis methods," *Geophysics*, vol. 36, no. 4, pp. 661–675, 1971.

[14] R. O. Schmidt, "Multiple emitter location and signal parameter estimation," *IEEE Transactions on Antennas and Propagation*, vol. 34, no. 3, pp. 276–280, Mar. 1986.

[15] A. Paulraj, R. Roy, and T. Kailath, "Estimation of signal parameters via rotational invariance techniques-ESPRIT," in *Proc. IEEE Nineteeth Asilomar Conference on Circuits, Systems and Computers*, Oct. 1985, pp. 83–89.

[16] R. Roy and T. Kailath, "ESPRIT-estimation of signal parameters via rotational invariance techniques," *IEEE Transactions on Acoustics, Speech and Signal Processing*, vol. 37, no. 7, pp. 984–995, Jul. 1989.

[17] T. Kailath and R. H. Roy III, "ESPRIT–estimation of signal parameters via rotational invariance techniques," *Optical Engineering*, vol. 29, no. 4, pp. 296–313, 1990.

[18] B. D. Rao and K. S. Hari, "Performance analysis of root-MUSIC," *IEEE Transactions on Acoustics, Speech, and Signal Processing*, vol. 37, no. 12, pp. 1939–1949, Dec. 1989.

[19] D. Nion and N. D. Sidiropoulos, "A PARAFAC-based technique for detection and localization of multiple targets in a MIMO radar system," in *Proc. IEEE International Conference on Acoustics, Speech and Signal Processing*, 2009, pp. 2077–2080.

[20] H. Wang and M. Kaveh, "Coherent signal-subspace processing for the detection and estimation of angles of arrival of multiple wide-band sources," *IEEE Transactions on Acoustics, Speech and Signal Processing*, vol. 33, no. 4, pp. 823–831, Aug. 1985.

[21] A. Vesa, "Direction of arrival estimation using MUSIC and root–MUSIC algorithm," in *18th Telecommunications Forum TELFOR*, 2010, pp. 23–25.

[22] J. F. Gu, "Direction of arrival estimation and tracking with sparse arrays," Ph.D. dissertation, Concordia University, 2013.

[23] R. Muhamed, "Direction of arrival estimation using antenna arrays," Ph.D. dissertation, Virginia Polytechnic Institute and State University, 1996.

[24] Y.-S. Yoon, "Direction-of-arrival estimation of wideband sources using sensor arrays," Ph.D. dissertation, Citeseer, 2004.

[25] M. Zhou, X. Zhang, X. Qiu, and C. Wang, "Two-dimensional DOA estimation for uniform rectangular array using reduced-dimension propagator method," *International Journal of Antennas and Propagation*, 2014.

[26] R. T. Hoctor and S. A. Kassam, "The unifying role of the coarray in aperture synthesis for coherent and incoherent imaging," *Proceedings of the IEEE*, vol. 78, no. 4, pp. 735–752, 1990.

[27] R. J. Kozick and S. A. Kassam, "Coarray synthesis with circular and elliptical boundary arrays," *IEEE Transactions on Image Processing*, vol. 1, no. 3, pp. 391–405, Jul. 1992.

[28] S. U. Pillai, Y. Bar-Ness, and F. Haber, "A new approach to array geometry for improved spatial spectrum estimation," *Proceedings of the IEEE*, vol. 73, no. 10, pp. 1522–1524, 1985.

[29] S. Pillai and F. Haber, "Statistical analysis of a high resolution spatial spectrum estimator utilizing an augmented covariance matrix," *IEEE Transactions on Acoustics, Speech, and Signal Processing*, vol. 35, no. 11, pp. 1517–1523, Nov. 1987.

[30] A. Moffet, "Minimum-redundancy linear arrays," *IEEE Transactions on antennas and propagation*, vol. 16, no. 2, pp. 172–175, Mar. 1968.

[31] Y. I. Abramovich, D. A. Gray, A. Y. Gorokhov, and N. K. Spencer, "Positive-definite toeplitz completion in DOA estimation for nonuniform linear antenna arrays. i. fully augmentable arrays," *IEEE Transactions on Signal Processing*, vol. 46, no. 9, pp. 2458–2471, Sep. 1998.

[32] Y. I. Abramovich, N. K. Spencer, and A. Y. Gorokhov, "Positive-definite Toeplitz completion in DOA estimation for nonuniform linear antenna arrays.

ii. partially augmentable arrays," *IEEE Transactions on Signal Processing*, vol. 47, no. 6, pp. 1502–1521, Jun. 1999.

[33] D. A. Linebarger, H. Sudborough, and I. G. Tollis, "Difference bases and sparse sensor arrays," *IEEE Transactions on Information Theory*, vol. 39, no. 2, pp. 716–721, Mar. 1993.

[34] D. Pearson, S. U. Pillai, and Y. Lee, "An algorithm for near-optimal placement of sensor elements," *IEEE Transactions on Information Theory*, vol. 36, no. 6, pp. 1280–1284, Nov. 1990.

[35] C. S. Ruf, "Numerical annealing of low-redundancy linear arrays," *IEEE Transactions on Antennas and Propagation*, vol. 41, no. 1, pp. 85–90, Jan. 1993.

[36] C.-Y. Chen and P. P. Vaidyanathan, "Minimum redundancy MIMO radars," in *Proc. IEEE International Symposium on Circuits and Systems*, May 2008, pp. 45–48.

[37] B. Porat and B. Friedlander, "Direction finding algorithms based on high-order statistics," *IEEE Transactions on Signal Processing*, vol. 39, no. 9, pp. 2016–2024, Sep. 1991.

[38] P. Chevalier, L. Albera, A. Ferréol, and P. Comon, "On the virtual array concept for higher order array processing," *IEEE Transactions on Signal Processing*, vol. 53, no. 4, pp. 1254–1271, Apr. 2005.

[39] P. Chevalier and A. Férréol, "On the virtual array concept for the fourth-order direction finding problem," *IEEE Transactions on Signal Processing*, vol. 47, no. 9, pp. 2592–2595, Sep. 1999.

[40] M. C. Doğan and J. M. Mendel, "Applications of cumulants to array processing. i. aperture extension and array calibration," *IEEE Transactions on Signal Processing*, vol. 43, no. 5, pp. 1200–1216, May 1995.

[41] W.-K. Ma, T.-H. Hsieh, and C.-Y. Chi, "DOA estimation of quasi-stationary signals via Khatri-Rao subspace," in *Proc. IEEE International Conference on Acoustics, Speech and Signal Processing*, April 2009, pp. 2165–2168.

[42] D. Bliss and K. Forsythe, "Multiple-input multiple-output (MIMO) radar and imaging: degrees of freedom and resolution," in *Proc. IEEE Asilomar Conference on Signals, Systems and Computers*, vol. 1, Nov. 2003, pp. 54–59.

[43] P. Pal and P. Vaidyanathan, "Nested arrays: a novel approach to array processing with enhanced degrees of freedom," *IEEE Transactions on Signal Processing*, vol. 58, no. 8, pp. 4167–4181, Aug. 2010.

[44] N. Wagner, Y. C. Eldar, and Z. Friedman, "Compressed beamforming in ultrasound imaging," *IEEE Transactions on Signal Processing*, vol. 60, no. 9, pp. 4643–4657, Sep. 2012.

[45] M. Lustig, J. M. Santos, J.-H. Lee, D. L. Donoho, and J. M. Pauly, "Application of compressed sensing for rapid MR imaging," *SPARS,(Rennes, France)*, 2005.

[46] M. Herman, T. Strohmer *et al.*, "High-resolution radar via compressed sensing," *IEEE Transactions on Signal Processing*, vol. 57, no. 6, pp. 2275–2284, Jun. 2009.

[47] D. Malioutov, M. Çetin, and A. S. Willsky, "A sparse signal reconstruction perspective for source localization with sensor arrays," *IEEE Transactions on Signal Processing*, vol. 53, no. 8, pp. 3010–3022, Aug. 2005.

[48] J. Yin and T. Chen, "Direction-of-arrival estimation using a sparse representation of array covariance vectors," *IEEE Transactions on Signal Processing*, vol. 59, no. 9, pp. 4489–4493, Sep. 2011.

[49] A. Xenaki, P. Gerstoft, and K. Mosegaard, "Compressive beamforming," *The Journal of the Acoustical Society of America*, vol. 136, no. 1, pp. 260–271, 2014.

[50] R. Tibshirani, "Regression shrinkage and selection via the lasso," *Journal of the Royal Statistical Society. Series B (Methodological)*, pp. 267–288, 1996.

[51] H. Zou, "The adaptive lasso and its oracle properties," *Journal of the American Statistical Association*, vol. 101, no. 476, pp. 1418–1429, 2006.

[52] A. Panahi and M. Viberg, "On the resolution of the LASSO-based DOA estimation method," in *Proc. IEEE International ITG Workshop on Smart Antennas*, Feb. 2011, pp. 1–5.

[53] A. A. Salama, "Design and analysis of smart array antennas system for guidance stations applications," Master's thesis, Alexandria University, EGYPT, 2012.

[54] Z.-M. Liu, Z.-T. Huang, and Y.-Y. Zhou, "Direction-of-arrival estimation of wideband signals via covariance matrix sparse representation," *IEEE Transactions on Signal Processing*, vol. 59, no. 9, pp. 4256–4270, Sep. 2011.

[55] P. Stoica, P. Babu, and J. Li, "Spice: A sparse covariance-based estimation method for array processing," *IEEE Transactions on Signal Processing*, vol. 59, no. 2, pp. 629–638, Feb. 2011.

[56] K. Lee, Y. Bresler, and M. Junge, "Subspace methods for joint sparse recovery," *IEEE Transactions on Information Theory*, vol. 58, no. 6, pp. 3613–3641, Jun. 2012.

[57] Z.-M. Liu, Z.-T. Huang, and Y.-Y. Zhou, "Sparsity-inducing direction finding for narrowband and wideband signals based on array covariance vectors," *IEEE Transactions on Wireless Communications*, vol. 12, no. 8, pp. 1–12, Aug. 2013.

[58] H. Yu, X. Qiu, X. Zhang, C. Wang, and G. Yang, "Two-dimensional direction of arrival (DOA) estimation for rectangular array via compressive sensing trilinear model," *International Journal of Antennas and Propagation*, vol. 2015, 2015.

[59] Z.-b. Shen, C.-x. Dong, Y.-y. Dong, G.-q. Zhao, and L. Huang, "Broadband DOA estimation based on nested arrays," *International Journal of Antennas and Propagation*, vol. 2015, 2015.

[60] M. Carlin, P. Rocca, G. Oliveri, F. Viani, and A. Massa, "Directions-of-arrival estimation through Bayesian compressive sensing strategies," *IEEE Transactions on Antennas and Propagation*, vol. 61, no. 7, pp. 3828–3838, Jul. 2013.

[61] A. A. Salama, M. O. Ahmad, and M. N. S. Swamy, "Underdetermined DOA estimation using MVDR-Weighted LASSO," *Sensors*, vol. 16, no. 9, pp. 1549 (pages 1–28), 2016.

[62] M. J. Gans, "A power-spectral theory of propagation in the mobile-radio environment," *IEEE Transactions on Vehicular Technology*, vol. 21, no. 1, pp. 27–38, Feb. 1972.

[63] J. Namgoong and J. S. Lehnert, "Performance analysis for multicarrier DS/SSMA in frequency-selective fading channels," in *Proc. IEEE Military Communications Conference, 2001. MILCOM 2001. Communications for Network-Centric Operations: Creating the Information Force.*, vol. 2, 2001, pp. 1365–1369.

[64] A. G. Kanatas and P. Constantinou, "Fading prediction model for non-GEO satellites at land mobile satellite channels," in *Proc. IEEE Symposium on Computers and Communications*, Jul. 1997, pp. 375–383.

[65] M. S. Mezghanni, N. Kandil, and N. Hakem, "Performance study of IEEE 802.15. 4/4g waveforms over the mobile underground mine radio-channel," in *Proc. IEEE 84th Vehicular Technology Conference*, Sep. 2016, pp. 1–6.

[66] P. Swerling, "Probability of detection for fluctuating targets," *IRE Transactions on Information Theory*, vol. 6, no. 2, pp. 269–308, Apr. 1960.

[67] ——, "Radar probability of detection for some additional fluctuating target cases," *IEEE Transactions on Aerospace and Electronic Systems*, vol. 33, no. 2, pp. 698–709, Apr. 1997.

[68] ——, *More on detection of fluctuating targets.* CA, USA: Rand Corporation, 1965.

[69] J. A. Gansman, M. D. Zoltowski, and J. V. Krogmeier, "Multidimensional multirate DOA estimation in beamspace," *IEEE transactions on signal processing*, vol. 44, no. 11, pp. 2780–2792, 1996.

[70] H. W. Engl, M. Hanke, and A. Neubauer, *Regularization of inverse problems.* Netherlands: Springer Science & Business Media, 1996, vol. 375.

[71] C. R. Vogel, *Computational methods for inverse problems.* PA, USA: Siam, 2002, vol. 23.

[72] A. Neumaier, "Solving ill-conditioned and singular linear systems: A tutorial on regularization," *SIAM review*, vol. 40, no. 3, pp. 636–666, 1998.

[73] P. C. Hansen, "Regularization tools: A Matlab package for analysis and solution of discrete ill-posed problems," *Numerical algorithms*, vol. 6, no. 1, pp. 1–35, 1994.

[74] A. Tikhonov, "Solution of incorrectly formulated problems and the regularization method," in *Soviet Math. Dokl.*, vol. 5, 1963, pp. 1035–1038.

[75] W. C. Karl, "Regularization in image restoration and reconstruction," *Handbook of Image and Video Processing*, pp. 141–160, 2000.

[76] B. Jiang, Y.-F. Liu, and Z. Wen, "L_p-norm regularization algorithms for optimization over permutation matrices," *SIAM Journal on Optimization*, vol. 26, no. 4, pp. 2284–2313, 2016.

[77] R. E. Burkard, "Quadratic assignment problems," *Handbook of combinatorial optimization*, pp. 2741–2814, 2013.

[78] E. J. Candes, J. K. Romberg, and T. Tao, "Stable signal recovery from incomplete and inaccurate measurements," *Communications on pure and applied mathematics*, vol. 59, no. 8, pp. 1207–1223, 2006.

[79] Z. Lu, "Iterative reweighted minimization methods for l_p regularized unconstrained nonlinear programming," *arXiv preprint arXiv:1210.0066*, 2012.

[80] J. Liang, "Joint azimuth and elevation direction finding using cumulant," *IEEE Sensors Journal*, vol. 9, no. 4, pp. 390–398, 2009.

[81] C. Zhu, W.-Q. Wang, H. Chen, and H. C. So, "Impaired sensor diagnosis, beamforming, and DOA estimation with difference co-array processing," *IEEE Sensors Journal*, vol. 15, no. 7, pp. 3773–3780, 2015.

[82] W.-K. Ma, T.-H. Hsieh, and C.-Y. Chi, "DOA estimation of quasi-stationary signals with less sensors than sources and unknown spatial noise covariance: a Khatri–Rao subspace approach," *IEEE Transactions on Signal Processing*, vol. 58, no. 4, pp. 2168–2180, April 2010.

[83] P. P. Vaidyanathan and P. Pal, "Sparse sensing with co-prime samplers and arrays," *IEEE Transactions on Signal Processing*, vol. 59, no. 2, pp. 573–586, Feb. 2011.

[84] Y. D. Zhang, M. G. Amin, and B. Himed, "Sparsity-based DOA estimation using co-prime arrays," in *Proc. IEEE International Conference on Acoustics, Speech and Signal Processing*, May 2013, pp. 3967–3971.

[85] K. Adhikari, J. R. Buck, and K. E. Wage, "Beamforming with extended co-prime sensor arrays," in *Proc. IEEE International Conference on Acoustics, Speech and Signal Processing*, May 2013, pp. 4183–4186.

[86] Q. Shen, W. Liu, W. Cui, S. Wu, Y. D. Zhang, and M. G. Amin, "Low-complexity direction-of-arrival estimation based on wideband co-prime arrays," *IEEE/ACM Transactions on Audio, Speech, and Language Processing*, vol. 23, no. 9, pp. 1445–1456, Sep. 2015.

[87] M. Lustig, D. Donoho, and J. M. Pauly, "Sparse MRI: The application of compressed sensing for rapid MR imaging," *Magnetic resonance in medicine*, vol. 58, no. 6, pp. 1182–1195, 2007.

[88] P. Gerstoft, A. Xenaki, and C. F. Mecklenbräuker, "Single and multiple snapshot compressive beamforming," *The Journal of the Acoustical Society of America*, vol. 138, no. 4, pp. 2003–2014, 2015.

[89] J. Fan and R. Li, "Variable selection via nonconcave penalized likelihood and its oracle properties," *Journal of the American statistical Association*, vol. 96, no. 456, pp. 1348–1360, 2001.

[90] S. S. Chen, D. L. Donoho, and M. A. Saunders, "Atomic decomposition by basis pursuit," *SIAM journal on scientific computing*, vol. 20, no. 1, pp. 33–61, 1998.

[91] B. Efron, T. Hastie, I. Johnstone, R. Tibshirani *et al.*, "Least angle regression," *The Annals of statistics*, vol. 32, no. 2, pp. 407–499, 2004.

[92] M. Elad, *The Quest for a Dictionary.* New York, USA: Springer, 2010.

[93] P. Sinha, A. D. George, and K. Kim, "Parallel algorithms for robust broadband MVDR beamforming," *Journal of Computational Acoustics*, vol. 10, no. 01, pp. 69–96, 2002.

[94] S. Balakrishnan and L. T. Ong, "GNU radio based digital beamforming system: BER and computational performance analysis," in *Proc. IEEE European Signal Processing Conference*, Aug. 2015, pp. 1596–1600.

[95] T. B. Lavate, V. Kokate, and A. Sapkal, "Performance analysis of MUSIC and ESPRIT DOA estimation algorithms for adaptive array smart antenna in mobile communication," in *Proc. IEEE Second International Conference on Computer and Network Technology*, April 2010, pp. 308–311.

[96] M. Priyadarshini and R. Vinutha, "Comparative performance analysis of MUSIC and ESPRIT on ULA," in *Proc. IEEE International Conference on Radar, Communication and Computing*, 2012, pp. 120–124.

[97] U. Mujahid, M. Mukhtar, J. Ahmed, A. Rehman, M. Abbas, and U. Shahid, "Spectral estimation for smart antenna system," in *Proc. IEEE International Conference on Computer, Control & Communication*, Sep. 2013, pp. 1–5.

[98] V. A. Morozov, "On the solution of functional equations by the method of regularization," in *Soviet Math. Dokl*, vol. 7, no. 1, 1966, pp. 414–417.

[99] B. W. Rust, *Truncating the singular value decomposition for ill-posed problems.* MD, USA: US Department of Commerce, Technology Administration, National Institute of Standards and Technology, 1998.

[100] G. Wahba, "Practical approximate solutions to linear operator equations when the data are noisy," *SIAM Journal on Numerical Analysis*, vol. 14, no. 4, pp. 651–667, 1977.

[101] P. C. Hansen, T. K. Jensen, and G. Rodriguez, "An adaptive pruning algorithm for the discrete L-curve criterion," *Journal of computational and applied mathematics*, vol. 198, no. 2, pp. 483–492, 2007.

[102] P. C. Hansen and D. P. O'Leary, "The use of the L-curve in the regularization of discrete ill-posed problems," *SIAM Journal on Scientific Computing*, vol. 14, no. 6, pp. 1487–1503, 1993.

[103] L. Qu and P. Routh, "Determination of regularization parameter using L-curve by the LARS-LASSO algorithm," in *The 2006 Joint Statistical Meetings in Seattle, Washington, JSM 2006*. American Statistical Association (ASA), 2006.

[104] M. Grant and S. Boyd, "CVX: Matlab software for disciplined convex programming, version 2.1," http://cvxr.com/cvx, Mar. 2014.

[105] ——, "Graph implementations for nonsmooth convex programs," in *Recent Advances in Learning and Control*, ser. Lecture Notes in Control and Information Sciences, V. Blondel, S. Boyd, and H. Kimura, Eds. Springer-Verlag Limited, 2008, pp. 95–110.

[106] R. H. Tütüncü, K. C. Toh, and M. J. Todd, "Solving semidefinite-quadratic-linear programs using SDPT3," *Mathematical programming*, vol. 95, no. 2, pp. 189–217, 2003.

[107] P. Stoica and N. Arye, "MUSIC, maximum likelihood, and Cramer-Rao bound," *IEEE Transactions on Acoustics, Speech and Signal Processing*, vol. 37, no. 5, pp. 720–741, May 1989.

[108] P. Stoica and A. Nehorai, "Performance study of conditional and unconditional direction-of-arrival estimation," *IEEE Transactions on Acoustics, Speech and Signal Processing*, vol. 38, no. 10, pp. 1783–1795, Oct. 1990.

[109] A. G. Jaffer, "Maximum likelihood direction finding of stochastic sources: A separable solution," in *Proc. IEEE International Conference on Acoustics, Speech, and Signal Processing*, Apr. 1988, pp. 2893–2896.

[110] A. A. Salama, M. O. Ahmad, and M. N. S. Swamy, "Compressive Sensing-based DOA Estimation using the Dantzig Selector," in *Proc. IEEE International Midwest Symposium on Circuits and Systems*, Aug. 2017, pp. 859–862.

[111] J. P. Le Cadre, "Parametric methods for spatial signal processing in the presence of unknown colored noise fields," *IEEE Transactions on Acoustics, Speech and Signal Processing*, vol. 37, no. 7, pp. 965–983, Jul. 1989.

[112] H. Ye and R. D. DeGroat, "Maximum likelihood DOA estimation and asymptotic Cramér-Rao bounds for additive unknown colored noise," *IEEE Transactions on Signal Processing*, vol. 43, no. 4, pp. 938–949, Apr. 1995.

[113] J. Li, B. Halder, P. Stoica, and M. Viberg, "Computationally efficient angle estimation for signals with known waveforms," *IEEE Transactions on Signal Processing*, vol. 43, no. 9, pp. 2154–2163, Sep. 1995.

[114] M. Viberg, P. Stoica, and B. Ottersten, "Array processing in correlated noise fields based on instrumental variables and subspace fitting," *IEEE Transactions on Signal Processing*, vol. 43, no. 5, pp. 1187–1199, May 1995.

[115] Q. Wu and K. M. Wong, "UN-MUSIC and UN-CLE: An application of generalized correlation analysis to the estimation of the direction of arrival of signals in unknown correlated noise," *IEEE Transactions on Signal Processing*, vol. 42, no. 9, pp. 2331–2343, Sep. 1994.

[116] T. Li and A. Nehorai, "Maximum likelihood direction finding in spatially colored noise fields using sparse sensor arrays," *IEEE Transactions on Signal Processing*, vol. 59, no. 3, pp. 1048–1062, Mar. 2011.

[117] M. Bhandary, "Estimation of covariance matrix in signal processing when the noise covariance matrix is arbitrary," *Journal of Modern Applied Statistical Methods*, vol. 7, no. 1, p. 16, 2008.

[118] V. Nagesha and S. Kay, "Maximum likelihood estimation for array processing in colored noise," *IEEE Transactions on Signal Processing*, vol. 44, no. 2, pp. 169–180, Feb. 1996.

[119] B. Liao, S.-C. Chan, L. Huang, and C. Guo, "Iterative methods for subspace and DOA estimation in nonuniform noise." *IEEE Transactions on Signal Processing*, vol. 64, no. 12, pp. 3008–3020, Jun. 2016.

[120] S. Vorobyov, A. B. Gershman, K. M. Wong *et al.*, "Maximum likelihood direction-of-arrival estimation in unknown noise fields using sparse sensor arrays," *IEEE Transactions on Signal Processing*, vol. 53, no. 1, pp. 34–43, Jan. 2005.

[121] L. C. Godara, "Limitations and capabilities of directions-of-arrival estimation techniques using an array of antennas: a mobile communications perspective," in *Proc. IEEE International Symposium on Phased Array Systems and Technology*, 1996, pp. 327–333.

[122] A. A. Salama, M. O. Ahmad, and M. N. S. Swamy, "Compressed Sensing DOA Estimation in the Presence of Unknown Noise," (under review).

[123] M. Hyder and K. Mahata, "An approximate ℓ_0 norm minimization algorithm for compressed sensing," in *Proc. IEEE International Conference on Acoustics, Speech and Signal Processing*, Apr. 2009, pp. 3365–3368.

[124] C. R. Berger, J. Areta, K. Pattipati, and P. Willett, "Compressed sensing-a look beyond linear programming," in *Proc. IEEE International Conference on Acoustics, Speech and Signal Processing*, Mar. 2008, pp. 3857–3860.

[125] L. Mancera and J. Portilla, "ℓ_0-norm-based sparse representation through alternate projections." in *ICIP*, vol. 2092. Citeseer, 2006.

[126] G. H. Mohimani, M. Babaie-Zadeh, and C. Jutten, "Fast sparse representation based on smoothed ℓ_0 norm," in *Independent Component Analysis and Signal Separation*. Springer, 2007, pp. 389–396.

[127] E. J. Candès, "The restricted isometry property and its implications for compressed sensing," *Comptes Rendus Mathematique*, vol. 346, no. 9, pp. 589–592, 2008.

[128] R. Baraniuk, M. Davenport, R. DeVore, and M. Wakin, "A simple proof of the restricted isometry property for random matrices," *Constructive Approximation*, vol. 28, no. 3, pp. 253–263, 2008.

[129] E. J. Candès, J. Romberg, and T. Tao, "Robust uncertainty principles: Exact signal reconstruction from highly incomplete frequency information," *IEEE Transactions on Information Theory*, vol. 52, no. 2, pp. 489–509, Feb. 2006.

[130] D. L. Donoho, "Compressed sensing," *IEEE Transactions on Information Theory*, vol. 52, no. 4, pp. 1289–1306, Apr. 2006.

[131] E. J. Candes and T. Tao, "Near-optimal signal recovery from random projections: Universal encoding strategies," *IEEE Transactions on Information Theory*, vol. 52, no. 12, pp. 5406–5425, Dec. 2006.

[132] A. A. Salama, M. O. Ahmad, and M. N. S. Swamy, "Beamspace compressed Sensing for DOA Estimation," (under review).

[133] Y. Yang, C. Wan, and C. Sun, "Broadband beamspace DOA estimation algorithms," in *Proc. IEEE OCEANS*, vol. 3, Sep. 2003, pp. 1654–1660.

[134] G. Bournaka, C. Schwark, D. Cristallini, and H. Kuschel, "Beam space transformation based direction of arrival estimation and auto calibration for a circular array in passive radar," in *Proc. IEEE Radar Conference*, May 2017, pp. 0745–0748.

[135] Z. Guo, X. Wang, and W. Heng, "Millimeter-wave channel estimation based on two-dimensional beamspace MUSIC method," *IEEE Transactions on Wireless Communications*, Jun. 2017.

[136] D.-J. Yeom, S.-H. Park, J.-R. Kim, and M.-J. Lee, "Performance analysis of beamspace MUSIC with beamforming angle," in *Proc. IEEE International Conference on Signal Processing and Communication Systems*, Dec. 2014, pp. 1–5.

[137] V. Vasylyshyn, "Improved beamspace ESPRIT-based DOA estimation via pseudo-noise resampling," in *Proc. IEEE 9th European Radar Conference*, Oct. 2012, pp. 238–241.

[138] Y. Guo, Y. Zhang, and N. Tong, "Beamspace ESPRIT algorithm for bistatic MIMO radar," *Electronics letters*, vol. 47, no. 15, pp. 876–878, 2011.

[139] J. Li and X. Zhang, "Direction of arrival estimation of quasi-stationary signals using unfolded coprime array," *IEEE Access*, vol. 5, pp. 6538–6545, 2017.

[140] O. A. Paiva and R. d. O. Moreira, "Raspberry pi: a 35-dollar device for viewing dicom images," *Radiologia brasileira*, vol. 47, no. 2, pp. 99–100, 2014.

[141] G. Havariyoun and N. Christofi, "Coding with pediatric patients at king's college hospital: Experience from a london hospital," *Journal of Medical Imaging and Radiation Sciences*, vol. 47, no. 4, pp. 294–297, 2016.